

University of Nottingham

UK | CHINA | MALAYSIA

Vibrational Spectroscopic Studies into Impurities in Ionic Liquids

Steven J. Maxwell-Hogg. Msci (Hons)

Thesis submitted to the University of Nottingham

for the degree of Doctor of Philosophy

September 2018

Some people graduate, but we still stupid

K.W

Abstract

Additional components present within an ionic liquid (IL) system have readily shown to alter the physiochemical properties and spectroscopic characteristics of the parent IL. Vibrational spectroscopy has been proven to be a powerful tool in probing these systems and identifying spectral changes as a result of the changing environment

This work presents a range of imidazolium-based ILs that have been probed with vibrational spectroscopy. The ILs investigated possess a 1-alkyl-3-methylimidazolium cation with corresponding anions ranging from $[BF_4]^-$, $[Ac]^-$, Cl^-, $[DMP]^-$, and $[MeSO_4]^-$. Each IL investigated was doped with an array of impurities that may commonly be retained in an IL system due to preparation and or exposure to the environment. Contamination is a common problem, leading to the perturbation of many physical and chemical properties, which can impact the overall efficiency of an IL.

Vibrational spectroscopy allows for the investigation into perturbations created by impurities and how varying concentrations ultimately affect the vibrational nature of the IL. These interactions have further been studied with the use of multivariate analysis to provide further insight into these changes. The combination of multiple vibrational spectroscopic techniques and analysis has allowed for an in-depth investigation into contaminated IL systems.

Declaration

This work has not previously been accepted in substance for any degree and is not being concurrently submitted in candidature for any degree.

Signed: _____ (Candidate)

Date: _____

Statement 1

This Thesis is the result of my own investigations, except where otherwise stated. Other sources are acknowledged by footnotes giving explicit references. Bibliographies are appended.

Signed: _____ (Candidate)

Date: _____

Signed: _____ (Supervisor)

Date: _____

Statement 2

I hereby give consent for my Thesis, if accepted, to be available for photocopying and for inter - library loan, and for the title and summary to be made available to outside organisations.

Signed: _____ (Candidate)

Date: _____

Acknowledgements

Firstly I would like to acknowledge Prof. Peter Licence and Prof. Andrei Khlobystov for their complimentary nature and encouragement in the final year of my undergraduate studies. Their kind words and reassurance was the key motivation for pursuing the Centre for Doctoral Training in Sustainable Chemistry.

I would like to personally thank my supervisor Prof. Pete Licence for his constant reinforcement throughout the four years of the CDT programme. Without his encouragement, belief in my potential as a researcher and positive support, this research and thesis would not have come together.

There are many people for whose help and guidance, no matter how small, aided in bringing this research and thesis together. I must thank Dr Calum Welsh for his guidance throughout, constant support with MATLAB, his knowledge of vibrational spectroscopy and overall help with this research. I must thank all the members of the Nottingham IL Group, past and present: Coby, Becca, Zoe, Ana, Ejike, Mags, Linda, Astrid, Meike, Zé, Patrick and Aki, who all provided continual support and advice whilst boosting the morale around the lab and office. I would like to thank all of Cohort One of the CDT, with a special thanks to Meg, Tatianna and Tim who were there both in and out of the chemistry bubble.

I would also like to thank the help of the technical staff in the school of chemistry and the CNL all of which provided assistance and knowledge when asked and were of great help to this research.

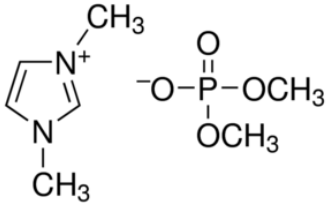
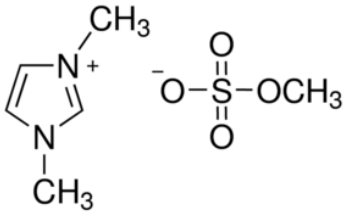
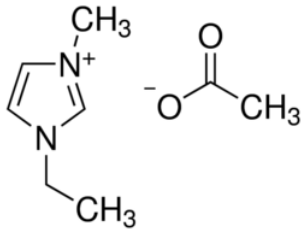
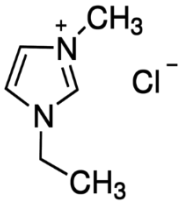
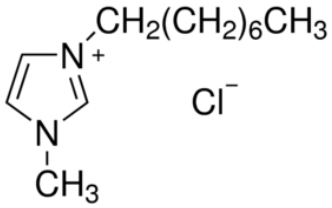
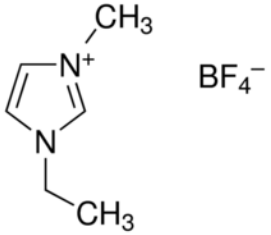
Last but not least, I would like to acknowledge family and friends who supported me during the four years of the PhD. First and foremost I would like to thank Mum, Dad,

Wiggy, Gabby and Franky for their constant support at every point in this process. Without them being there at the end of many phone calls and visits, this thesis would not be possible.

Abbreviations and Acronyms

$[A]^-$	Anions
ACN	Acetonitrile
[AHAs]	Aprotic Heterocyclic Anions
atm	Atmospheres
ATR-FTIR	Attenuated Total Reflection Fourier-Transform Infrared Spectroscopy
COSMO-RS	Conductor like Screening Model for Real Solvents
d	Doublet
DCM	Dichloromethane
DFT	Density Functional Theory
ESI-MS	Electrospray Ionisation Mass Spectrometry
EtOH	Ethanol
GCMD	Grained Molecular Dynamic Simulations
hr	Hour
IC	Ion Chromatography
IL	Ionic Liquid
IR	Infrared Spectroscopy
κ	Electrolytic Conductivity
K	Kelvin
m	Multiplet
mbar	Millibar

MC	Monte Carlo
MCR	Multivariate Curve Resolution
MD	Molecular Dynamics
MeOH	Methanol
Min	Minute
Mol	Mole
NMR	Nuclear magnetic resonance
P	Pressure
Ppm	Parts per Million
Q	Quartet
R	Alkyl Group
RT	Room Temperature
S	Singlet
T	Triplet
T	Time
T	Temperature
vol	Volume
Wt	Weight
E	Dielectric Constant
η	Viscosity
ρ	Density
Σ	Conductivity

Ionic Liquids			
Structure	**Name**	**Hydrophilicity**	**Methodology**
	1, 3-Dimethylimidazolium dimethyl phosphate, [MMIM] [DMP]	Hydrophilic	Chapter 2, Ref: [11-13]
	1, 3-Dimethylimidazolium methyl sulphate, [MMIM] [$MeSO_4$]	Hydrophilic	Chapter 2, Ref: [13-14]
	1-Ethyl-3-methylimidazolium acetate, [EMIM] [Ac]	Hydrophilic	Chapter 2, Ref: [13,15,16]
	1-Ethyl-3-methylimidazolium chloride, [EMIM] Cl	Hydrophilic	Chapter 2, Ref: [13,17]
	1-Methyl-3-octylimidazolium chloride, [OMIM] Cl	Hydrophilic	Chapter 2, Ref: [18-19]
	1-Ethyl-3-methylimidazolium tetrafluoroborate, [EMIM] [BF_4]	Hydrophobic	Chapter 2, Ref: [22]

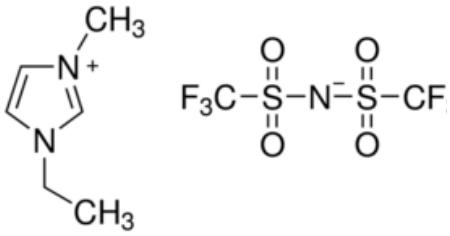
	1-Ethyl-3-methylimidazolium bis (trifluoromethylsulfonyl) imide, [EMIM] [Tf_2N]	Hydrophobic	Chapter 2, Ref: [22-23]

Table of Contents

Chapter 1. Introduction

1.1 Background……..
1.2 Properties of Ionic Liquids……..
1.2.1 Bulk Physical Properties……...
1.3 Impurities in Ionic Liquids……...
1.3.1 Preparation of Ionic Liquids……..
1.4 Water Impurities in Ionic liquids…….
1.4.1 Impact of Water on the Viscosity of Ionic Liquids……..
1.4.2 Impact of Water on Ionic Liquid Facilitated Chemistry……..
1.4.3 Spectroscopic Analysis of Ionic Liquid Water Systems……
1.4.4 Computational Analysis of Ionic Liquid Water Systems……...
1.4.5 Ionic Liquids and Bulk Water Mixtures……
1.5 Further Impurities in Ionic liquids……..
1.5.1 Solvent Impurities in Ionic liquids……
1.5.2 Halide Impurities in Ionic liquids……..
1.5.3 Alkali Salt Impurities in Ionic liquids……
1.6 Aims and Objectives……...
1.7 References……..

Chapter 2. Experimental and Methodology

2.1 Vibrational Spectroscopy……
2.1.1 ATR-FTIR…….
2.1.2 Raman Spectroscopy…….

2.1.3 Multivariate Analysis……

2.1.4 Multivariate Curve Resolution……

2.1.5 Analysis of Datasets……

2.2 Karl Fischer Titration……

2.2.1 Coulometric Karl Fischer Titration……

2.3 Instruments……

2.4 Materials……

2.5 Synthesis of Ionic Liquids……

2.5.1 Preparation of 1, 3-dimethylimidazolium dimethyl phosphate, [MMIM] [DMP]……..

2.5.2 Preparation of 1, 3-dimethylimidazolium methyl sulphate, [MMIM] [$MeSO_4$]……..

2.5.3 1-Ethyl-3-methylimidazolium acetate, [EMIM] [Ac]…….

2.5.4 1-Ethyl-3-methylimidazolium chloride, [EMIM] Cl……..

2.5.5 Preparation of 1-methyl-3-octylimidazolium chloride, [OMIM] Cl……..

2.6 General Procedure for Metathesis Products……

2.6.1 Ethyl-3-methylimidazolium bis (trifluoromethylsulfonyl) imide, [EMIM] [Tf_2N]....

2.5.2 Ethyl-3-methylimidazolium tetrafluoroborate, [EMIM] [BF_4]……..

2.7 Preparation of Binary Solutions of Water and Ionic Liquids……

2.8 Preparation of Binary Solutions of Solvent and Ionic Liquids ……

2.9 Preparation of Binary Solutions of Metathesis Salts and Ionic Liquids …….

2.10 References…….

Chapter 3. Vibrational Spectroscopic Analysis of Water and Ionic Liquids

3.1 Introduction……...

3.1.1 Regional ATR-FTIR Vibrations of Ionic liquids……...

3.1.2 Linear Combination of Spectra……..

3.1.3 Initial Investigation into Atmospheric Water…….

3.2. [MMIM] [$MeSO_4$] Absorption of Atmospheric Water……...

3.2.1 Physical Properties of [MMIM] [$MeSO_4$] ……..

3.3 Hydration of [MMIM] [$MeSO_4$] ……

3.3.1 Physical Properties of [MMIM] [$MeSO_4$] upon Hydration……

3.3.2 Multivariate Curve Resolution Results …….

3.4 Hydration of [MMIM] [$MeSO_4$] at Lower Concentrations of Water…….

3.4.1 Multivariate Curve Resolution Results …….

3.5 Conclusion……

3.6 References……

Chapter 4. Vibrational Spectroscopic Analysis of Molecular Solvents and Ionic Liquids

4.1 Introduction……...

4.2 Preparation of Solvent Ionic Liquid Binary Mixtures……

4.3 Impact of Miscible solvents on Ionic Liquids…….

4.4 Impact of Immiscible solvents on Ionic Liquids…….....

4.5 Ionic Liquids, Molecular Solvents and Water Tertiary Mixtures…….

4.6 Conclusion……

4.7 References……

Chapter 5. Vibrational Spectroscopic Analysis of Alkali Salts and Ionic Liquids

5.1 Introduction……...

5.1.1 Current Research into Alkali Salt Ionic Liquid Systems……..

5.1.2 ATR-FTIR of Alkali Salt Based Ionic Liquids ……..

5.2 ATR-FTIR of [EMIM] [Tf_2N] doped with $LiNTf_2$……

5.2.1 Physical Properties of [EMIM] [Tf_2N] ……

5.3 ATR-FTIR Analysis of Additional Ionic Liquid Alkali Salt Combinations…….

5.4 Conclusions……..

5.5 References……

Chapter 6. Conclusion and Future Work

Chapter 7. Appendix

Appendix A: NMR and Mass Spectrometry analysis for Chapter 2……..

Appendix B: ATR-FTIR, Raman and Multivariate Spectra for Chapter 3……

Appendix C: ATR-FTIR Spectra for Chapter 4……

Chapter 1

Introduction to Ionic Liquids and Impurities

1. Introduction

1.8 Background

ILs are a class of ionic salts that are present in the liquid phase at unusually low temperatures. The composition of common ILs is that of a non-symmetrical, sterically encumbered organic cation with a weakly coordinating anion. Figure 1.1 details a selection of cations and anions that can be interchangeable. Other compositions, such as ILs with symmetrical cations and multicationic ILs are known. ILs exhibit very low vapour pressures, which is attributable to the strong coulombic charge that holds the individual ions together. ILs exhibit many other characteristics that include: wide liquid regions, favourable solvating properties and high thermal stability to name but a few [1-3].

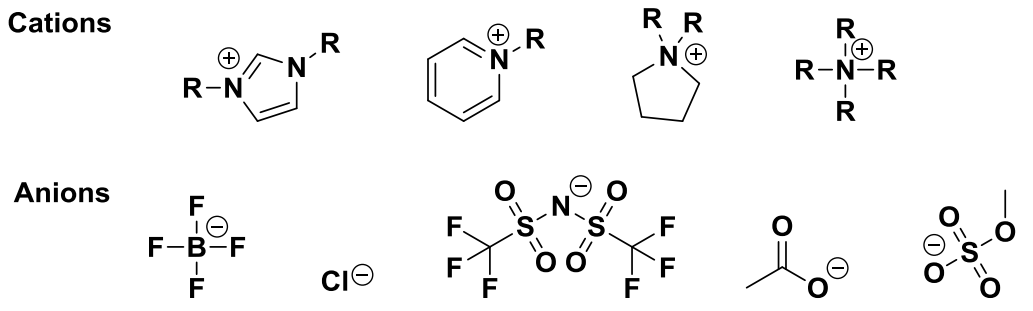


Figure 1.1. Examples of frequently used ILs detailing the cationic (top row) and anionic (bottom row) components.

Despite their extremely low vapour pressures, some ILs can be distilled under harsh conditions of low pressure and high temperatures. The favourable solvating properties allow ILs to facilitate organic, bioorganic and inorganic reactions, enabling optimization of yield and tunability that provides the title of designer solvent. The applications of ILs are widespread throughout diverse areas of chemistry, including electrochemistry, nuclear chemistry and polymer chemistry[2-3].

ILs have readily been labelled as 'green solvents' since their introduction. Most of the justification for this classification rests upon the properties of ILs. ILs non-volatility, low flammability and ease of containment are just a selection of properties that are often used to support their 'Green' label. The classification of ILs in this manner has been challenged on several occasions. Concerns with toxicity, environmental persistence and price are noted as the major negative factors associated with commonly used ILs. As a response to the negative factors associated with ILs, further research has been carried out into the design of ILs with lower toxicity, and even ILs that can be derived from natural and biodegradable forms[1,4,5].

The 'greenness' of ILs however, should be judged accordingly to other process solvents with the environmental impact of the overall process being the main concern. For example, if a more hazardous solvent, be that a widely common IL, provided significant improvements to the overall environmental impact of the reaction process compared with a less hazardous alternative, then the 'greener' choice is less favoured. The takeaway message from this would be that the term green solvent is inaccurate and a 'true green' solvent is idealistic. Approaching chemistry in terms of sustainability provides a more comprehensive outlook. Improving the sustainability of chemical processes is more beneficial than the constituents that make up the process. ILs have already achieved success in this area by replacing molecular solvents and improving the overall efficiency of the chemistry they assist. The potential ability to recycle ILs

further increases the sustainability profile of not only the IL but the overall chemical processes they are involved in[4-5].

1.2 Properties of Ionic Liquids

ILs display a variety of physical properties that allow them to be a more attractive replacement for traditional molecular organic solvents. These properties are common to all ILs and are the defining characteristics of these solvents. ILs non-volatility allows them to be used in high vacuum environments; their non-flammability proves of value when they are used as solvents for exothermic reactions. ILs also possess the ability to dissolve a wide range of inorganic and organic compounds including amino acids, biopolymers and proteins[35]. The properties of ILs can be altered by the selection of distinctive anion cation combinations. The somewhat infinite groupings of these ions give rise to the definition of tuneable and designer solvents for ILs. ILs can ultimately be purposefully designed based around the role that is required of them[1,6].

Unintentional altering of the properties of ILs can be induced due to the presence of residual impurities or contaminants present within the IL system. In order for ILs to be effective and efficient as replacement solvents and chemical facilitators, it is imperative that care is taken in their preparation, synthesis and drying. The properties that are the most influenced by impurities are the bulk properties of ILs. Viscosity and density are two main examples of bulk properties that are directly affected by IL contamination [3,6].

1.2.1 Bulk Physical Properties

Viscosity (η)

Generally, ILs are much more viscous than conventional molecular solvents, and the viscosity values of most ILs are 2 - 3 orders of magnitude larger than molecular solvents. The anionic and cationic combination of an IL has a significant influence on the viscosity. Changing the length of alkyl substituents on the cationic counterpart is another way in which viscosity can be altered and tuned. The lengthening of alkyl substituents increases the viscosity due to the greater cohesive energy between cations, which is caused by the stronger van der Waals interactions in the hydrophobic domains of the liquid. Evidently, high viscosity can be problematic within IL chemistry, handling of severely viscous ILs can limit the usage of ILs. It is, therefore, necessary to prepare ILs with an ideal viscosity value based on the function required of them. A fundamental understanding of the relationship between viscosity and ionic structure is necessary to more rationally design ILs with the desired viscosity value[7,36].

Density (ρ)

The density of ILs is higher than common molecular organic liquids due to the strong attraction between cation and anion. The density values of ILs fall in the range of 1.1-2.5 g cm^{-3}. In general, the altering of the density of an IL is seen when changing the size of the ionic system. Trends in density can be rationalised in terms of the packing efficiency of the individual ions, which will determine the mass per volume. An example of this is the enlargement of alkyl substituents on the cation, as a result, a decrease in density is observed. The density is decreased due to the individual ions being unable to pack effectively due to the flexible alkyl chains[8].

1.3 Impurities in Ionic Liquids

The presence of additional components or impurities within an IL system will ultimately have an impact on properties associated with the IL (both physical and chemical) associated with the IL. The degree to which these additional components impact the IL will vary depending on the nature of both the added constituent and the IL. To understand the effect impurities have on ILs and their properties it is first necessary to develop an understanding of the assortment of impurities that can be retained in an IL medium. An insight into how these impurities find their way into the resulting 'pure' IL is necessary, as is an understanding of what research has already been done in investigating the impact on ILs and IL facilitated chemistry. The field of research into impurities in ILs has been active for a considerable amount of time and with significant success however, there are still details that pose a challenge to our understanding. There is scope to provide additional knowledge into how impurities effect and alter ILs and their properties. The area continues to grow and further adding to this further aids in a more efficient design, purification and storage of ILs; the ultimate goal here is in improving the sustainability profile of ILs.

1.3.1 Preparation of Ionic Liquids

The initial point of contamination for any IL lies in the synthesis of these 'designer' solvents. The design and preparation of an IL differ depending on the desired combination of anion and cation counterparts. Most common ILs follow a similar synthetic route of an initial alkylation step followed by further synthetic steps that assist in diversifying the anion. The combination of anion and cation is chosen in order to tune the IL properties causing them to become task specific solvents[1-3,6].

The ILs studied in this thesis are all imidazolium-based ILs with variation in the anionic counterpart. A select few of the ILs were generated from a simple methylation reaction whilst others were derived from a corresponding common precursor, the 1-alkyl-3-methylimidazolium halide, in general, the chloride. Figure 1.2 details a schematic for a selection of general preparation and work-up procedures for widely used imidazolium ILs[6].

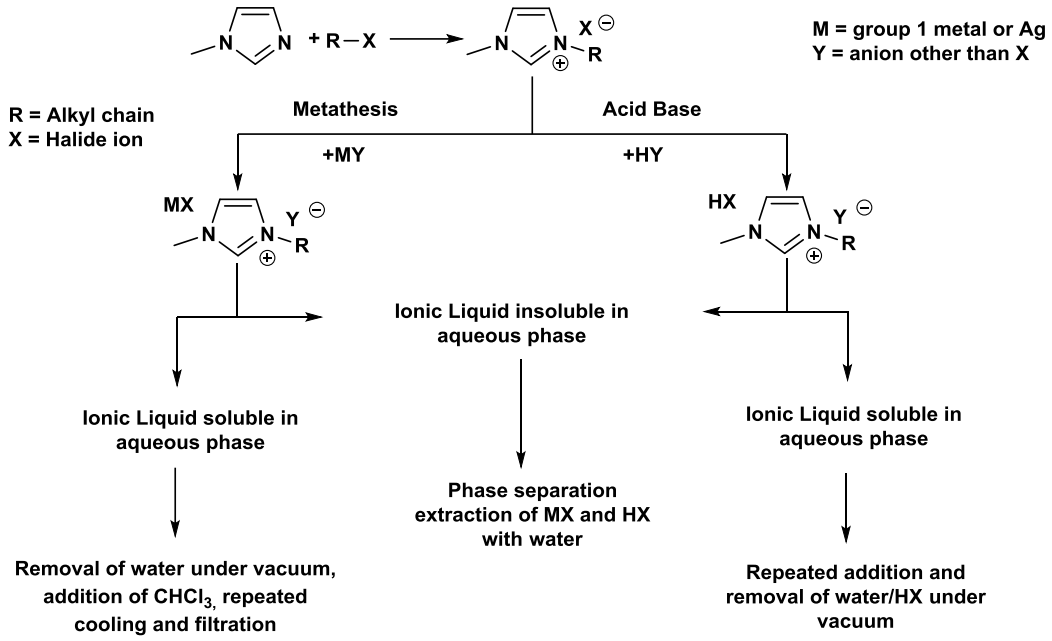


Figure 1.2. Preparation and work-up procedures for commonly used imidazolium-based ILs.

The first step in Figure 1.2 features an alkylation reaction that occurs between methylimidazole and an alkyl halide. Due to the stoichiometry of this initial reaction, it is possible that the generated IL may retain surplus halide ions that can pose as problematic further down the line. Variation of the anionic counterpart of the IL requires further synthetic steps, Figure 1.2 displays two examples of potential anionic exchange routes. The two routes presented are a metathesis step and an acid-base reaction. Both steps see the halide based IL reacted with either an alkali salt, acid or base in

order to force an anion exchange. In all cases, it is possible that the use of excess reactants will lead to trace contaminants being upheld within the final IL.

The use of several purification steps such as solvent washes and extractions aims to reduce the level of contaminants, most commonly the residual halide, as this is used in excess to ensure full alkylation of the imidazolium precursor. The initial purification steps are followed by a severely intense schlenk drying process. The process sees the IL dried under a reduced atmosphere ranging from 10^{-3} to 10^{-6} mbar with a temperature range of 50 - 60°C which aims to further eliminate any volatiles retained in the IL. The effective nature of ILs as solvents allow them to confine residuals to their ionic system. Regardless of the attempt of impurity elimination, an inefficient drying process, human error or simple exposure to the atmosphere will cause ILs to sustain low levels of contaminants.

As seen in Figure 1.2 there are a number of steps within the synthetic process of ILs that can be viewed as contaminant introducing steps. Low-level contamination can have a severe impact on the physiochemical properties and spectroscopic characteristics of ILs. Use of contaminated ILs for further chemistry can cause problems with the efficiency of the process. It is why it must be stressed that the purification, drying and storage steps must be approached meticulously and not underestimated.

As already highlighted, there are numerous contaminant introducing steps within the synthesis of ILs. This thesis will tackle a selection of the most prevalent impurities that can become entrapped in ILs. The most sizeable impurity that impacts the physiochemical properties of ILs is that of water. The hygroscopic nature of ILs instantaneously triggers the absorption of water from a variety of sources. Water sources range from trace amounts present in solvents used for IL synthesis to water present in the atmosphere. Other common impurities include halide ions, solvents and alkali salts. Halide ions and alkali salt impurities can be retained due to an overage

amount of reagents required to force IL synthesis to completion. Solvent impurities are predominately introduced at purification steps. This chapter will explore how these impurities impact the properties of ILs, the chemistry that ILs facilitate and the spectroscopic characteristics of ILs.

1.4 Water Impurities in Ionic liquids

A major impurity that is seemingly present in the vast majority of ILs is that of water. Water contamination can occur at multiple points during the synthesis of ILs, such as metathesis steps adopted for most ILs. Common metathesis reactions utilise water as the reaction solvent. If not dried sufficiently, water will be retained in the final IL and will ultimately pose a risk with further usage of the IL.

Most common ILs are hygroscopic and readily absorb water from a variant of sources such as bulk water, water present in reagents and even atmospheric water. Examples of hydrophilic ILs include halide, acetate and phosphate-based ILs. These anions produce ILs that are miscible in any proportion with water. In comparison ILs that contain anions such as $[PF_6]$, and $[Tf_2N]$ are viewed as hydrophobic. Even these commonly labelled ‘’hydrophobic’’ ILs, are somewhat hygroscopic and will readily absorb water, be that to a lesser extent of the hydrophilic ILs. The absorption of water, however, is non-negligible and has proven to bring about significant changes to the IL[6,9]. The intentional addition of water has also been seen in IL chemistry as a viscosity modifier, which is readily deployed as a useful tool to aid countless chemical processes[37-38]. Many ILs retain water as a result of being inefficiently dried, human error and atmospheric exposure. The resulting ‘wet’ IL differs significantly to its ‘dry’ counterpart, leading to small compositional changes that can have a large effect on intermolecular reactions. The preservation of water in an IL will also have an impact

on solvents properties such as polarity, viscosity and density[39-40]. Seddon and co-workers have emphasized that an efficient drying process is necessary if ILs are to be used as solvents for moisture sensitive substances[6].

The investigation into how residual water influences the nature of ILs has been approached from a multitude of angles within the literature. This section aims to explore a selection of these perspectives, emphasising how successful water is in altering the properties of ILs and how the presence of water can be detrimental to IL use within chemistry.

The introduction of water into an IL system, be that in the form of trace amounts from the atmosphere or purposeful hydration causes the IL system to transition from a pure IL to a binary mixture. A binary mixture is simply the 'mixing' of two liquids that are entirely miscible with one another. The combination of two components may cause significant changes to the original properties of the pure individual components. In the case of a binary solution of an IL and water, water significantly alters the properties of the IL. The alterations observed can be viewed as both advantageous and disadvantageous dependent on the desired use of the IL.

1.4.1 Impact of Water on the Viscosity of Ionic Liquids

A perfect example of how the formation of a binary mixture with water brings about changes to the properties of ILs can be seen when looking at viscosity values. It has already been discussed in this chapter that ILs are generally viscous liquids and their viscosity can be altered by the simple selection of different anion and cation combinations. It is well documented within in the literature that the combination of ILs with varying organic liquids, even other ILs, will modify ILs viscosity. Joseph J. Fillion and Joan F. Brennecke demonstrated this by investigating the viscosities of 23 IL - IL

mixtures at various temperatures and mole fractions. The IL - IL mixtures investigated contained ILs where both the cations and anions differed. The focus was put on phosphonium and imidazolium cations and $[Tf_2N]^-$ and aprotic heterocyclic anions [AHAs]. The results showed that IL - IL mixtures that showed higher than expected viscosities were mixtures of phosphonium [AHAs] ILs with imidazolium $[Tf_2N]$, whilst imidazolium [AHAs] ILs mixed with phosphonium $[Tf_2N]$ ILs showed lower than expected viscosities. The changing viscosities observed upon mixing can be related back to the combination of the counterions and ultimately IL - IL interactions.

When creating binary mixtures of two ILs, the combination of ions will play a role in tuning the viscosity of the system. In turn, the ions of the IL will play a lesser role when molecular organic liquids are used in conjunction to create the binary mixture. The organic liquid will aim to disrupt the coulombic interaction of the IL and form new interactions that will determine the viscosity. This is observed fittingly upon addition of water to an IL system, the mixing with water unquestionably brings about a dilution of the IL system. The viscosity of water at RT is approximately 0.89 mPa s.[41]. Combining this liquid with an IL, of which has a relatively high viscosity, will cause an overall change in the value for the viscosity of the IL. Fendt *et al*. showed that the presence of water within ILs resulted in an overall decrease in the viscosity and density of ILs[10]. Figure 1.3 displays the effect of an increasing water concentration on the viscosity of [EMIM] [Ac] at RT.

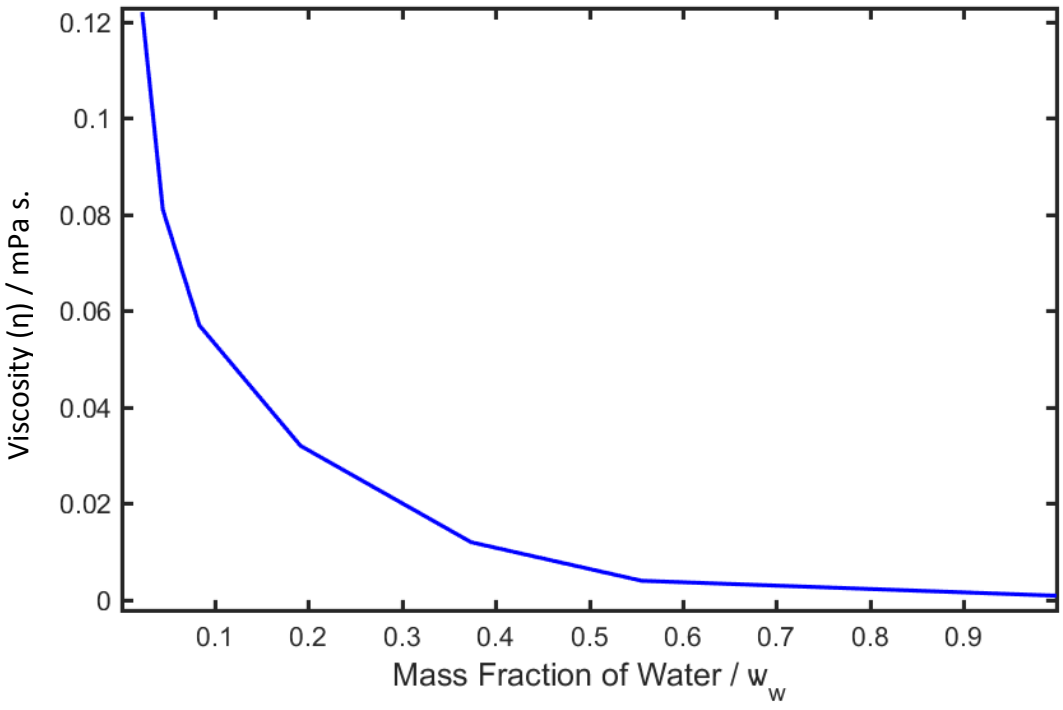


Figure 1.3. Reconstructed data showing the decline of viscosity, η, of [EMIM] [Ac] at 25 °C with increasing mass fraction of water.

Figure 1.3 details an overall decrease in viscosity. The ILs studied by Fendt *et al.* and many other groups within the literature display an overall decline in both viscosity and density[10,42-44]. This is expected as ILs have higher densities compared to water and the hydration of an IL will cause an overall dilution of the ionic system and hence a reduction in viscosity.

The reduction in viscosity upon mixing with water has been shown to be useful in many applications. Viscosity modification by dilution has been seen in electrochemistry and in the production of suitable lubricants. As discussed, ILs in their pure form are viscous liquids with a lower conductivity than expected and are often difficult to handle in many applications. The addition of water has shown to reduce the viscosity and in doing so increases their conductivity and enables easier handling of these solvents.

Huaping Xiao *et al.* detailed ILs being used as lubricants both in their neat form and mixed with water, with water being the additive[48]. The combination of water with ILs produces a remarkable reduction in friction and wear. The extent of water IL mixing is dependent on the role of the lubricant. The main point to stress here is that the mixing of these two liquids is carried out with the aim of enhancing the lubricant allowing it to perform more efficiently and effectively. This is an example of how water doping of an IL can be used in a positive manner, which is why research into water IL mixtures is necessary.

1.4.2 Impact of water on Ionic Liquid Facilitated Chemistry

It can be conclusively observed from research within the literature that the properties of dry and wet ILs drastically differ. Illustrating that the presence of water be that as an impurity will considerably impact most ILs. In most cases, water retention in ILs is undesirable as ILs are most commonly being purposefully designed in order to facilitate moisture sensitive chemistry. In other cases, the presence of water within the IL can aid in chemical facilitation and improve the overall reaction. Selected examples of the effects that water contamination or mixing has on chemistry facilitated by ILs are shown below.

One major example to illustrate water negatively influencing IL assisted chemistry is the role it plays when ILs are used for dissolution chemistry. ILs are readily used within dissolution chemistry and are purposely designed in order to dissolve a wide range of substances, with the major group being biopolymers. Over the past few years, ILs have become enormously popular for dissolving biopolymers such as keratin, cellulose and lignin. The IL is designed in order to disrupt the bonding network that is upheld within the biopolymer and ultimately lead to its dissolution followed by subsequent recovery of the desirable products. In comparison, the use of bulk water for dissolution of

biopolymers is unheard of due to the failure of water to cleave the tight structure of common biopolymers. Water present in an IL reduces the purity of the IL to a binary mixture. The result of having a binary mixture will have an impact on the dissolution efficiency of biopolymers. Retention of low concentrations of water can alter the solvation power of the IL and thus influence the amount of biopolymer that can be dissolved by the IL. Water also has the ability to interact with ILs via hydrogen bonding. By being present within the IL system, water will compete with any biopolymer to engage in hydrogen bonding. The reduction in hydrogen bonding between the IL and any biopolymer reduces the overall dissolution process. Minnick *et al.* explored the reduction in the dissolution in the 1-ethyl-3-methylimidazolium diethyl phosphate, [EMIM] [DEP], IL. Figure 1.5 displays their findings[11-12].

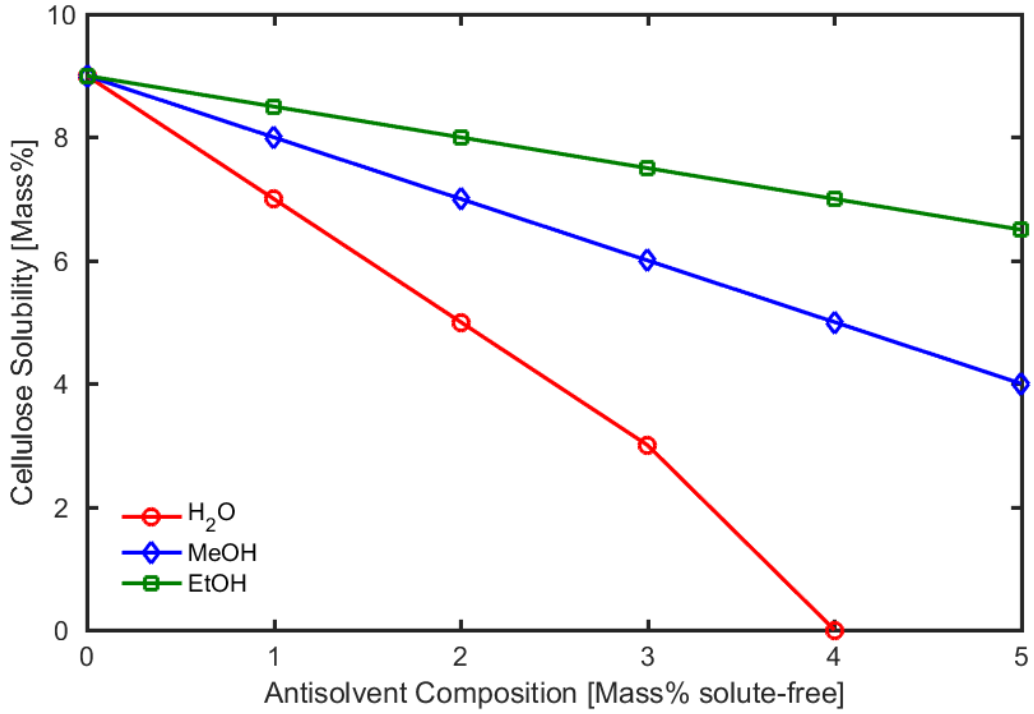


Figure 1.5. Reconstructed thermodynamic solubility limit of cellulose in [EMIM] [DEP] anti-solvent mixtures at 40°C. Lines are smoothed data[11].

Figure 1.5 shows that compared to the cellulose capacity of the pure IL which dissolves 9.1 mass % cellulose at 40°C, cellulose solubility in mixtures of [EMIM] [DEP] with just 1 mass % anti-solvent are 8.3 mass %, 7.6 mass %, and 6.6 mass % for ethanol, methanol, and water respectively. At 3 mass % anti-solvent loading, cellulose solubility in the same anti-solvent systems are 6.9 mass %, 5.5 mass % and 0.5 mass % respectively. It is evident that the presence of water or solvent in IL systems causes a reduction in the dissolution power and hence impacts the efficiency of the dissolution process[11].

Further examples of how wet ILs can be problematic to the overall chemical process can be seen when ILs are utilised to assist catalysis. A number of critical aspects have made ILs an interesting medium in which to catalyse chemical reactions. ILs low volatility is a major improvement to that of conventional molecular solvents and is what benefits their use in catalysis. The tuneable properties of ILs allow not only control over the processing of the reaction but also control over solvent - solute interactions. The latter is important, and the fact that these solvents are ionic and highly structured can give rise to distinct chemistry of their own compared with molecular solvent systems in both achiral and chiral processes. In any process, the steps following reaction are often at least as important for the overall environmental impact and economics. In this respect, ILs have been shown to have a significant advantage over conventional solvents for homogeneously catalysed reactions. In order for IL facilitated catalysis to proceed effectively and efficiently, it is imperative that the chemical host is free of all impurities and dried sufficiently. This is particularly important in catalysis where the impurity in the solvent can have a significant impact on the selectivity and activity of the catalyst. Residual water has been shown to directly coordinate to the metal centre of some catalysts, by doing so the rate of the desired reaction is reduced. Heightened

water levels in ILs may lead to aggregation around the catalyst and in severe cases cause the deactivation of the catalyst[2-3].

The two examples thus far have shown that trace amounts of water can have a strong influence in impacting the chemistry ILs facilitate. The hydration of ILs with water is not always viewed as negative. Purposeful doping of ILs with water is widely observed in the literature inducing positive results. To *et al.* demonstrated the positive effect water doping has on the performance of ILs used for extraction of carbohydrates and lipids from algae[49]. It was shown that the use of choline amino acid based IL aqueous solutions (65 % IL - 35 % water) instead of the neat ILs gave an extraction of up to 51 % of total lipids from algal biomass.

Additional examples into the intentional doping of ILs with water utilise water as an additive to alleviate viscosity concerns and boost the conductivity of ILs. As detailed in this chapter water is widely used to tune the physical properties of ILs for further use. An example of this is put forward by Basile *et al.* who showed that the plating and stripping performance of sodium metal in an IL electrolyte is improved when including water as an additive[50]. It is suggested that an ideal solid electrolyte interface may be formed through the use of water as an additive in $[Tf_2N]^-$ based highly concentrated IL electrolytes. Approximately 500 ppm of water is shown to perform well for both improving bulk physicochemical properties of the electrolyte, in addition to improving the sodium surface for cycling.

Overall the formation of IL - water binary system impact IL facilitated chemistry in both positive and negative ways. ILs are most often purposefully designed to serve a function. Cases in which water hinders the function of ILs can be seen when they are deployed for moisture sensitive chemistry. Minute traces of water within an IL system can damage their use for this branch of chemistry. Retention of water is undesired and therefore must be eliminated in order for moisture sensitive chemistry to proceed effectively and efficiently. In select cases, as mentioned above, purposeful hydration

of ILs can be advantageous. The addition of water aids in reducing viscosity which can be viewed as beneficial for a range of chemical systems. Overall the presence of water within an IL system will bring about changes be that as a hindrance to ILs or in order to manipulate ILs for positive gain. It is imperative that the water content in ILs is suitably quantified before deploying the IL for a specific role.

1.4.3 Spectroscopic Analysis of Ionic Liquid Water Systems

Due to the hygroscopic nature of most ILs and the impact water can have on the physicochemical properties, it is no surprise that there is an abundance of spectroscopic and computational data and studies on IL water systems. Studies into IL water systems have provided significant data in regards to bonding interactions between the two components alongside structural arrangements present in the system. It has been shown in a wide range of studies that intermolecular hydrogen bonding is the dominant interaction between the individual components of the binary system.

Spectroscopic investigations into the impact water has on ILs mainly focuses in on the most commonly used ILs, with [BMIM] [BF_4] being the archetypal IL used for these studies. The investigation into fluorinated imidazolium ILs have been conducted by several groups. Giammanco *et al*. report how water effects [BF_4] ILs with differing chain lengths on the imidazolium cation[14]. Yamada *et al*. investigated water IL mixtures with a wide variety of fluorinated anions, such as [BF_4], [PF_6] and [OTf][15-16]. Fazio *et al.* exclusively investigated [BMIM] [BF_4] with water present[17]. Wang *et al*. added temperature as a secondary variable and explored not only the effect that water has on [BMIM] [BF_4] but coupled this with the effect that temperature has on the binary mixtures[47]. All the groups utilized vibrational spectroscopy in their studies and concluded similar results. Significant evidence provided from ATR-FTIR spectroscopy, Raman spectroscopy and 2D correlation experiments showed significant perturbations

in the anionic region. Danten *et al*. put forward that the predicted structures show that the water molecule preferentially interacts with the fluorinated anions by forming associations of type (A…H–O–H…A)[18]. This predicted structure is further reinforced by Da-Yong *et al*. who studied the H-bonding interactions in [EMIM] OTf water system[51]. It was shown that water molecules could fill in the interstices and form (OTf…HOH…OTf) complexes[18,33,51]. Kazarian *et al*. systematically studied the molecular states of atmospheric water in RTILs by attenuated total reflection infrared (ATR-IR) spectroscopy, which indicated that most of the water molecules at low concentrations (up to 1.5 %, wt : wt) mainly interacted with the anions and exist in symmetric 1 : 2 type H bonded complexes (anion …HOH…anion)[19].

The literature substantially agrees that the dominant interaction between water and ILs occurs predominantly at the anion and is that of hydrogen bonding between bond acceptor and donor functionalities of the anion and water respectively. The structure of this interaction is conclusively put forward as an (A…H–O–H…A) association[16,18,33].

Further studies into IL water systems revealed that as well as the known interaction between water and the anion, which is viewed as the dominant interaction, there are further interactions observed. Many groups report a secondary interaction occurring at the C2 position on the imidazolium ring. Both Chen *et al*. and Noack *et al*. showed that upon co-solvent addition the strong interactions between the anion and the C2 position of the imidazolium cation are weakened, and at high dilution, they are replaced by cation - co-solvent interactions[20-21]. A prominent blueshift observed for the C2-H indicates a weakening interaction.

NMR studies further corroborate the observations from ATR-FTIR spectroscopy. Mele *et al*. presented direct experimental evidence of the interaction between ILs and water through NMR spectroscopy[52]. NMR results indicated the existence of tight ion pairs in the pure liquid, even with the presence of small amounts of water. Saihara *et al*.

showed that ^{1}H NMR studies can be used to investigate the varying states of water confined in the nano-domain structures of typical RTILs[34]. The results showed that the NMR peaks for water in $[BF_4]^-$ based ILs were clearly split, indicating the presence of two discrete states of confined water.

The literature has proved the use of spectroscopic techniques as a powerful tool in which to probe IL water systems. The probing of these systems provides a base level understanding of how residual water interacts with a selection of ILs. Further research into more diverse ILs may provide additional information and further confirm the findings already present in the literature.

1.4.4 Computational Analysis of Ionic Liquid Water Systems

Along with physicochemical investigations, computational studies using various approaches have and continue to provide a key insight into solvation, molecular aggregation and phase behaviour of IL water binary mixtures. Knowledge in the field of IL water mixtures has been greatly advanced by studies performed with the application of quantum chemical calculations, ab initio, atomistic molecular dynamics (MD) and coarse-grained molecular dynamic simulations (GCMD)[23].

Interactions between water and ILs have been investigated by Wang *et al*. using density functional theory (DFT), in which the strength of the interaction between water and the anionic counterpart was explored[22]. Further computational work involving empirical potential MD and MC simulations provided insight into the solubility of ions in water and the interactions responsible for structural behaviour. Shah and Maginn conducted MC simulations to study the solubility of water in the IL [BMIM] $[PF_6]$. It was speculated that the higher solubility observed in simulations was due to stronger interactions between the water and the IL. It was further suggested that the variation in force field parameters resulted in better agreement with experiments[30].

Computational studies into IL water systems have also been used in conjunction with spectroscopic studies in order to substantiate the findings already made. Khan *et al*. presented experimental water activity coefficient data[31]. It was found that the interaction study of water ILs is affected by increasing alkyl chain length on the imidazolium ring. COSMO-RS was found to be a reliable predictive method in estimating at least qualitatively, the excess enthalpies and Gibbs free energy of binary mixtures of water and ILs. COSMO-RS highlighted that hydrogen bonding as the dominant interaction in the studied binary systems.

1.4.5 Ionic Liquids and Bulk Water Mixtures

As for mixtures of ILs solvated by bulk water, the infrared spectra properties are relatively less studied in comparison to small concentrations of water, especially the water-rich region.

Singh *et al*. investigated various thermophysical properties of IL water mixtures with water content varying from 20 wt % to 95 wt % over a temperature range of 298 K to 343 K[32]. The use of MD simulations provided an insight into each of the binary mixtures. Singh *et al*. found that there is a greater temperature induced disintegration of IL ion water interactions in dense systems, compared to dilute ones. Inferring that the faster loosening of the IL water interaction of the dense solution is the cause of its experimentally observed sharper decrease in density and viscosity, and an increase in compressibility[32]. The dilute solutions exhibited structural features very similar to that of pure water. Three distinct structural regimes were assigned to ILs in the presence of water: (i) expanded IL structure with interspersed water (ii) bicontinuous IL - water system and (iii) collapsed IL structure as floating icebergs in continuous water.

The study carried out by Singh *et al*. suggests that as the water concentration of the binary mixture is increased the IL and water transition through a variance of environments and thus the interaction between the two should also be changing[32]. Although there are two changing variables here (water concentration and temperature), separating the two out and carrying out independent studies may perhaps reveal further information and aid in pinpointing the distinct structural regimes proposed by Singh *et al*[32].

A more in-depth investigation into bulk water IL systems alongside further analysis into the smaller concentrations are required to pinpoint the point at which an IL stops being classified as an IL and resembles more of a solution of ions.

1.5 Further impurities in Ionic liquids

It is clear from the literature that water impurities heavily impact ILs and that this area of research is a hot topic and under continual investigation. It is imperative to note that other impurities can also be introduced into the IL system and can severely alter the physiochemical properties along with the spectroscopic characteristics of ILs. Residual solvents, halide ions and alkali salts are further examples of potential impurities that can be problematic to IL systems. Retention of solvents can occur at various points in the purification process. The retention of halide ions and alkali salts are due to an initial alkylation reaction followed by subsequent anion diversification steps that utilise excess quantities of starting material. The presence of any of these reagents in the final IL can pose as problematic in the long run. Examples of this have been identified within the literature and are explored below.

1.5.1 Solvent impurities in Ionic liquids

Multiple organic solvents are used to facilitate IL synthesis and in their subsequent purification. The use of multiple solvents can lead to trace concentrations ending up in the final 'pure' IL. In general, ILs are miscible with liquids of medium to high dielectric constant and immiscible with liquids with low dielectric constants. An example of this is [BMIM] [BF_4] which is completely miscible with methanol (ε = 32.66) whereas toluene (ε = 2.38) is only miscible to up to 50 mol %. Contamination is possible with both miscible and immiscible solvents[6]. Trace amounts of co-solvents in an IL system will have an overall effect on the physical properties of the IL

The addition or retention of co-solvents in ILs can cause displacement of the original physical properties of the IL and create new properties based around the co-solvent. Very much like water, molecular solvents cause a decrease in the viscosity of the original IL. Decrease of the viscosity of ILs by the addition of co-solvents however, will follow a different pattern depending on the nature of the co-solvent. This is possibly due to differences in polarities which lead to different interactions with the ions of the ILs. Le *et al.* explored the physical properties of a selection of ILs and found that the addition of co-solvents impacted the melting and glass transition temperatures as well as showing a decrease in the viscosity and noticeable increases in conductivity values[25].

As discussed section 1.4, the presence of water in ILs causes a reduction in the solvation power of the IL when looking at dissolution chemistry. This observation is clearly displayed in Figure 1.5. Also noted in Figure 1.5 are ethanol and methanol binary. It can be seen that both solvents cause a decrease in solvation power. The results shown are not to the same extent as water, but still significant enough to show that molecular solvents conserved in ILs can negatively impact the dissolution process[11-12].

1.5.2 Halides as impurities in Ionic liquids

Surplus halide ions are readily introduced into ILs due to the stoichiometry of either the alkylation or metathesis reaction steps. Excess halide reagents are utilised in order to force the synthesis of ILs to completion. Multiple purification steps aim to reduce or eliminate the number of halide ions in the final IL however, halide retention is observed for many ILs. Residual halide ions in the ionic system have shown to affect the physical properties of ILs and directly hinder IL facilitated catalysis.

Seddon *et al*. showed the extent to which surplus chloride ions impact the physical properties of ILs[6]. Known quantities of [CnMMIM] Cl were deliberately added to each IL in order to assess the magnitude of the viscosity increase caused by an excess of chloride ions. Table 1.1. Illustrates the results obtained.

IL	$[Cl^-]$ / mol kg^{-1}	η / mPa s.
[EMIM] $[BF_4]$	0.01	67
	1.80	92
[BMIM] $[BF_4]$	0.01	154
	0.50	201
[BMIM] $[NO_3]$	0.02	67
	1.70	220
[OMIM] $[NO_3]$	0.01	1240
	2.20	8470

Table 1.1. Comparison of the viscosity of chloride contaminated and low chloride content batches of ILs at 20 °C[6].

It is evident that an increased chloride concentration for each IL studied caused an increase in the viscosity of the IL. Density measurements were also recorded by Seddon *et al*, with the results showing an overall decrease in the physical parameter[6].

Similar to other impurities that can be found in ILs, additional halide ions can impact the reactions ILs are used for. The main example of this is observed when ILs are used for catalysis. Similar to water, halides are known to coordinate to the transition-metal centres of catalysts, and thus influence (usually negatively) the rate of reaction. Halide ions will, however, bind much more readily and engage in a stronger interaction with the metal centre due to an increased electronegativity. Chloride impurities have been reported to have a detrimental effect on transition-metal catalysed reactions, such as hydrogenations. Boxwell *et al.* reported the use of [BMIM] [BF_4] for the hydrogenation of olefins using Wilkinson's and related catalysts, seen in Figure 1.6[26].

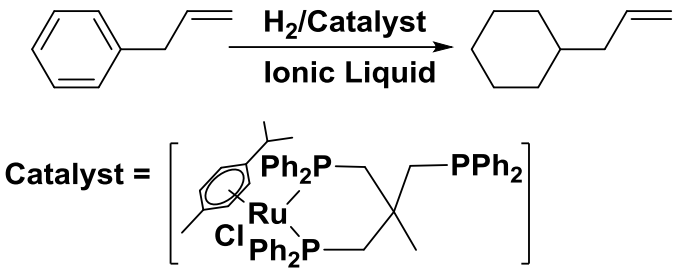


Figure 1.6. Example of a catalytic dehydrogenation reaction that utilises an IL to facilitate the reaction. The ruthenium catalyst is shown and is the point of interaction for any impurities present in the IL[26].

Whilst these catalysts are moderately effective they are deactivated by trace quantities of chloride ions persisting in the IL from its preparation. The chloride binds to the ruthenium metal centre and may displace one or more of the triphenylphosphine ligands due to their lability. Ligand exchange disables the catalyst and negatively impacts the overall reaction.

1.5.3 Alkali Salt impurities in Ionic liquids

As discussed throughout this chapter, the contamination of ILs with alkali salts occurs when the IL undergoes a metathesis reaction. The preservation of alkali salts in the IL, like other impurities discussed in this chapter, bring about a change the physiochemical properties of the IL. Within the literature, there are many studies that explore the effect of excess alkali salt on the conductivity of ILs for their use in electrochemistry. Computational studies on these mixtures further allude to the arrangement of the excess salts within the IL medium.

Pereiro *et al.* explored the solubility of inorganic salts in pure ILs and determined that the behaviour is largely dependent on the anion and cations of both the IL and the inorganic salt present in the mixture[27]. In general, binary mixtures containing the bis (trifluoromethylsulfonyl) imide anion or the ammonium thiocyanate inorganic salt exhibited the largest solubility. On the other hand, inorganic salts with a divalent atom (Na_2 [SO_4] and $CaCl_2$) exhibited lower solubility in the IL.

Mendez-Morales concluded, that the solvation of excess $[Li]^+$ cations in select ILs takes place by means of an inhomogeneous nanostructural mechanism. $[Li]^+$ cations are proposed as being embedded in the polar domains of amphiphilically nanostructured poly ionic liquids (PIL). This causes solid like $[Li]^+$ - [NO_3] - $[Li]^+$ structures to progressively evolve until saturation; where they act as crystallization nuclei. This could possibly be a universal type of ion solvation in ILs, but more work is needed to prove this hypothesis[28].

It is clear from the literature that research into impurities is an ongoing area of research that is ever growing. The significant effect impurities have on ILs and the chemistry that they facilitate is of importance in order to improve the purification and synthetic approaches to ILs. Purity measurements should always accompany reported physical

data to aid in explaining any anomalies within results. By highlighting how problematic trace contaminants can be within these designer solvents allow for precautions to be taken.

1.6 Aims and Objectives

This chapter has established how impurities within ILs can have a pronounced effect on their physical and chemical properties as well as the spectral characteristics of ILs. As outlined, understanding how the various interactions and structural organisations of impurities present in an IL influences chemical and physical processes is essential. In order to improve the overall efficiency and in turn sustainability of the reaction a greater understanding is needed.

Although there is significant research into how impurities affect the physiochemical properties and the spectroscopic characteristic of ILs, further understanding of impure IL systems is still needed. To efficiently investigate the relationship between impurities and ILs a systematic approach was taken towards the synthesis of the ILs used, the levels of impurities within the IL system and the analytical techniques used. Details of this are found in Chapter 2.

Spectroscopic studies into the effect of impurities in the literature are dominated by water studies. Further spectroscopic studies are required to further confirm the pre-existing results and provide additional information with regards to water and IL systems. Chapter 3 explores the effects that atmospheric water along with a wider concentration range of water has on a series of ILs that would be most commonly used in dissolution chemistry. The main spectroscopic technique utilised to explore the binary mixtures of IL and water was vibrational spectroscopy. A combination of

ATR-FTIR spectroscopy, Raman spectroscopy and multivariate analysis were used to probe the binary mixtures. The aim of this chapter is to confirm pre-existing findings whilst providing additional information about IL systems with ranging concentrations of water. The use of the selected analytical techniques, wide water concentration gradient and the diverse ILs studied will enhance literature conclusions.

Spectroscopic studies into other impurities that are present in ILs are scarce and the area is in its infancy with room for spectroscopic data to be added and improved. Chapter 4 and 5 explore the effect of residual solvents and alkali salts have on ILs. As with Chapter 3, the main spectroscopic technique used to probe these systems was vibrational spectroscopy. A series of ATR-FTIR experiments were conducted in order to explore these impurities. The intention of both chapters is to explore the less researched impurities spectroscopically and probe the systems for any significant changes brought about due to this contamination.

1.7 References

1. P. Wasserscheid and T. Welton, T. (eds). Ionic Liquids in Synthesis (Wiley-VCH, 2007).
2. T. Welton, *Chem. Rev.* **1999**, *8***,** 2071 - 2084.
3. J. P. Hallett and T. Welton, *Chem. Rev*. **2011**, *5*, 3508 - 357.
4. S. Zhu, R. Chen, Y. Wu, Q. Chen, X. Zhang and Z. Yu, *Chem. Biochem. Eng*. **2009**, *23*, 207 - 211.
5. M. J. Earle and K. R. Seddon, *Pure Appl. Chem*. **2000**, *72*, 1391 - 1398
6. K. R. Seddon, A. Stark and M.-J. Torres, *Pure Appl. Chem*. **2000**, *72*, 2275 - 2287.
7. G. Yu, D. Zhao, L. Wen, S. Yang and X. Chen, *AIChE J*. **2011**, *58*, 2885 - 2899.
8. J. Jacquemin, P. Husson, A. A. H. Padua and V. Majer , *Green Chem.* **2006**, *8*, 172 - 180.
9. J. G. Huddleston, A. E. Visser, W. M. Reichert, H. D. Willauer, G. A. Broker and R. D. Rogers, *Green Chem*. **2001**, *3*, 156 - 164.
10. S. Fendt, S. Padmanabhan, H. W. Blanch and J. M. Prausnitz, *J. Chem. Eng. Data.* **2011**, *56*, 31 - 34.
11. D. L. Minnick, R. A. Flores, M. R. Destefano and A. M. Scurto, *J. Phys. Chem. B*. **2016**, *32*, 7906 - 7919.
12. R. P. Swatloski, S. K. Spear, J. D. Holbrey and R. D. Rogers, *J. Am. Chem. Soc.* **2002**, *18*, 4974 - 4975.
13. A. Jarosik, S. R. Krajewski, A. Lewandowski and P. Radzimski, *J. Mol. Liq.* **2006**, *123*, 43 - 50.
14. C. H. Giammanco, P. L. Kramer, D. B. Wong and M. D. Fayer, *J. Phys. Chem. B*. **2016**, *120*, 11523 - 11538.
15. T. Yamada, Y. Tominari, S. Tanaka and M. Mizuno, *J. Phys. Chem. B*. **2017**, *121*, 3121 - 3129.
16. T. Yamada, Y. Tominari, S. Tanaka and M. Mizuno, *J. Phys. Chem. B*. **2015**, *119*, 15696 - 15705.
17. B. Fazio, A. Triolo and G. Di Marco, *J. Raman Spectrosc.* **2008**, *39*, 233 - 237.

18. Y. Danten, M. I. Cabaço and M. Besnard, *J. Mol. Liq.* **2010**, *153*, 57 - 66.
19. L. Cammarata, S. G. Kazarian, P. A. Salter and T. Welton, *Phys. Chem. Chem. Phys*. **2001**, *3*, 5192 - 5200.
20. *Y*. *Chen*, *Y*. *Cao*, *Y*. *Zhang*, and *T*. *Mu*, *J. Mol. Struct.* **2014**, *1058*, 244 - 251.
21. K. Noack, A. Leipertz and J. Kiefer, *J. Mol. Struct.* **2012**, *1018*, 45 - 54
22. H. Wang, M. Liu, Y. Zhao, X. Xuan, Y. Zhao and J. Wang, *Green Chem*. **2017**, *60*, 970 - 978.
23. B. L. Bhargava, Y. Yasaka and M. L. Klein, *Chem. Commun.* **2011**, *47*, 6228 - 6241
24. Y. Gao, L. Zhang, Y. Wang and H. Li, *J. Phys. Chem. B*. **2010**, *114*, 2828 - 2833.
25. M. L. P. Le, L. Cointeaux, P. Strobel, J.-C. Leprêˆ, P. Judeinstein and F. Alloin, *J. Phys. Chem. C*. **2012**, *116*, 7712 - 7718.
26. C. J. Boxwell, P. J. Dyson, D. J. Ellis and T. Welton, *Chem. Commun.* **2002**, *0*, 3010 - 3011.
27. A. B. Pereiro, J. M. M. Araújo, F. S. Oliveira, J. M. S. S. Esperança, J. N. Canongia Lopes, I. M. Marrucho and L. P. N. Rebelo, *J. Chem. Thermodyn*. **2012**, *55*, 29 - 36.
28. T. Méndez-Morales, J. Carrete, Ó. Cabeza, O. Russina, A. Triolo, L. J. Gallego and L. M. Varela, *Phys. Chem. Chem. Phys.* **2015**, *17*, 5298 - 5307.
29. J. A. Widegren, E. M. Saurer, K. N. Marsh and J. W. Magee, *J. Chem. Thermodyn*. **2005**, 37, 569 - 575
30. P. Yee, J. K. Shah and E. J. Maginn, *J. Phys. Chem. B*. **2013**, *117*, 12556 - 12566.
31. M. S. Khan, C. S. Liew, K. A. Kurnia, B. Cornelius and B. Lal, *J. Phys. Conf. Ser.* **2016**, *148*, 862 - 869.
32. D. K. Singh, S. Cha, D. Nam, H. Cheong, S.-W. Joo and D. Im, *ChemPhysChem*, **2016**, *17*, 3040 - 3046.
33. Q. G. Zhang, N. N. Wang and Z. W Yu, *J. Phys. Chem. B*. **2010**, *14*, 4747 - 4754
34. K. Saihara, Y. Yoshimura, S. Ohta, and A. Shimizu. *Sci. Rep.* **2015,** *0*, 1 - 10.
35. E. S. Sashina and N. P. Novoselov, *Russ J Gen Chem*. **2009**, *79*, 1057 - 1062.
36. J. J. Fillion and J. F. Brennecke, *J. Chem. Eng. Data*. **2017**, *62*, 1884 - 1901.
37. C. Kliemann, M. Kleiber and K. Müller, *Chem. Eng. Tech.* **2018**, *41*, 819 - 826.

38. C. Zhao, A. M. Bond, R. G. Compton, A. M. O'Mahony and E. I. Rogers, *Anal. Chem.* **2010**, *9*, 3856 - 3861
39. J. D. Holbrey and K. R. Seddon, *J. Chem. Soc. Dalton Trans*. **1999**, *0*, 2133 - 2139.
40. H. V. Spohr and G. N. Patey, *J. Chem. Phys*. **2010**, *132*, 234510.
41. J. R. Coe Jr. *and* T. B. Godfrey, *J. Appl. Phys.* **1944,** *15*, 625.
42. J. Wang, Y. Tian, Y. Zhao and K. Zhuo, *Green Chem*. **2003**, *5*, 618 - 622.
43. E. Rilo, J. Vila, J. Pico, S. García-Garabal, L. Segade, L. M. Varela and O. Cabeza, *J. Chem. Eng. Data*. **2010**, *55*, 639 - 644.
44. C. A. Hall, K. A. Le, C. Rudaz, A. Radhi, C. S. Lovell, R. A. Damion, T. Budtova and M. E. Ries, *J. Phys. Chem. B*. **2012**, *42*, 12810 - 12818.
45. A. Stark, P. Behrend, O. Braun, A. Müller, J. Ranke, B. Ondruschka and B. Jastorff, *Green Chem*, **2008**, *10*, 1152 - 1161.
46. K. Wippermann, J. Giffin and C. Korte, *J. Electrochem. Soc.* **2018**, *165*, 263 - 270.
47. Y. Wang, G.A. Voth. *J. Am. Chem. Soc.* **2005**, *127***,** 12192 - 12193.
48. H. Xiao, T*ribology Transactions.* **2016***,* 1, 20 - 30.
49. T. To, K. Procter, B. A. Simmons, S. Subashchandrabose and R. Atkin, *Faraday Discuss.* **2018**, 206, 93 - 112
50. A. Basile , S. A. Ferdousi, F. Makhlooghiazad, R. Yunis, M. Hilder, M. Forsyth, P. C. Howlett, *J. Power Sources*. **2018**, 379, 344 - 349
51. S. Da-Yong, C. Jing, *Physico-Chimica Sinica*, **2014**, 30, 605 - 1610
52. A. Mele, C. Tran, S. Lacerda, *Angew. Chem.* **2003**, 115, 4500 - 4502.

Chapter 2

Experimental and Methodology

This chapter details the main vibrational spectroscopic analytical techniques, sample preparation and synthesis of the ILs used within this thesis.

2.1 Vibrational Spectroscopy

Absorption in the infrared region results in changes in the vibrational and rotational status of a molecule. The absorption frequency depends on the vibrational frequency of a molecule, whereas the absorption intensity depends on how effectively the infrared photon energy can be transferred to the molecule. This depends on the change in the dipole moment that occurs as a result of molecular vibration. As a consequence, a molecule will absorb infrared light only if the absorption causes a change in the dipole moment. Thus, all compounds except for elemental diatomic gases such as N_2, H_2 and O_2, have an infrared spectra. The collective vibration of bonds display a highly characteristic absorption pattern that is uniquely attributed to the molecule under investigation (in the case of this thesis, ILs). This is prominently shown in the fingerprint region (*ca.* 1200 - 400 cm^{-1}). As a result, IR spectroscopy is widely used in the determination of the chemical content and molecular structure of an analyte[1,2].

For quantification of several components absorbing in the mid-infrared region (2.5 - 25 μm or 4000 - 400 cm^{-1}), either conventional dispersive infrared analysis or Fourier Transform Infrared (FTIR) spectroscopy can be used. For the purpose of this thesis, ATR-FTIR was deployed as the appropriate vibrational spectroscopic technique. This introduction aims to provide an insight into the areas of IR

spectroscopy that are central to this thesis, it in no way aims to deliver an extensive overview of vibrational spectroscopy.

2.1.1 ATR-FTIR

ATR-FTIR spectroscopy is a two-component technique, comprised of attenuated total internal reflection (ATR) and Fourier transform infrared spectroscopy (FTIR).

In an FTIR instrument, the monochromator and the slits are replaced by an interferometer, usually of Michelson type. In the interferometer, a beam of IR radiation is divided into two beams by means of a beamsplitter. A path difference between the beams is introduced whereupon they are allowed to recombine. In this way, interference between the beams is obtained and the intensity of the output beam from the interferometer can be monitored as a function of path difference using an appropriate detector[1,2,23]. A schematic of an interferometer is shown in Fig. 2.1.

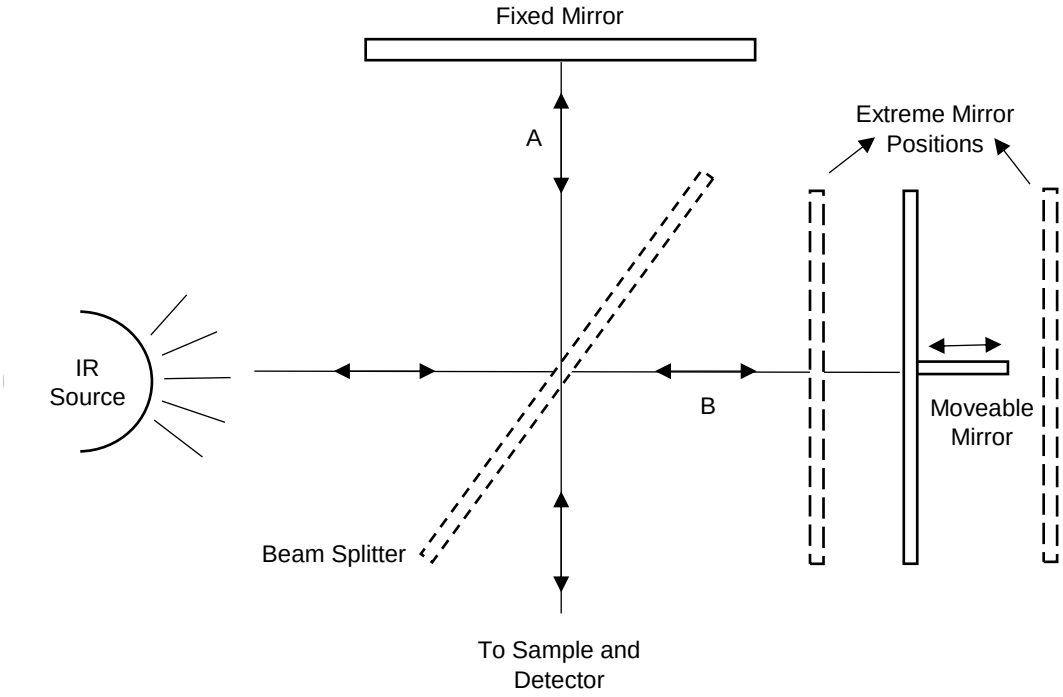


Figure 2.1. Schematic diagram of the optical layout of a Michelson interferometer[23].

Infrared radiation is projected onto the beamsplitter. An ideal beamsplitter consists of a non-absorbing film which transmits 50% of the radiation to the mirror, which is moving back and forth at a constant speed, whereas 50% of the radiation is reflected to the fixed mirror. After being reflected, the two beams will recombine at the beamsplitter where interference between the beams takes place.

An ATR accessory operates by measuring the changes that occur in a totally internally reflected infrared beam when the beam comes into contact with a sample (indicated in Fig. 2.2).

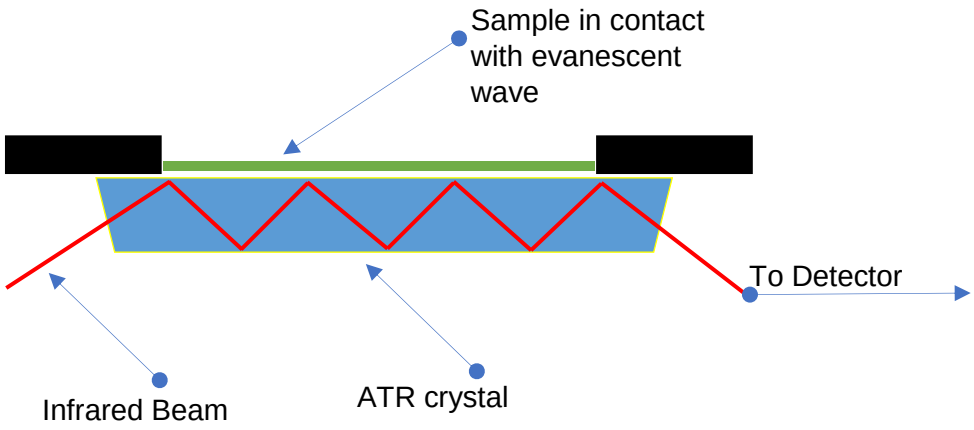


Figure 2.2. Schematic representation of an ATR-FTIR system[2].

Traditional IR spectrometers have been used to analyse solids, liquids and gases by means of transmitting the infrared beam directly through the sample, ATR uses the reflectance of the sample instead. An ATR measures the change that occurs in a totally internally reflected infrared beam when the beam comes in contact with the sample. The infrared beam hits an optically dense crystal (usually diamond, as used in this thesis) which then creates an evanescent wave that subsequently protrudes the sample (0.5 - 5 µm). The evanescent wave is altered in the regions where the sample absorbs energy, this is then detected and translated into the IR spectra[1,2,23].

It is important that the sample has good contact with the ATR crystal to ensure that the evanescent wave can easily penetrate. This can be accomplished by applying moderate pressure to the sample during the measurement. This is most effective when dealing with solid samples, liquid samples can be easily spread onto the crystal with sufficient contact being made. Full and intimate contact of the sample onto the ATR crystal is essential to achieve high-quality results[2].

The refractive index of the crystal has to be significantly greater than the one of the sample.

Whilst ATR is widely used to analyse a variance of samples, there are several factors that can affect the quality of the final spectrum such as, the refractive indices of the ATR crystal and the sample ($n_{crystal} > n_{sample}$), angle of incident IR beam, depth of penetration, wavelength of the IR beam, number of reflections, quality of the sample contact with ATR crystal, etc. The critical angle is given by:

$$\theta c = \sin^{-1}\left\{\frac{n_{sample}}{n_{crystal}}\right\}$$

If the refractive index of the sample is higher than the refractive index of the crystal, derivative shaped absorbance bands are observed, since the critical angle requirement was not met. The resulting spectrum is a mix of the ATR and external reflectance. The penetration depth is directly proportional to the wavelength of the incident beam, which means that photons with higher wavenumbers penetrate the sample less than photons with lower wavenumbers. Consequently, peaks on the left-hand side of the spectra often appear a smaller than expected i.e. OH peaks etc. It is important to correct this effect by applying the ATR correction to the raw spectrum[2,23].

For all of the ATR-FTIR spectra displayed in this thesis, the following general experimental parameters were used. A drop of each IL was smeared onto the diamond

of the ATR-FTIR, repeat measurements were taken for each IL in order to detect and monitor changes to each system. Each experiment was repeated to ensure consistency of results and the parameters used are detailed in Table 2.1.

ATR-FTIR Spectroscopy Parameters	
Resolution	4 cm^{-1}
Scan time	24 s
Number of spectra collected	100

Table 2.1. ATR-FTIR spectroscopy parameters utilised for the collection of all spectra within this thesis.

FTIR spectra over the range from 4000 - 500 cm^{-1} were collected at room temperature (RT), (~25°C) using an ALPHA II's platinum ATR single reflection diamond ATR. Spectra were recorded with a resolution of 4 cm^{-1}. The spectra were recorded for approximately 1.6 hrs, with 100 spectra being recorded for each IL.

2.1.2 Raman Spectroscopy

Raman spectroscopy was used to further augment the findings and conclusions drawn from the use of ATR-FTIR spectroscopy. The Raman spectra were collected on a prototype Raman spectrometer built by an instrument manufacturer (confidential) and collected by Calum Welsh. The prototype Raman spectrometer utilised two lasers, a 680 and 785 nm to collect both the higher and lower wavenumber (2000 - 4000 and

0 - 2000 cm^{-1}) regions of the spectrum separately. The use of two different lasers, with special optics, effectively allowed the instrument to function as two separate spectrometers. As a result, each spectrum displayed within this thesis has been stitched together. For the pure IL samples, significant fluorescence was observed and the integration times required adjusting. The spectral dataset was post-processed by Calum Welsh to give meaningful chemical information.

2.1.3 Multivariate Analysis

The interpretation of IR spectra in complex systems, such as the binary and tertiary mixtures analysed within this thesis can often further be aided by multivariate analysis[4,5]. The fundamental concept of multivariate analysis is the observation and analysis of multiple statistical variables simultaneously. The use of multivariate analysis allows for the analysis of changes in the intensity of multiple wavelengths simultaneously, compared to the univariate analysis of peak height or position that can be deduced from observations made from the intensity of a single peak in ATR-FTIR spectroscopy[5-7].

2.1.4 Multivariate Curve Resolution

Multivariate Curve Resolution (MCR) attempts to decompose a matrix into non-negative factors i.e. pure analytical spectra. MCR is part of a collective of techniques referred to as self-modelling curve resolution, of which are based on a ‘un-mixing’ method in an attempt to decompose data. The result of this is that concentrations and pure component spectra can be extracted and further meaning can be drawn out from these results[5-8].

To demonstrate the applicability and interpretation of MCR to systems monitored with vibrational spectroscopy it is best to view MCR in action with an example. Simulated spectra with overlapping bands have been generated and subsequently analysed *via* MCR. This pseudo-chemical system has been purposefully simulated to illustrate a two-component system in which both components are changing as a result of one another. Over the course of the experiment component 1 decreases in intensity whilst component 2 increases in intensity. This pseudo chemical system is monitored by ATR-FTIR spectroscopy. Figure 2.2 shows a simulated spectra and displays two overlapping bands. Component 1 has a peak maxima at 100 and component 2 has a peak maxima at 175. Going from blue to red component 1 is consumed, with its concentration falling from 100 % to 0 % and component 2 is produced, with its concentration increasing from 0 % to 100 % at a linear rate.

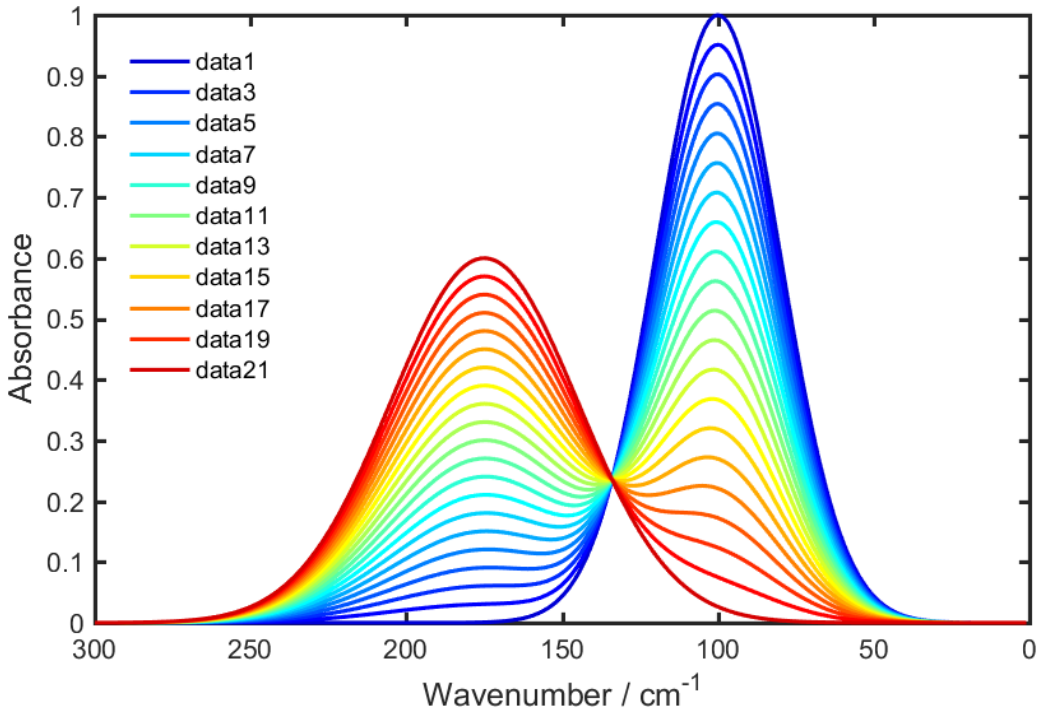


Figure 2.3. Simulated spectra (with overlapping bands) of a pseudo-chemical system comprising of two components; 1 and 2.

As discussed, the spectra displayed in Figure 2.2 is comprised of overlapping bands and although interpretation using classical univariate methods is possible, a multivariate approach can yield band separation and interpretation. MCR attempts to separate the data out and extract pure component spectra along with scores that are closely related to concentrations profiles of the individual components. The results for the MCR analysis calculated on the data represented in Figure 2.2 can be seen in Figure 2.3. The top spectra show the spectral variance of the system and the bottom spectra show the scores or concentration profiles of each component.

The top spectra in Figure 2.3 show the two components from the MCR decomposition of the pseudo dataset. The MCR components closely resemble real chemical spectra. These components exactly replicate the chemical species 1 and 2 as described in Figure 2.2. What is apparent is that the dataset has been simplified with a point of overlap being more distinguishable. The bottom spectra of Figure 2.3 display the scores, or concentration profiles of each of the components. As the system is a two-component system it is quite simple to establish the dynamic between the two components. The bottom spectra show that at the start of the experiment, component 1 (blue line) accounts for 100 % of the mixture and there is no evidence of component 2 (red line). As the pseudo-chemical system progresses, the concentration of component 1 (blue line) decreases at a linear rate, and the concentration of component 2 (red line) increases at a linear rate. At the end of the experiment, the system is comprised solely of component two. MCR has thus allowed the system to firstly be simplified and secondly for conclusions to be drawn from this simplified data. Conclusions garnered from the use of MCR can augment that of the conclusions established from univariate approaches to the data.

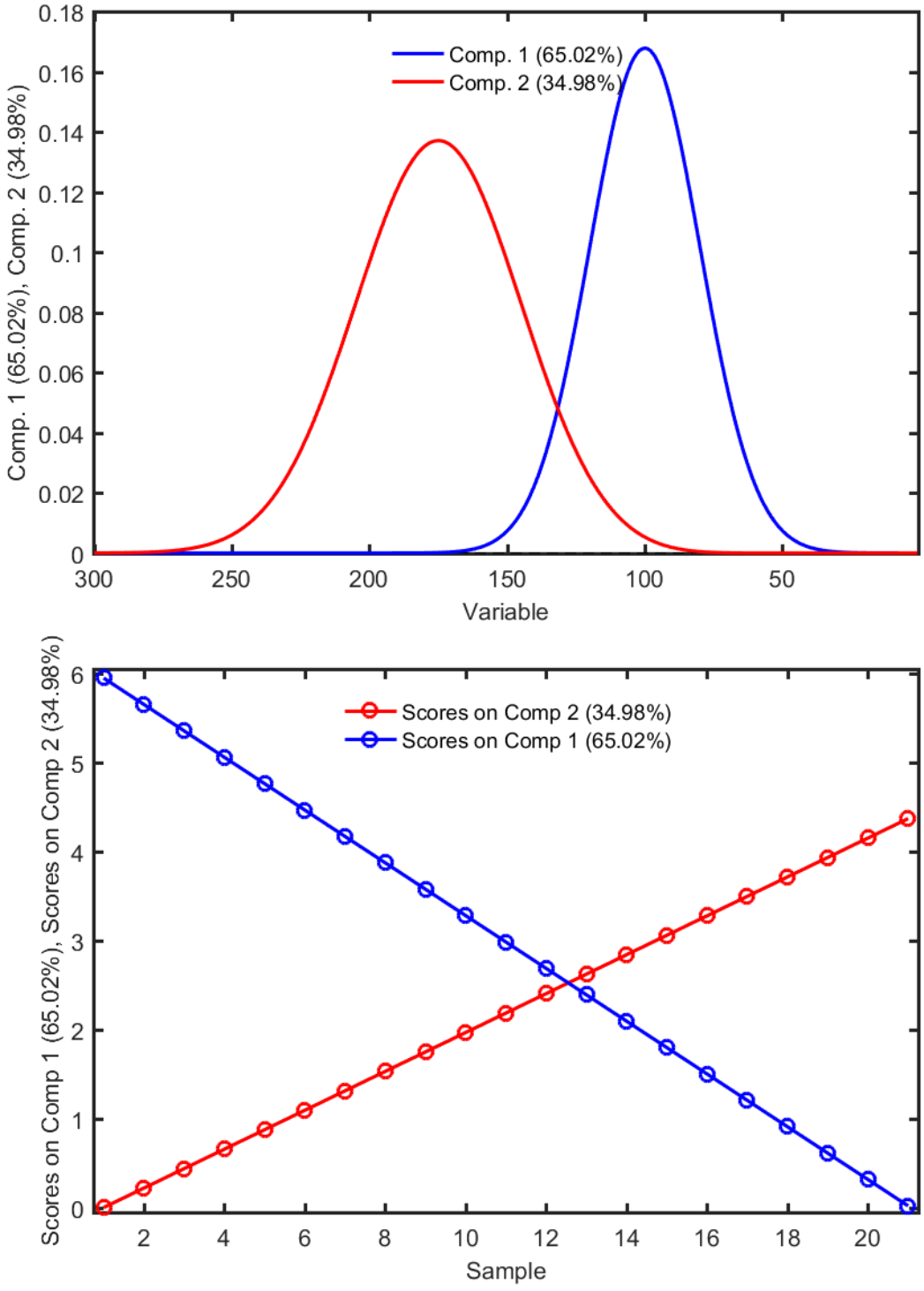


Figure 2.4. MCR of the pseudo data. (Top) MCR components showing the pure spectra (Bottom) MCR scores, or concentration profiles showing the change in the concentration of each component over the course of the experiment.

2.1.5 Analysis of Datasets

MATrix LABoratory (MATLAB), is a product of Mathworks Inc. It is a computational environment especially suited for problems in matrix algebra. All analyses within this thesis were performed with MATLAB, making use of its abilities to perform complex matrix computations in a command language with a similar notation to matrix algebra. Although some toolboxes and scripts (obtained through MATLABs File Exchange) were used during the analysis[9]. This thesis also makes extensive use of the PLS Toolbox, produced by Eigenvector[10]. PLS Toolbox is a collection of essential and advanced chemometric routines built within MATLABs computational environment.

2.2 Karl Fischer Titration

Karl Fischer Titration is a classic titration method deployed to measure the water content in most types of substances. For the purpose of this thesis, all substances measured were liquid at RT. Karl Fischer Titration is based on an iodine - iodide reaction. Water readily reacts with iodine generating iodide anions. The endpoint of the titration is reached when all the water present is consumed. A generalised titration reaction can be seen below.

$$SO_2 + CH_3OH + B \leftrightarrow CH_3SO^{3-} + HB + CH_3SO^{3-} + H2O + I_2 + 2B \rightarrow CH_3SO_4^- + 2HB + 2I^-$$

The process sees an organic base (B), sulphur dioxide, iodine and an alcohol. The original Karl Fischer titration method used pyridine as an organic base and methanol as the alcohol. Nowadays the Karl Fischer titration reagents are much less toxic with imidazole being used as the organic base and ethanol as the alcohol. The replacement of the original reagents for the less toxic ones also showed a fastened rate of reaction[25-26].

The Karl Fischer Titration method can either be coulometric or volumetric. In general, it can be said that the titration method chosen is dependent on the water content of the samples being measured:

- Coulometric titration is suitable for samples with low water content (10 µg - 100 mg)
- Volumetric titration is suitable for samples with higher water content (0.1 - 500 mg).

The water measurements documented within this thesis were carried out using a coulometric Karl Fischer titration. Coulometric Karl Fischer titration was utilised due to the hygroscopic nature of ILs and their ability to take in minute amounts of water present in the atmosphere[25-26].

2.2.1 Coulometric Karl Fischer Titration

The main compartment of the titration cell contains the anode solution plus the analyte.

The anode solution consists of an alcohol (ROH), a base (B), SO_2 and I_2. The titration cell also consists of a smaller compartment with a cathode immersed in the anode solution of the main compartment. The two compartments are separated by an ion permeable membrane. The Pt anode generates I_2 when current is provided through the electric circuit. The net reaction as shown below is the oxidation of SO_2 by I_2. One mole of I_2 is consumed for each mole of H_2O[25-26].

$$B{\cdot}I_2 + B{\cdot}SO_2 + B + H_2O \rightarrow 2BH^+I^- + BSO_3$$

$$BSO_3 + ROH \rightarrow BH^+ROSO_3^-$$

The endpoint is detected most commonly by a bipotentiometric method. A second pair of Pt electrodes are immersed in the anode solution. The detector circuit maintains a constant current between the two detector electrodes during titration. Prior to the

equivalence point, the solution contains I^- but little I_2. At the equivalence point, excess I_2 appears and an abrupt voltage drop marks the endpoint. The amount of charge needed to generate I_2 and reach the endpoint can then be used to calculate the amount of water in the original sample[25-26].The volumetric titration is based on the same principles as the coulometric titration except that the anode solution is used as the titrant solution.

Coulometric titrators offer one decisive advantage compared to volumetric titrators: No titer has to be determined. The coulometric method is an absolute method, there is a strictly quantitative relationship between the amount of electric charge and the quantity of iodine generated[25-26].

A small pre-weighed amount of each IL was injected into the Karl Fischer apparatus, with the process being repeated in triplicate in order to generate consistent results.

2.3 Instruments

All compounds were dried in *vacuo* ($P \leq 10^{-3}$ mbar) at 50 - 70°C and stored under argon before being characterised by ^{1}H, ^{13}C and ^{19}F-{1H} and ^{31}P-{1H} NMR spectroscopy when appropriate. NMR spectra were acquired on Bruker DPX300, AV400, AV (III) 400, AV (III) 400HD, DPX400, or AV (III) 500 spectrometers at RT unless otherwise stated. All chemical shifts are reported in parts per million (ppm) with reference to residual traces of protonated solvents in commercial NMR solvents. For $CDCl_3$, the shifts are referenced to 7.27 ppm for ^{1}H NMR spectroscopy and 77.0 ppm for ^{13}C NMR spectroscopy. For DMSO-d_6, the shifts are referenced to 2.50 ppm for ^{1}H NMR spectroscopy and 39.5 ppm for ^{13}C NMR spectroscopy. Coupling constants (*J*) are given in Hz and multiplicities were labelled (s) singlet, (d) doublet, (t) triplet, and (q) quartet and (m) multiplet.

Note: ^{1}H NMR and ^{19}F NMR chemical shifts are represented together in the compound structure. ^{13}C NMR chemical shifts are represented separately.

High-resolution mass spectra were recorded using electrospray ionization (ESI) techniques at the Carbon Neutral Laboratory, University of Nottingham. Infra-red spectra were recorded on an ALPHA II FTIR instrument on the neat compound using the attenuated total refraction technique.

For synthesis which involved anion exchange chemistry, Ion Chromatography (Dionex ICS-5000 machine fitted with AS20 analytical column and AG20 guard column) showed that residual halide was below the detection limits of the instrument (≈ 1 ppm).

Viscosity and Density measurements were recorded simultaneously at RT for each sample (Anton Paar SVM 3000 Viscometer). Each measurement required 3 mL of the sample and each sample was measured in triplicate in order to generate consistent results. Measurements were recorded at RT for all samples.

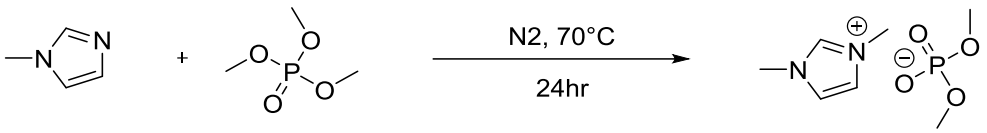
Water content determination for each IL and solvent were recorded using Karl Fischer techniques (CA-200 Moisturemeter). Each sample was measured in triplicate in order to generate consistent results.

2.4 Materials

Compounds investigated herein were prepared in our laboratory using modified literature procedures. Chemical precursors were obtained from the commercial supplier Sigma Aldrich and used without further purification unless stated otherwise. Lithium bis (trifluoromethylsulfonyl) imide was obtained from 3M. All water used in this work was Millipore Milli-Q 18.2 MΩ ultrapure and deionised. All solvents were analytical grade with the exception of anhydrous solvents (≥ 99.7 %)

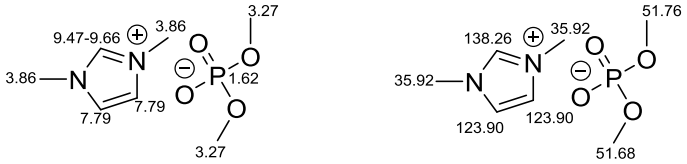
2.5 Synthesis of Ionic Liquids

2.5.1 Preparation of 1, 3-dimethylimidazolium dimethyl phosphate, [MMIM] [DMP]



Methylimidazole (7.20 mL, 90.0 mmol) was cooled to 0 °C and allowed to stir. Trimethyl phosphate (10.5 mL, 90.0 mmol) was subsequently added dropwise over a period of 1 hr. Upon completion of the dropwise addition, the reaction was allowed to warm to RT and was stirred for a further 24 hr at 70 °C. The reaction mixture was dried under vacuum at 70 °C for 24 hr, yielding a clear viscous liquid of 1, 3-dimethylimidazolium dimethyl phosphate (19.6 g, 96 %).

1, 3-Dimethylimidazolium dimethyl phosphate



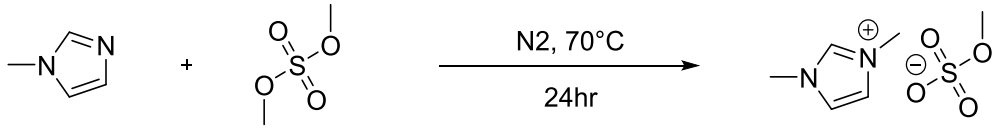
^{1}H NMR (400 MHz, DMSO-d_6) δ = 9.47 - 9.66 (1H, s, NC**H=**N), 7.79 (2H, d, NC**H=**C**H**N), 3.86 (6H, s, C**H₃**N), 3.27 ppm (6H, d, *J*=10.2 Hz, C**H₃**O).

^{13}C NMR (75 MHz, DMSO-d_6) δ = 138.26 (CH), 123.90 (CH_2), 51.76 (CH_3), 51.68 (CH_3), 35.92 (CH_3).^{31}P NMR (162 MHz, DMSO-d_6) δ 1.62 (h, *J* = 10.3 Hz).

ESI-MS (-ve) $[PO_4C_2H_6]^-$, calcd 125.04, found 125.00.

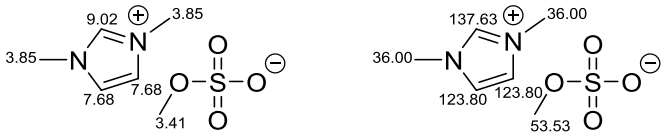
Spectroscopic data were in accordance with that reported previously[11-13].

2.5.2 Preparation of 1, 3-dimethylimidazolium methyl sulphate, [MMIM] [$MeSO_4$]



Methylimidazole (19.14 mL, 240.0 mmol) was cooled to 0 °C and allowed to stir. Diethyl sulphate (13.95 mL, 250.0 mmol) was subsequently added dropwise over a period of 1 hr. Upon completion of the dropwise addition, the reaction was allowed to warm to RT and was stirred for a further 24 hr at 70 °C. The reaction mixture was dried under vacuum at 70 °C for 24 hr, yielding a yellow viscous liquid of 1, 3-dimethylimidazolium methyl sulphate (47.3 g, 95 %).

1, 3-Dimethylimidazolium methyl sulphate



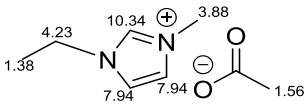
^{1}H NMR (400 MHz, DMSO-d_6) δ 9.02 (1H, s, NC**H**=N), 7.68 (d, *J* = 1.7 Hz, 2H, d, NCH**=**C**H**N), 3.85 (d, *J* = 1.1 Hz, 6H, s, C**H$_3$**N), 3.41 (3H, s, C**H$_3$**N).

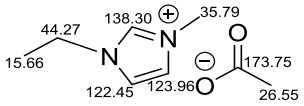
^{13}C NMR (101 MHz, DMSO-d_6) δ 137.63, 123.80, 53.53, 36.00.

ESI-MS (-ve) $[CH_3O_4S]^-$, calcd 110.98, found 110.9757.

Spectroscopic data were in accordance with that reported previously[13-14].

2.5.3 1-Ethyl-3-methylimidazolium acetate, [EMIM] [Ac]





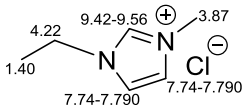
1-Ethyl-3-methylimidazolium acetate was purchased from Sigma Aldrich, at a purity of 97 %. H NMR (300 MHz, DMSO-d_6) δ 10.34 (1H, s, NC**H=**N), 7.94 (2H, d, NC**H=**C**H**N), 4.23 (2H, q, *J* = 7.3 Hz, $CH_3C\mathbf{H_2}N$), 3.88 (3H, s, NC$\mathbf{H_3}$), 1.58 (3H, s, OCC$\mathbf{H_3}$), 1.38 (3H, t, *J* = 7.4 Hz, $C\mathbf{H_3}CH_2N$).

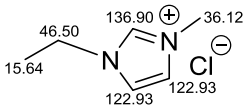
^{13}C NMR (75 MHz, DMSO-d_6) δ 173.75 (C), 138.30 (CH), 123.96 (CH), 122.45 (CH), 44.27 (CH_2), 35.79 (CH_3), 26.55 (CH_3), 15.66 (CH_3).

ESI-MS (+ve) $[C_6H_{11}N_2]^+$ calcd 111.09, found 111.36.

Spectroscopic data were in accordance with that reported previously[13,15,16].

2.5.4 1-Ethyl-3-methylimidazolium chloride, [EMIM] Cl





1-Ethyl-3-methylimidazolium chloride was purchased from Sigma Aldrich, of which the purity was 98 %.

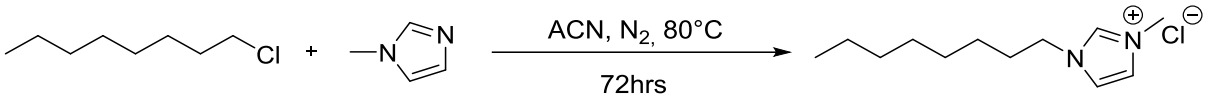
^{1}H NMR (300 MHz, DMSO-d_6) δ = 9.42 - 9.56 (1H, s, NC**H=**N), 7.74 - 7.90 (2H, d, NC**H=**C**H**N), 4.22 (2H, q, *J*=7.3 Hz, $CH_3C\mathbf{H_2}N$), 3.87 (3H, s, $NC\mathbf{H_3}$), 1.40 ppm (3H, t, *J*=7.3 Hz, $C\mathbf{H_3}CH_2N$).

^{13}C NMR (75 MHz, DMSO-d_6,) δ = 136.90 (CH), 123.98 (CH), 122.43 (CH), 44.50 (CH_2), 36.12 (CH_3), 15.64 (CH_3).

ESI-MS (+ve) $[C_6H_{11}N_2]^+$ calcd 111.09, found 111.36.

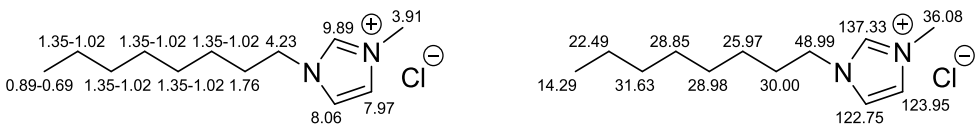
Spectroscopic data were in accordance with that reported previously[13,17].

2.5.5 Preparation of 1-methyl-3-octylimidazolium chloride, [OMIM] Cl



Chlorooctane (17.67 mL, 104.0 mmol) was added dropwise to methylimidazole (7.11 g, 86.6 mmol) and allowed to stir at 80 °C for 72hrs under an inert atmosphere. The reaction mixture was dried under vacuum at 70 °C for 24 hr, yielding a clear viscous liquid of 1-methyl-3-octylimidazolium chloride (18.4 g, 92 %).

1-Methyl-3-octylimidazolium chloride



^{1}H NMR (400 MHz, DMSO-d_6) δ 9.89 (1H, s, NC**H=**N), 8.06 (1H, d, NC**H**=CHN), 7.97 (1H, d, NCH=C**H**N), 4.23 (2H, t, *J* = 7.2 Hz, $CH_3C\mathbf{H_2}N$), 3.91 (3H, s, $NC\mathbf{H_3}$), 1.76

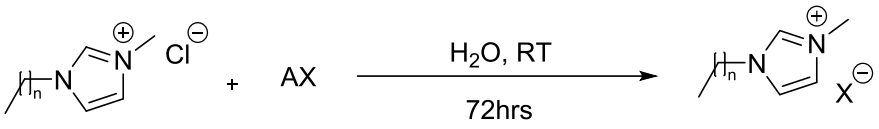
(2H, m , *J* = 7.2 Hz, NC**H₂**CH_2), 1.35 - 1.02 (10H, CH_2(C**H₂**)$_5CH_3$), 0.89 - 0.69 (3H, m, CH_2C**H₃**).

^{13}C NMR (101 MHz, DMSO-d_6) δ 137.33, 123.95, 122.75, 48.99, 36.08, 31.63, 30.00, 28.98, 28.85, 25.97, 22.49, 14.29.

ESI-MS (+ve) $[C_{12}H_{23}N_2]^+$ calcd 195.19, found 195.49.

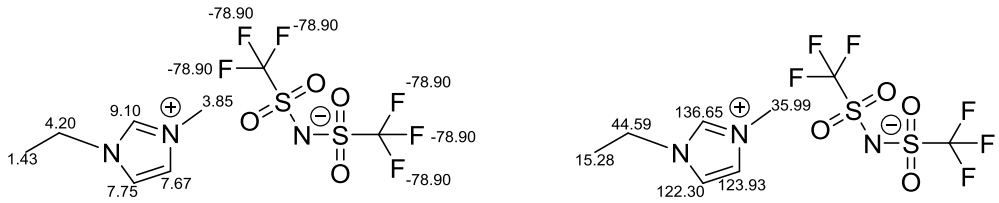
Spectroscopic data were in accordance with that reported previously[18,19].

2.6 General Procedure for Metathesis Products



1-N-3-methylimidazolium chloride was dissolved in water (20 mL). The corresponding salt in water (10 mL) was added and the mixture stirred at 0 °C and gradually allowed to warm up to RT for 24 hr. Dichloromethane (20 mL) was added to recover the IL and washed with cold water (5 x 5 mL). The organic layer was collected, the solvent removed and stirred *in vacuo* overnight at 50 °C[20,21].

2.6.1 1-Ethyl-3-methylimidazolium bis (trifluoromethylsulfonyl) imide, [EMIM] [Tf_2N]



$LiNTf_2$ (15.8 g, 55.0 mmol) was added to 1-ethyl-3-methylimidazolium chloride (7.5 g, 51.0 mmol) to yield 1-ethyl-3-methylimidazolium bis (trifluoromethylsulfonyl) imide (16.2 g, 81 %) as a clear viscous liquid.

^{1}H NMR (400 MHz, DMSO-d_6) δ 9.10 (s, 1H), 7.74 (d, 1H), 7.66 (d, 1H), 4.20 (q, J = 7.3 Hz, 2H), 3.86 (s, 3H), 1.43 (t, J = 7.3 Hz, 3H).

^{19}F NMR (376 MHz, DMSO-d_6) δ -79.02.

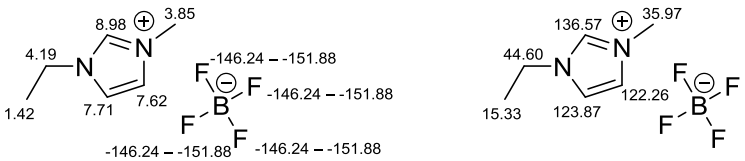
^{13}C NMR (101 MHz, DMSO-d_6) δ 136.65, 123.93, 122.30, 44.59, 35.99, 15.28.

ESI-MS (+ve) $[C_6H_{11}N_2]^+$ calcd 111.09, found 111.09.

ESI-MS (-ve) $[C_2F_6NO_4S_2]^-$, calcd 279.92, found 279.91.

Spectroscopic data were in accordance with that reported previously[22-23].

2.6.2 1-Ethyl-3-methylimidazolium tetrafluoroborate, [EMIM] [BF_4]



$NaBF_4$ (12.2 g, 110.0 mmol) was added to 1-ethyl-3-methylimidazolium chloride (14.7 g, 100.0 mmol) to yield 1-ethyl-3-methylimidazolium tetrafluoroborate (15.5 g, 78 %) as a yellow viscous liquid.

^{1}H NMR (400 MHz, DMSO-d_6) δ 8.98 (1H, s, NC**H=**N), 7.71 (1H, d, NC**H**=CHN), 7.62 (1H, d, NCH=C**H**N), 4.19 (2H, q, *J* = 7.3 Hz, $CH_3C\mathbf{H_2}N$), 3.85 (3H, s, NC**H$_3$**), 1.42 (3H, t, *J* = 7.3 Hz, $C\mathbf{H_3}CH_2N$).

^{19}F NMR (376 MHz, DMSO-d_6) δ -146.24 - -151.88 (m).

^{13}C NMR (101 MHz, DMSO-d_6) δ 136.57, 123.87, 122.26, 44.60, 35.97, 15.33.

ESI-MS (+ve) $[C_6H_{11}N_2]^+$, calcd 111.09, found 111.09.

Spectroscopic data were in accordance with that reported previously[22].

2.7 Preparation of Binary Solutions of Water and Ionic Liquids

Chapter 3 involves the investigation into how water effects ILs and vice versa. For several of the experiments, a series of IL water binary mixtures were prepared initially by volume. The water doped ILs were prepared by the addition of ultra-pure water (Millipore Milli-Q 18.2 MΩ) to each IL. Each binary mixture was mixed to ensure complete miscibility. The IL : water volume gradient ranged from 5 : 95 vol : vol % to 95 : 5 vol : vol % for every 5 % for the initial hydration experiment. Table 2.2 details the vol % and mol % of ILs to water for each individual IL investigated as well as each individual water concentration investigated.

Sample Number	IL : Water vol : vol %	[MMIM] [$MeSO_4$] : Water mol : mol %	[MMIM] [DMP] : Water mol : mol %	[EMIM] [Ac] : Water mol : mol %	[OMIM] Cl : Water mol : mol %
1	100 : 0	100 : 0	100 : 0	100 : 0	100 : 0
2	95 : 5	69 : 31	66 : 34	67 : 33	60 : 40
3	90 : 10	51 : 49	48 : 52	49 : 51	41 : 59
4	85 : 15	39 : 61	37 : 63	38 : 62	31 : 69
5	80 : 20	31 : 69	29 : 71	30 : 70	24 : 76
6	75 : 25	26 : 74	23 : 77	25 : 75	19 : 81
7	70 : 30	21 : 79	19 : 81	20 : 80	16 : 84
8	65 : 35	18 : 82	16 : 84	17 : 83	13 : 87
9	60 : 40	15 : 85	13 : 87	14 : 86	11 : 89
10	55 : 45	12 : 88	11 : 89	12 : 88	9 : 91
11	50 : 50	10 : 90	9 : 91	10 : 90	7 : 93
12	45 : 55	9 : 91	8 : 92	8 : 92	6 : 94
13	40 : 60	7 : 93	7 : 93	7 : 93	5 : 95
14	35 : 65	6 : 94	5 : 95	6 : 94	4 : 96
15	30 : 70	5 : 95	4 : 96	4 : 96	3 : 97
16	25 : 75	4 : 96	3 : 97	4 : 96	3 : 97
17	20 : 80	3 : 97	3 : 97	3 : 97	2 : 98
18	15 : 85	92 : 8	2 : 98	2 : 98	1 : 99
19	10 : 90	1 : 99	1 : 99	1 : 99	1 : 99
20	5 : 95	1 : 99	1 : 99	1 : 99	0 : 100

Table 2.2 mol and vol % values for ILs and water for each forceful hydration experiment.

Upon investigation and analysis of the initial water doping experiment, a secondary hydration experiment was carried out to further analyse the effect of lower concentrations of water on the IL [MMIM] [$MeSO_4$]. Table 2.3 details vol % and mol % of [MMIM] [$MeSO_4$] to water for each sample studied.

Sample Number	[MMIM] [$MeSO_4$] : Water vol : vol %	[MMIM] [$MeSO_4$] : Water mol : mol %
1	100 : 0	100 : 0
2	99 : 1	89 : 11
3	97 : 3	79 : 21
4	96 : 4	71 : 29
5	94 : 6	64 : 36
6	92 : 8	58 : 42
7	91 : 9	53 : 47
8	90 : 10	48 : 52
9	89 : 11	44 : 56
10	87 : 13	40 : 60
11	85 : 15	37 : 63
12	84 : 16	35 : 65
13	82 : 18	33 : 67
14	81 : 19	31 : 69
15	80 : 20	29 : 71
16	78 : 22	28 : 72
17	77 : 23	26 : 74
18	76 : 24	25 : 75
19	74 : 26	24 : 76
20	73 : 27	23 : 77
21	71 : 29	22 : 78
22	71 : 29	21 : 79
23	70 : 30	20 : 80

Table 2.3. mol and vol % values for [MMIM] [$MeSO_4$] and water for the detailed hydration experiment.

2.8 Preparation of Binary Solutions of Solvent and Ionic Liquids

Chapter 4 details the investigation into the impact that residual solvents have on a range of ILs. A series of IL solvent binary mixtures were thus prepared by volume. The solvent doped ILs were prepared by the addition of acetonitrile (ACN), dichloromethane (DCM), hexane and toluene to many of the ILs above. Prior to the subsequent mixing of IL and solvent, the water content for each solvent was determined *via* Karl Fischer measurements. Table 2.4 details the water content of the solvents used.

Solvent	Residual Water Content (ppm)
ACN	**4.0 ± 0.8**
DCM	**1.3 ± 1.2**
Hexane	**1.6 ± 1.4**
Toluene	**2.1 ± 0.4**

Table 2.4. Karl Fischer measurements for the solvents used in conjunction with the ILs. Karl Fischer measurements were recorded in triplicate.

Each solvent contained minimal concentrations of water and required little or no further drying. The gradient for the IL solvent mixtures was selected as, 1.00 : 1.00 (vol : vol), 1.00 : 0.50 (vol : vol) and 1.00 : 0.25 (vol : vol). Table 2.5 details the mol % of each of the IL solvent mixtures.

Solvent : IL mol : mol % for Binary Mixture of 1.0 : 1.0 vol : vol %						
	[MMIM] [DMP]	[MMIM] [$MeSO_4$]	[EMIM] [Ac]	[EMIM] [BF_4]	[EMIM] Cl	[OMIM] Cl
ACN	77 : 23	75 : 25	76 : 24	75 : 25	70 : 30	81 : 19
DCM	73 : 27	71 : 29	72 : 28	71 : 29	66 : 34	78 : 22
Hexane	57 : 43	54 : 46	56 : 44	54 : 46	48 : 52	63 : 37
Toluene	62 : 38	60 : 40	61 : 39	59 : 41	54 : 46	68 : 32

Solvent : IL mol : mol % for Binary Mixture of 0.5 : 1.0 vol : vol %						
	[MMIM] [DMP]	[MMIM] [$MeSO_4$]	[EMIM] [Ac]	[EMIM] [BF_4]	[EMIM] Cl	[OMIM] Cl
ACN	62 : 38	60 : 40	61 : 39	59 : 41	54 : 46	69 : 31
DCM	58 : 42	55 : 45	56 : 44	55 : 45	49 : 51	64 : 36
Hexane	40 : 60	37 : 63	39 : 61	37 : 63	32 : 68	46 : 54
Toluene	45 : 55	42 : 58	44 : 56	42 : 58	37 : 63	52 : 48

Solvent : IL mol : mol % for Binary Mixture of 0.25 : 1.0 vol : vol %						
	[MMIM] [DMP]	[MMIM] [$MeSO_4$]	[EMIM] [Ac]	[EMIM] [BF_4]	[EMIM] Cl	[OMIM] Cl
ACN	45 : 55	43 : 57	44 : 56	42 : 58	32 : 68	52 : 48
DCM	41 : 59	38 : 62	39 : 61	37 : 63	33 : 67	47 : 53
Hexane	25 : 75	23 : 77	24 : 76	23 : 77	19 : 81	30 : 70
Toluene	29 : 71	27 : 73	28 : 72	26 : 74	23 : 77	35 : 65

Table 2.5. mol % values for the binary solutions of each IL and each solvent studied in this thesis.

2.9 Preparation of Binary Solutions of Metathesis Salts and Ionic Liquids

Chapter 5 explores the relationship between ILs and residual contamination due to alkali salts from metathesis reactions. A series of metathesized ILs, as prepared above, was mixed with varying concentrations of the initial alkali salt used during the synthesis process. The binary mixtures were prepared by weight. The ATR-FTIR spectra were taken for each sample that underwent full dissolution with the metathesis salt. Table 2.6 details the wt : wt % and the mol : mol % of each IL and salt intended for analysis. Table 2.6 also highlights the point at where dissolution broke down for each IL.

Sample Number	IL : Salt wt : wt %	[EMIM] [Tf_2N] : $LiNTF_2$ mol : mol %	[EMIM] [BF_4] : $NaBF_4$ mol : mol %	[EMIM] [BF_4] : $LiBF_4$ mol : mol %	[EMIM] [Ac] : LiAc mol : mol %
1	98 : 2	97 : 3	97 : 3	96 : 4	95 : 5
2	96 : 4	95 : 5	93 : 7	92 : 8	90 : 10
3	94 : 6	92 : 8	90 : 10	88 : 12	86 : 14
4	92 : 8	89 : 11	86 : 14	85 : 15	82 : 18
5	90 : 10	87 : 13	83 : 17	81 : 19	77 : 23
6	88 : 12	84 : 16	80 : 20	78 : 22	74 : 26
7	86 : 14	82 : 18	77 : 23	74 : 26	70 : 30
8	84 : 16	79 : 21	74 : 26	71 : 29	67 : 33
9	82 : 18	77 : 23	72 : 28	68 : 32	64 : 36
10	80 : 20	75 : 25	69 : 31	65 : 35	61 : 39
11	70 : 30	63 : 37	56 : 44	53 : 47	48 : 52
12	60 : 40	52 : 48	45 : 55	42 : 58	37 : 63
13	50 : 50	42 : 58	36 : 64	32 : 68	28 : 72
14	40 : 60	33 : 67	27 : 73	24 : 76	21 : 79
15	30 : 70	24 : 76	19 : 81	17 : 83	14 : 86
16	20 : 80	16 : 84	12 : 88	11 : 89	9 : 91
17	10 : 90	8 : 92	6 : 94	5 : 95	4 : 96

Table 2.6. mol % values for the binary solutions of each IL and each alkali salt studied in this thesis. The yellow highlight indicates the point of dissolution, mol % beyond this point did not show full dissolution

2.10 References

1. G. Ramer and B. Lendl. *Encyclopedia of Analytical Chemistry*. J. Wiley and Sons: Chichester, United Kingdom, 2013.

2. T. Buffeteau, B. Desbat and D. Eyquem, *Vibrational Spectroscopy*. **1996**, *11*, 29 - 36.

3. S. E. Glassford, B. Byrne and S. G. Kazarian, *Biochim. Biophys. Acta*. **2013**, *1834*, 2849 - 2858.

4. B. Stuart. *Infrared spectroscopy*; J. Wiley and Sons: Chichester, United Kingdom, 2009.

5. A. de Juan and R. Tauler, *Crit. Rev. Anal. Chem*. **2006**, *36*, 163-176.

6. J. J. Andrew and T. M. Hancewicz , *Appl. Spectrosc.* **1998**, *52*, 797 - 807.

7. R. Tauler, Chemom. Intell. Lab. Syst. **1995**, *30*, 133 - 146.

8. R. Tauler, A. Smilde and B. Kowalski , *J. Chemom*. **1995**, *9*, 31 - 58.

9. UK.mathworks.com. (**2018**). *File Exchange - MATLAB Central*. [Online] Available at: https://uk.mathworks.com/matlabcentral/fileexchange/.

10. UK.mathworks.com. (**2018**). PLS_Toolbox Eigenvector Research, Inc. [Online] Available at: http://www.eigenvector.com/software/pls_toolbox.htm.

11. D. L. Minnick, R. A. Flores, M. R. Destefano and A. M. Scurto, *J. Phys. Chem. B*. **2016**, *32*, 7906 - 7919.

12. H. F. Sangian, J. Kristian, S. Rahma, H. K. Dewi, D. A. Puspasari, S. Y. Agnesty, S. Gunawan and A. Widjaja, *Bull. Chem. React. Eng. Catal*. **2015**, *10*, 1978 - 2993.

13. Wasserscheid, P.; Welton; T. Ionic Liquids in Synthesis; Wiley-VCH: Weinheim, Germany, 2008.

14. A. B. Pereiro, F. Santamarta, E. Tojo, A. Rodríguez and J. Tojo, *J. Chem. Eng. Data*. **2006**, *51*, 952 - 954.

15. M. B. Shiflett and A. Yokozeki, *J. Chem. Eng. Data*. **2009**, *54*, 108 - 114.

16. J. Bian, F. Peng, X.-P. Peng, X. Xiao, P. Peng, F. Xu and R.-C. Sun, *Carbohydrate*

Polymers. **2014**, *100*, 211 - 217.

17. P.-Y. Chen and I.-W. Sun, *Electrochim. Acta*, **2000**, *45*, 3163 - 3170.

18. K. R. Seddon, G. Srinivasan, M. Swadźba-Kwaśny and A. R. Wilson, *Phys. Chem. Chem. Phys*. **2013**, *15*, 4518.

19. D. C. Apperley, C. Hardacre, P. Licence, R. W. Murphy, N. V. Plechkova, K. R. Seddon, G. Srinivasan, M. Swadźba-Kwaśny and I. J. Villar-Garcia, *Dalton Trans.* **2010**, *39*, 8679 - 8687.

20. J. P. Hallett and T. Welton, *Chem. Rev.*, **2011**, *5*, 3508 - 3576.

21. M. Y. Lui, L. Crowhurst, J. P. Hallett, P. A. Hunt, H. Niedermeyer and T. Welton, *Chem. Sci.* **2011**, *2*, 1491 - 1496

22. P. Bonhôte, A.-P. Dias, N. Papageorgiou, K. Kalyanasundaram and M. Grätzel, *Inorg. Chem.* **1996**, *35*, 1168 - 1178.

23. C. H. Giammanco, P. L. Kramer, D. B. Wong and M. D. Fayer, *J. Phys. Chem. B*. **2016**, *44*, 11523 - 11538.

24. B. C. Smith. *Fundamentals of Fourier Transform Infrared Spectroscopy*; Taylor & Francis Group: United States of America, 2011.

25. P Bruttel, R Schlink. *Water Determination by Karl Fischer Titration;* Metrohm monograph: Herisau, Switzerland, 2003.

26. E Scholz. *Karl Fischer Titration: Determination of Water;* Springer: Berlin, 2012.

Chapter 3

Vibrational Spectroscopic Analysis of Water and Ionic Liquids

3.1 Introduction

This chapter focuses on the application of vibrational techniques to probe interactions between ILs and water as both a contaminant and upon hydration with known quantities of water. The work displayed in this chapter investigates a number of hydrophilic ILs that readily absorb atmospheric water and upon doing so, display clear and distinct interactions with the absorbed water.

ILs are naturally hygroscopic and readily absorb water when exposed to the atmosphere[1-2]. The extent of hydration is determined by the combined properties of both the anion and cation[2-3]. As discussed in Chapter 1, the degree of hydration is much more attributed to the structural changes made to the anionic counterpart[4-5]. The results discussed in this chapter are centred on imidazolium-based ILs with the most noticeable difference between these ILs being the choice of the anion. The ILs chosen for investigation were based on their application within varying chemical processes, such as biopolymer dissolution[6-7]. All anions chosen have the ability to act as both hydrogen bond acceptors and donors, a feature of which is desirable in dissolution chemistry[6-7]. Upon interaction with atmospheric and bulk water the anion assumes one or both of these roles. As discussed in Chapter 1, many groups have reported predicted structures that show that the water molecule preferentially interacts with the anion of the IL by forming associations of type (A…H–O–H…A). This chapter aims to build on this work by exploring further anions and probing the effects of a wider concentration gradient of water.

This chapter aims to explore a diverse range of ILs in order to assess if the same pattern is followed in regards to bonding interactions as already observed in the literature. Building upon the spectroscopic results obtained from atmospheric water and ILs, each IL was hydrated further with bulk water. The intention of increasing the concentration gradient of water present in each IL allows for the effects of water on ILs and *vice versa* to be explored on a varying scale. The interactions between water and ILs will ultimately change as a result of each IL slowly transitioning into a solution of ions upon hydration.

IR and Raman spectroscopy are utilised in this chapter as the main spectroscopic techniques to probe the effects of varying water concentrations on each IL. Vibrational spectroscopy has been proven to be a powerful tool for the investigation of ILs and can be used to monitor changes that may arise as a result of contamination or the presence of lasting reagents[8]. Analysis of the spectra, using statistical techniques such as multivariate analysis, has been applied and developed in order to retrieve additional information that can be mathematically excavated. The use of multivariate analysis allows for a deeper insight into how the ILs and water change as a result of multicomponent systems being formed.

3.1.1 Regional ATR-FTIR Vibrations for Ionic Liquids

ILs are comprised of both a cationic and anionic counterpart. Each counterpart will possess a number of vibrational bonds that will be noticeably displayed in an IR spectrum[8]. The vibrational bands will be unique to each IL, dependent on the combination of the anion and the cation. Figure 3.1 shows an example IL, [MMIM][DMP], to illustrate the general positioning of the cationic and anionic regions. The individual regions are highlighted in blue.

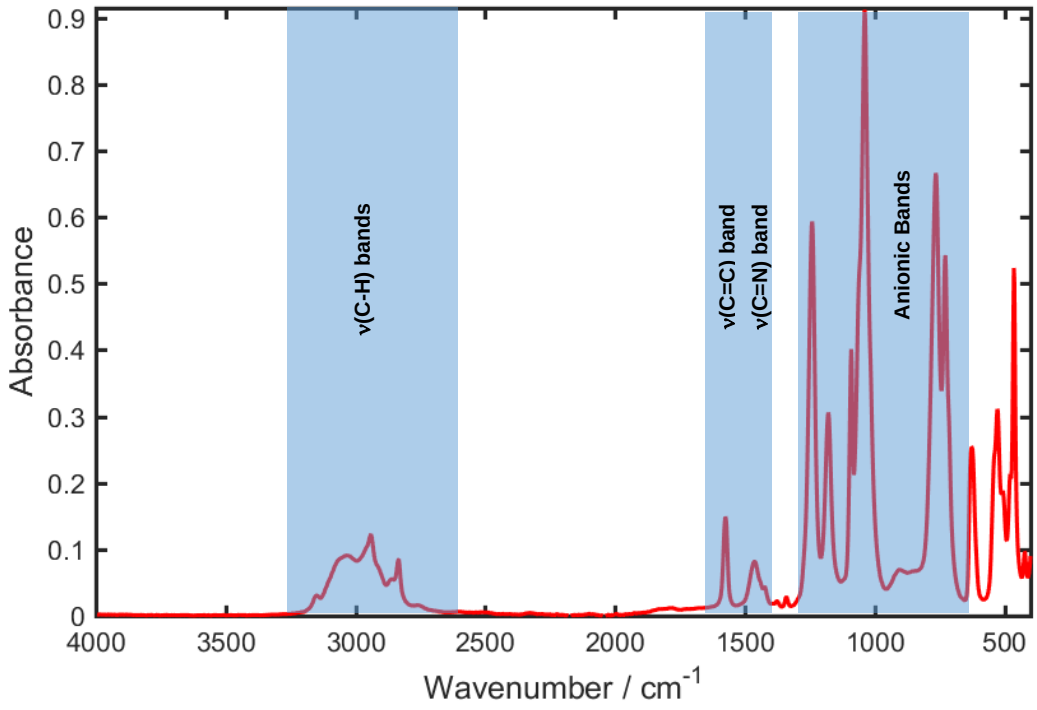


Figure 3.1 IR spectrum of [MMIM] [DMP] with both the cationic and anionic regions clearly highlighted. The cationic region comprises of the ν(C-H), ν(C=C) and ν(C=N) bands, the anionic region has been generalised as most anionic peaks are displayed in the lower wavenumber region.

The cation, in this case, dimethyl imidazolium comprises of C=C, C-H, C-N and C=N bonds which are all displayed prominently in the IR spectrum[8-10]. The bonds present within the cation are somewhat sensitive to change as a result of alterations in IL composition. All of the ILs investigated in this chapter possess imidazolium cations and will all have prominent peaks in these positions. Noticeable shifts concerning the C-H vibrations are observed in many ILs upon changing the overall structure and or environment[8,11,12]. Simple lengthening of alkyl substituents will create changes in both the positioning and the intensity of ν(C-H) peaks[13]. The anionic region of the IR spectrum attracts considerable interest due to the presence of multiple vibrational modes that are highly sensitive to change as a result of additional impurities or

contamination[14-15]. For each IL the positioning of the anionic region is dependent on the associated vibrational bonds. The anionic region in Figure 3.1 represents the $[C_2H_6PO_4]^-$ anion and falls in the region of 1300 - 700 cm^{-1}. [16,17] Distinct peaks at 1241, 1039, 764 cm^{-1} [16,17] represent the phosphorus-oxygen bonding environments. Any changes to the nature of these bonds will have an effect on the shape, position and intensity of these peaks.

Within this thesis, the ILs investigated all possess an imidazolium-based cation, with small differences in the length of the alkyl chain. The noticeable difference as mentioned is that of the anion. It can be noted that Figure 3.1 is a basic representation of the cationic and anionic regions for the ILs studied. Variation in both regions will be observed for each individual IL.

Table 3.1 shows the main spectral features of interest for the ILs investigated herein. The structure of the various ILs as stated is determined by the combination of the anionic and cationic counterparts. The varying combination of ions leads to specific stretching frequencies unique to each IL. Various other methods have been deployed to investigate the effect of impurities and contaminants on ILs such as NMR spectroscopy and computational methods[18-19]. ATR-FTIR spectroscopy however, has become a rapid and efficient way to determine and visualise the effects of contaminants. The migration towards vibrational spectroscopy is primarily down to the power of ATR-FTIR spectroscopy as a spectroscopic technique. The ease of sample preparation coupled with the non-destructive nature of the technique and the clear visual representation of the results are all features which favour ATR-FTIR spectroscopy for this research.

Wavenumber/ cm^{-1}	Functional Group	IL	Ref
3120-3160	C4,5 - H sym	All	8,9,20
3120-3160	C4,5 - H asym	All	8,9,20
3104,	C2-H	All	8,9,20
2980 - 3030	(N)-CH_3 asym	All	8,9,20
3099-3135	(N)-CH_2-CH_3 asym	[EMIM] [Ac], [EMIM] Cl	8,21,22
2900-2850	(N)-CH_2 asym	[EMIM] [Ac], [EMIM] Cl, [OMIM] Cl	8, 21,22
2943	(N)-CH_3 sym	All	9,20
2899-2910	(N)-CH_2-CH_3 sym	[EMIM] [Ac], [EMIM] Cl	8, 21,22
1150-1085	O-C	[MMIM] [DMP], [MMIM] [$MeSO_4$]	16,20,21
1678	C=C	All	8,9,20
1574	C=N	All	8,9,20
1300-1200	SO_3 asym	[MMIM] [$MeSO_4$]	20,23
1014	SO_3 sym	[MMIM] [$MeSO_4$]	20,23
1334	COO asym	[EMIM] [Ac]	21,22
1567	COO sym	[EMIM] [Ac]	21,22
1320-1140	P=O	[MMIM] [DMP]	16
1030-917	P-O	[MMIM] [DMP]	16
727,	O-C	[MMIM] [DMP]. [MMIM] [$MeSO_4$]	16,20,21

Table 3.1. The main spectral features for the functional groups of both the cationic and anionic counterparts for the ILs studied in this chapter.

As discussed thus far, the ATR spectrum of ILs can simply be split into cationic vibrational frequencies and anionic vibrational frequencies. The cationic region tends to fall approximately in the region of 3200 - 1500 cm^{-1} and the anionic region falling in the region of 1500 - 400 cm^{-1} [8]. Closer inspection of each region provides a further understanding of the vibrational nature of both the cation and anion. Figure 3.2 comparatively displays the C-H region for the imidazolium-based ILs discussed in this chapter.

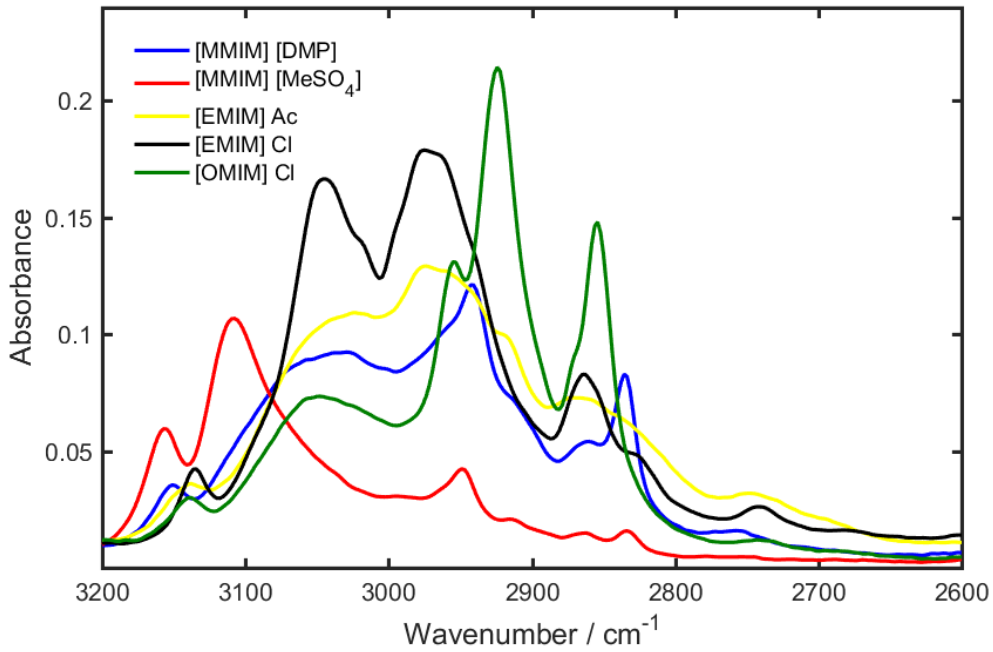


Figure 3.2. Comparative overlay of the higher wavenumber region for several ILs, detailing specifically the C-H vibrations.

The peaks present in the frequency range of 2800 and 3000 cm^{-1} can be assigned to the symmetric and asymmetric stretching vibrations of the ν(C-H) bands associated with the imidazolium ring[8,9,20]. We can separate this frequency range into varying C-H environments. The absorption bands in the range between 3000 and 3200 cm^{-1} are assigned to C2-H stretching mode, [8,9,20] C4, 5-H asymmetric stretching mode, and C4,

5-H symmetric stretching mode, under some portion of the contribution of Fermi resonances and overtones [8,9,20]. Although absorption bands due to these modes tend to overlap and their assignment varies within the literature, a general consensus is that the C2-H stretching mode exists at a lower frequency and the C4, 5-H asymmetric and symmetric modes exist at higher frequencies[8-9]. The lower frequency values for the C2-H stretching mode is credited to the C2 hydrogen being acidically labile and therefore creating a point of interaction which causes a change in the vibrational nature. Diversifying the anionic counterpart causes the C2-H position to fluctuate, it has been shown that a smaller more electronegative anion will interact more effectively at the point of the C2-H,[12,24] thus causing the weakening of this particular bond and hence a redshift being observed in the IR spectrum. The positioning of the C2-H is seemingly dependent on the coulombic interaction with the anion.

The absorption bands in the frequency range between 2800 and 2950 cm^{-1} represent the methylene and methyl groups in the alkyl chain[8-9]. In this region, the absorption frequencies and absorption intensities depend on the alkyl chain length present on the imidazolium cations. For example, by comparatively assessing [EMIM] Cl (black spectrum) against [OMIM] Cl (green spectrum) in Figure 3.2, it is observed that the relative intensity of the methylene peak differs. [OMIM] Cl presents a more intense peak in comparison to the [EMIM] Cl due to the greater number of methylene groups present and ultimately being sampled during the measurement process.

For the ILs studied within this thesis the diversity observed amongst the IL is predominately present in the anion. As a result, the anionic region, which is detailed in the lower wavenumber region will be unique to each IL. The ILs investigated within this chapter all possess anions that have the ability to engage in multiple interactions. The choice of anion was initially selected based on their active role in dissolution chemistry and their ability to disrupt the overall structure of biopolymers by engaging in hydrogen bonding. It is this ability to engage in intermolecular hydrogen bonding that allows for

the vibrational nature of the anionic region to be studied. This chapter is concerned with the interactions between water and ILs with the predominant interactions being that of intermolecular hydrogen bonding. The point of interaction between water and IL will be unique to each IL, which is dependent on the anion. Any changes in the vibrational nature of the anionic functionalities will be represented as a shift.

3.1.2 Linear Combination of Spectra

In order to understand the impact contaminants have on ILs, it is necessary to produce a series of ILs that have been knowingly doped with contaminants and asses them with vibrational spectroscopic techniques. The combination of an IL with a contaminant can be viewed as an A+B type system. With such systems, it may be assumed that when viewing the resulting spectrum it is simply a combination of the spectra of the two individual components that the system is composed of. The addition of two spectra in such a way is known as a linear combination of spectrum[25-26]. For systems where there is little or no interaction, a linear combination of spectra can be assumed to be the correct analysis of the system. For systems where component one changes the nature of component two and *vice versa* then the concept of linear combination breaks down and the system will display distinct prominent changes. The systems investigated within this thesis contain components that will have an impact on one another and therefore should not follow a simple linear combination of spectra. Simply showing that systems do not undergo a linear combination of the spectrum provides preliminary evidence that upon contamination of ILs, the system is changing.

The initial investigation into contaminant effects on ILs for this thesis shows the manner in which water impacts the vibrational nature of each IL. Figure 3.3 displays the pure IL [MMIM] [DMP], [MMIM] [DMP] with the maximum absorption of atmospheric water and a pure spectrum of water.

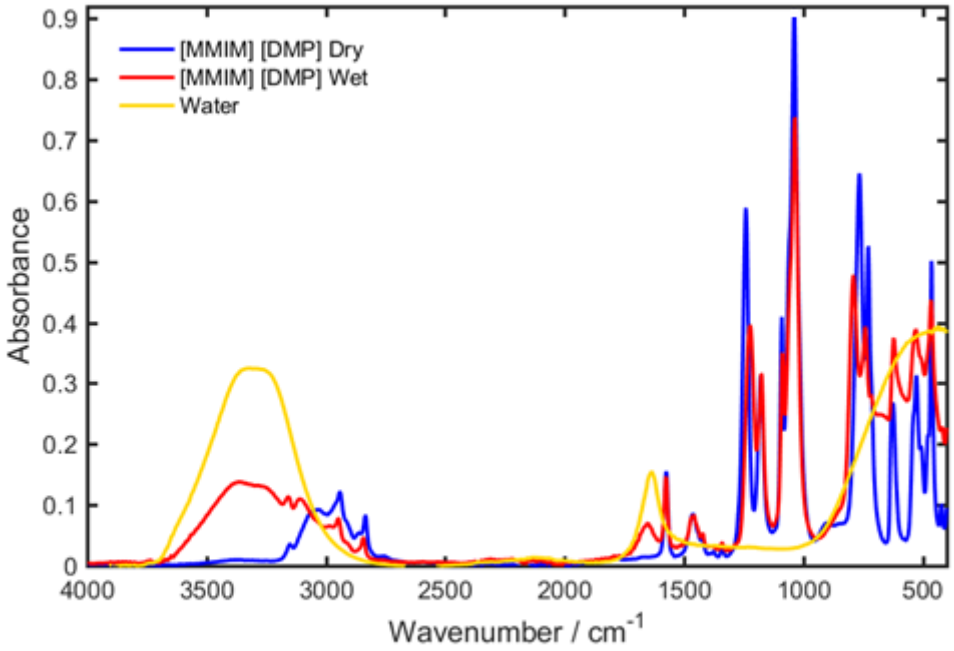


Figure 3.3. ATR-FTIR spectra of dry [MMIM] [DMP] (blue line), hydrated [MMIM] [DMP] (red line) and bulk water (yellow line).

Treating this as an A+B type system, where A is the pure IL (blue line) and B is water (yellow line) we observe that the combination of the two (red line) is not the linear combination of the two spectra. As the IL undergoes hydration with atmospheric water prominent changes become apparent in the IR spectrum. The system has broken away from a linear combination and distinct changes are observed in the regions corresponding to IL bands, due to atmospheric water growing in at 3500 cm^{-1} and 1624 cm^{-1}. The observed changes in Figure 3.3 are unique to [MMIM] [DMP], but all the ILs studied in this chapter all show changes and as a result, do not follow a simple linear combination of spectra. A non-linear combination of spectra is also observed for many other ILs as reported by Welton and co-workers[5]. Further investigation into the effect of atmospheric water and bulk water on the vibrational nature of ILs can be found later in this chapter.

3.1.3 Initial Investigation into Atmospheric Water

The initial experiments into water as a contaminant involved the absorption of atmospheric water by a range of ILs. In these experiments, a droplet of IL was smeared onto the diamond ATR crystal allowing for moisture from the atmosphere to be absorbed at ambient conditions (RT, atm) into the IL until apparent saturation at a given humidity. Each ATR-FTIR spectroscopy experiment aimed to be at the same humidity however, minimal fluctuations in humidity will ultimately have an effect on the amount of water absorbed by the IL.

Karl Fischer measurements were taken before and after exposure to the environment to display the extreme changes in water content from the start of the experiment to the end stage. Table 3.2 displays the Karl Fischer values for each IL.

Karl Fischer Measurements		
IL	**Before Exposure to Atmospheric Water : ppm**	**After Exposure to Atmospheric Water : ppm**
[MMIM] [DMP]	114	1200
[MMIM] [$MeSO_4$]	40	1900
[EMIM] [Ac]	293	1600
[EMIM] Cl	157	16000
[OMIM] Cl	287	12000

Table 3.2. Water content measurements for each IL before and after exposure to the atmosphere.

It can be seen that after exposure to the atmosphere the presence of water retained within the IL system has drastically increased for each IL. The extent of water absorption differs for each IL studied, this may be linked to the differing hygroscopic

nature of each IL. Fluctuations in the amount of water absorbed can also be related to the expanse of surface area exposed to the atmosphere. Surface area exposed is inversely proportional to the droplet size, so in general, reducing the droplet radius by a factor of N will multiply the surface area by a factor of N. A greater exposed surface area will inevitably lead to more water being absorbed by the IL. With each ATR-FTIR spectroscopy experiment, it was intended that droplet size of the IL would be constant however, small fluctuations in droplet size may have occurred inducing small fluxes in the amount of water retained. The Karl Fischer measurements aim to provide an insight into how drastic atmospheric water absorption is for ILs.

As a result of atmospheric water absorption by each IL, distinct spectroscopic changes were brought about. Alterations in peak position and intensity are observed for a range of cationic and anionic peaks. Not all peaks display fluctuations and it can thus be concluded that interactions between ILs and water occur at specific points. For now, we are going to focus in on the higher wavenumber region in order to understand what is happening in this region when atmospheric water is absorbed for each IL. Figure 3.4 displays the ν(O-H) and ν(C-H) stretches for a number of saturated ILs. The spectra displayed is the combination of the final ATR-FTIR spectrum measured for each IL. Initial observations of the ν(O-H) stretch shows a flux in the environment of this band dependent on the IL. Changes in the peak maxima and wavenumber of the ν(O-H) stretch is indicative of different interactions between water and the ILs.

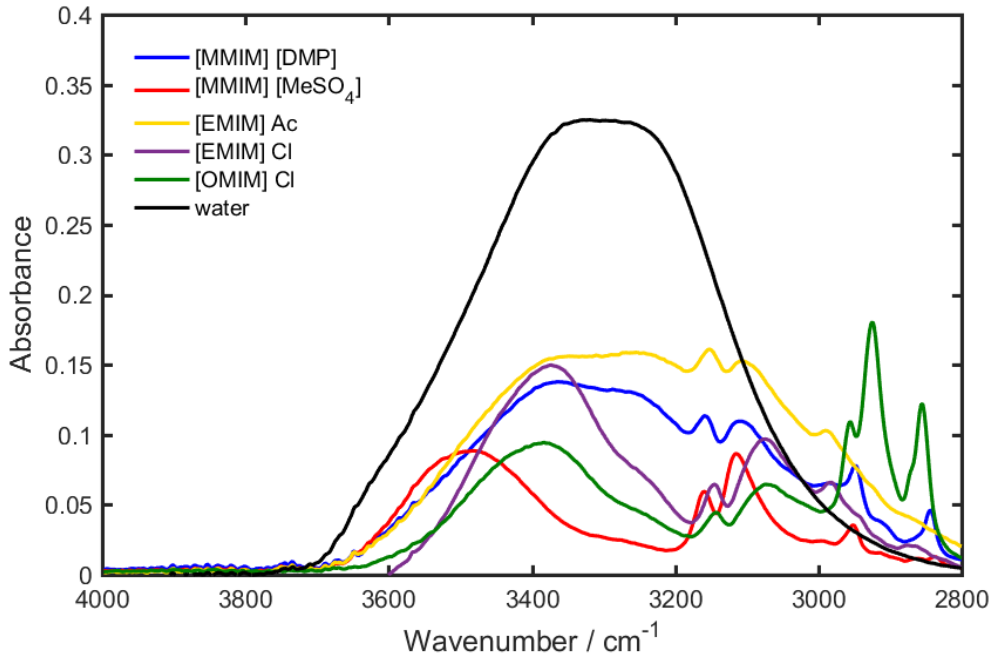


Figure 3.4. ATR-FTIR spectra of maximum water absorption from the atmosphere for a selection of ILs, showing differing water states / conformations, seen by the change in the shape of the OH stretching mode. Pure water has been shown for comparison.

The shape and position of the ν(O-H) peak for [MMIM] [DMP] and [EMIM] [Ac] are comparable, suggesting that absorbed water in these ILs display similar hydrogen bonding. These two ILs also have significantly more absorbed water compared to the other ILs. Both [MMIM] [DMP] and [EMIM] [Ac] have superseded the distinct shape of bound water, with the shape of the peaks showing an unresolved structure. The saturation point for these ILs is dominated by strong broad bands comparable to 'free' water. The noticeable difference between [MMIM] [DMP] and [EMIM] [Ac] is the intensity of the two. [MMIM] [DMP] displays a smaller intensity in comparison. Changes in intensity may be due to the amount of water being sampled, which as discussed may be related to the absorption capacity of the IL. Further reasoning for this change in intensity may relate to fluctuations in laboratory or experimental conditions. A change in humidity and or droplet size being sampled could play a part in intensity variations.

[EMIM] Cl and [OMIM] Cl also show peaks of equal shape and position with a variance in intensity. Both ILs possess the same anion with the variance here being observed with the cation, a lengthening of the alkyl chain for [OMIM] Cl is the key difference. This change in cation may contribute to the changes observed in intensity for the ν(O-H) stretch, equally changes in laboratory conditions such as humidity and temperature may be contributing factors. What can be deduced from these two ILs is that the water stretch has the same energy maxima and therefore the same H bond environment in these ILs. Comparing the two sets of ILs discussed thus far it is apparent that the key differences between the two sets are the shape and peak maxima of the ν(O-H) stretch. This distinct change may be attributed to water interacting differently for the two groups of ILs which can allude to the strength of the hydrogen bond formed between water and the IL.

[MMIM] [$MeSO_4$] shows the ν(O-H) stretch positioned furthest left (highest energy shift) of the spectra compared to the other ILs. The shape here is similar to that of the peaks observed for the chlorinated ILs, which suggests that the conformation of water may be similar. The positioning of the peak to the left of the spectra can be accredited to the strength of the hydrogen bond. An observed redshift for the ν(O-H) band in comparison to that observed in the other ILs is suggestive of a decrease in bond length for the O-H bond, which may be a result of a stronger interaction with the sulphate anion compared to the other anions displayed.

Figure 3.4 clearly displays changes in the ν(O-H) stretch for each IL water mixture suggestive of a varying level of hydrogen bonding between water and ILs as a result of the changing anion. IR spectroscopy proves to be an optimal technique for displaying and analysing these results.

Figure 3.4 not only displays distinct changes for the ν(O-H) stretch but also changes for the C-H region. As discussed earlier in this chapter, the ν(C-H) bands fall *c.a.*

2800 - 300 cm^{-1} with each C-H environment falling at a unique position[8-9]. The ν(C-H) bands existing directly on the imidazolium ring, C2-H, C4 and C5-H are the most affected by the introduction of atmospheric water. These bands fall in the frequency range of 3000-3200 cm^{-1} [8,9,20]. Figure 3.5 shows an example of how the C-H region changes upon hydration with atmospheric water. The IL shown as the example is [MMIM] [$MeSO_4$].

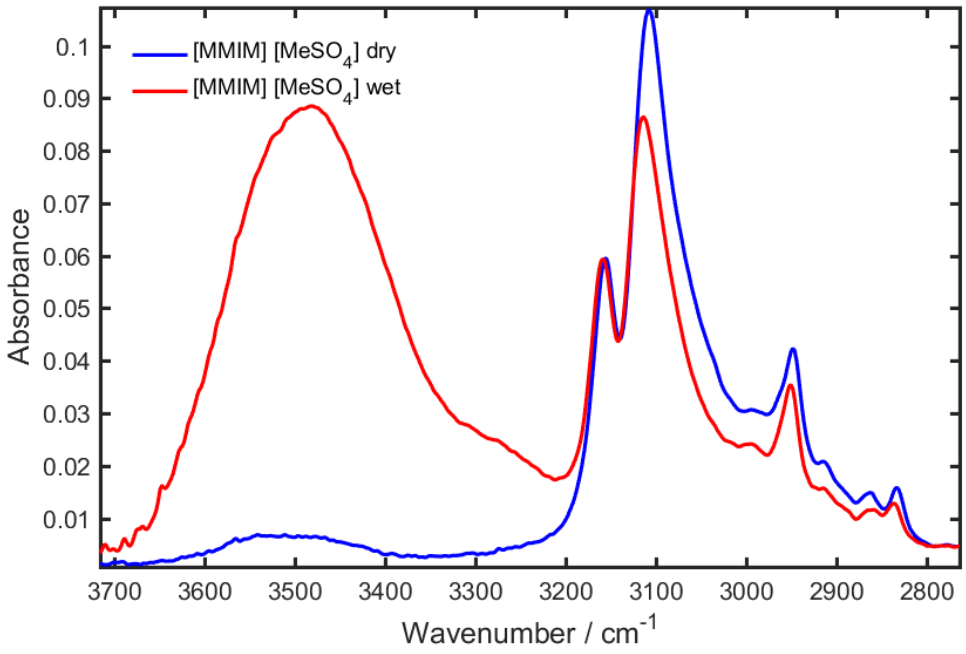


Figure 3.5. The higher wavenumber region for [MMIM] [$MeSO_4$] before (blue line) and after (red line) exposure to the atmosphere. The C-H region falls in the range of 2800-3000 cm^{-1}.

The major changes present in the C-H region associated with hydration are concerned with the hydrogens on the imidazolium ring. We observe changes in intensity and peak maxima for the C2-H (3108 cm^{-1}), C4 and C5-H (3155 cm^{-1}), [27,28] with the major change being observed for the C2-H. The fluctuations in intensity and peak maxima blueshifting are indicative of changes in the vibrational nature of the bonds pertained to the cation. Changes associated with the cation suggests a possible interaction

between atmospheric water or a change to the original anion - cation interaction. The blueshift to higher energy seen for the C2-H stretch may be associated with the acidic lability of this proton and its willingness to engage in interactions. It is well documented within the literature that a point of interaction between the anionic and cationic counterparts of the IL occurs at the C2-H position[4,24]. Cha *et al.* showed that with a decreased halide anion size, the C2-H peak is more redshifted in the IR spectrum, which suggests that the hydrogen bonding is stronger for C2-H with a smaller halide anion[29]. Applying this knowledge to the binary systems explored within this thesis, two hypotheses can be made. The initial one is that upon hydration the blueshift observed for the C2-H stretch suggests a reduction in the original coulombic interaction between that cation and anion. The second is that as well as a reduction in coulombic interaction, water engages in hydrogen bonding at the C2-H position, with this new bond being weaker in comparison to the original anion - cation bond. The new weaker hydrogen bond would cause the C2-H band to be less redshifted in comparison to the original C2-H anionic bonding interaction. The ν(C-H) bands present on the alkyl side chains of the imidazolium ring display minimal changes in intensity suggestive of lessened or no interactions with atmospheric water.

From herein [MMIM] [$MeSO_4$], will be the IL of focus in order to illustrate the impact of water contamination and hydration. [MMIM] [$MeSO_4$] has been selected as the example IL as it perfectly displays the vibrational effects absorbed atmospheric water has on ILs and *vice versa*. The $[MeSO_4]^-$ anion is comprised of multiple bonding sites, specifically hydrogen bonding acceptor sites. It is the abundance of hydrogen bonding sites that allows [MMIM] [$MeSO_4$] to display clear and prominent changes that can be viewed with vibrational spectroscopy.

3.2. [MMIM] [$MeSO_4$] Absorption of Atmospheric water

To gauge a general impression of the influence that atmospheric water has on the vibrational spectra of the main functional groups associated with [MMIM] [$MeSO_4$]. A preliminary experiment was conducted, in which [MMIM] [$MeSO_4$] was spread on an ATR crystal and exposed to the atmosphere at RT for 100 min. IR spectra were collected as a function of time. It was expected that as [MMIM] [$MeSO_4$] absorbed atmospheric water it would engage in intermolecular hydrogen bonding, resulting in spectral changes in the cationic and anionic regions of the ATR spectrum. Figure 3.6 shows the IR spectra obtained. Closer analysis of the different regions uncovers a further understanding of the system.

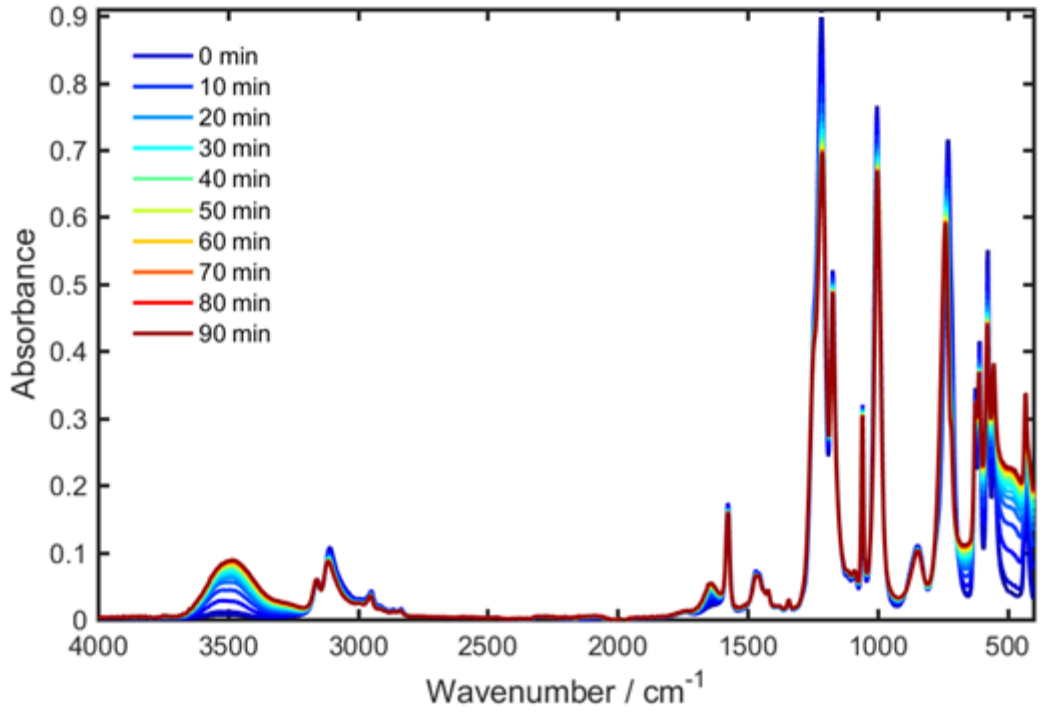


Figure 3.6. ATR-FTIR spectra of [MMIM] [$MeSO_4$] as atmospheric water is absorbed over time (blue to red).

In order to understand the changes occurring as a result of each IL absorbing water and transitioning into a binary system, it is imperative to separate the spectra out and focus in on each changing band. Starting with the vibrational bands associated with water itself, it can be seen that as the water content increases, there is an observed absorbance increase of the ν(O-H) stretch at 3500 cm^{-1} coupled with the bend at 1650 cm^{-1}. Assessment of both vibrational bands reveals that the rate at which water is absorbed by the IL is not constant throughout the duration of the experiment. Figure 3.7 shows the rate of change in absorbance of the ν(O-H) bend. Here the ν(O-H) bend has been plotted against the ν(C-N) band of the imidazolium ring present at 1176 cm^{-1}. The reasoning behind plotting the ν(O-H) bend in this format as opposed to plotting the ν(O-H) stretch is due to the fact that the bend is not subject to as much vibrational change compared to that of the stretch. Both the ν(C-N) and ν(O-H) bands are less perturbed and less affected by the change in environment. The ν(O-H) stretching band as discussed is perturbed as the concentration of water in the system is increased. There is also clear overlap with the ν(C-H) bands of the IL, which would provide a false impression of the rate of absorption. Figure 3.7 shows that as the experiment runs the course of the 100 min timescale we see an exponential increase in the change in absorbance until *ca.* 60 - 70 min. This suggests that the IL is rapidly absorbing atmospheric water within the first hour of the experiment. Beyond 60 - 70 min the rate of change of absorbance is reduced and the curve begins to level out. It would be expected that after 100 min the curve would transition into a straight line as the IL would be saturated with atmospheric water.

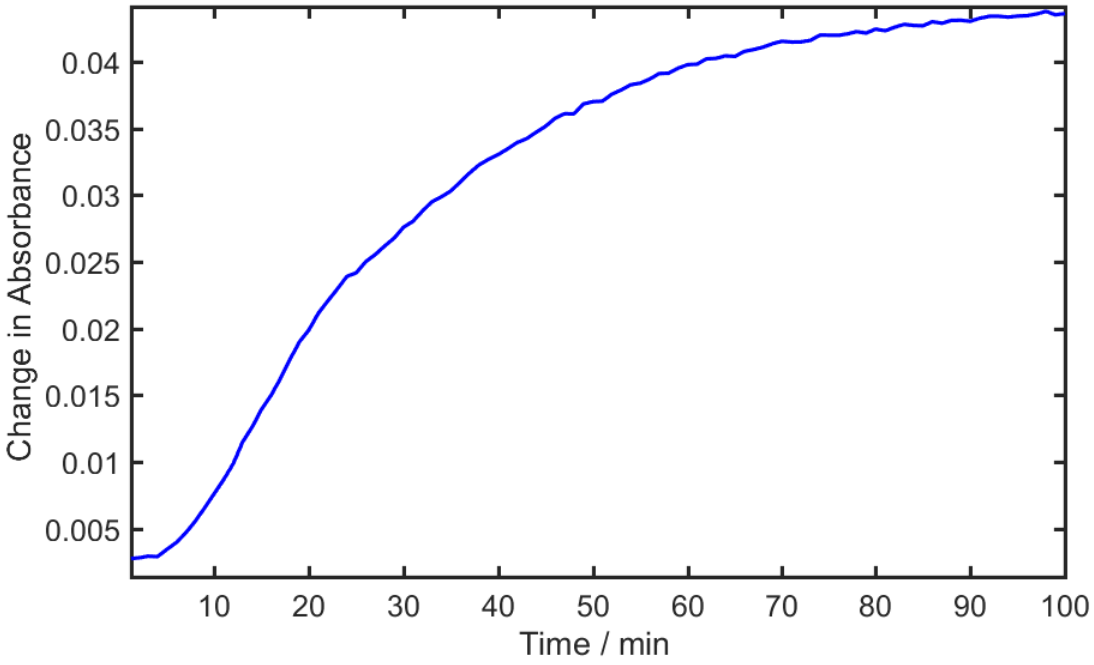


Figure 3.7. The rate of change in absorbance of atmospheric water in [MMIM] [$MeSO_4$], generated by plotting the absorbance of the ν(O-H) bend against the absorbance of the ν(C-N) stretch on the imidazolium ring.

Figure 3.6 not only displays prominent changes associated with each water band, bands linked with the cation and anion also display distinct changes in shape, intensity and peak maxima. Figure 3.8 focuses in on the major spectral changes observed for the major functional groups including the ν(C-H) bands for the cation and the -SO_3 vibrations of the anion. Figure 3.8 presents four enhanced spectra, A - D, for the different regions of the IR spectra; with hydration of the IL occurring from blue to red.

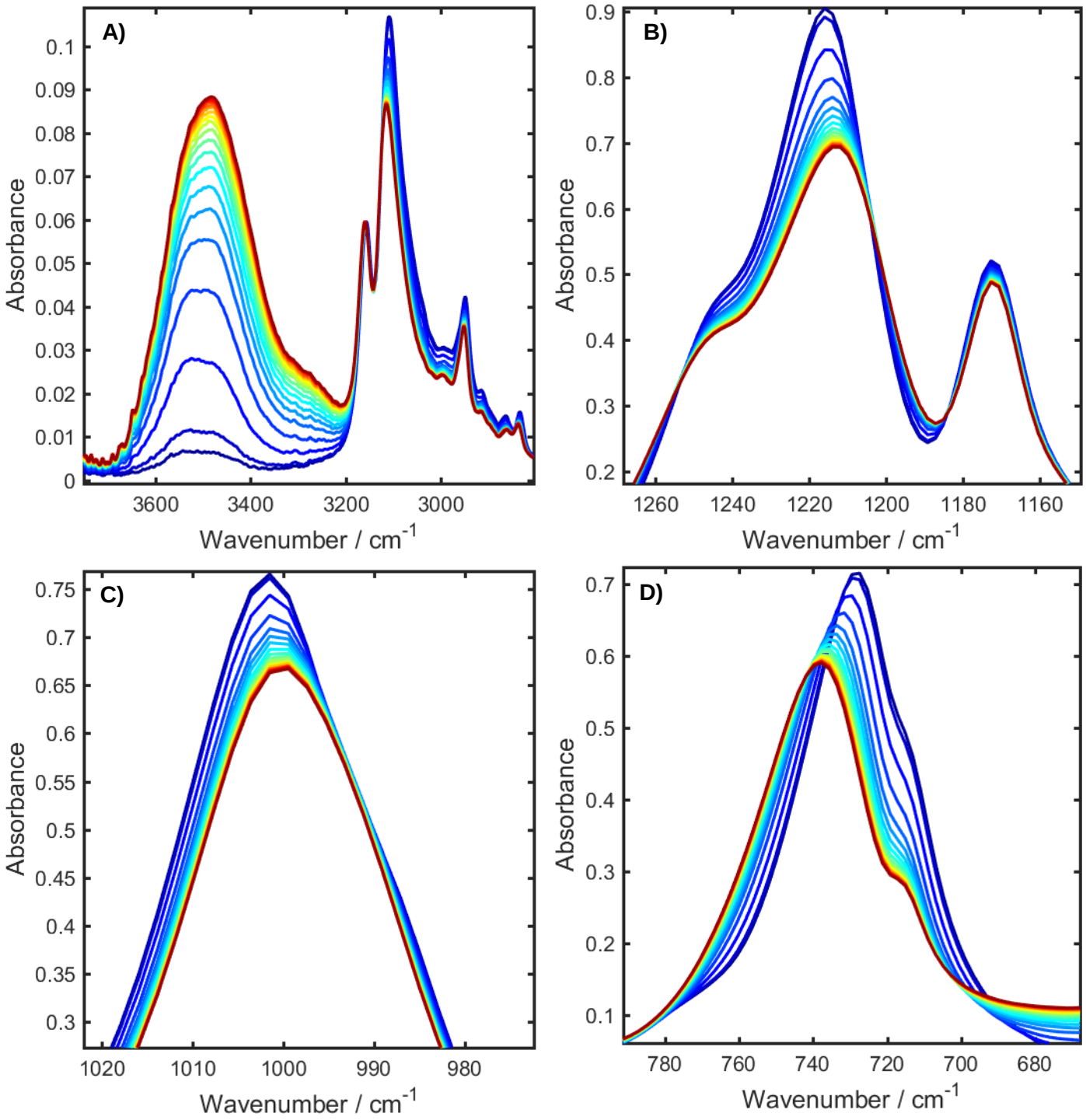


Figure 3.8. Enhanced spectra for the major spectral changes observed in [MMIM] [$MeSO_4$]. A) ν(O-H) and ν(C-H), B) ν(S=O), C) ν(S=O), D) ν(S-O) as atmospheric water is absorbed over time (blue to red).

Spectra A displays the absorbance of the ν(O-H) stretching band at *ca.* 3500 cm^{-1}. The information that can be distilled from this section of the spectra is not just the obvious growth of the band but the rate in which the band grows. It is observed that the rate of the band growth is rapid to start; as the IL is absorbing atmospheric water. The rate of absorption decreases upon saturation of the IL, with the band eventually displaying no further change. This observation is seen and explained in Figure 3.7 spectra A additionally highlights the C-H region associated with the IL, as previously discussed the major change for the C-H region is observed for the C2-H of the imidazolium ring. The peak maxima for the C2-H stretch shows an increase in wavenumber (blueshift), indicating a decrease in the bond length and thus a change in the vibrational environment as [MMIM] [$MeSO_4$] absorbs atmospheric water. As noted earlier in the chapter, this change in the C2-H stretching frequency may be attributed to either a reduction in the original coulombic interaction observed for the IL and or coupled with a new weaker hydrogen bond as the water interacts at this point.

Spectra B, C and D show the vibrational bands corresponding to the $–SO_4$ vibrations of [MMIM] [$MeSO_4$]. The perturbation of these bands seems to be consistent with the absorption of water. As water is absorbed there is an increased possibility for the IL to engage in intermolecular hydrogen bonding with the anion largely dominating. The peak maxima associated with the ν(S=O) band (*ca.* 1200 - 1000 cm^{-1}) moves to lower energy whilst the peak maxima corresponding to the ν(S-OR) band (*ca.* 900 - 700 cm^{-1}) shifts to a higher energy[20,23]. The frequency shifts observed in ATR-FTIR spectroscopy is indicative of a change in the molecules vibrational nature. The perturbation of the anionic bands can be related to interactions with atmospheric water, with intermolecular hydrogen bonding being the dominant interaction. The shift to lower energy for the S=O bond and higher energy for the S-OR bond is due to intermolecular hydrogen bonding with the [$MeSO_4$] anion. As the anion is composed of four available points for hydrogen bonding, interactions at one or more of these

points cause a change in the vibrations of each of the individual bonds that the anion is composed of. Engagement of bonding at one hydrogen bonding site will have a knock on effect to the other bonds that the anion is composed of. The redshifts observed for the SO_3 moiety of the anion would indicate direct hydrogen bonding with water and as a result of this changing environment. The S-OR bond may adjust in an attempt to balance the changing vibrational nature of the anion, hence an observed blueshift.

3.2.1 Physical Properties of [MMIM] [$MeSO_4$]

From the analysis of the ATR-FTIR spectra of [MMIM] [$MeSO_4$], it is clear that upon hydration of the IL with atmospheric water, strong changes are observed with the vibrational nature of the bonds in both the cation and anion regions. The fluctuations detailed in the ATR-FTIR analysis are coupled with changes in the physical properties of the ILs. Keeping [MMIM] [$MeSO_4$] as the IL example, small quantities of water absorbed from the atmosphere bring about changes to the physical appearance, viscosity and density of the IL. Table 3.3 and Figure 3.9 details the water content and changes in viscosity and density over the same time period as the initial IR experiment and then at 20 min intervals with a final measurement being taken at 24 hrs after exposure to the atmosphere. It is imperative to note that the measurements associated with the physical properties of the IL were recorded from a larger volume of IL. A larger volume of IL was required in order to record these measurements as the viscometer required 3 mL of IL for one measurement. A change in volume and surface area compared to that presented in the ATR-FTIR spectroscopy experiments will impact the rate and concentration of water absorbed by the IL. The main point here is to illustrate how atmospheric water impacts the physical properties of the IL.

Time	Water Content / ppm
Dry IL (0 min)	62
20 min	107
40 min	828
60 min	7180
80 min	9770
120 min	13500
140 min	13800
160 min	18700
180 min	25400
200 min	25500
220 min	29900
240 min	30500
260 min	32000
24hrs	153000

Table 3.3. Measured water content, via Karl Fischer for [MMIM] [$MeSO_4$] over a period of 260 mins exposed to the atmosphere and then again for 24 hrs exposure.

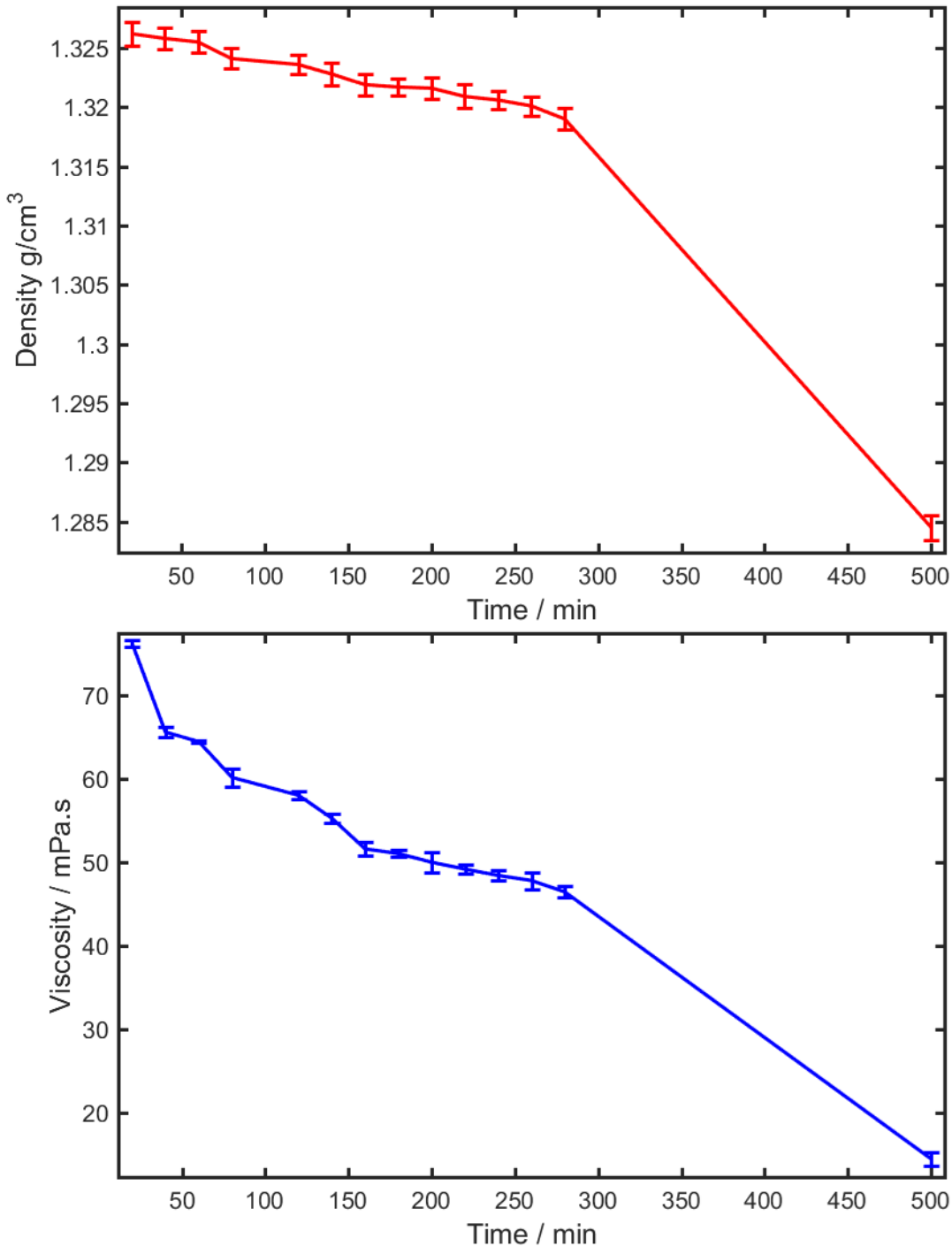


Figure 3.9. Density (Top) and Viscosity (Bottom) measurements for [MMIM] [$MeSO_4$] over a period of 260 mins exposed to the atmosphere, and then again for 24 hrs exposure.

From Table 3.3 and Figure 3.9 we see that over the time period set, there is an increase in water content. As a result of the increased water content, both density and viscosity values show an overall decrease. The density of [MMIM] [$MeSO_4$] saturated with atmospheric water are somewhat lower when compared with the dried sample; the observed difference, of 1 to 3 %, is almost negligible from the practical point of view. With regards to the viscosity of [MMIM] [$MeSO_4$], the presence of atmospheric water strongly decreases the viscosity of the IL compared to the dried sample. The point at which the initial ATR-FTIR spectroscopy experiment was terminated (100 min) a *c.a.* 25 % decrease in viscosity is observed. After 24hrs an overall 80 % decrease in viscosity is observed for the IL.

It is clear from the analysis conducted *via* ATR-FTIR spectroscopy and the measurements of the physical properties of [MMIM] [$MeSO_4$] that exposure to atmospheric water drastically changes the IL. The drastic changes observed in this section, in turn, could affect the overall chemical properties of ILs as a result of improper drying and exposure to just the atmosphere.

It is necessary to note at this point, that each IL studied for this chapter follows a near identical trend to that observed with our example IL of [MMIM] [$MeSO_4$]. Each IL displays vibrational changes in both the cationic region (predominantly at the C2-H position) and the anionic region (available hydrogen bonding sites). The anionic region is unique to each IL however, the same approach taken for assessing the example IL can be applied to each IL.

In regards to the physical properties associated with the individual ILs, each IL exhibits an overall decrease in the values for both density and viscosity as the water content is increased.

The variation between ILs can be found when assessing the water region at *c.a.* 3500 $cm^{-1.}$ The shape and positioning of the water stretch differ dependant on the IL

investigated, more specifically variation of the anion. At the beginning of this chapter Figure 3.4 displayed an overlay of the ν(O-H) stretch for each IL investigated in this thesis. The explanation provided is based on the strength of hydrogen bonding between the IL and water. The overall sequence for the strength of the hydrogen bond is as followed: [MMIM] [$MeSO_4$] < [EMIM] Cl ~ [OMIM] Cl < [MMIM] [DMP] ~ [EMIM] [Ac]. This sequence is based on the extent to which the ν(O-H) stretch is blueshifted. The further variation observed between the individual IL water systems lies in the rate at which water is absorbed. With each IL displaying varying levels of hygroscopicity it comes as no surprise that the rate of absorption would differ.

3.3 Hydration of [MMIM] [$MeSO_4$], ATR-FTIR and Raman Spectroscopy Results

The previous section determined that the vibrational structure of ILs is heavily influenced by the introduction of small quantities of water absorbed from the atmosphere. Observed changes in both the cationic region (the C-H vibrations) and anionic region (-SO_4^- vibrations) distinctly display the influence water absorption has on the IL. Changes represented well in the IR spectra are paralleled with changes in the physical properties of the IL such as density and viscosity. The observed change in both the chemical and physical properties of the IL due to varying quantities of impurities, in this case, low levels of water, can adversely affect the use of ILs. As previously stated, ILs are used in a wide range of chemical processes and the presence of minor impurities play a significant role in these processes. In order to further investigate how water interacts and affects the properties of ILs, a dilution experiment was designed and implemented. Each IL investigated was hydrated with varying concentrations of ultrapure water as displayed in Table 3.4.

Sample Number	IL : Water vol : vol %	[MMIM] [$MeSO_4$] : Water mol : mol %
1	100 : 0	100 : 0
2	95 : 5	69 : 31
3	90 : 10	51 : 49
4	85 : 15	39 : 61
5	80 : 20	31 : 69
6	75 : 25	26 : 74
7	70 : 30	21 : 79
8	65 : 35	18 : 82
9	60 : 40	15 : 85
10	55 : 45	12 : 88
11	50 : 50	10 : 90
12	45 : 55	9 : 91
13	40 : 60	7 : 93
14	35 : 65	6 : 94
15	30 : 70	5 : 95
16	25 : 75	4 : 96
17	20 : 80	3 : 97
18	15 : 85	92 : 8
19	10 : 90	1 : 99
20	5 : 95	1 : 99

Table 3.4. vol and mol % values for [MMIM] [$MeSO_4$] and water for each sample investigated.

As with the investigation into atmospheric water, [MMIM] [$MeSO_4$] has been chosen as the example IL to focus in on the changes brought about by hydration. The use of ATR-FTIR spectroscopy augmented with Raman spectroscopy and multivariate analysis allowed for an in-depth approach to analysing the binary mixtures. Both vibrational techniques present fundamental molecular vibrations at both ends of the energy range. With a change in selection rules for Raman, which requires a change in polarizability and not dipole like ATR-FTIR spectroscopy; an intensity inversion between polar and non-polar bonds is observed[29-31]. Bands such as the ν(O-H) stretch appear to be less prominent in Raman spectroscopy compared to ATR-FTIR spectroscopy where other vibrations, such as peaks associated with C-H bonds are Raman active even at 95 % water. These vibrational techniques allow semi-quantification of the percentage composition of the binary mixtures as well as the investigation into the states of the molecules at different mixture percentages.

Figure 3.10 shows the ATR-FTIR and Raman spectra of a 5 % by volume increase of water in [MMIM] [$MeSO_4$]. The ATR-FTIR spectra for this experiment display distinct features which are comparable to the spectra obtained from atmospheric absorption. For both experiments, the influence of water on the main functional groups of the IL appears near identical. For the C-H region, specifically, the C2-H present on the imidazolium ring shows an overall blueshift. The anionic functional groups, the -SO_4^- peaks, show both blue and redshifting vibrations. The changes observed here mirror that found in the initial experiment. Hydration of the IL causes intermolecular interaction between water and each counterpart of the IL. The interaction observed for the cation is less prominent compared to the anion, here the site of interaction revolves around the acidically labile proton present on the C2 position of the imidazolium ring. The interactions associated with the anion are more distinct as there are numerous sites available for hydrogen bonding.

The main difference to address between the two experiments is the rapid decrease in intensity of the IL peaks in the hydration experiment. The decrease in intensity is accredited to the hydration of the IL with increasing concentrations of water. The binary mixtures being analysed are increasingly becoming less of a binary mixture where the IL is solvating water and more of a binary mixture where water is solvating the IL. The drastic change in intensity can be accredited to less IL being sampled for each mixture as water begins to dominate. As we are observing similar changes that have already been discussed in the previous section, the main focus will now be on the differences between the two experiments. The key variance between the two experiments revolves around the higher wavenumber region, specifically the region where the water stretch prevails.

For the hydration experiment, allowing for the exchange of the initial coulombic interaction with that of an interaction with water, which may cause the observed blue prominent growth of the ν(O-H) stretching band is clearly observed, as expected as the IL is being hydrated. As the stretching band grows in there are noticeable features that change going from each concentration of water. A change in intensity, shape and position are the key features of the –OH stretch that will be further discussed from herein.

The Raman spectra for the hydration of [MMIM] [$MeSO_4$] presents complimentary information to the spectra obtained from ATR-FTIR spectroscopy. Focusing in on the regions of most interest were we observe multiple changes. The ν(O-H) stretch shows growth going from each hydration point as expected. A change in band shape is parallel to the ν(O-H) region observed in the ATR-FTIR spectra, further supporting fluctuations of the state of water during the hydration process. Raman spectroscopy allows for the -C-H region to be prominently observed at each hydration concentration. The clear changes viewed in this region is an increase in intensity as the water concentration is increased, coupled with a blueshift, specifically for the C2-H band. As

previously discussed the C2-H on the imidazolium cation is labile and acidic allowing for exchange of the initial coulombic interaction with that of an interaction with water, which may cause the observed blueshift present in both the Raman and ATR spectra. The anionic peaks display fluctuations in intensity paired with prominent shifts, with the $-SO_3$ stretches undergoing redshift and the ν(O-C) stretch undergoing a blueshift. All the spectral changes observed in Raman spectroscopy coincide with the spectral changes in the ATR.

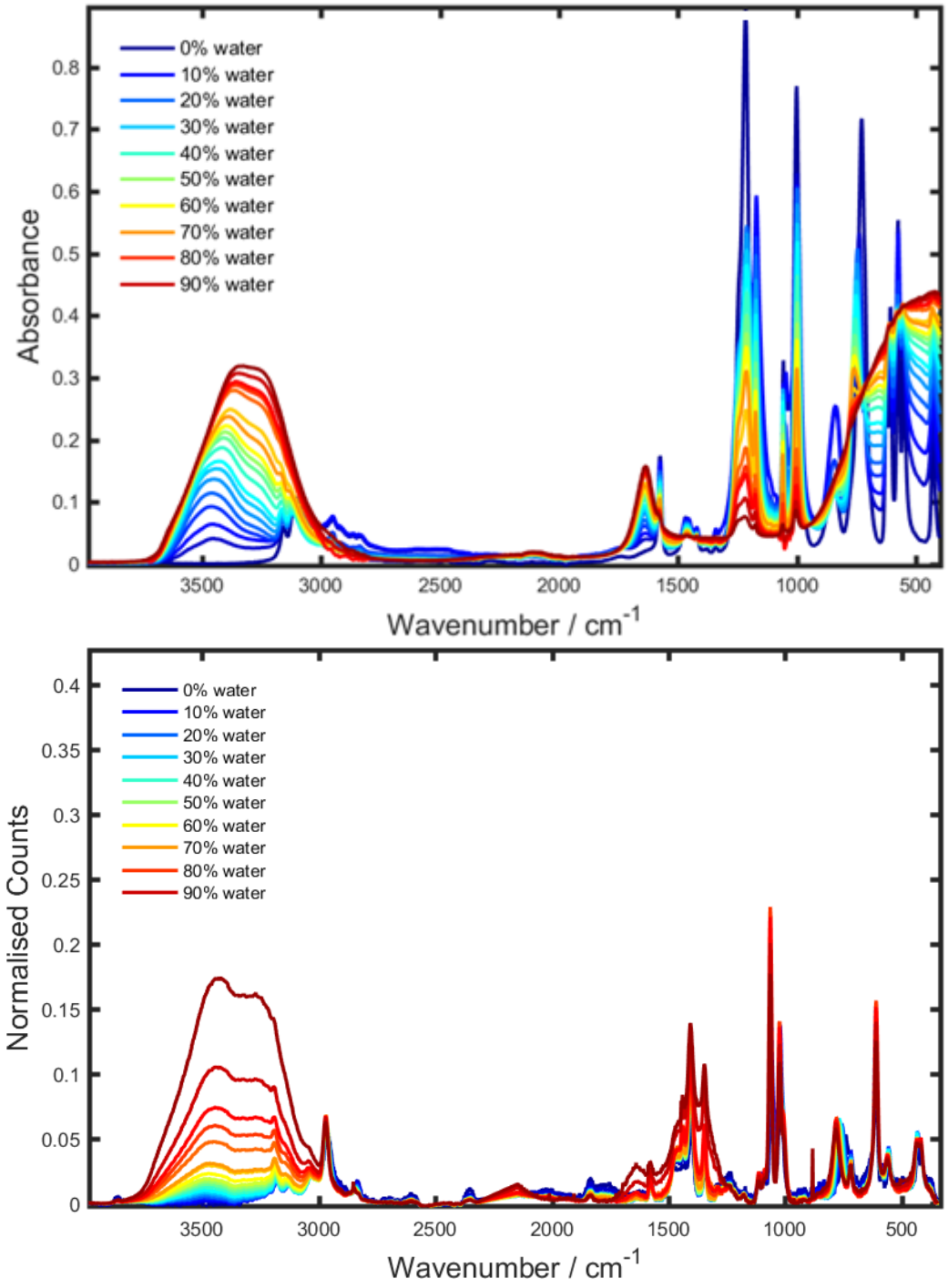


Figure 3.10. ATR-FTIR and Raman (Top and Bottom, respectively) spectra of a 5 % by volume increment (blue to red) of water in [MMIM] [$MeSO_4$].

Figure 3.11 displays the recorded ATR and Raman ν(O-H) band for each concentration of water in [MMIM] [$MeSO_4$]. An accepted growth is observed for the ν(O-H) band relative to the IL peaks, specifically the ν(C-H) modes, as the IL is being hydrated. The key spectral changes observed in this region are concerned with the shape of the band and position of the peak maxima for the ν(O-H) stretch. As previously observed with the absorption of atmospheric water, the shape of the water band differs from that of pure water. Small concentrations of water residing in the IL creates possibilities for intermolecular hydrogen bonding with the main functional groups associated with the IL. The participation in hydrogen bonding between water and the IL constrains water into a bound environment which is reflected in the IR as a change in the shape of the ν(O-H) stretch. In regards to the hydration of [MMIM] [$MeSO_4$] an increase in the concentration of water in the IL causes the shape of ν(O-H) band in the ATR spectra to evolve from a shape representative of bound water, as observed with atmospheric water to that of the shape of bulk water. Further inspection reveals distinct points of change in the shape of the ν(O-H) stretch. Changes observed at *ca.* 10 %, 30 % and 70 %. At 10% the shape of water stretch is comparable to that observed upon saturation with atmospheric water, this may be considered as the initial state that water assumes upon engaging in hydrogen bonding with the IL. The third shape of the water stretch begins at 70 %, the ν(O-H) stretch here is displayed as a broadened peak which is very representative of bulk water. The broadening of the peak is expected at this point as the binary solution is predominantly water. A conjectured second shape of the water stretch emerges around 30 % hydration. The peak maxima is slightly shifted with the peak sharpening to an extent and a small shoulder is also seen to grow in. The noticeable second shape of the water stretch may have two possible explanations. Firstly the new shape may be a separate state of water, with water now interacting with the IL distinctly differently to the initial bound water state. A secondary explanation could be that the shape is actually a combination of the initial bound state of water and

bulk water, with the result being a new shape present in the IR. Further investigation is needed to separate out the individual shapes of water as a result of hydration.

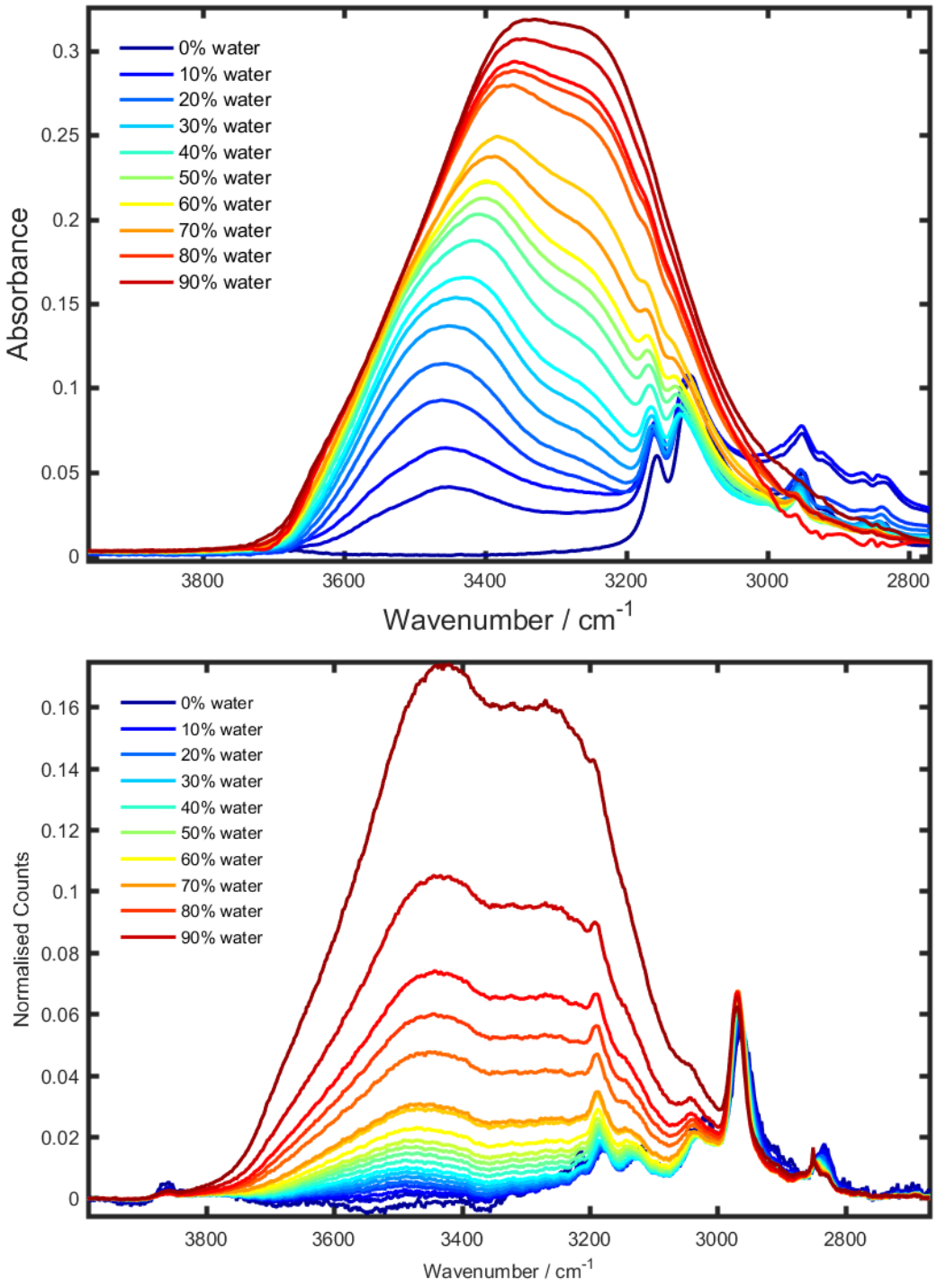


Figure 3.11. ATR-FTIR and Raman (Top and Bottom, respectively) spectra showing redshifting as the water content in [MMIM] [$MeSO_4$] is increased. The Raman spectra have been baselined and scaled and show complementary information to the IR spectra.

Figure 3.12 shows the ATR-FTIR and Raman spectra of the vibrational mode that represents a ring and sulphate combination. The predominant observation in the ATR-FTIR spectra is the blueshifting that occurs upon hydration as a result of molecular interactions with water, as seen in the atmospheric water experiments. A noticeable difference observed is an increase in the intensity at 640 - 680 cm^{-1}. Changes in this region of the ATR-FTIR spectra can be attributed to vibrational overtones combined with librations. These librations further provide evidence for hydrogen bonding with the IL. Librations in this region of the ATR-FTIR spectra are due to the restrictions imposed by hydrogen bonding of the water molecule. The noticeable feature of the Raman spectra is again a blueshifting peak with an intensity drop which can be used to support the findings from the ATR-FTIR spectroscopy experiment. The same explanation of hydrogen bonding can be used to describe the vibrational changes in the Raman spectra. Univariate analysis of the peak maxima in both spectra, shows non-linearity between 5 - 20 % water, possibly indicating an approximate concentration when the binary mixture is no longer a ‘pure’ IL. This is based on the premise that the IL no longer solvates the water present in the system and it is the water solvating the IL.

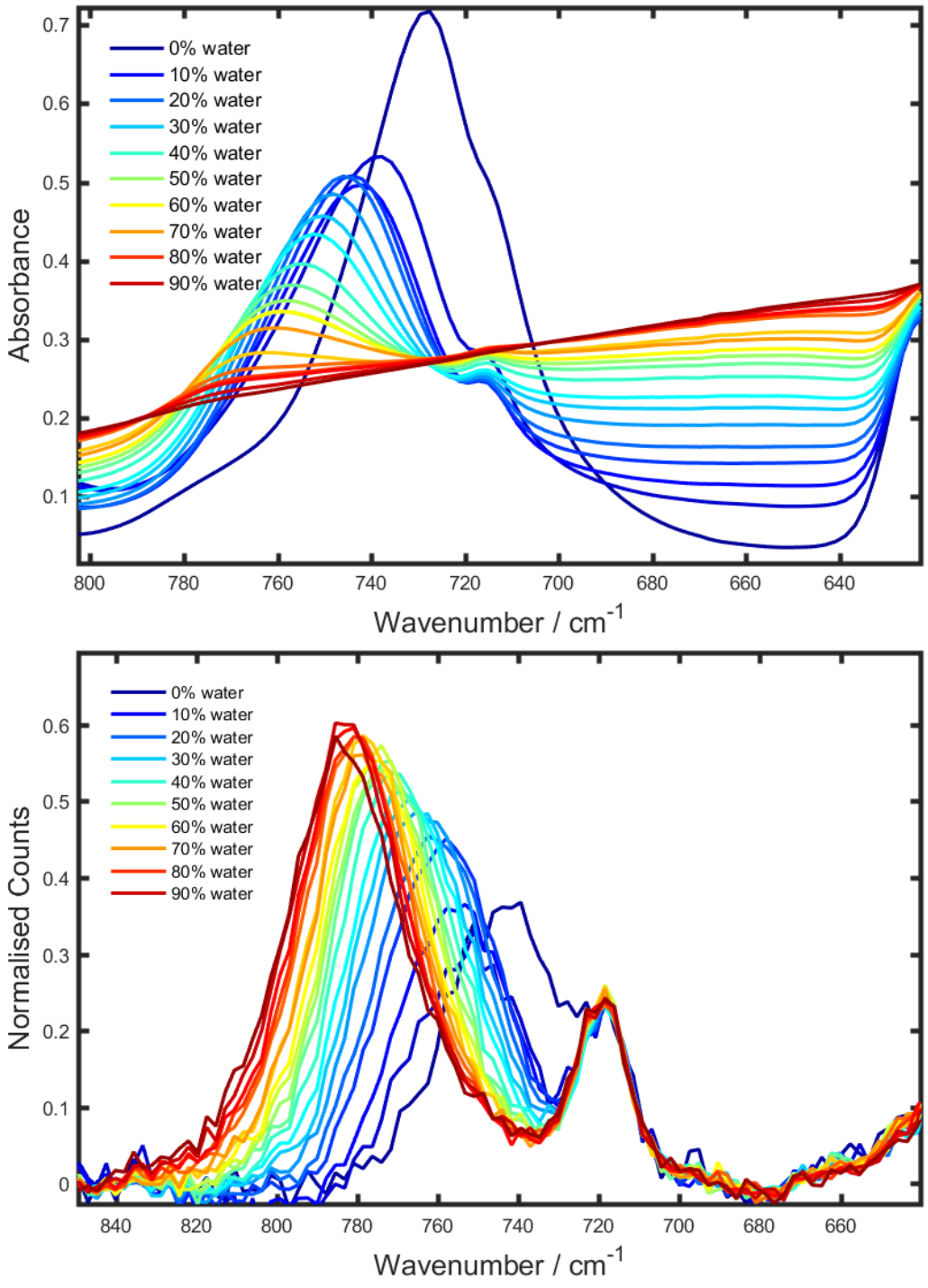


Figure 3.12. ATR-FTIR Raman spectra of -SO_4^- and ring combination band. The Raman spectra have been baselined and normalised to the integration area of the ring combination band, 700 - 730 cm^{-1}. Both spectra display the blueshifting of the -SO_4^- and ring combination band as the water content is increased.

Figure 3.13 provides supplementary evidence of both vibrational techniques complementing one another. Figure 3.13 displays the change in the peak maxima for $\nu(SO_2)$ for both the ATR-FTIR and Raman spectra. By plotting the change in peak maxima it can clearly be seen that the resulting increase in peak maxima is realised for both methods of vibrational analysis; as the percentage of water is increased. The increase in peak maxima for both techniques changes in a somewhat linear fashion at a near identical rate. With ATR-FTIR and Raman spectroscopy showing near identical results it can be assured that the use of both techniques in conjunction with one another allows for a clearer explanation of the changing system.

.

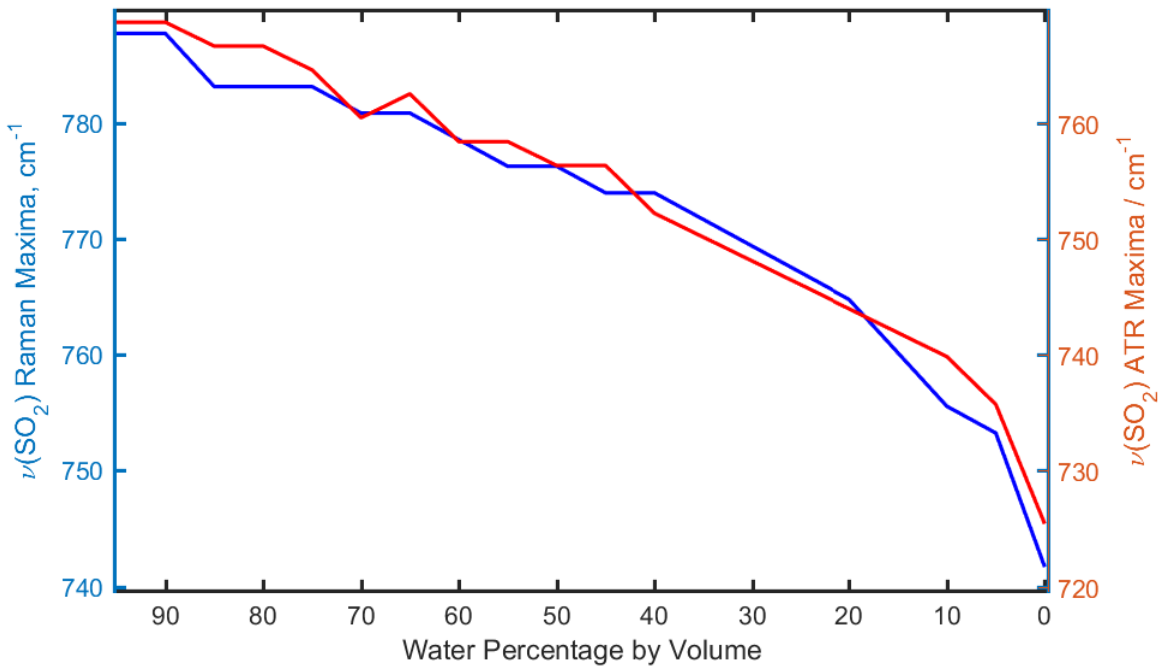


Figure 3.13. Changes in the peak maxima for the $\nu(SO_2)$ band in both the FTIR (red line) and Raman (blue line) spectra, showing an overall decrease as the percentage of water is increased.

3.3.1 Physical Properties of [MMIM] [$MeSO_4$] upon Hydration

As observed in the initial experiment, that showed [MMIM] [$MeSO_4$] absorb atmospheric water, the physical properties of the IL drastically changed. Now, upon hydration of said IL, the physical properties, viscosity and density, continue to change as the IL transitions from an environment in which the IL solvates water to a one where water solvates the IL. Figure 3.14 details measured viscosity and density parameters for the concentration gradient covered in the hydration experiment.

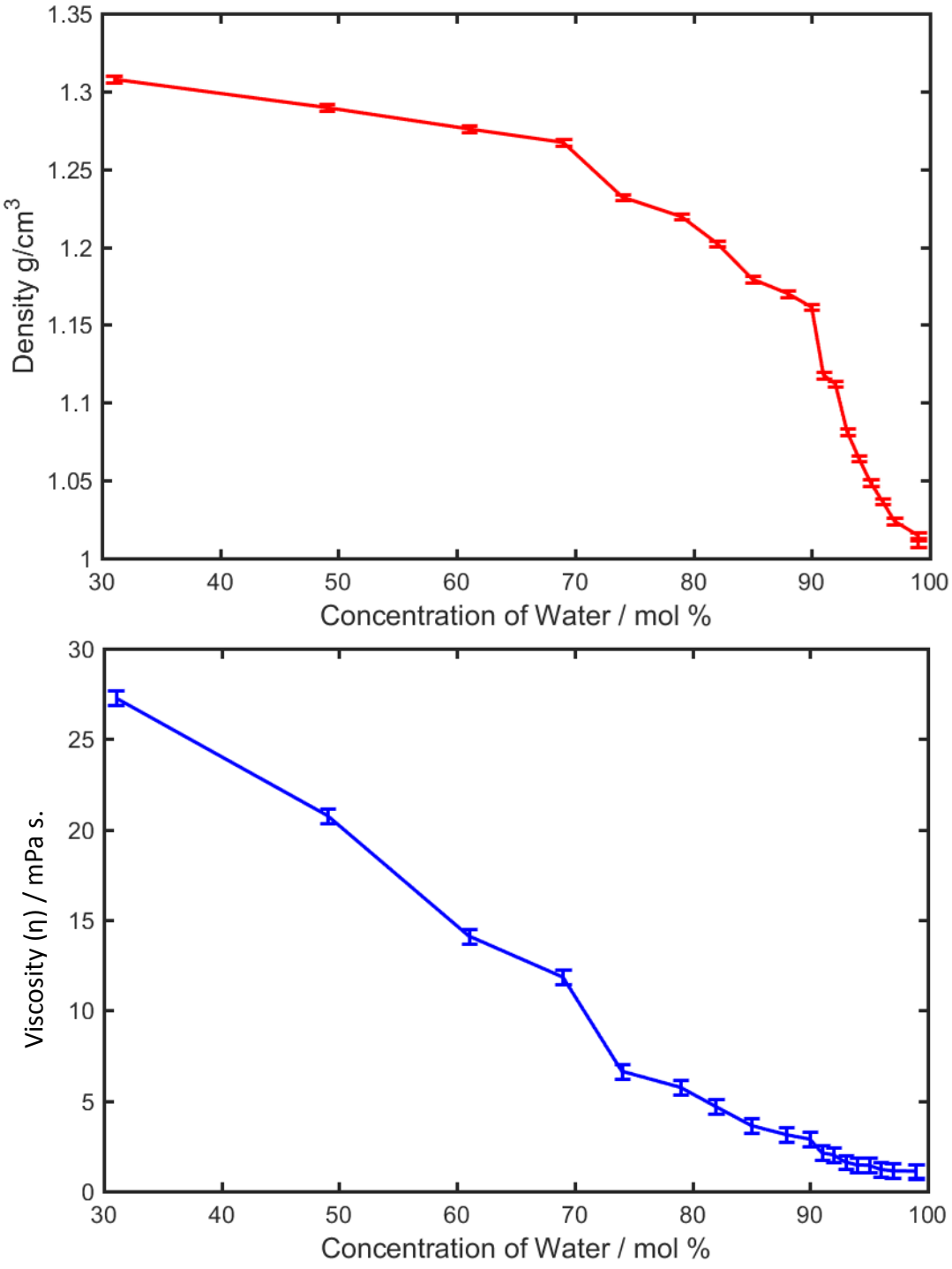


Figure 3.14. Density (Top) and Viscosity (Bottom) measurements for the binary mixtures of [MMIM] [$MeSO_4$] and water, with the mol % of the water in each mixture being detailed.

As with the initial experiment, both parameters display a decrease in value. As the concentration of water is increased the binary mixture becomes more solution like and in thus doing so, causes a drastic decrease in both the viscosity and density parameters. The noticeable change in both these parameters are expected as water is knowingly being added to the IL displacing the once tightly held IL environment for a more ionic solution like environment. With the increase in water concentration for each binary mixture, the parameters move away from that observed for pure 'dry' [MMIM] [$MeSO_4$] to be more in alignment with that observed for pure 'bulk' water.

3.3.2 Multivariate Curve Resolution Results

Univariate analysis of the peak maxima for the changing peaks present in the [MMIM] [$MeSO_4$] binary mixtures provides limited analysis. Additional analysis of this data set using multivariate approaches attains a further understanding of the systems. MCR, is described in Chapter 2, section 2.1.4. The objectives of MCR are to probe spectral variation in the binary IL and water mixtures, MCR allows for the separation of the variance into pure spectra and concentration profiles that can reveal additional information buried within the dataset[32].

With MCR the number of components is pre-defined, with the determination of the number of components achieved by comparison of the scores and loadings[32]. The number of components for the water and [MMIM] [$MeSO_4$] mixtures are represented in Figure 3.15. The cumulative percentage plot shows seven components for the water and [MMIM] [$MeSO_4$] mixtures. For this system, only the first four components were further analysed. To ensure the correct number of components were chosen for the system, MCR models with n+1 components (where n is the assigned number of components). Each component contains a percentage amount of variance and is not a repeat of any other component. For this system, the extra components contained a very small amount of total variance. The loadings and scores of the fifth component

represented a variance that was non-representative of real spectra. All of these factors suggest that mathematical artefacts are being introduced by forcing the MCR model to fit a higher number of components than the real system contained; indicating the correct number of components were originally chosen.

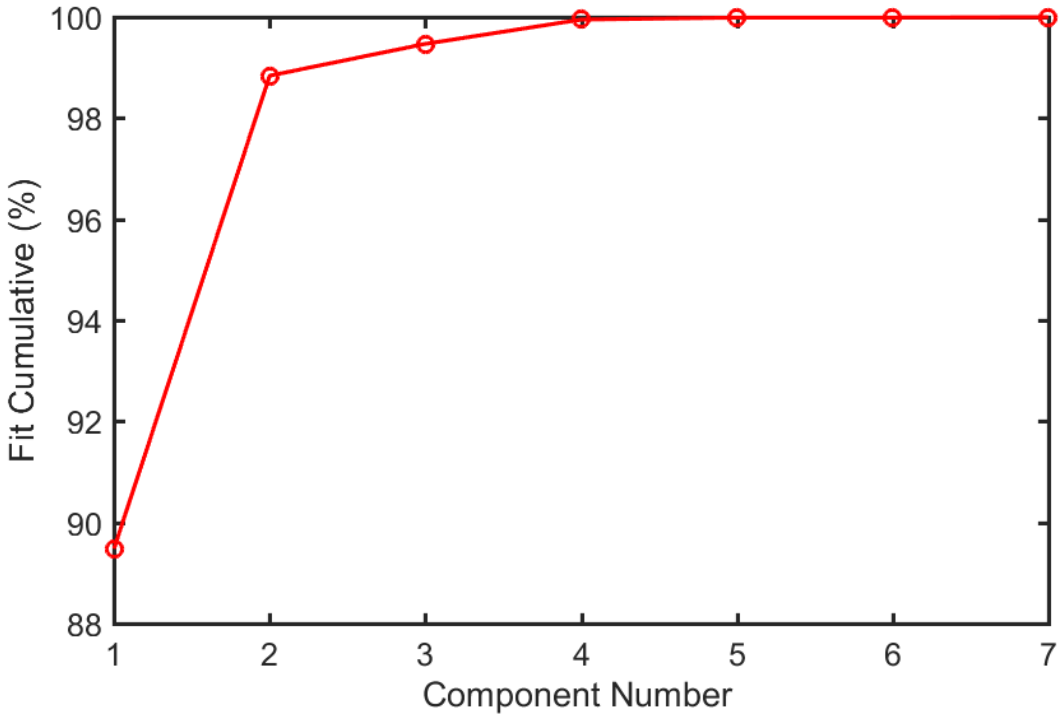


Figure 3.15. Fit cumulative % for MCR analysis per number of components for MCR of [MMIM] [$MeSO_4$] as the water content is increased, monitored by ATR-FTIR spectroscopy.

As explained in Chapter 2, the loadings and scores can be analysed to give insight into the system undergoing perturbation. It is hoped that the resulting component loading and scores are spectrally significant due to the non-negativity constraints applied during the optimisation phase of the modelling. Each loading is analysed to ensure that the response shows real chemical spectral variance.

As stated earlier in this section, the changes observed in the IL peaks for atmospheric water absorption are mirrored in the hydration experiment. The main focus of this

section has been on the higher wavenumber region, specifically the water stretch. The MCR data reflects this and displays only the higher wavenumber region. Figure 3.16 shows the scores and loadings obtained from the MCR analysis of the IR spectra of the IL [MMIM] [$MeSO_4$] doped with varying amounts of water in 5 % intervals. The number of components is predefined and are represented in the percentage fit model above.

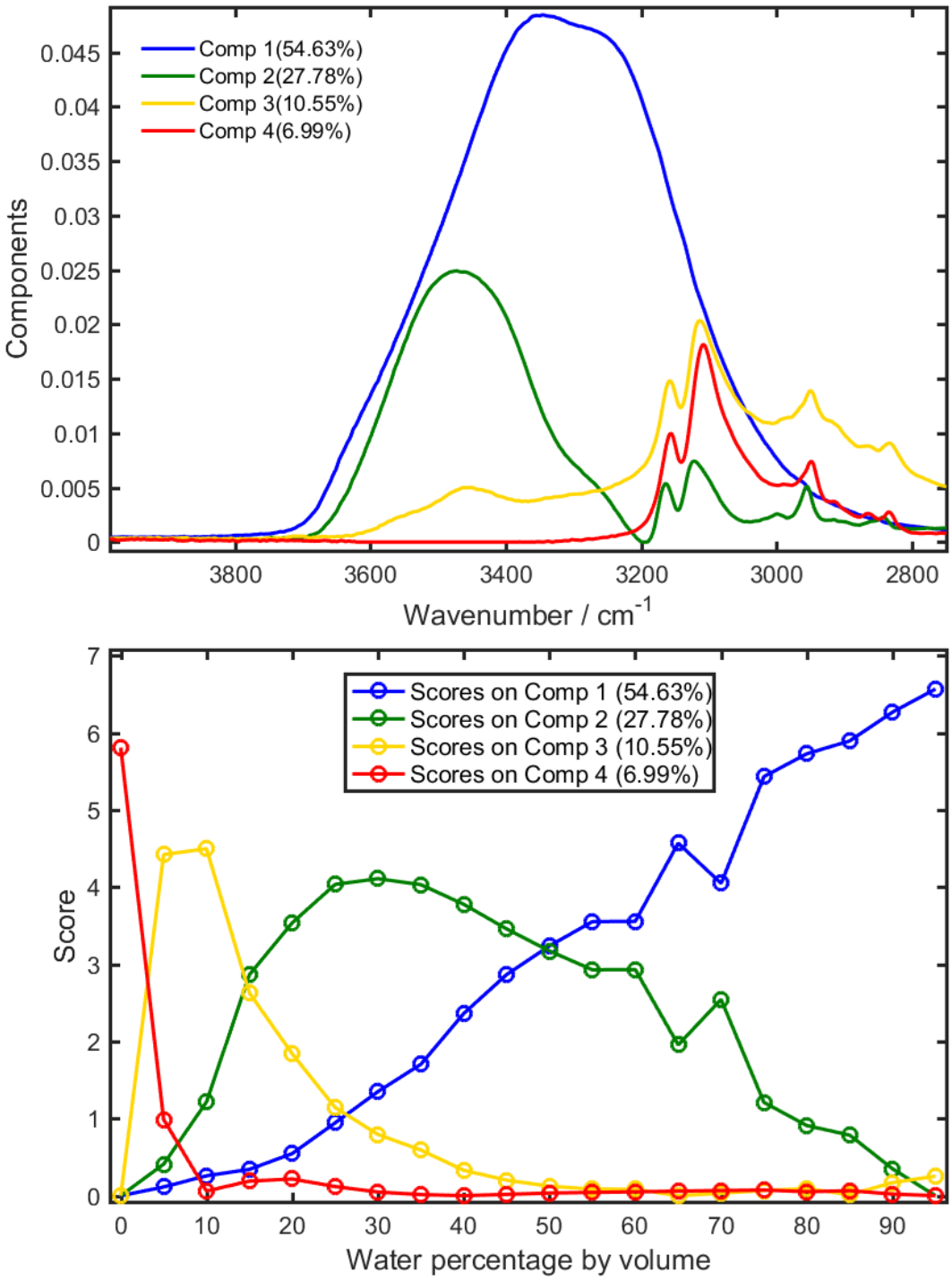


Figure 3.16. MCR components (top) and scores "concentrations" (bottom) for 0 - 95 % water in [MMIM] [$MeSO_4$] mixture monitored by ATR-FTIR, showing only the high wavenumber region.

Figure 3.16 shows a four-component MCR decomposition using an ALS algorithm of the 0 - 95 % water in [MMIM] [$MeSO_4$] mixture. The extracted pure component spectra are shown in the top of the Figure and their corresponding concentrations in the bottom section. Analysis of the MCR data reveals four components with spectral features that correspond to pure water (blue), pure [MMIM] [$MeSO_4$] (red), and [water]$_x$ [MMIM] [$MeSO_4$]$_y$ (green and yellow). The green and yellow traces show that the shape of the ν(O-H) stretching mode of water is similar to that previously observed with both the atmospheric and hydration experiments. It is assumed that the green and yellow traces are showing either the ν(O-H) stretching mode to be restricted, indicative of bound water, or a combination of bound and bulk water. The difference between the green and yellow traces is identified by a change in the wavenumber of the peak maxima.

The scores (or concentrations) show, that as the water content is increased, the blue (water) component increases and the red (IL) component decreases. With regards to the yellow and green components (IL water complex), each component increases at low water percentages proceeded by a decrease at higher concentrations. Distinct score gradient changes are observed for both components with the yellow component displaying changes at *ca.* 10 vol : vol % and 40 vol : vol % water (49 and 85 mol % respectively) and the green component displaying changes at *ca.* 30 vol : vol % and 60 vol : vol % water (79 and 93 mol % respectively).

3.4 Hydration of [MMIM] [$MeSO_4$] at Lower Concentrations of Water

Upon analysis of the results acquired for the hydration experiment, it was decided that in order to allow for a deeper insight into changing water, a more precise smaller concentration gradient would be investigated. The points of interest gained from the hydration experiment lay in the initial hydration range between 5 - 30 vol %, Table 3.5 details the mol % calculated for the new hydration experiment.

As with the previous section regarding hydration of the IL, this section will only be concerned with the higher wavenumber region. As it has been established the changes brought about in the IL regions are mirrored at a range of water concentrations. Using a smaller concentration gradient will add no new additional information for these peaks and thus are not included in this section.

Sample Number	[MMIM] [$MeSO_4$] : Water vol : vol %	[MMIM] [$MeSO_4$] : Water mol : mol %
1	100 : 0	100 : 0
2	99 : 1	89 : 11
3	97 : 3	79 : 21
4	96 : 4	71 : 29
5	94 : 6	64 : 36
6	92 : 8	58 : 42
7	91 : 9	53 : 47
8	90 : 10	48 : 52
9	89 : 11	44 : 56
10	87 : 13	40 : 60
11	85 : 15	37 : 63
12	84 : 16	35 : 65
13	82 : 18	33 : 67
14	81 : 19	31 : 69
15	80 : 20	29 : 71
16	78 : 22	28 : 72
17	77 : 23	26 : 74
18	76 : 24	25 : 75
19	74 : 26	24 : 76
20	73 : 27	23 : 77
21	71 : 29	22 : 78
22	71 : 29	21 : 79
23	70 : 30	20 : 80

Table 3.5. mol % values for [MMIM] [$MeSO_4$] and water for the detailed hydration experiment.

Figure 3.17 shows the ATR-FTIR spectra of the hydration of [MMIM] [$MeSO_4$], this experiment was tailored to explore lower concentrations of water, with the aim of separating out differing states of water. The concentration gradient for this experiment ranged from 11 - 79 mol % of the water in [MMIM] [$MeSO_4$]. Tailoring the experiment

resulted in further changes in the shape of the water band. At these lower concentrations, the appearance of the band is seemingly split into two. The effect of the lower concentrations of water on the cationic and anionic bands is mirroring what has already been observed in the previous hydration experiment and the initial experiment involving the absorption of atmospheric water.

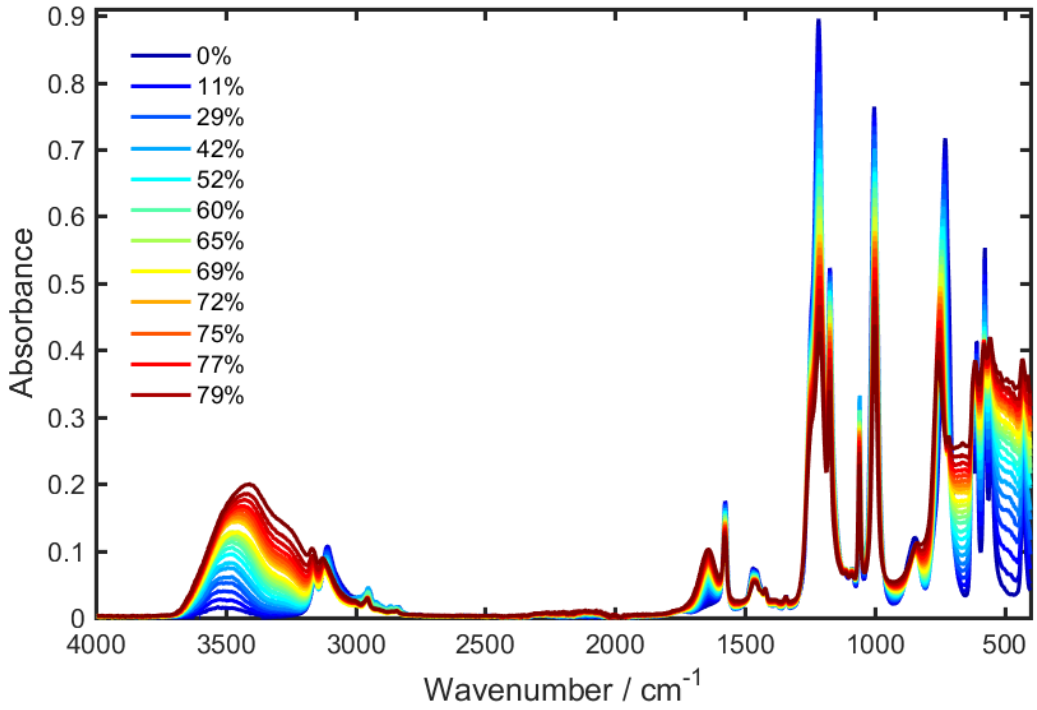


Figure 3.17. Hydration of [MMIM] [$MeSO_4$] exploring the effect of the lower concentrations of water. The amount of water by volume present in IL.

Figure 3.18 shows the ATR-FTIR spectra of the ν(O-H) stretch as the water content in [MMIM] [$MeSO_4$] is increased. Unlike the initial hydration experiment, this experiment explores the lower concentrations of water. The concentration range explored here is 11 - 79 mol % water in [MMIM] [$MeSO_4$], the major difference observed in this data is the shape of the water stretch. At lower concentrations, the water stretch appears to be present as a combination of two peaks, as the concentration of water is increased the shape no longer resembles this and has fully merged into a more broadened

singular peak. A further increase in the concentration of water sees a shoulder introduced at *ca* 3280 cm^{-1}.

The varying shapes of water throughout the experiment may be accredited to different states of water at varying concentrations. At lower concentrations, water may be assuming an initial bound state with the IL. A possible second explanation could be that the peak is a combination of the symmetric and asymmetric water stretch. As the water concentration exceeds that of the concentrations observed for atmospheric water absorption, the water shape is broadened and is more symbolic of bulk water towards the end of the experiment.

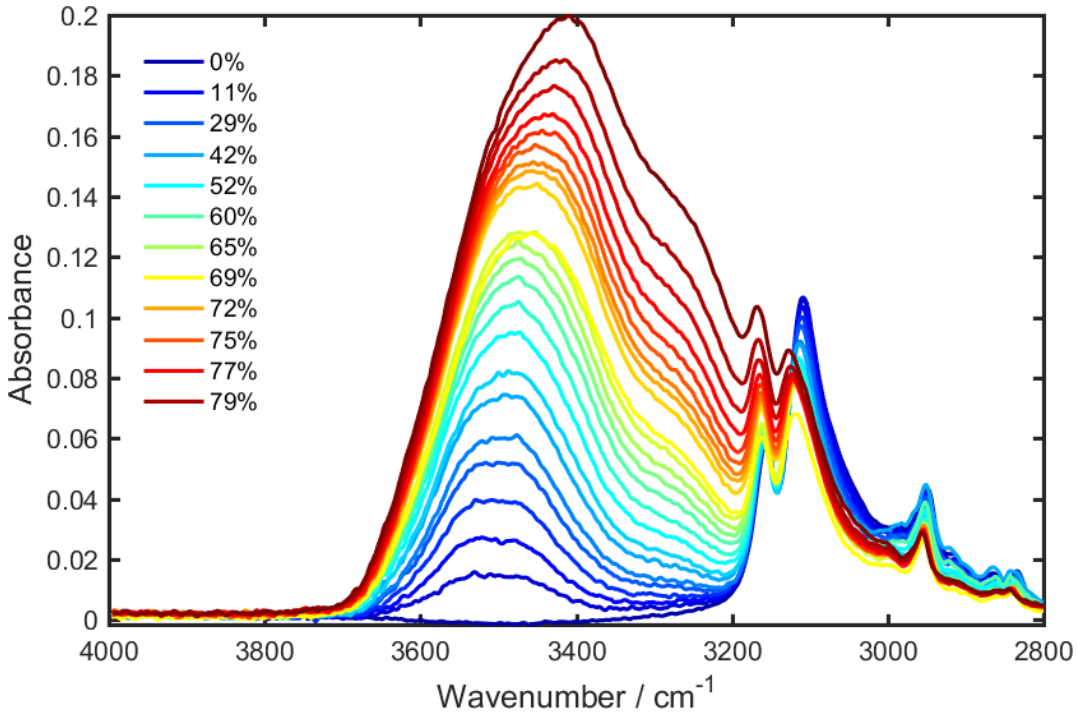


Figure 3.18. The ATR-FTIR spectra of the ν(O-H) band as the water content in [MMIM] [$MeSO_4$] is increased.

3.4.1 Multivariate Curve Resolution Results

Figure 3.19 shows a three-component MCR decomposition using an ALS algorithm in the higher wavenumber region for 11 - 79 mol % water in [MMIM] [$MeSO_4$] mixture. The extracted pure component spectra are shown in the top spectrum and their corresponding concentrations in the bottom spectrum.

Analysis of the MCR data reveals three components, all features show varying levels of water with the yellow component possessing the least amount of water and thus having a higher weighted IL contribution. The resultant components, red and blue display the ν(O-H) bending mode in two possible bound states. As previously discussed, the different water shapes presented may be a result of the asymmetric and symmetric stretch combining. Comparatively analysing the MCR data collected for this hydration experiment against the initial hydration experiment further provides evidence of a shifting peak maxima for the individual environments of water upon hydration.

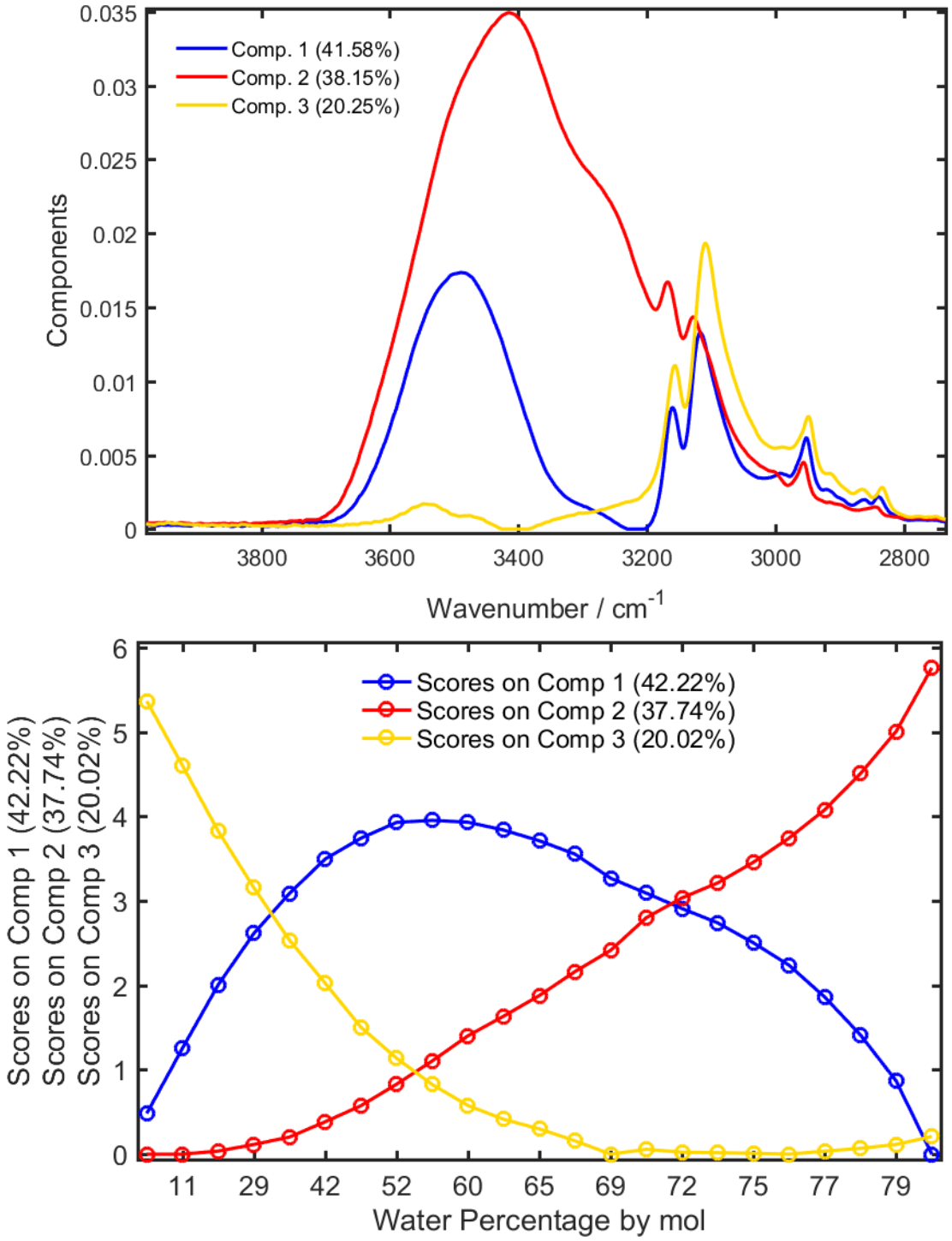


Figure 3.19. MCR components (top) and scores "concentrations" (bottom) for 11 - 79 mol % water in [MMIM] [$MeSO_4$] mixture monitored by ATR-FTIR, showing only the high wavenumber region.

The OH stretch vibration of the first component appears to display a double maxima, although this is very small. It does however, mirror what has been observed more prominently in the ATR-FTIR spectra. Further tailoring this experiment with a variance of concentration either side of the already explored concertation gradient for this mixture would allow for this two peaked feature to be observed more prominently. The blue and red components are indicative of bound water that has already been observed in the initial hydration experiment.

The scores (or concentrations) show, that as the water content is increased, the red component (hydrated [MMIM] [$MeSO_4$]) increases and the yellow component (most representative of pure [MMIM] [$MeSO_4$]) decreases. With regards to the blue component (IL water complex), there is an observed steady increase as the concentration of water is increased. The blue component begins to decrease *ca.* 56 mol % of water. The blue component shows a steady gradient change as the red component decrease, indicative of water transitioning from one state to another. Relating this back to the first hydration experiment, we observe a similar effect in relation to bound water, we see an increase in the gradient of the component aligned with bound water followed by a decrease in gradient as the component representative of bulk water comes into effect.

The hydration experiments have further confirmed the changes associated with the IL bands as a result of interactions with water. A combination of ATR-FTIR spectroscopy, Raman spectroscopy and multivariate analysis has provided further probing into the binary mixtures and has revealed varying states of water at specific concentrations of water.

3.5 Conclusion

This chapter has utilised ATIR-FTIR spectroscopy augmented with Raman spectroscopy to investigate the effect of varying concentrations of water on ILs. Multivariate techniques were used in conjunction to study the effects further. The data collated indicates that IR spectroscopy is a powerful technique to monitor spectral changes observed at the varying concentrations levels of water. In this chapter [MMIM] [$MeSO_4$] has been used as the example IL to illustrates the many changes observed to both components of the binary mixture as the water component is varied.

The initial focal point of this chapter explored the effect of atmospheric water on a range of ILs, of which greatly differed in terms of the anionic counterpart. The chapter focused in on [MMIM] [$MeSO_4$], as this IL best displayed the changes brought about by water. [MMIM] [$MeSO_4$] has a multitude of sites that readily interact with water and in doing so produce sharp, clear peaks in the IR spectra. [MMIM] [$MeSO_4$] was exposed to atmospheric water in order to gain a general impression on the influence on the vibrational nature of the main functional groups associated with this IL. The immediate conclusions drawn from this experiment showed that the major spectral changes were associated with the anionic counterpart of the IL, suggestive of stronger intermolecular interactions between atmospheric water and the sulphate anion. The cation was slightly impacted with the main point of interaction occurring at the C2-H stretching band situated on the imidazolium ring. The perturbation observed here was a blueshifting of the peak maxima coupled with an intensity decrease. The blueshifting was attributed to the changing coulombic environment associated with the hydration of the IL as atmospheric water was being absorbed. As the concentration of water increased within the IL, possible aggregation may be occurring between the anion and cation causing an increase in the distance between the two ions. A change in the distance between the counterparts weakens the original coulombic interaction

between the ions and thus allowing the acidically labile C2-H to be more localised within the cation.

With regards to the anionic counterpart, there are multiple changes observed in the bands associated. As it has been stated the sulphate anion has a number of points of interaction that will readily engage in intermolecular hydrogen bonding with water as it is absorbed. The most prominent changes in the ATR-FTIR spectra that we observed for the sulphate anion were concerned with the $-SO_3$ symmetric and asymmetric stretches as well as changes in the ν(O-C) stretch. Both the symmetric and asymmetric $-SO_3$ stretches display a redshift, with the peak maxima associated with these bands shifting to lower energy. Such changes in the IR spectra are associated with a change in the vibrational environment and can be linked to direct hydrogen bonding of the $-SO_3$ division of the anion. Interaction at the oxygens may cause elongation of these bonds and hence bring about the weakening of said bonds and thus cause a shift to lower energy. The ν(O-C) stretch displays the opposite, the perturbation associated with this band is that of a shift to higher energy, denoted a blueshift. The blueshifting nature of this band may be explained as a knock on effect caused by hydrogen bonding occurring at the other oxygen bonds. As a result of one half of the anion engaging in hydrogen bonding with water, a redistribution in charge density may lead to the strengthening of the C-O bond to counteract the changes brought about from the interaction with atmospheric water.

Further conclusions were drawn upon continued hydration of [MMIM] [$MeSO_4$]. Hydrating the IL with varying concentrations of water showed a number of spectral changes. Prominent changes were observed in the water region. A difference in intensity and shape coupled with slight shifts are all features that are indicative of changing water. Water is seemingly progressing from varying states of bound water through too bulk water, where the concentration of water solvates [MMIM] [$MeSO_4$]. The Raman spectroscopy data compliments the data attained from ATR-FTIR

spectroscopy. The changes displayed in the cationic and anionic regions are mirrored in both vibrational techniques. The –C-H groups in the dialkyl-imidazolium ring however, are predominantly present in the Raman spectra compared to the ATR-FTIR spectra. Raman spectroscopy data shows that at high concentrations of water (95 % water) the C-H region is preserved, allowing for the changes to be clearly analysed. The shape changes for the ν(O-H) band are observed which supports the findings from the ATR-FTIR spectra.

MCR analysis further probes the data obtained *via* ATR-FTIR and Raman spectroscopy. MCR allows for spectral variance to be separated out and the overall dataset simplified into pure spectra and 'scores' which can be seen as concentration profiles. MCR was applied to the hydration experiments in an attempt to further explore the higher wavenumber region and to probe the variance in the ν(O-H) stretching vibration. The conclusions that can be drawn from the MCR data is that for the initial hydration experiments, the system is separated out into four components. Two of the components represent that of pure IL and that of pure bulk water. The other two components observed represent the IL water bound complex, the separation of the system out into two components that represent this suggests that the two complexes may be different. The difference between the two may be associated with the conformation water is in or the way in which the water is hydrogen bonding to the IL. Noticeable changes in these two components at 10 and 30 % by volume resulted in a secondary hydration experiment that explored this region. The MCR results for the secondary hydration experiment showed a three-component system. The first component represents that of the near pure IL. The other two components representing either different bound water states or a combination of a bound water state and the separation of the ν(O-H) stretch into its asymmetric and symmetric stretching mode.

Overall this chapter has provided an insight into the impact that varying concentrations of water have on the vibrational nature and physical properties of a selection of ILs. It

has also showcased the powerful nature of vibrational spectroscopic techniques and multivariate analysis when probing IL binary systems.

3.6 References

1. J. G. Huddleston, A. E. Visser, W. M. Reichert, H. D. Willauer, G. A. Broker and R. D. Rogers, *Green Chem*. **2001**, *3*, 156 - 164.

2. Wasserscheid, P.; Welton; T. Ionic Liquids in Synthesis; Wiley-VCH: Weinheim, Germany, 2008.

3. J. P. Hallett and T. Welton, *Chem. Rev*. **2011**, *5*, 3508 - 3576.

4. K. Noack, A. Leipertz and J. Kiefer, *J. Mol. Struct*. **2012**, *1018*, 45 - 53.

5. L. Cammarata, S. G. Kazarian, P. A. Salter and T. Welton, *Phys. Chem. Chem. Phys.* **2001**, *3*, 5192 - 5200 .

6. Richard P. Swatloski, Scott K. Spear, and John D. Holbrey and R. D. Rogers, *J. Am. Chem. Soc.* **2002**, *18*, 4974 - 4975.

7. D. L. Minnick, R. A. Flores, M. R. Destefano and A. M. Scurto, *J. Phys. Chem. B*. **2016**, *32*, 7906 - 7919.

8. V. H. Paschoal, L. F. O. Faria and M. C. C. Ribeiro, *Chem. Rev*. **2017**, *117*, 7053 - 7112.

9. J. Grondin, J.-C. Lassègues, D. Cavagnat, T. Buffeteau, P. Johansson and R. Holomb, *J. Ram. Spectrosc.* **2011**, *42*, 733 - 743.

10. C. Roth, S. Chatzipapadopoulos, D. Kerlé, F. Friedriszik, M. Lütgens, S. Lochbrunner, O. Kühn and R. Ludwig, *New J. Phys*. **2012**, *14*, 105026.

11. K. Fumino and R. Ludwig, *J. Mol. Liq.* **2013**, *192* ,1 - 9.

12. K. Fumino, A. Wulf and R. Ludwig, *Angew Chem.* ***2008***, *20*, 3830-3834.

13. T. Yamada, Y. Tominari, S. Tanaka and M. Mizuno. *J. Phys. Chem. B*. **2017**, *121*, 3121 - 3129.

14. K. Fumino, K. Wittler and R. Ludwig, *J. Phys. Chem. B*. **2012**, *31*, 9507 - 9511.

15. Q. R. Sheridan, W. F. Schneider and E. J. Maginn, *J. Phys. Chem. B*. **2016**, *49*, 12679 - 12686.

16. C. Hampton, D. Demoin, Vibrational Spectroscopy Tutorial: Sulfur and Phosphor, (2010) Available from: https://faculty.missouri.edu/~glaserr/8160f10/A03_Silver. pdf.

17. A. Dahi, K. Fatyeyeva, C. Chappey, D. Langevin, S. P. Rogalsky, O. P. Tarasyuk and S. Marais, *RSC Adv.* **2015**, *5*, 76927 - 76938.

18. C. H. Giammanco, P. L. Kramer, D. B. Wong and M. D. Fayer, *J. Phys. Chem. B*. **2016**, *44*, 11523 - 11538.

19. B. L. Bhargava, Y. Yasaka and M. L. Klein, *ChemComm*. **2011**, *47*, 6228 - 6241.

20. J. Kiefer, J. Fries and A. Leipertz. *Appl. Spectrosc.* **2007**, *61*, 1306 - 1311.

21. J. E. S. J. Reid, R. J. Gammons, J. M. Slattery, A. J. Walker and S. Shimizu, *J. Phys. Chem. B*. **2017**, *3*, 599 - 609.

22. C. A. Hall, K. A. Le, C. Rudaz, A. Radhi, C. S. Lovell, R. A. Damion, T. Budtova and M. E. Ries, *J. Phys. Chem. B*. **2012**, *42*, 12810 - 12818.

23. Q. G. Zhang, N. N. Wang and Z. W. Yu, *J. Phys. Chem. B*. **2010**, *14*, 4747 - 4754.

24. Y. Jeon, J. Sung, C. Seo, H. Lim, H. Cheong, M. Kang, B. Moon, Y. Ouchi and D. Kim, *J. Phys. Chem. B*. **2008**, *15*, 4735 - 4740.

25. B. Stuart. *Infrared spectroscopy*; J. Wiley and Sons: Chichester, United Kingdom, 2009.

26. S. R. Ryu, I. Noda, C. H. Lee, P. H. Lee, H. Hwang and Y. M. Jung, *Appl. Spectrosc*. **2011**, *4*, 359 - 68.

27. Q.-G. Zhang, N.-N. Wang and Z.-W. Yu, *J. Phys. Chem. B*. **2010**, *14,* 4747 - 4754.

28. J. Kiefer, J. Fries and A. Leipertz, *Appl. Spectrosc*. **2007**, *61*, 1306 - 1311.

29. S. Cha, M. Ao, W. Sung, B. Moon, B. Ahlström, P. Johansson, Y. Ouchi and D. Kim, *Phys. Chem. Chem. Phys.* **2014**, *16*, 9591 - 9601.

30. D. K. Singh, S. Cha, D. Nam, H. Cheong, S.-W. Joo and D. Im, *ChemPhysChem*. **2016**, *19*, 3040 - 3046.

31. N. E. Heimer, R. E. Del Sesto, Z. Meng, J. S. Wilkes and W. R. Carper, *J. Mol. Liq*.

2006, *124*, 84 - 95.

32. A. de Juan & R. Tauler, *Crit. Rev. Anal. Chem.* **2006**, *36*, 163 - 176.

33. martin.chaplin@btinternet.com, m. (2018). Water absorption spectrum. [Online] www1.lsbu.ac.uk. Available at: http://www1.lsbu.ac.uk/water/water_vibrational_spectrum.html [Accessed 26 Jul. 2018].

Chapter 4

Vibrational Spectroscopic Analysis of Molecular Solvents and Ionic Liquids

4.1 Introduction

This thesis is concerned with the investigation into impurities within ILs and how their presence can impact the properties of ILs. The focal point of this chapter is centred around the investigation into the impact residual molecular organic solvents may have on the spectroscopic characteristics of a range of ILs.

The use of vibrational techniques allows for the probing of the IL solvent systems in order to establish how these binary systems are influenced dependent on the components they are composed of. As discussed in Chapter 1, molecular solvents are widely used in the synthesis, preparation and purification of ILs[1-3]. The IL synthetic process sees the use of both miscible and immiscible solvents, which have the potential to be retained in the final IL to varying extents [2,4]. Table 4.1 details the range of ILs and molecular solvents investigated in this chapter. The ILs investigated in this chapter were all alkyl imidazolium-based ILs. The choice of IL was one that was aligned with their use in many processes, such as dissolution chemistry, catalysis and lubricants[5-7,33]. The molecular solvents investigated herein were chosen based on their extensive usage alongside ILs and due to their assistance in the synthetic procedure for ILs.

Ionic Liquids			
[MMIM] [DMP]	[MMIM] [$MeSO_4$]	[EMIM] [Ac]	
[EMIM] Cl	[EMIM] [BF_4]	[OMIM] Cl	
Molecular Solvents			
ACN	DCM	Hexane	Toluene
Miscible	Miscible	Immiscible	Immiscible

Table 4.1. The range of ILs and molecular solvents used to generate the binary mixtures that are investigated within this chapter

ILs are deployed for a wide range of chemical processes. One particular area of chemistry which sees a wide interest in the use of ILs is the area of electrochemistry. ILs have the potential to be used as safe solvents for Li^+ ion batteries and dye-sensitized solar cells[7-8]. Chapter 1 discussed the general properties of ILs showing them to have low conductivity and high viscosity[9-10]. The addition of molecular additives such as molecular solvents has been explored within the literature in order to design safer IL electrolytes that simulate all the required properties for efficient electrochemical usage (i.e., low viscosity, electrochemical stability, and non-flammability)[11-12].

Numerous groups have shown how the use of solvents as additives impact the viscosity, density and conductivity of ILs. Wang *et al.* investigated the physical properties of a range of imidazolium-based ILs with a selection of miscible solvents, including ACN and DCM[13]. It was shown that upon dissolution with the IL, the overall

bulk properties were altered. As a result of the combination of the IL with the solvent additive, both the density and viscosity of the IL showed an overall decrease for each solvent used. The same observations were made by Seddon *et al*. who further confirmed that the introduction of a solvent additive brought about a decrease in both viscosity and density and caused an increase in the conductivity of the ILs investigated[14]. Abdallah *et al.* and Guerfi *et al.* both demonstrated that the non-flammability of an electrolyte is maintained with the incorporation of organic solvents up to a concentration of 20 - 40 wt % in ILs[15-16]. Both groups observed no flammability in [Tf_2N] based ILs doped with ACN, DCM and propylene. Molecular solvents as additives permit the improvement of ILs for suitable solid electrolyte interfaces whilst their transport properties are also advantageously enhanced. The reduction in viscosity triggers an increase in the diffusion and mobility of IL. Disruption to the original coulombic interaction of the IL will cause an increase in the number of charge carriers in the system. A change in any of these parameters is seen to be highly beneficial for electrochemistry[16-17].

Supplementary NMR spectroscopy data on ILs indicate a large contribution of ionic association. The addition of molecular solvent additives, more specifically polar solvents causes IL solvent interactions to develop at the expense of the original IL - IL interactions. The addition of additives here aims to increase ion dissociation all of which benefits the use of these binary mixtures. Tokuda *et al.* showed that the addition of 1, 2-dichloroethane and propylene carbonate positively impacted the ionic association of ammonium-based ILs with a range of anions[18]. Comparison of the molar conductivity of the IL solvent mixtures and the pure ILs at the same viscosity showed that the more polar the solvent is, the greater the salt dissociation.

As a result of changing physical properties of the IL due to the addition of solvent additives, as seen in the literature,[12,16,18] this chapter aims to investigate if the presence of these molecular additives causes a change in the vibrational nature of a range of

ILs. As seen with the investigation into IL water binary systems, vibrational spectroscopy is a highly useful analytical technique in order to easily identify any changes caused to the IL system as a result of potential interaction between the individual components that make up a mixed system. Applying the same process as seen for the IL water mixtures, to the now solvent IL binary mixtures, this chapter aims to identify potential interactions that may be occurring between the ILs and the range of solvent additives presented. Unlike water the interactions between the IL and the range of solvent additives may not be exclusively hydrogen bonding, the added variable of differing polarities and miscibility poses new challenges when identifying potential interactions in the systems.

4.2 Preparation of Solvent Ionic Liquid Binary Mixtures

Binary mixtures were prepared for each solvent and IL, which saw the mixing of each component to form a 1 : 1 by volume solution. Both ACN and DCM were completely miscible with the IL generating a homogenous binary solution. Hexane and toluene were seemingly immiscible with the IL however, a scintilla of these supposed immiscible solvents has the capacity to be retained within the IL medium and thus potentially bring about changes to the system.

Two ATR-FTIR spectroscopy experiments were set up in parallel to explore the solvent IL systems. The first experiment saw the ATR-FTIR spectroscopy measurements for the solvent IL systems conducted within a glovebox. The aim here was to remove the influence of atmospheric water on the systems and to solely identify changes brought about due to the influence of just the molecular solvents. The second experiment saw the ATR-FTIR measurements for the solvent IL systems conducted in the presence of the atmosphere. There were multiple aims for conducting this secondary experiment.

The main aims were to understand if the presence of atmospheric water created a means for competition in terms of interaction with the IL, if a tertiary system would be created or if water would completely dominate the system similar to that of the binary systems in Chapter 3.

As the initial ATR-FTIR spectroscopy experiment was conducted within a glovebox, all ILs were dried under schlenk conditions (50°C, $x10^{-6}$ bar) to remove any water absorbed through the synthetic process. All solvents were obtained as anhydrous from solvent towers and further dried under a slightly reduced pressure in order to ensure that IL solvent binary systems would be void of any water. Although the water content of each solvent was below that of the detection limit in IR, spectra were collected to confirm the lack of water. The absence of water allows for any changes to be solely identified as ones brought about by interactions between the molecular solvents and the IL.

4.3 Impact of Miscible solvents on Ionic Liquids

The miscibility of ILs with common molecular solvents is dependent on the anionic and cationic combination of the IL. Ultimately the properties of the IL will determine the solubility of these solvents with molecular solvents[14,19]. Most common ILs readily mix with ACN and DCM due to the polarity of these solvents and their ability to readily interact with the constituents of most ILs. The prevalent use of these two solvents in the preparation, synthesis and purification of ILs makes them the perfect candidates for investigation[1]. The use of these solvents in conjunction with ILs allows for small concentrations to be retained within the IL system. As seen for water, preservation of unwanted reagents can have a pronounced impact on the properties and spectroscopic characteristics of the IL[20-22].

This chapter will use [MMIM] [DMP] as the example IL to illustrate the effect that both miscible and immiscible solvents have on the vibrational nature of ILs. This section will focus on the spectral relationship between [MMIM] [DMP] and the miscible solvents of ACN and DCM.

Figure 4.1 shows an overlayed ATR-FTIR spectra of the 1 : 1 vol : vol % binary mixture of [MMIM] [DMP] and ACN The pure IL, [MMIM] [DMP] and pure ACN have been overlayed in order for comparison and to ensure that any spectral changes observed are not just a simple linear combination of the two components. All spectra were collected under glovebox conditions. The Intensities of the ACN peaks have been enhanced by a factor of five to illustrate where each individual peak associated with this solvent falls.

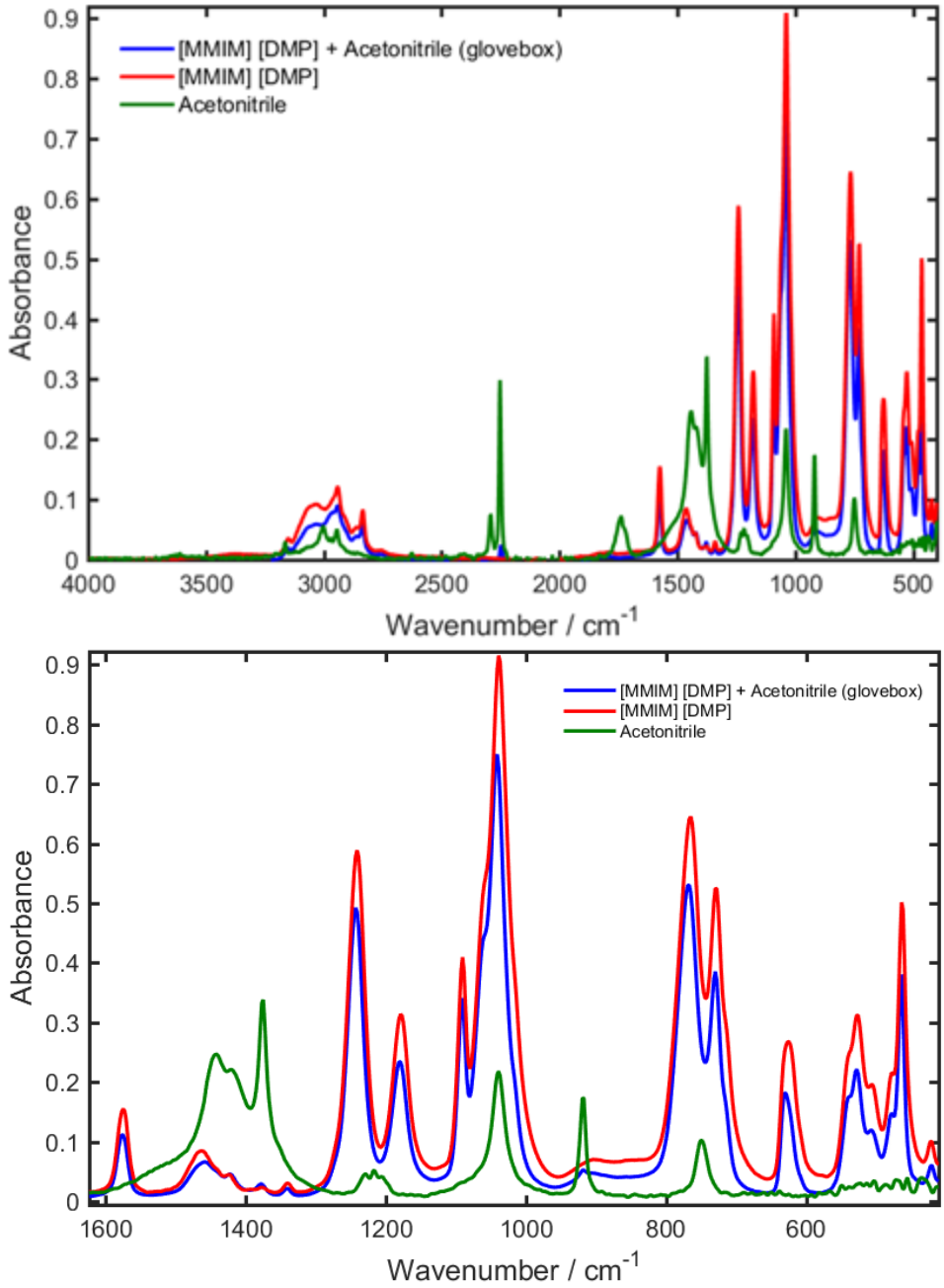


Figure 4.1. ATR-FTIR spectra of MMIM] [DMP] ACN binary mixture overlayed with pure [MMIM] [DMP] and ACN (top spectra) a zoomed in version displaying the fingerprint region of the IL (bottom).

From initial observations of the overlayed spectra, the IL ACN mixture does not seem to display any spectral variance. The bottom spectra provide a zoomed in version of

the fingerprint region, showing bands and features associated with the anion, providing further insight into potential interactions of the binary mixture. Analysis of the fingerprint region shows a general decrease in the intensity of the IL peaks. This is expected for a binary component mixture, as the IL is now occupying less of the sampling volume and hence displaying a decrease in absorbance.

The intensity drop observed for the binary mixture is also coupled with small changes in the peak maxima for a selection of the anionic peaks. The prominent points for interaction on the anion are the phosphorous oxygen moieties. Both the ν(P=O) and ν(P-O) stretches that appear at 1239, 768 and 729 cm^{-1} respectively,[23,24] shift slightly to higher energy, indicating that theses anionic bands may be strengthening as a result of ACN as an additive. It is imperative to note that for these anionic peaks there is overlap with peaks associated with ACN component. The overlap of peaks may enhance the anionic peaks and cause small shifts which may be identified as shifts due to interactions or as the linear combination of the two components. Selecting non-overlapping peaks for analysis of the binary mixtures is of importance when attempting to distinguish between real interactions and simple linear combinations. For the [MMIM] [DMP] ACN binary mixture, the peak of choice to establish this falls at 625 cm^{-1}. It is clear that this peak displays a slight blueshift to higher energy suggesting that there is an interaction between the two components of the system.

Figure 4.2 shows comparative spectra between the initial and final spectrum recorded for the [MMM] [DMP] ACN binary mixture. In comparison, the spectra for the final measurement of the ACN doped system resembles that of the spectra for the original pure [MMIM] [DMP] suggesting that the system has reverted back to that of pure IL. Upon further inspection of the spectra, there is seemingly a loss of ACN from the system, which causes the reversal of the spectral changes initially observed. The loss of ACN may also be used to explain the differences observed in the intensity of the peaks. Differences in absorbance as previously discussed, arise due to a difference in

concentration[25-26]. The drop in intensity for the initial spectra for the ACN doped IL can be attributed to the IL occupying less of the sampling volume. As the ACN is lost form the binary mixture, the IL is then re-concentrated and hence a regression back to the original intensity observed for the pure IL.

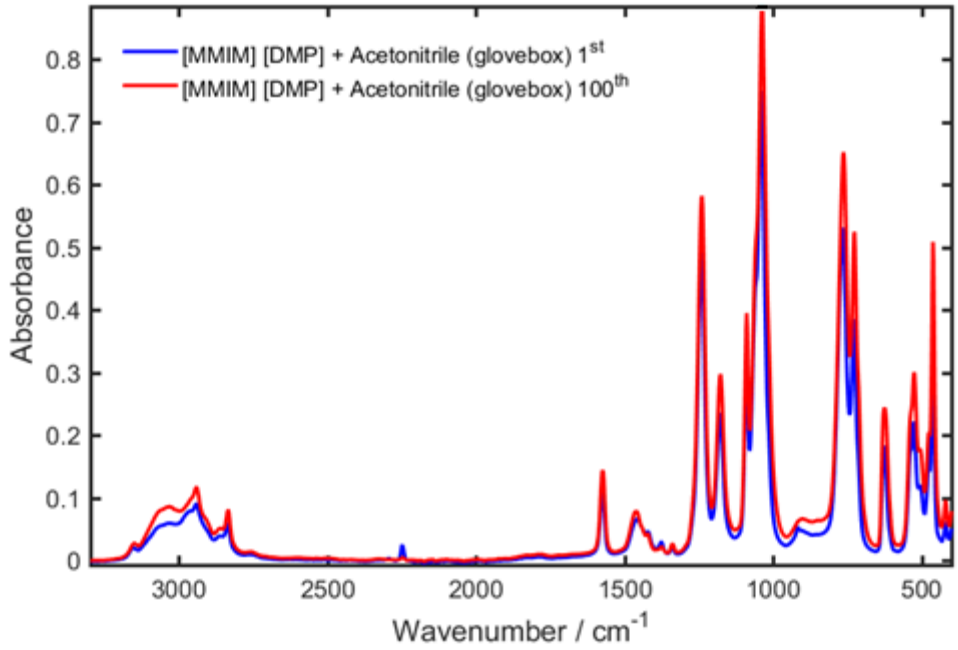


Figure 4.2. ATR-FTIR spectra of first (blue line) and last (red line) measurement for the [MMIM] [DMP] ACN binary mixture, recorded under glovebox conditions.

This loss of ACN from the system may further be analysed by inspecting the changing ν(C≡N) feature associated with ACN [27]. The feature is clearly present at the initial point of spectral collection, as the ATR-FTIR spectroscopy experiment runs its course the peak diminishes and is no longer detectable by ATR-FTIR spectroscopy. The most likely suggestion is that the ACN has evaporated from the binary system and was not engaged in significantly strong interactions. Figure 4.3 shows the change in absorbance of the ν (C≡N) peak for the duration of the ATR-FTIR spectroscopy experiment. The overall trend is negative, showing that ACN is being evaporated from the system over the 100 mins of the experiment.

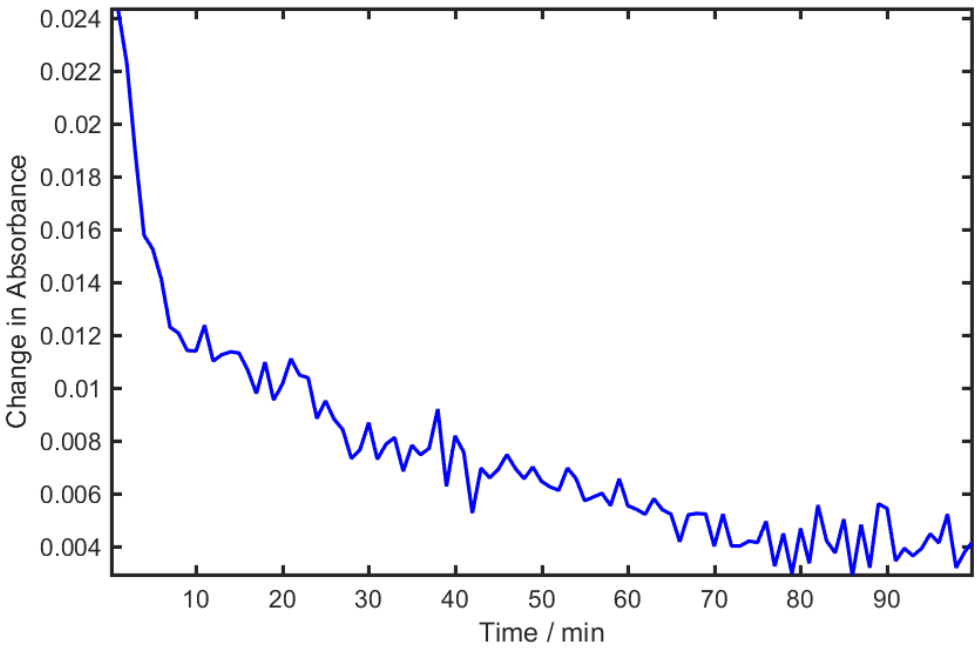


Figure 4.3. The rate of change in absorbance of the ν (C≡N) feature for the [MMIM] [DMP], ACN binary mixture.

The same analytical procedure was carried out for the investigation of the DCM binary mixtures. Figure 4.4 shows an overlayed ATR-FTIR spectra of the 1 : 1 vol : vol % binary mixture of [MMIM] [DMP] and DCM. The pure IL, [MMIM] [DMP] and pure DCM have been overlayed for comparison. Much like that of the other solvents explored in Table 4.1, this overlay approach is assumed in order to identify any spectral changes arising as a result of a changing system as opposed to a linear combination of the two components. Initial analysis of the top spectra reveals significant spectral variance. Compared to the ACN IL binary mixture, a drastic decrease in the intensity is observed for all IL peaks associated with the DCM IL doped system, with this being maintained throughout the entirety of the ATR-FTIR spectroscopy experiment. There is no regression back to the original IL spectrum compared to the observation with the ACN doped system. Enhanced spectral variance can be seen in the lower wavenumber

region, where many of the anionic bands reside. The bottom spectra of Figure 4.4 provide a zoomed in version of the fingerprint region of which contains the vibrational bands associated with the anion of the IL. Analysis of the functional groups associated with the anion reveals minor blueshifts similar to that observed for the ACN doped systems. Both the ν(P=O) and ν(P-O) stretches shift slightly to higher energy, again indicating that theses anionic bands may be strengthening as a result of DCM being present as an additive. The ν(P=O) and ν(P-O) stretches fall at 1239, 768 and 729 cm^{-1} respectively, analysis of the spectra shows that for these peaks, there is an overlap with the peaks associated with DCM. The blueshifts observed for the DCM IL binary mixture may be shaped by these underlying bands, in order to gauge if these shifts are in fact due to potential interactions with DCM, it is imperative to analyse any peaks absent of underlying solvent peaks. The peak at 626 cm^{-1} is one of the peaks with no association with solvents peaks. The peak is blueshifted to higher energy suggesting that the presence of DCM is impacting the vibrational nature of [MMIM] [DMP]. The blueshift to higher energy observed for anionic bands may be a result of the DCM component interrupting anionic and cationic coulombic interactions, causing each counterpart to be pushed further away from one another. A reduction in the original coulombic IL interaction would create the strengthening of the individual bonds for each moiety, which in turn would be represented by a blueshift in the ATR-FTIR spectra.

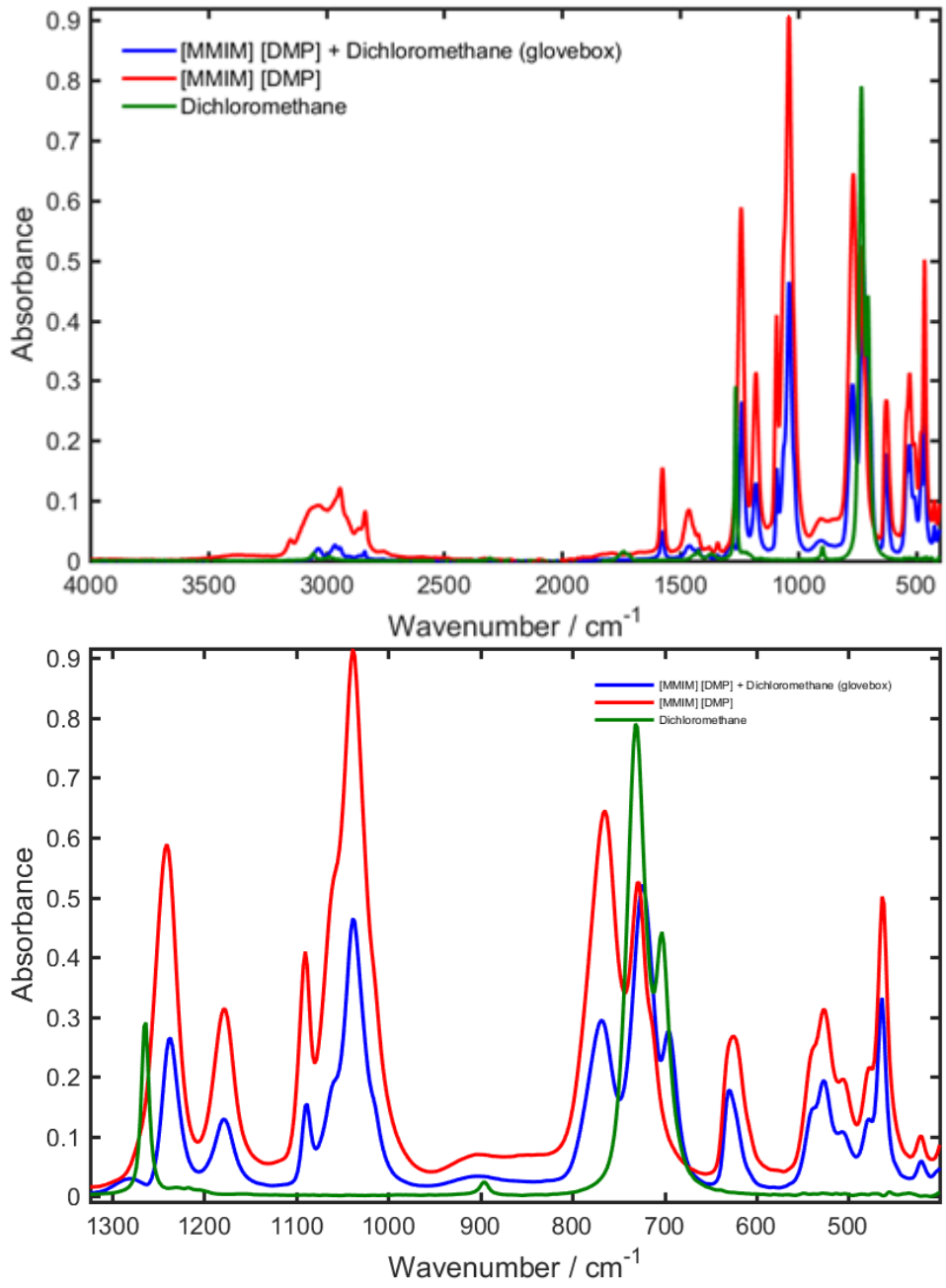


Figure 4.4. ATR-FTIR spectra of [MMIM] [DMP] doped with DCM overlayed with pure [MMIM] [DMP] and DCM (top spectra) a zoomed in version displaying the anionic region of the IL (bottom).

As discussed above, analysis of the relative intensities of the peaks associated with the DCM IL binary mixtures shows a lowering of intensity compared to the pure [MMIM]

[DMP]. The change in intensity can be explained due to a lowering of the concentration of the IL in the sampling volume of the mixture as it is diluted with DCM. Comparing the changing intensity with that of the ACN IL binary mixture, it can be noted that unlike the regression back to the original intensity observed for the ACN mixtures; the DCM mixtures do not display this. The lowered intensity is maintained throughout the entirety of the ATR-FTIR spectroscopy experiment. With the ACN mixtures, it was shown that the ACN was being evaporated from the system, one would expect the same to occur with DCM. DCM is much more volatile compared to ACN, with the former having a boiling point of 39.8°C and the latter 81.6°C,[28] it would thus be expected that DCM would be evaporated much more readily than ACN. Figure 4.5 displays an enhanced section of the spectra for the DCM IL binary mixture. The vibrational bands shown are that of the ν(P-O) stretches. It can be seen that for the DCM IL binary mixture (blue spectra) the shoulder at 695 cm^{-1}, as a result of the DCM component, is still present in the 100th spectra recorded. The intensity of the shoulder is lowered in the final spectra however, its presence indicates that the DCM is seemingly being retained within the IL more effectively compared to the ACN mixtures. The retention of DCM in the IL may be due to DCM and the IL interacting with one another. The presence of the chlorine moiety in DCM may interact with the IL at the C2-H position, similar to that of a chloride anion based ILs, but to a lesser extent. A potential extension of the timing of the experiment may see the system revert back as DCM is eventually evaporated off.

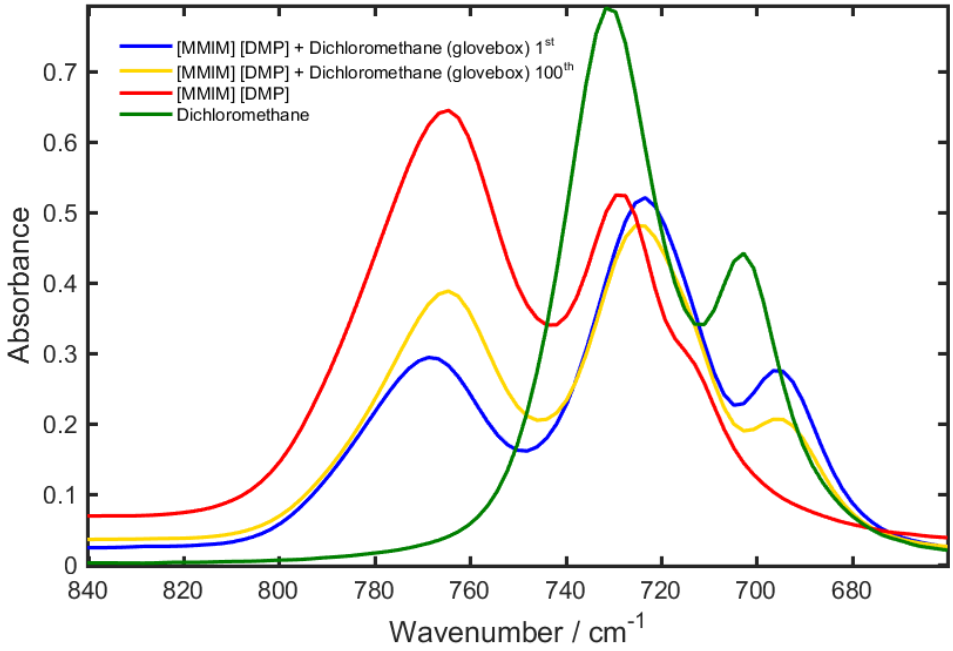


Figure 4.5. Enhanced ATR-FTIR spectra of the DCM [MMIM] [DMP] binary mixture, showing the retention of DCM within the mixture for the entirety of the experiment.

4.4 Impact of Immiscible solvents on Ionic Liquids

Along with the use of miscible solvents in IL preparation, immiscible solvents are also widely utilised. The use of immiscible solvents can mainly be found in the purification process for ILs, such as solvent extractions and recrystallizations[29-30]. Although the term immiscible is used to describe these solvents in conjunction with ILs, they aren't completely immiscible. It has been shown that low levels of immiscible solvents can be dissolved and retained within an IL. One main example of this is the retention of water within hydrophobic ILs such as [EMIM] [Tf_2N]. It has been shown that due to washing with water, [EMIM] [Tf_2N] will retain < 50 ppm of water[31].

As with the miscible solvents, the same experimental and analytical procedure was utilised. Figure 4.6 shows the initial and final ATR-FTIR spectra for [MMIM] [DMP] doped with hexane (top spectra) and toluene (bottom spectra) displaying overlay spectra of the pure IL [MMIM] [DMP] and pure solvent for comparative purposes. Unlike ACN and DCM that show some spectral variance when comparing the pure and doped spectra both hexane and toluene exhibit near zero spectral variance. The only change observed is a minute change in intensity of the peaks, but not significant enough to suggest a vast change in the concentration of the IL. It can thus be said that the immiscible solvents fail to change the vibrational nature of the pure IL and no changes are detected by utilising ATR-FTIR spectroscopy.

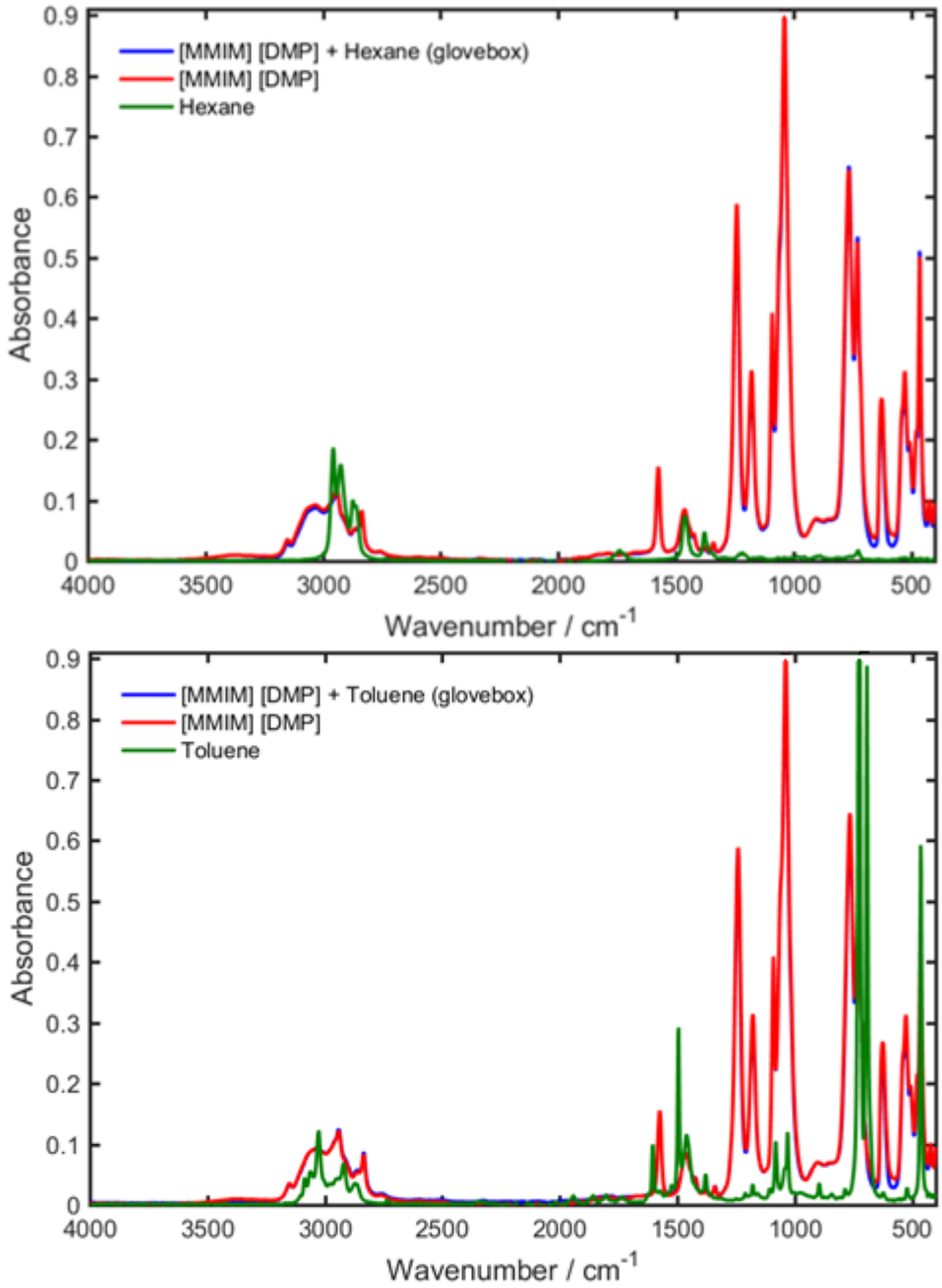


Figure 4.6. ATR-FTIR spectra of [MMIM] [DMP] doped with hexane (top) and toluene (bottom) overlayed with pure [MMIM] [DMP] and the corresponding pure solvent.

It is clear that the amount of spectral variance brought about from common molecular solvents compared to that brought about by atmospheric and bulk water is somewhat minimal. The difference in interactions may be accounted for by examining the polarity

and solubility of the additives present in the IL binary mixtures. Comparing and contrasting the polarities of the additives thus far investigated, it can be noted that the polarity scale can be viewed as, water > ACN > DCM > toluene > hexane, this is based on the dielectric constant and dipole moment of each additive[31]. Although heavily related, it would be more correct to use the dipole moment for each solvent when analysing the binary mixtures in this chapter, as the IL is solvating the solvent. Table 4.2 details the values for each parameter and the classification of each solvent.

Solvent	**Dielectric Constant**	**Dipole Moment**	**Solubility**	**Classification**
Water	80	1.85 D	Miscible	Polar protic
CAN	37	3.92 D	Miscible	Polar aprotic
DCM	9.1	1.60 D	Miscible	Borderline polar aprotic
Toluene	2.3	0.36 D	Immiscible	Non-polar
Hexane	1.8	0.00 D	Immiscible	Non-polar

Table 4.2. Solvent parameters and classifications of the solvents used within this thesis.

Comparison of the results obtained from the vibrational spectroscopic experiments to the already existing investigations carried out by Tokuda *et al.* may further explain the systems[18]. Tokuda *et al.* carried out NMR studies into how more polar solvents cause a greater salt dissociation in the IL system and thus display more prominent solvent IL interactions at the expense of the original IL - IL interactions [18]. It is clear from the ATR-FTIR spectroscopy experiments that the results seemingly match up with the

NMR findings. Water being the most polar solvent used creates the most disturbance and hence the most prominent changes to the vibrational nature of the IL system. ACN and DCM seem to show similar results, with slight perturbations being observed in the ATR-FTIR spectra. There is a slight deviation here, as one would expect ACN to display more prominent perturbations, or at least compared to DCM. The reasoning behind this may be the fact that DCM has the halogen moiety which may play a role in creating further interactions with the IL, specifically at the C2-H position. The final two solvents investigated are toluene and hexane, of which are both non-polar solvents and display no significant perturbations in the ATR-FTIR spectra.

Further ATR-FTIR spectroscopy research into polar solvents that lie between the polarities of water and ACN should further corroborate the NMR findings made by Tokuda *et al.* and follow the pattern that is being suggested in this chapter[18]. Further examples of this can be seen in research conducted by Noack et al., who investigated the impact of ethanol and methanol on the vibrational nature of a range of ILs[32]. Ethanol and methanol are both polar aprotic solvents that are less polar than water and more polar than ACN and DCM. Both solvents are miscible with most common ILs and effectively change the vibrational nature of ILs through the engagement of intermolecular hydrogen bonding. Noack *et al.* illustrated the extent of change for both alcohols and compared that against the changes brought about by water[32]. It was shown that water exhibited the greatest perturbation in the ATR-FTIR spectra followed by MeOH and then EtOH. The observations indicate that the strength of the molecular interactions between the IL and the solvent additive decreases from water to EtOH. Relating this back to the solvent polarity, this is in agreement with Tokuda's NMR results. Both MeOH and EtOH exhibit dipole moments, with the alcohols fitting in the sequence in the following way, H_2O > MeOH > EtOH. The positioning in the sequence reflects the solvents individual ability to form interactions involving hydrogen atoms[32].

4.5 Ionic Liquids, Molecular Solvents and Water Tertiary Mixtures

Alongside the ATR-FTIR spectroscopy experiment conducted within the glovebox, a secondary ATR-FTIR spectroscopy experiment was conducted under atmospheric conditions. By carrying out the ATR-FTIR spectroscopy experiment out in the atmosphere, the once binary mixture of solvent and IL has the ability to progressively transition into a tertiary mixture of solvent, IL and atmospheric water as time passes. As noted several times in this thesis ILs are hygroscopic and will readily absorb atmospheric water. The introduction of a solvent additive into the IL system will impact the extent of this absorption of atmospheric water. The investigation into both miscible and immiscible solvents allows for a variety of explanations as to how the absorption of water is influenced due to a multicomponent system. This section will explore the impact that creating tertiary mixtures has upon each component present in the mixture.

The initial binary mixtures of solvent and IL were prepared in the same fashion to that for the glovebox experiment. Each IL and solvent was dried prior to mixing and stored in a desiccator before each measurement. A small sample of the solvent IL mixture was placed on the ATR-FTIR under ambient conditions (RT, atm) and allowed to absorb atmospheric water over a period of 100 min. The results for each solvent investigated can be seen below.

In order to evaluate the changes for each tertiary mixture, it is necessary to compare and contrast the spectra obtained against the results obtained in Chapter 3. Figure 4.7 displays the ATR-FTIR spectra for the binary mixture of atmospheric water and [MMIM][DMP], which was recorded over a period of 100 mins in order to allow sufficient absorption of water. As discussed in Chapter 3, the absorption of atmospheric water fundamentally changes the way in which the IL interacts. The availability of additional

hydrogen bonding sites paired with a reduced coulombic interaction between ionic constituents all contributes to the observed changes detected in the ATR-FTIR spectra. Chapter 3 provides an in-depth look at this. The main focus in this section is to compare the original data against the data recorded for the tertiary mixtures and isolate points of change.

The major point of change identified from investigating IL water binary mixtures was that of the anionic region, which is displayed in the lower wavenumber region of the ATR-FTIR spectra. Figure 4.7 shows an enhanced section of the initial ATR-FTIR spectra, showing only the fingerprint region and highlighting the changes brought about as a result of the absorption of atmospheric water. Clear shifts for the peak maxima of the anionic bands and drops in intensity are all observed for the anionic bands. It will therefore be the anionic section that will be focused in on when concerning the tertiary mixtures. This region presents a diverse range of changes and thus provides a point for comparative analysis.

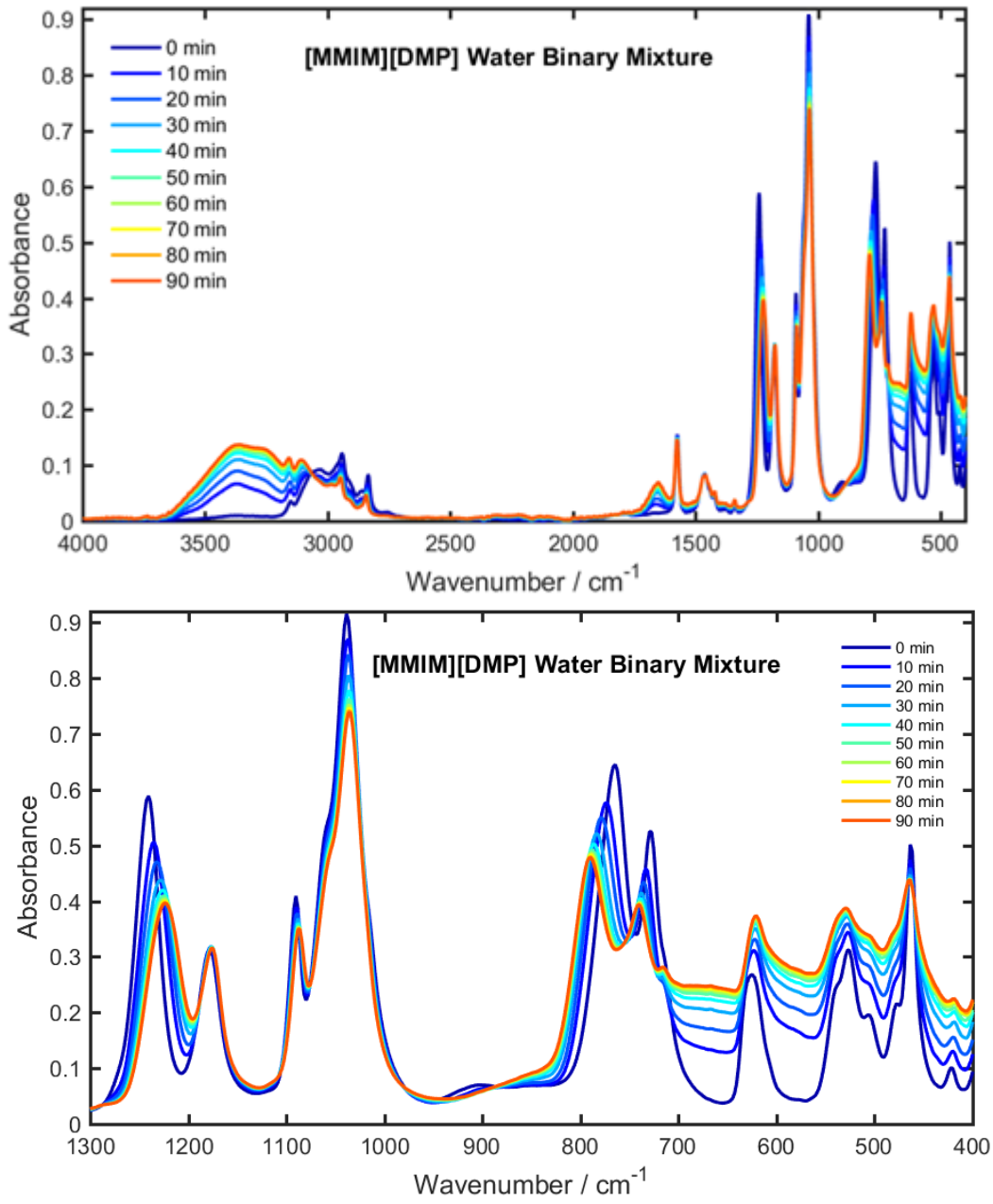


Figure 4.7. ATR-FTIR spectra of [MMIM] [DMP] upon the absorption of atmospheric water over a period of 100 min (blue to red) with a zoomed in spectra of the anionic region (bottom).

Figure 4.8 shows the fingerprint region of the tertiary mixtures for the miscible and immiscible solvents studied in this chapter. It is clear that there are noticeable changes being observed as a result of a now three-component mixture. Comparatively analysing the spectrum for each solvent against that of the binary IL water mixture allows for any significant changes to be observed. Each solvent spectrum has been overlayed against the spectrum obtained for the binary mixture of IL and water.

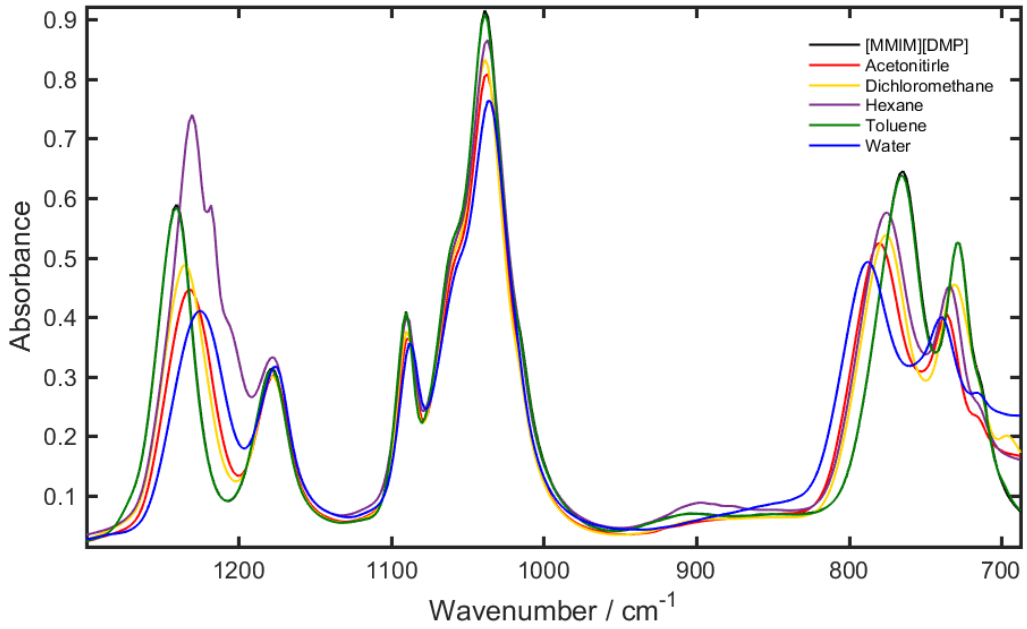


Figure 4.8. A zoomed in ATR-FTIR spectra of the anionic region (1300 - 700 cm^{-1}) for [MMIM] [DMP] tertiary mixtures.

The major spectral variance can be seen for the ν(P=O) and the symmetric and asymmetric ν(P-O) bands, which appear at 1239, 768 and 729 cm^{-1} respectively. It is important to note that the spectrum for the toluene tertiary mixture is near identical to the original dry [MMIM] [DMP] with the spectrum showing a scintilla of change. This suggests that toluene does an effective job of preventing water from being absorbed

by the IL, this may be due to toluene within the tertiary mixture rearranging itself to form a biphasic layer that sits above the IL.

The symmetric and asymmetric ν(P-O) bands for each solvent tertiary mixture (excluding toluene) are redshifted to lower energy coupled with decreasing intensity. The extent of the shift varies for each solvent with water showing the greatest shift, followed by ACN, DCM and then hexane. A similar observation is made for the ν(P=O) band, however, due to the overlapping of hexane and IL peaks present in this area, the spectrum for the hexane tertiary mixture is offset and dominated by solvent peaks. The ν(C-O) band at 1039 cm^{-1} shows little variations in comparison with the other anionic peaks. There is a slight redshift to lower energy coupled with a decrease in intensity.

In order to explain the changes observed for each solvent, it is imperative to note that as a result of having a mixture of solvent, IL and atmospheric water there is now a system in which new interactions are possible. There is a potential for IL - solvent, IL - water and solvent - water interactions or a mix of the three that can all contribute to the changes within the system. Identifying the exact interaction that is occurring is difficult as the tertiary systems are fairly complex. What can be deduced is that the interactions occurring at the anionic bands are represented by a redshift and a decrease in intensity. If this change is representative of an IL - water interaction, similar to that seen for the binary mixture, then what can be determined is that the strength of the hydrogen bond is impacted as a result of the additional solvent component present in the system. The strength of the hydrogen bond from the observation in the ATR-FTIR spectra would be ordered in the following way, water binary mixture > ACN tertiary mixture > DCM tertiary mixture > hexane tertiary mixture > toluene tertiary mixture.

An alternative explanation could simply be that as a result of the mixing of the IL with the miscible and immiscible solvents, the storage capacity of IL is subsequently reduced and thus the amount of atmospheric water that can be absorbed by the IL is also reduced. A reduction in absorption of atmospheric water will, in turn, affect the extent of change for the anionic peaks. As the solvents evaporate from the mixture, then it would be expected that the system would return to that of the binary mixture of IL and atmospheric water.

Much like the initial binary mixture of water and IL, the tertiary mixtures absorb atmospheric water as the ATR-FTIR spectroscopy experiment proceeds. This is clearly indicated by the growth of the OH stretch at 3500 cm^{-1} paired with the bend at 1650 cm^{-1}. The rate at which each band grows in varies depending on the solvent present in the tertiary mixture. Figure 4.9 shows the rate of change in absorbance of the O-H bend for each of the tertiary mixtures, with the IL water system overlayed for comparison. The same reasoning for plotting the O-H bend for the binary systems is applied here (see Chapter 3).

The tertiary mixture consisting of toluene (purple line) shows that for the first 45 mins of the experiment, atmospheric water fails to be absorbed into the system. After this, there is an observed increase in the absorption of water by the system. For the hexane system (yellow line) we see an overall increase in the absorption of atmospheric water, however, there is flux in the first 35 mins of the ATR-FTIR spectroscopy experiment, we observe a drastic increase for the first 15 mins followed a slight levelling of the curve until 35 mins, upon which, we observe an increase in the absorption of water. Both the curves for ACN and DCM systems show an overall increase in the absorption of atmospheric water, the distinct change here, however, is that the exponential increase for both of these systems is lessened, compared to the binary IL water system. Overall each tertiary mixtures shows a reduction in the gradient of the curve

suggestive that the rate of absorption for atmospheric water is reduced as a result of co-solvents being present within the IL system.

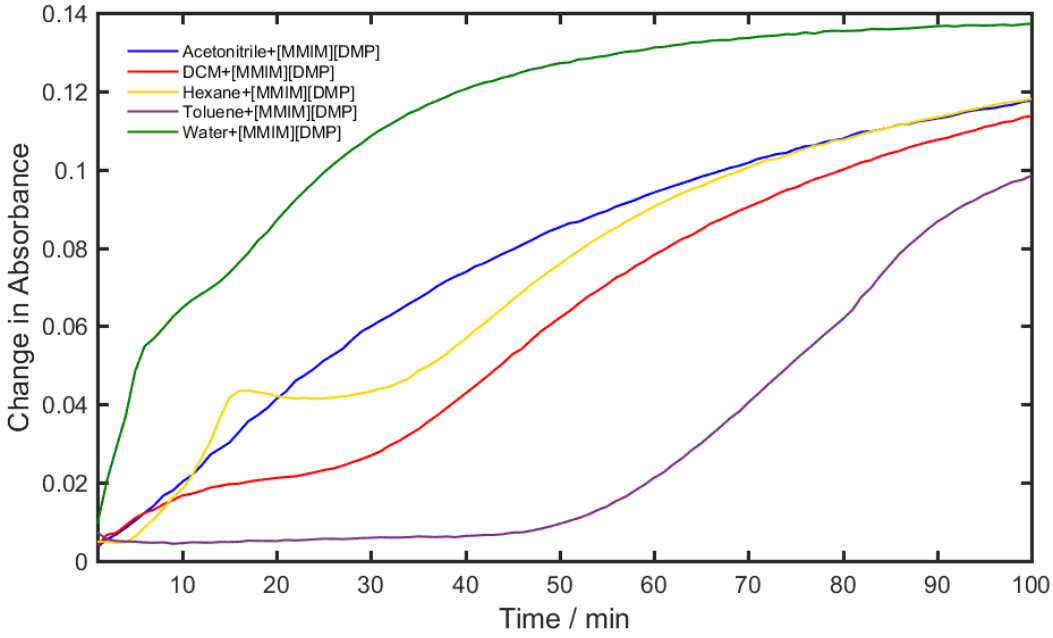


Figure 4.9. The rate of change in absorbance of the ν(O-H) bend in [MMIM] [DMP] (green line) doped with a co-solvents, ACN (blue line), DCM (red line), hexane (yellow line) and toluene (purple line).

There are a number of explanations as to why the rate of atmospheric is reduced for the tertiary mixtures. The explanations used to describe the vibrational changes in the IL peaks for each tertiary mixtures can also be used to rationalise the difference in the rate of water absorption for each tertiary mixture. Firstly one of the obvious explanations is that as a result of the IL already solvating the molecular solvent, the storage capacity of the IL Is reduced and the amount of water that can initially be absorbed is also reduced. Eventual evaporation of the molecular solvent allows for the IL to absorb more atmospheric water, which may be one of the reasons as to why the rate of water absorption differs for each solvent. This explanation can be applied to the miscible solvents much more rationally than the immiscible solvents as there is full

dissolution observed for the miscible solvents. Further explanation as to why the rate of water absorption is reduced for the immiscible solvents may rely on the notion that the immiscible solvents form a biphasic system with the IL. When the mixture is placed on the ATR-FTIR for sampling, the arrangement of the mixture could be that of a biphasic system with the toluene being present on the surface of the IL and hence creating a barrier preventing the absorption of atmospheric water. An immiscible surface layer without evaporation would prevent water from entering the IL, eventual evaporation would lead to exposure to atmospheric water and subsequent absorption. This may be the case at 45 min when there is an increase in the absorbance of the ν(O-H) stretch.

There are a number of variables associated with the tertiary mixtures that can be used to explain the difference in the rate at which water is absorbed by the IL. The complexity of these systems creates difficulty in isolating a sole reason to explain the differences observed for each tertiary mixture. It is much more practical to assess each tertiary mixture individually and use a multitude of explanations.

4.6 Conclusion

This chapter investigated the impact solvent additives have on the vibrational nature of a range of ILs. It was observed that upon the formation of binary mixtures between ILs and solvent additives, there were minimal changes to the vibrational nature. Of all the solvents investigated the miscible solvents of ACN and DCM showed small changes to the peak maxima and position of the anionic peaks of the IL, suggesting a small interaction between these solvent additives and the anionic moiety of the IL.

The immiscible solvents displayed no change to the vibrational nature of the IL, it is possible that none of the immiscible solvents was retained by the IL. If any retention of

the immiscible solvents occurred then the small quantity failed to interact with the IL effectively for any changes to be detected by IR.

The ATR-FTIR spectroscopy results were compared against the NMR spectroscopy results within the literature, which stated the more polar the solvent the greater the impact on the original IL - IL interaction, of which is readily replaced by solvent interactions. Although the changes observed in this study were minimal, the solvents seemed to fit into the pattern proposed by Noack *et al.* the polar solvents displayed some change to the vibrational nature and the non-polar solvents displayed no change[32]. Further analysis of more polar solvent IL mixtures would provide confirmation of this.

The second half of this chapter explored the formation of tertiary mixtures of IL, solvent and atmospheric water. The results of the formation of tertiary mixtures varied for each solvent additive used. Overall, each solvent appeared to cause a reduction in the impact atmospheric water had on the vibrational nature of the IL. A comparative overlay (Figure 4.8) showed the extent of this. The more immiscible solvents persevered the IL and prevented the impact of water much more effectively compared to the miscible solvents. Additional analysis into the rate of absorption of atmospheric water by the IL solvent mixtures showed a reduction into the amount of atmospheric water being absorbed by the system. There may be multiple explanations into why there is a reduction in the impact atmospheric water has on the IL as a result of a solvent additive being present. Firstly, there may be a reduction in the storage capacity of the IL. As the solvent is present within the IL system, the amount of atmospheric water that can be absorbed is subsequently reduced. As a result of a three-component system, there is also the possibility for the formation of additional interactions. There is the potential for IL - water, solvent - IL, solvent - water interactions within the system, all of which may play a role in the difference between the tertiary mixtures and the IL water binary mixtures. Another simple explanation is that for the immiscible solvents,

the formation of a biphasic system may occur on the ATR-FTIR diamond. The IL is then protected from atmospheric water absorption until the immiscible solvent is evaporated from the system.

Overall this chapter has provided an insight into the relationship between molecular solvent additives and ILs on a vibrational spectroscopic front. Although the results for the solvent IL binary mixtures were minimal, it has opened up the potential for the exploration of solvent IL mixtures based on polarity. The investigation into tertiary mixtures of ILs, water and molecular solvents revealed that as a result of extra components being present in the IL (molecular solvents), the amount and rate at which water is absorbed is altered.

4.7 References

1. P. Nockemann, K. Binnemans and K. Driesen, *Chem. Phys. Lett.* **2005**, *415*, 131 - 136.
2. T. Welton, *Chem. Rev*. **1999**, *99*, 2071 - 2083.
3. R. Rogers, K. Seddon and S. Volkov. (2003). *Green Industrial Applications of Ionic Liquids*. Dordrecht: Springer Netherlands, pp.30-41.
4. D. W. Armstrong, L. He and Y.-S. Liu, *Anal. Chem.* **1999**, *71*, 3873 - 3876.
5. R. Ratti, *Adv. Chem. Phys*. **2014**, *2014*, 1 - 16.
6. P. Sun, D.W. Armstrong, *Anal. Chim. Acta,* **2010***, 666*, 1 - 16.
7. S. Zhu, R. Chen, Y. Wu, Q. Chen, X. Zhang and Z. Yu, *Chem. Biochem. Eng. Quart*. **2009**, *23*, 207 - 211.
8. M. H. Chakrabarti, F. Sabri Mjalli, I. M. Alnashef, M. A. Hashim, M. A. Hussain, L. Bahadori, C. Tong and J. Low, *Renew. Sust. Energ. Rev*. **2013**, *30*, 254 - 270.
9. H. Tokuda, K. Hayamizu, K. Ishii, Md. A.B. H. Susan and M. Watanabe, *J. Phys. Chem*. B. **2004**, *108***,** 16593 - 16600.
10. J. J. Fillion and J. F. Brennecke, *J. Chem. Eng. Data*. **2017**, *62*, 1884 - 1901.
11. M. L. P. Le, L. Cointeaux, P. Strobel, J.-C. Leprêtre, P. Judeinstein and F. Alloin, *J. Phys. Chem. C*. **2012**, *116*, 7712 - 7718.
12. N. D. Khupse and A. Kumar, *J. Sol. Chem*. **2009**, *38*, 589 - 600.
13. J. Wang, Y. Tian, Y. Zhao and K. Zhuo, *Green Chem*. **2003**, *5*, 618.
14. K. R. Seddon, A. Stark and M.-J. Torres, *Pure Appl. Chem*. **2000**, *72*, 2275 - 2287.
15. T. Abdallah, D. Lemordant and B. Claude-Montigny, *J. Power Sources*. **2012**, *201*, 353 - 359.
16. A. Guerfi, M. Dontigny, P. Charest, M. Petitclerc, M. Lagacé, A. Vijh and K. Zaghib, *J. Power Sources*, **2010**, *195*, 845 - 852.

17. T. Tsuda and C. L Hussey, *Electrochem. Soc. Interf.* **2007**, *16*, 42 - 49.

18. H. Tokuda, S.-J. Baek and M. Watanabe, *Electrochemistry*. **2005**, *73*, 620 - 622.

19. S. Zhang, N. Sun, X. He, X. Lu and X. Zhang, *J. Phys. Chem. Ref. Data*. **2006**, *35*, 1475 - 1517.

20. S. Cha, M. Ao, W. Sung, B. Moon, B. Ahlström, P. Johansson, Y. Ouchi and D. Kim, *Phys. Chem. Chem. Phys.* **2014**, *16*, 9591 - 9601.

21. Y. Jeon, J. Sung, D. Kim, C. Seo, H. Cheong, Y. Ouchi, R. Ozawa and H. O. Hamaguchi, *J. Phys. Chem. B*. **2008**, *112*, 923 - 928.

22. L. E. Ficke and J. F. Brennecke, *J. Phys. Chem. B*. **2010**, *114*, 10496 - 10501.

23. C. Hampton, D. Demoin, Vibrational Spectroscopy Tutorial: Sulfur and Phosphor, (2010) Available from: https://faculty.missouri.edu/~glaserr/8160f10/A03_Silver. pdf.

24. E.-L. Karjalainen, A. Hardell and A. Barth, *Biophys. J.* **2006**, *91*, 2282 - 2289.

25. V. H. Paschoal, L. F. O. Faria and M. C. C. Ribeiro, *Chem. Rev.* **2017**, *117*, 7053 - 7112.

26. J. Grondin, J.-C. Lassègues, D. Cavagnat, T. Buffeteau, P. Johansson and R. Holomb, *J. Ram. Spectrosc.* **2011**, *42*, 733 - 743.

27. T. Takamuku, M. Tabata, A. Yamaguchi, J. Nishimoto, M. Kumamoto, H. Wakita and T. Yamaguchi, *J. Phys. Chem. B*. **1998**, *102*, 8880 - 8888.

28. Solvent--recycling.com. (2018). Boiling Points of Solvents for Solvent Recycling. [Online] Available at: http://www.solvent--recycling.com/boiling_points.html, [accessed 28 th August 2018].

29. Organicdivision.org. (2018). Common Organic Solvents: Table of Properties. [Online] Available at: https://www.organicdivision.org/orig/organic_solvents.html [accessed 28th August 2018].

30. L. C. Branco, J. N. Rosa, J. J. Moura Ramos and C. A. M. Afonso, *Chem. Eur. J.* **2002**, *8*, 3671.

31. K. Wippermann, J. Giffin and C. Korte, *J. Electrochem. Soc.* **2018**, *165*, 263 - 270.

32. K. Noack *et al*. *J. Mol. Struct.* **2012**, *1018*, 45 - 53.

33. N. V. Plechkova and K. R. Seddon, *Chem. Soc. Rev.* **2008**, *37*, 123 - 150.

Chapter 5

Vibrational Spectroscopic Analysis of Alkali Salts and Ionic Liquids

5.1 Introduction

This chapter aims to build upon the premise set by the research already discussed within this thesis by using spectroscopic techniques to probe IL systems that possess further impurities. The work in this chapter is focused around an excess of alkali salts that may be retained in imidazolium-based ILs during their preparation process. Both the vibrational nature of the ILs and their physical properties were investigated to assess any changes caused by residual contamination. Alkali salts are readily used in conjunction with ILs in order to diversify the anionic counterpart and ultimately change the properties of the IL for a specific use[1-2]. Alcalde *et al*. showed the impact changing the anion has on the properties of an IL, specifically a change in viscosity[3]. It was shown for imidazolium-based ILs with the cation of choice being $[EMIM]^+$ the viscosity ordering for common anions was $Cl^- > [HS]^- > [DEP]^- > [Tf]^- > [ES]^- > [OA]^- > [BF_4]^- > [Tf_2N]^-$. The viscosity ordering in these ILs is representative of the strength of anion-cation interactions, which have a pivotal role in ILs viscosity. ILs generated from halide ILs *via* metathesis, display a lower viscosity compared to the original halide based IL suggestive of a reduction in the anion - cation interaction.

The synthetic process for the metathesis reaction involves the combination of an IL, commonly the halide version, with an alkali salt. Both components for the reaction are mixed as ready-made solutions, usually generated by using ultrapure water. The

resulting reaction mixture is then stirred for 48 hrs to generate the final IL[4-5]. Figure 5.1 illustrates a general metathesis procedure for an imidazolium-based IL.

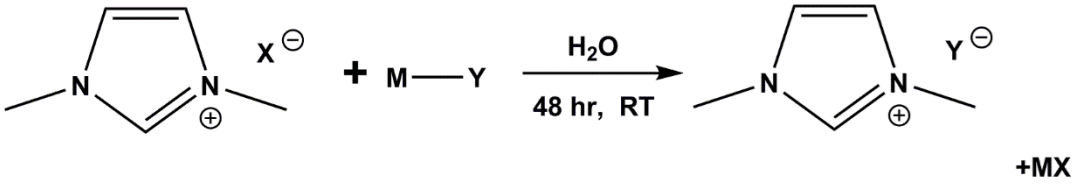


Figure 5.1. General metathesis procedure for imidazolium-based ILs. MY represents the metathesis salt where M is either a group 1 metal or Ag and Y is a corresponding anion.

Upon purification of the metathesis generated IL, residual amounts of the initial alkali salt may be retained within the IL as a result of the reactant initially being in excess in order for the metathesis reaction to proceed to completion. The purification process for ILs generated from metathesis involves the washing of the IL with ultrapure water, with the aim of removing any residual salts and or starting material from the IL medium. Error in the purification process, such as inefficient washing, may lead to unwanted material being retained within the IL system. Unlike contamination with water and molecular solvents (see results Chapters 3 and 4) the contaminant here is a charged molecule. The introduction of a charged molecule into an already charge species opens up the possibility for interactions not only including hydrogen bonding and Van der Waals but also electrostatic interactions. A mixture composed of two charged components allows for the dissociation of each charged species. This opens up the potential for new coulombic charges to be formed within the mixture. Taking the process of synthesising an IL from an alkali salt and a pre-existing IL as the example, there is the potential for a multitude of electrostatic interactions. Assuming that the reaction with the alkali salt has gone to completion and we have 100 % conversion, the only coulombic reaction is the one that occurs solely between the cation and anion

of the IL. Quite commonly with IL metathesis, this is not the case and there is retention of minute concentrations of starting material and or unwanted products. If retention of other charged species ensues there is the potential for interactions between these species and the desired IL. Examples of this include the IL interacting with the by-product of metathesis, the IL interacting with the alkali salt reactant and even the IL interacting with the anion of the original IL; if the full conversion is not achieved. Overall if there is retention of a charged substance within an IL and new interactions arise then changes to the properties of the IL may be impacted. This chapter aims to explore this by introducing excess alkali salt into the IL medium and analysing the mixtures with vibrational spectroscopy.

5.1.1 Current Research into Alkali Salt Ionic Liquid Systems

Current research within the literature that study IL alkali salt systems revolve around the purposeful doping of ILs with the corresponding alkali salt. [Tf_2N] based ILs are the prototypical ILs investigated within these studies, with the arrangement of the additional alkali salts being the main focus of many groups. Most groups deploy MD simulations in order to generate an idea of how the alkali salt is arranged. Accompanying experiments explore a change in viscosity and transport properties of the IL.

Borodin *et al*. conducted the first MD simulation study of an IL doped with a lithium salt, specifically pyrrolidinium based ILs doped with 25 % mol fraction of $LiNTf_2$ and reported analysis of the $[Li]^+$ cation environment and its transport mechanism[6]. This work showed that $[Li]^+$ cations are typically coordinated, on average, to approximately four oxygen atoms with each oxygen atom being contributed by different [Tf_2N] anions. It was also found that $[Li]^+$ transport in this system is heavily dependent on $[Li]^+$ coordination and occurs primarily through [Tf_2N] in the first coordination shell.

Research into the addition of alkali salts to ILs carried out by Chen and Forsyth showed simulations that elucidated to the formation of bulky anion - alkali complexes around the ILs. In their case, they demonstrated that the bulky anion - alkali complexes provided more opportunities for the restructuring of the ionic coordination environment through aggregate rearrangement, and thus enhancement of the dynamics of the alkali metal ions in a cluster environment[7]. Méndez-Morales *et al.* showed that the combination of bonding interactions between the metal alkali salt and the IL led to the formation of polar and apolar nanodomains as seen in Figure 5.2[8]. It was shown that the addition of the alkali salt led to a limited disruption of the structure of the IL with the main effect of the salt addition being the transference of anions to the inner regions of the polar nanodomains where $[Li]^+$ cations reside. The distribution of the anions in this way created a disruption in the network of hydrogen bonds upon solvation, clustering anions in their neighbourhood.

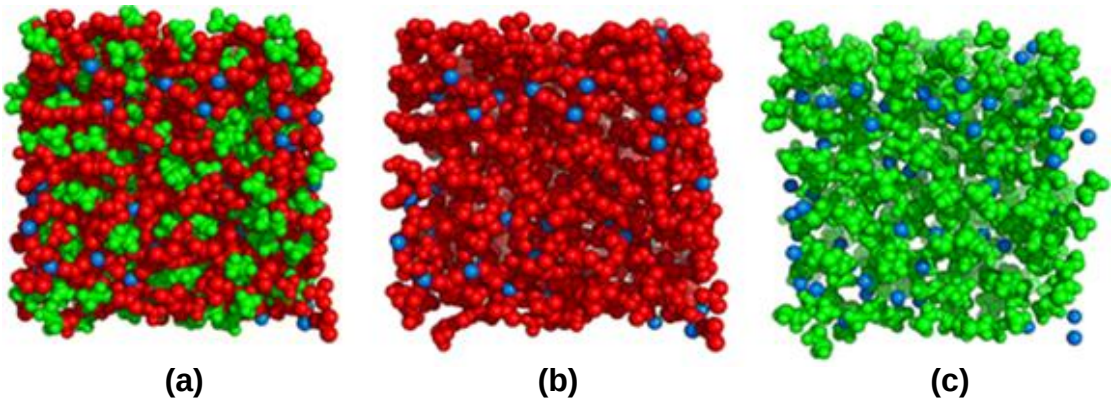


Figure 5.2. Reconstructed snapshots of the simulation box of a solution of $LiNO_3$ in EAN at a concentration of 25 % of lithium salt at T = 298.15 K and p = 1 at, proposed by Méndez-Morales et al. [8] The snapshots of the whole system (a), nitrate anions and ammonium groups of the cation (red) with lithium's (blue) (b) and apolar region of the ethyl ammonium cation (green) with lithiums (blue) (c) are presented.

Additional investigations into $LiNTf_2$ doped IL systems focused in on the use of these systems within electrochemistry. Howlett *et al*. investigated [N-methyl-N-propylpyrrolidinium] $[Tf_2N]$ ILs doped with $LiNTf_2$ as an electrolyte for battery applications and found great cycling efficiency and uniform, non-dendritic deposition of lithium[9]. The phase behaviour of doped pyrrolidinium ILs was also investigated by Henderson *et al*. The authors suggested that strong $[Li]^+$ - $[Tf_2N]^-$ interactions, most likely between the $[Li]^+$ cations and anion oxygen, exist in the crystal structures for all of the doped mixtures[10].

In summary, current research revolving around the presence of additional $LiNTf_2$ in the prototypical IL, [EMIM] $[Tf_2N]$ provides an insight into the structural arrangement of the additional alkali salt; alongside potential interactions. There is agreement within the literature that suggests excess alkali salts leads to aggregation and arrangement around the IL in the form of an anion - alkali complex. The dominant interaction is seemingly in the form of the $[Li]^+$ cation interacting with the oxygen moieties of the anion. Each $[Li]^+$ cation is typically coordinated, on average, to four oxygen atoms with each oxygen atom being contributed by different $[Tf_2N]$ anions. The aggregation around the IL and the interactions alluded to within the literature suggests that additional alkali salt will lead to a change in the vibrational nature of the original IL.

Spectroscopic studies into the doping of ILs with alkali salts is limited, with the literature focusing primarily on the arrangement of these salts using MD simulations and exploring doping to benefit the electrochemistry of ILs. Nicotera *et al*. however, carried out NMR characterization on $LiNTf_2$ doped ILs and investigated the interactions between the components within the system as well as transport properties of the electrolyte[11]. Examination of ^1H, ^1F, and ^7Li NMR spectra, Nicotera noted that interactions of the organic cations with $[Li]^+$ and $[Tf_2N]^-$ was very weak compared to the interactions between $[Li]^+$ and $[Tf_2N]^-$ with the latter resulting in a strong coordination between $[Tf_2N]^-$ and $[Li]^+$.

The general impression from the literature on the addition of alkali salts to IL is that the alkali salt forms aggregates around the IL. Aggregation of the IL causes disruption in interactions between the components of the IL thus bringing about changes in the interactions that are commonly seen in ILs[6-8]. There is a possibility for a disruption in the original coulombic interaction between the IL counterions, as well as the potential for new electrostatic interactions to occur as a result of excess charged components. This chapter aims to take the structural differences put forward from the research available in the literature between the pure IL and the alkali-doped IL and further explore these systems using vibrational spectroscopy. As we have already seen in Chapter 3 with water, an arrangement of an additional species around the IL leads to interactions between either the cation or anion or both. In the case of water, there is clear interaction between the anionic counterparts, resulting in a decrease in the original coulombic interaction of the IL. These changes are clearly identified and explained with the use of vibrational spectroscopy. Similarly, the arrangement of additional alkali salts within the IL medium should bring about changes to the original IL interaction, leading to a change in the spectroscopic nature of a number of the vibrational bands of the IL. The use of vibrational spectroscopy in this chapter will allow for further identification of the possible interactions occurring between excess alkali salt and IL.

This chapter initially explores the prototypical IL, [EMIM] [Tf_2N], with added $LiNTf_2$. The initial investigation aims to explore the main points made in the literature by using vibrational spectroscopy. This chapter additionally explores two other IL alkali salt systems in order to confirm or refute potential trends between the differing alkali salts.

5.1.2 ATR-FTIR Spectroscopy of Alkali Salt Based ILs

As with the other results chapters detailed in this thesis, this chapter utilises vibrational spectroscopy to probe the effects of varying concentrations of alkali salts on a range of ILs. The ILs in question and their alkali salts are detailed in Table 5.1.

IL	Alkali Salt
[EMIM] [Tf_2N]	$LiNTf_2$
[EMIM] [BF_4]	$LiBF_4$
[EMIM] [BF_4]	$NaBF_4$
[EMIM] [Ac]	LiAc

Table 5.1. Alkali salts and the corresponding ILs studied within this chapter.

It has been proven within the literature and in earlier chapters, vibrational spectroscopy is a powerful tool in the investigation into the changes in the vibrational nature of ILs as a result of resting impurities within the IL[12-14]. The general IR spectra of ILs can be split into cationic and anionic regions in accordance with the IL which allows for ease of identification of vibrational peaks. The ILs investigated within this chapter are all imidazolium-based ILs, the cation has been kept the same for each IL studied, with the cation choice being 1-ethyl-3-methylimidazolium. Consistency in the cation ensures any changes observed for the cationic bands can be compared and contrasted effectively. The noticeable differences between the ILs lie in the anion, each anion was selected based on the corresponding alkali salt that was utilised for the synthesis of the initial IL. Table 5.2 shows the main spectral features of interest for the ILs

investigated herein. The variation in the anion leads to specific stretching frequencies unique to each IL, the stretching frequencies for the cation will fall in the same position for each of the ILs investigated.

Wavenumber/ cm^{-1}	Functional Group	IL	Ref
3120-3160	C4,5 – H sym	All	15,14
3120-3160	C4,5 – H asym	All	15,14
3104,	C2-H	All	15,14
2980 - 3030	(N)-CH_3 asym	All	15,14
2899-2910	(N)-CH_2-CH_3 sym	All	15,14
2900-2850	(N)-CH_2 asym	All	15,14
1678	C=C	All	15,14
1574	C=N	All	15,14
1331-1354	S=O asym	[EMIM] [Tf_2N]	15
1228	C-F sym	[EMIM] [Tf_2N]	15
1014-1197	B-F	[EMIM] [BF_4]	14
1175	C-F asym	[EMIM] [Tf_2N]	15
1132-1136	S=O sym	[EMIM] [Tf_2N]	15
960	C-C	All	15,14
788-789	S-C	[EMIM] [Tf_2N]	15
760-763	N-S	[EMIM] [Tf_2N]	15
1334	COO asym	[EMIM] [Ac]	16
1567	COO sym	[EMIM] [Ac]	16

Table 5.2. The main spectral features for the functional groups of both the cationic and anionic counterparts for the ILs studied in this chapter.

As this chapter is dealing with residual alkali salts as the contaminant, all ILs were dried under schlenk conditions (50°C, $x10^{-6}$ bar) to remove any water absorbed through the synthetic process. The alkali salts used for the doping of the dry ILs were also dried under schlenk conditions to safeguard the system from water contamination. As seen in Chapter 3, water is readily absorbed by ILs from the atmosphere and engages in intermolecular hydrogen bonding with both the cation and anion counterpart. Removal of water allows for any changes in the IL system to be solely identified as ones brought about by residual starting material (alkali slats). All ATR-FTIR spectra were recorded within a glovebox (< 0.1 ppm H_2O, < 0.1 ppm O_2) to avoid absorption of atmospheric water. The preparation of the doped ILs was also carried out inside the glovebox to ensure complete elimination of water from the system. A concentration gradient for each IL and alkali salt was established with the details of the concentration gradient being displayed in Table 5.3.

Sample Number	IL : Salt wt : wt %	[EMIM] [Tf_2N] : $LiNTf_2$ Mol : Mol %	[EMIM] [BF_4] : $NaBF_4$ Mol : Mol %	[EMIM] [Ac] : LiAc Mol : Mol %
1	98 : 2	97 : 3	97 : 3	95 : 5
2	96 : 4	95 : 5	93 : 7	90 : 10
3	94 : 6	92 : 8	90 : 10	86 : 14
4	92 : 8	89 : 11	86 : 14	82 : 18
5	90 : 10	87 : 13	83 : 17	77 : 23
6	88 : 12	84 : 16	80 : 20	74 : 26
7	86 : 14	82 : 18	77 : 23	70 : 30
8	84 : 16	79 : 21	74 : 26	67 : 33
9	82 : 18	77 : 23	72 : 28	64 : 36
10	80 : 20	75 : 25	69 : 31	61 : 39
11	70 : 30	63 : 37	56 : 44	48 : 52
12	60 : 40	52 : 48	45 : 55	37 : 63
13	50 : 50	42 : 58	36 : 64	28 : 72
14	40 : 60	33 : 67	27 : 73	21 : 79
15	30 : 70	24 : 76	19 : 81	14 : 86
16	20 : 80	16 : 84	12 : 88	9 : 91
17	10 : 90	8 : 92	6 : 94	4 : 96

Table 5.3. Calculated wt : wt % and the corresponding mol : mol % of the IL : alkali salt binary solutions investigated.

ATR-FTIR spectroscopy was used to investigate each combination of IL and alkali salt under the condition that the alkali salt fully dissolved in the IL and that the resulting solution was a homogenous binary mixture of the two components. It was imperative that full dissolution occurred and that there was no sampling of the pure alkali salt as this would hinder the identification of any true spectral variance. For each combination, there was a dissolution endpoint in which the amount of alkali salt calculated for the

solution did not fully dissolve. Table 5.4 details the dissolution endpoints for each combination of IL and alkali salt.

IL : Alkali Salt	Dissolution endpoint mol : mol %
[EMIM] [Tf_2N] : $LiNTf_2$	75 : 25
[EMIM] [BF_4] : $NaBF_4$	77 : 23
[EMIM] [Ac] : LiAc	74 : 26

Table 5.4. Dissolution endpoints (mol : mol %) for the IL alkali salt combinations investigated in this chapter.

Each sample combination up until the dissolution endpoint was investigated with ATR-FTIR spectroscopy and the results were overlayed in order to assess any changes within the system. To ensure that the changes observed from knowingly doping the ILs with the corresponding alkali salt were, in fact, true spectral changes, it was necessary to initially assess the solutions in the form of an A+B system. As discussed in Chapter 3, an A+B system where both components are independent of one another produce a linear combination of spectra. If the system is undergoing true spectral change, in which component one effects component two then the system breaks away from a linear combination with the spectral changes being distinctly observed[17]. Figure 5.3 displays the pure IL [EMIM] [Tf_2N], [EMIM] [Tf_2N] doped with $LiNTf_2$ and pure spectra of $LiNTf_2$.

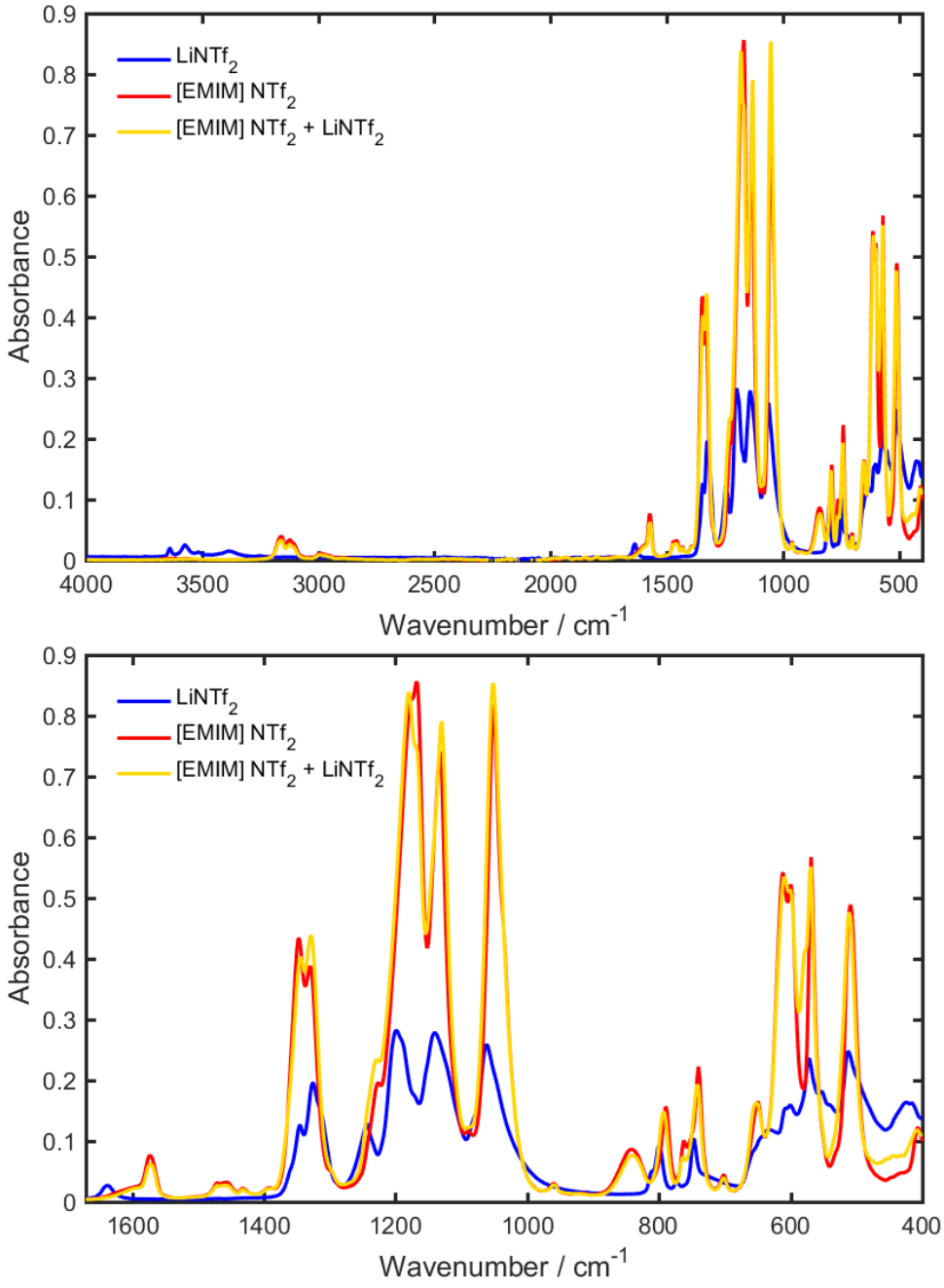


Figure 5.3. Full ATR-FTIR (top spectra) spectra showing the overlay of pure $LiNTf_2$ (blue line), pure [EMIM] [Tf_2N] (red line) and [EMIM] [Tf_2N] doped with $LiNTf_2$ (yellow line), and an enhanced fingerprint region showing the overlay of each component (bottom spectra).

Treating this as an A+B system, where A is the pure $LiNTf_2$ (blue line) and B is the pure [EMIM] [Tf_2N] (red line) we would then expect [EMIM] [Tf_2N] doped with $LiNTf_2$ (yellow line) to be the combination of these two spectra. Upon analysis of the [EMIM] [Tf_2N] doped with $LiNTf_2$ spectra, prominent shifts in peak maxima coupled with drops in intensity are observed for many of the peaks within the IL system. As with the other systems discussed in this thesis, in order to identify 'real' interactions, there must be prominent changes observed in peaks that are not overlapping with peaks associated with the impurity or additive. The bottom spectra in Figure 5.3 displays the enhanced fingerprint region for the mixture of [EMIM] [Tf_2N] and $LiNTf_2$. There is a huge overlap of peaks present within the system and it is difficult to distinguish if there is true interaction as some of the immediate and obvious shifts may be the result of overlapping bands combining. Analysis of the fingerprint region reveals a band at 843 cm^{-1} that has no overlap with the bands of $LiNTf_2$. The band displays a significant redshift towards lower energy for the [EMIM] [Tf_2N] $LiNTf_2$ mixture, when compared to the pure IL. The shift in the peak maxima of this band suggests that there is, in fact, a change in the vibrational nature of the IL as a result of additional $LiNTf_2$. The extent of change for each individual peak is difficult to decipher as there may be a combination of change as a result of overlapping peaks and changes due to molecular interactions. It can be stated, however, that this system is not a clear linear combination and the changes present for the [EMIM] [Tf_2N] doped with $LiNTf_2$ spectra are influenced by the components of the mixture impacting one another. The changes observed in this initial spectra suggests that there is a change in the original interaction as a result of $LiNTf_2$ being present in the system.

5.2 ATR-FTIR Spectroscopy of [EMIM] [Tf_2N] Doped with $LiNTf_2$

To develop a general impression of how alkali salts impact the vibrational nature of ILs, a vibrational spectroscopic experiment was devised in which spectra were recorded for a series of ILs doped with increasing concentrations of alkali salts. [EMIM] [Tf_2N] is the example IL of choice and displayed the most significant spectral change in the IL series studied within this thesis. It is also the IL that is the most miscible with its corresponding alkali salt allowing for a greater sample range to be investigated. The IR spectra were recorded within a glovebox at ambient conditions and the spectra collected as a function of concentration. Figure 5.4 shows the IR spectra obtained. Closer analysis of the different regions provides a further understanding of how the increasing concentration of $LiNTf_2$ effects [EMIM] [Tf_2N].

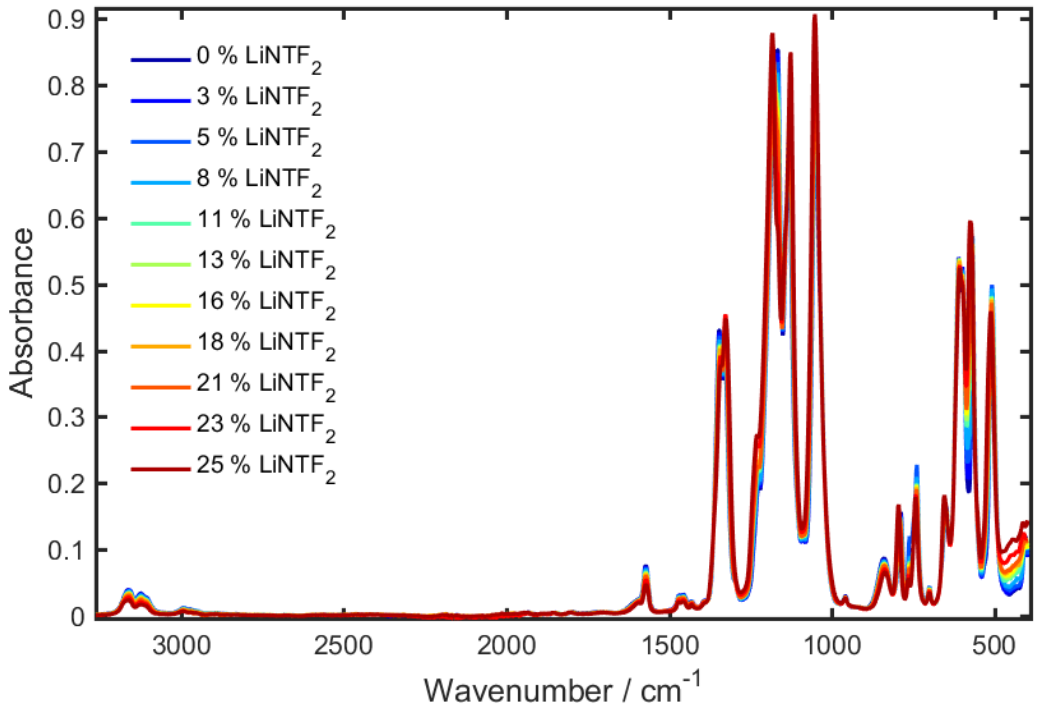


Figure 5.4. ATR-FTIR spectra of the [EMIM] [Tf_2N] with increasing concentrations of $LiNTf_2$ (blue to red).

As the concentration of $LiNTf_2$ is increased for each sample, the vibrational nature of the bonds associated with both the cation and anion moieties for [EMIM] [Tf_2N] display significant changes. Many of the peaks present in Figure 5.4 show a mixture of changes to the peak maxima and intensity, such perturbations are associated with a change in the vibrational nature of the bonds associated with these peaks. Changes in the vibrational nature of these bonds are indicative of a change in the environment of the pure [EMIM] [Tf_2N] and or interactions occurring between [EMIM] [Tf_2N] and $LiNTf_2$. Figure 5.5 focuses in on the major spectral changes observed for the major functional groups including the ν(C-H) bands for the cation and the NSO_2, and CF_3 vibrations of the anion. Figure 5.5 presents three enhanced spectra, A - C for the different regions of the IR spectra.

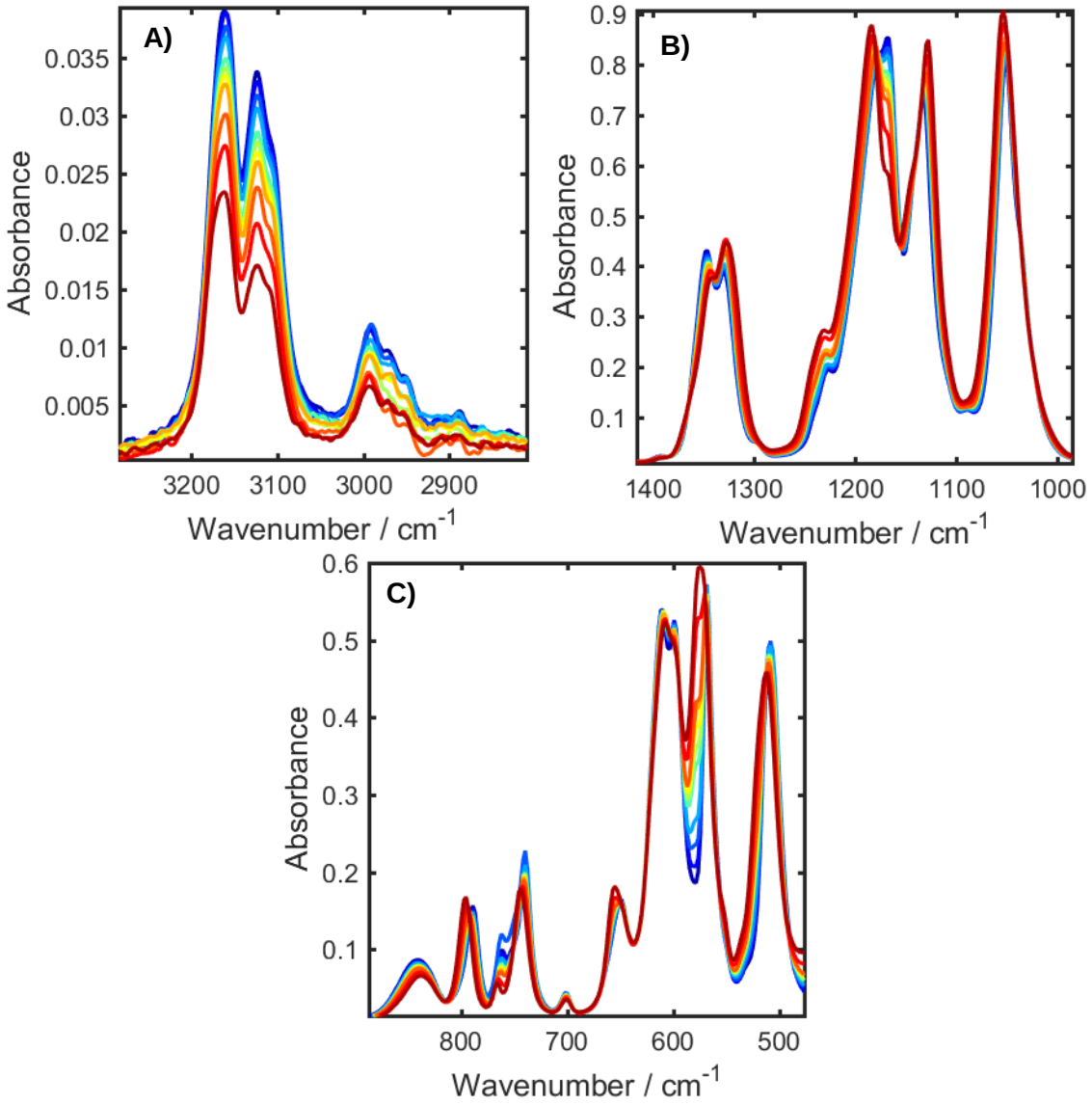


Figure 5.5. Enhanced spectra for the major spectral changes observed in [EMIM] [Tf_2N] as the concentration of $LiNTf_2$ is increased. A) ν(C-H), B) and C) display a combination of vibrations from the imidazolium ring, ν(C-F) and ν(S=O).

Spectra A of Figure 5.5 represents the higher wavenumber region of the $LiNTf_2$ doped [EMIM] [Tf_2N] mixture and focuses in on the C-H vibrations of the imidazolium ring and the associated alkyl groups. In contrast, the ν(C-H) stretching bands occurring between 2800 and 3200 cm^{-1} are remarkably weak in the IR spectra. In general, the

IR spectrum is strongly dominated by contributions from the $[Tf_2N]$ anion[18]. The major change that can be extracted from spectra A is that for each of the ν(C-H) bands there is a drop in intensity as the concentration of $LiNTf_2$ is increased. Generally, a drop in intensity represents a drop in the sampling of this region. As already discussed the ATR-FTIR spectra for [EMIM] $[Tf_2N]$ is strongly dominated by anionic peaks. The introduction of excess $[Tf_2N]^-$ anion into the IL may contribute to the increased dominance over the cationic peaks and hence an observed drop in intensity. There are no apparent peak shifts present in this region suggesting that there are no striking changes to the C-H bonds associated with the cation.

Spectra B - C represents the lower wavenumber region for the binary mixture of [EMIM] $[Tf_2N]$ and $LiNTf_2$. The bands of concern in this region are associated with both the cation and anion. Focusing first on spectra B, there are numerous peaks here that display significant change. The peaks at 1349 and 1329 cm^{-1} respectively represent the $\nu(SO_2)$ symmetric stretch of the anion and a combination of ring stretching of the cation with the $\nu(SO_2)$ asymmetric stretch of the anion[18]. Both peaks show an overall redshift with changes in intensity. The symmetric $\nu(SO_2)$ stretch displays a decrease in intensity, where the ring and asymmetric $\nu(SO_2)$ combination peak showing an increase in intensity. The introduction of a charged salt such as $LiNTf_2$ means that there is an increase in both $[Li]^+$ and $[Tf_2N]^-$ ions. An increase in both these ions will ultimately create a change in the electronic environment of the IL and in doing so bring about changes associated with the vibration of the bonds. The redshift observed for both peaks may be representative of elongation and weakening of the S=O bonds on the anion as a result of interactions with an excess of $[Li]^+$ cations. Peak shifts associated with the imidazolium ring suggests that there is a change in the vibrational environment of the ring as the concentration of $LiNTf_2$ is increased. As the concentration of $LiNTf_2$ is increased there is a surplus of $[Tf_2N]^-$ anions that can interact

with both cations available ($[EMIM]^+$ and $[Li]^+$). An increased interaction at the imidazolium ring and the neighbouring alkyl chains is perhaps causing fluctuations in the vibrational nature and hence an observed redshift.

Spectra C focuses in on bands associated with the imidazolium ring and the $-CF_3$ groups on the $[Tf_2N]^-$ anion. Peaks at 741 and 568 cm^{-1} are assigned to the $\nu(CF_3)$ symmetric and asymmetric stretch respectively[18]. Both of these peaks show a decrease in intensity and an overall redshift of the peak maxima. The redshift for the $-CF_3$ bands indicates a shortening and strengthening of the C-F bonds. This could be a possible side effect of the interaction happening at the SO_2 positions and as a way to combat the changing dipole of the anion due to the interactions from excess lithium ions.

As noted in the introduction of this chapter, MD research into $[Tf_2N]$ based ILs doped with $LiNTf_2$ revealed that $[Li]^+$ cations are typically coordinated, on average, by about four oxygen atoms with each oxygen atom being contributed by different $[Tf_2N]^-$ anions[9-11]. Further studies showed that interactions of the organic cation with $[Li]^+$ and $[Tf_2N]^-$ was very weak compared to the interactions between $[Li]^+$ and $[Tf_2N]^-$ with the latter resulting in a strong coordination between $[Tf_2N]^-$ and $[Li]^+$. The results from the literature can be matched with the results obtained from the vibrational spectroscopic experiments. The weak interaction between the organic cation and the other ions within the binary system may be used to explain why the appearance of the cationic peaks appear so weakly within the ATR spectra and why there is no significant change other than an intensity drop. The strong interaction and coordination observed between the $[Tf_2N]^-$ anions and the $[Li]^+$ cations explains the dominant presence in the anionic region of the ATR spectra. As stated by Borodin *et al.* the $[Li]^+$ ion coordinates to four individual $[Tf_2N]^-$ and the interactions take place at the oxygen atoms present on the

sulphur moiety of the anion[6]. The redshifts observed for the peaks corresponding to the S=O bonds, complement the findings from the MD simulations in the literature. The additional spectral variance observed from the ATR experiments may be a result of the IL system adjusting to the interaction occurring between the $[Li]^+$ cation and the oxygens on the sulphur moieties. Overall the results obtained from the ATR-FTIR spectroscopy experiments seemingly match up with the MD findings put forward in the literature.

It is imperative to stress that the changes observed from going from pure [EMIM] [Tf_2N] to a system with excess alkali salt may not be purely down to interactions and there may be an influence caused by overlapping peaks. As the concentration of $LiNTf_2$ is increased in the system, there is a greater absorbance for the anion peaks. An increased concentration of anionic peaks will impact the intensity of these peaks in the ATR-FTIR spectra. There is also a possible contribution due to varying anionic states. As discussed in the literature and noted above, the $[Li]^+$ cation interacts with the oxygen moieties of four different anions. The four anions may not necessarily be associated with the IL, with some being attributed to the alkali salt. There is potential for the changes identified above to be a combination of the disruption of the original anion - cation interaction due to the anion interacting with surplus $[Li]^+$ cations and the anion of the alkali salt aggregating alongside the anion of the IL.

5.2.1 Physical Properties of [EMIM] [Tf_2N]

It is clear from the analysis of the ATR-FTIR spectra of [EMIM] [Tf_2N] that an increase in the amount of excess $LiNTf_2$ brings about changes that are not easily observed and analysed with vibrational spectroscopy. The changes in the vibrational nature of both the cationic and anionic bonds present in [EMIM] [Tf_2N] are accompanied with definitive changes in the physical properties of [EMIM] [Tf_2N] as the concentration of

alkali salt increase. Figure 5.6 details viscosity and density measurements of the binary solutions of [EMIM] [Tf_2N] and $LiNTf_2$ at each mol %.

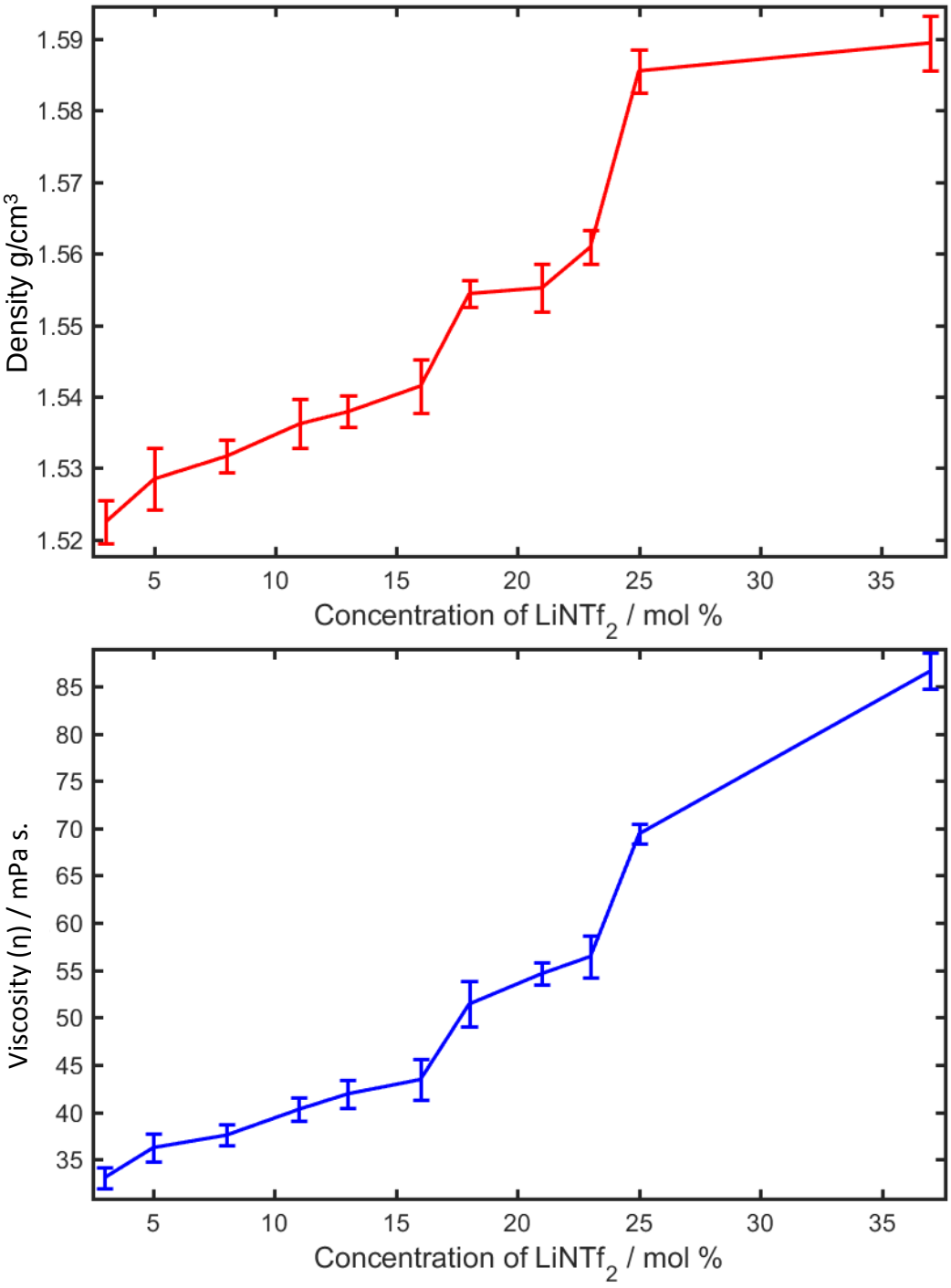


Figure 5.6. Density (Top) and Viscosity (Bottom) measurements for [EMIM] [Tf_2N] : $LiNTf_2$ binary mixtures investigated within this chapter.

From Figure 5.6 we see that as the concentration of $LiNTf_2$ present in [EMIM] [Tf_2N] increases both the density and viscosity show an overall increase in value. The density for the binary mixtures as the concentration of $LiNTf_2$ increases shows a steady increase at each concentration. As with the change in density observed for the water experiments, the observed difference, of 1 - 4 %, is negligible from a practical point of view. Changes in viscosity are much more drastic in comparison. The presence of excess $LiNTf_2$ causes the viscosity of the solution to increase from the initial viscosity of pure [EMIM] [Tf_2N]. Comparing the viscosity of the [EMIM] [Tf_2N] to that of the [EMIM] [Tf_2N] doped with $LiNTf_2$ we observe a 62 % increase in viscosity. Figure 5.6 graphically displays the change in viscosity against the change in density for [EMIM] [Tf_2N] as the concentration of $LiNTf_2$ is increased. It can be seen that there is a linear increase for both parameters, further indicating changes to the properties of the IL as a result of excess alkali salt.

It is clear from the analysis conducted *via* ATR-FTIR spectroscopy and the measurements of the physical properties of [EMIM] [Tf_2N], that the presence of additional $LiNTf_2$ creates a change in the IL. The changes observed in this section are just a small insight into how additional alkali salt behaves in an IL. Further investigation into other physical properties such as electrical conductivity would provide further insight and potential application of these binary solutions.

5.3 ATR-FTIR Spectroscopic Analysis of Additional IL Alkali Salt Combinations

At the beginning of this chapter, it was stated that a range of ILs knowingly doped with their corresponding alkali salt would be investigated. Thus far this chapter has given an insight into the way in which additional $LiNTf_2$ effects the vibrational nature of the IL

[EMIM] [Tf_2N]. The reasoning behind this is due to the [EMIM] [Tf_2N] : $LiNTf_2$ binary solutions being the only solutions to seemingly display significant changes in the ATR-FTIR spectra.

As a result of the significant changes observed from the [EMIM] [Tf_2N] : $LiNTf_2$ binary solutions, it was hypothesised that other alkali salts may also produce similar results. Further binary solutions were prepared (see Table 5.3) and investigated with ATR-FTIR spectroscopy in the same manner. Figure 5.7 shows the results of the ATR-FTIR spectra for the binary solutions of [EMIM] [Ac] : LiAc (top spectra) and [EMIM] [BF_4] : $NaBF_4$ (bottom spectra). It is clear from the analysis of both spectra that the presence of additional alkali salt in these ILs do not bring about significant changes to the vibrational nature of the bonds associated with the IL. Despite an increasing concentration of alkali salt in both binary mixtures, the systems here may seemingly follow an A+B system where neither component impacts the other.

Compared to the spectra obtained for the doped [EMIM] [Tf_2N], the ATR-FTIR spectra for these binary mixtures do not yield significant results. The minute changes observed for both of these systems are all intensity changes which can be related to the changing concentration of the components within the system. It can be seen that for the [EMIM] [Ac] : LiAc (top spectra) there is some spectral change present at *ca.* 3350 cm^{-1} and 440 - 400 cm^{-1} these bands are identified as water present within the system due to the highly hygroscopic nature of [EMIM] [Ac].

Bini *et al*. investigated the anion - cation strength of several ILs and showed that the $[Ac]^-$ and $[BF_4]^-$ are more tightly bound to imidazolium cations compared to the 'loosely' bound $[Tf_2N]^-$, with the latter being the least interacting amongst the ones investigated[19]. The strength of the anion - cation interaction highlighted here can be related to the lack of change in the ATR-FTIR spectra for both [EMIM] [Ac] and [EMIM] [BF_4]. The more tightly bound $[Ac]^-$ and $[BF_4]^-$ anions are less likely to be engaging in

interactions with the excess alkali salt, where the larger more diffuse $[Tf_2N]^-$ anion readily engages in interactions with surplus alkali salt; specifically $[Li]^+$.

Upon reflection, ATR-FTIR spectroscopy may not be the optimal spectroscopic technique to probe theses additional IL: alkali salt systems. Further investigation into these binary mixtures using MD simulations and NMR experiments would be needed. MD simulations into the arrangement of the additional alkali salts, LiAc and $NaBF_4$, would further corroborate the results obtained here or provide a deeper insight into potential interactions within the systems.

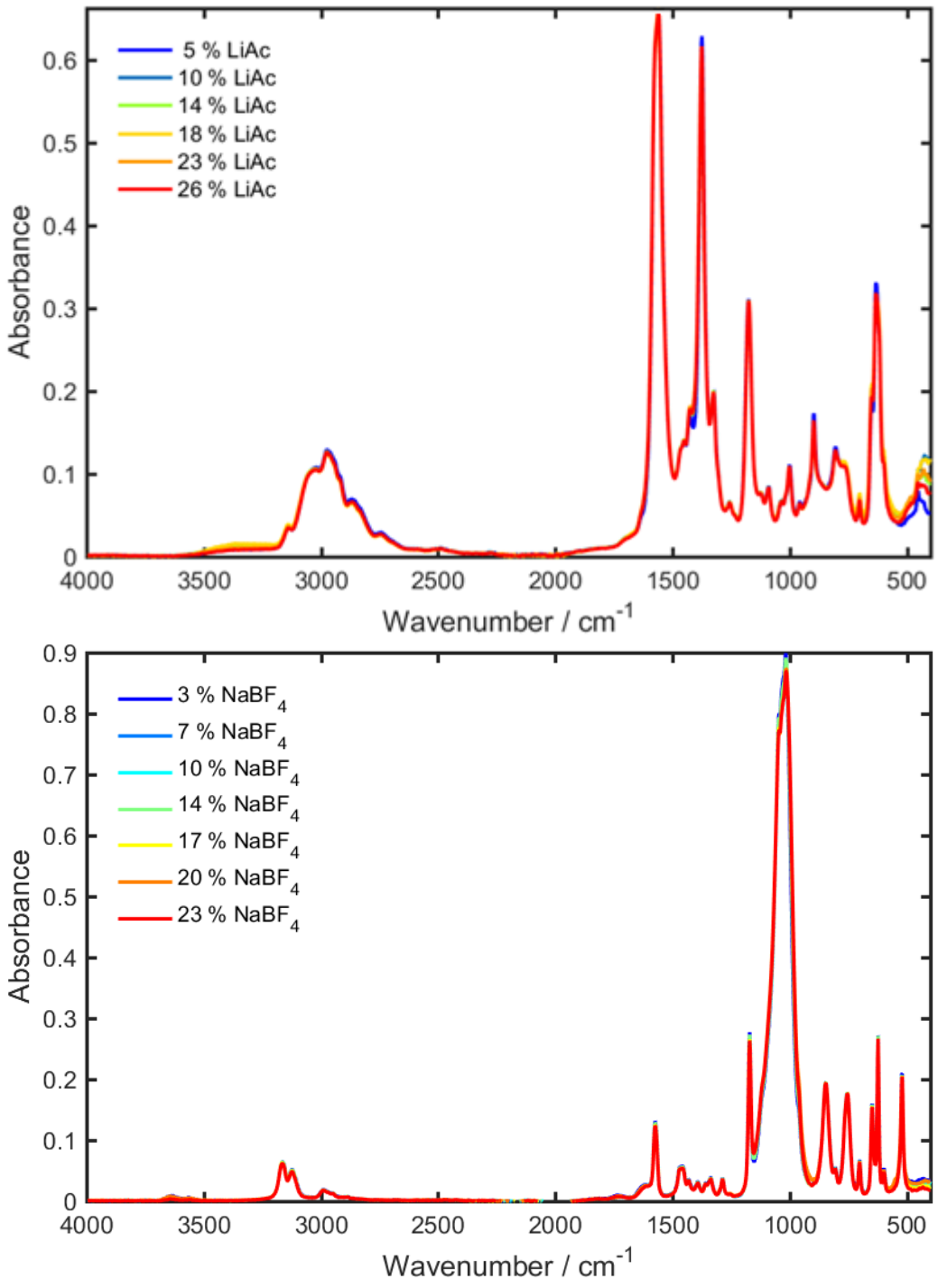


Figure 5.7. ATR-FTIR spectra for each completely miscible binary solution of [EMIM] [Ac] : LiAc (top spectra) and [EMIM] [BF_4] : $NaBF_4$ (bottom spectra).

5.4 Conclusions

This chapter has shown the impact that additional alkali salts have on a range of ILs. The chapter lead with the prototypical IL [EMIM] [Tf_2N] being doped with a range of $LiNTf_2$ concentrations and investigated with ATR-FTIR spectroscopy. The results of the ATR-FTIR showed significant changes in intensity and perturbations in many of the peaks associated with [EMIM] [Tf_2N] as the content of $LiNTf_2$ was increased.

The major spectral changes were observed in the anionic region with the SO_2 and CF_3 symmetric and asymmetric stretches displaying distinct perturbations. The bands associated with the SO_2 moiety of the IL displayed a redshift to lower energy with the CF_3 moiety blueshifting to higher energy. These spectral variations correspond to the analysis from the MD dynamic simulations present within the literature. The redshifting SO_2 bands corresponded to the MD simulation that states that due to an excess of $LiNTf_2$ in the IL system, $[Li]^+$ cations are bonded to four [Tf_2N] anions. The interaction takes place at the oxygen functionalities of the anion. As a result of this interaction at the anion, the redshift of the CF_3 functionality may be explained by the anion trying to counteract this interaction. The changes present in the ATR-FTIR spectra are accompanied by changes in both viscosity and density parameters. As the concentration of $LiNTf_2$ is increased both parameters show an overall increase.

The second section of this chapter explored variations of alkali salts and ILs and aimed to deduce if similar changes would occur upon changing the binary mixture. The ATR-FTIR spectroscopy results failed to display significant spectral changes for both binary mixtures of [EMIM] [Ac] LiAc and [EMIM] [BF_4] $NaBF_4$. The sole changes present in both of these systems centred on the minute differences in the intensity of many peaks, which can be attributed to the changing concentrations of individual components with the IL alkali salt mixtures. The lack of spectral variations suggests that ATR-FTIR spectroscopy may not be the optimal analytical technique to probe

these binary mixtures. The absence of perturbations for these binary mixtures may also imply that LiAc and $NaBF_4$ do not arrange themselves in the same fashion that $LiNTf_2$ assumes. In order to ensure that this is the case, MD simulations on both these binary mixtures would be required.

Overall this chapter has shown that excess $LiNTf_2$ in the prototypical IL [EMIM] [Tf_2N] causes the vibrational nature of the IL to change. Multiple bands associated with the IL display changes in both intensity and peak maxima as a result of an increased concentration of the alkali salt. The changes identified within the ATR-FTIR spectra have been related back to the MD findings presented in the literature and seemingly match with arrangement and interactions identified from MD simulations. This chapter also explored other ILs synthesised *via* metathesis, but failed to identify significant changes to the vibrational nature of these IL. The lack of vibrational change can be related back to the strength of the original anion - cation for each IL.

5.5 References

1. N. V. Plechkova and K. R. Seddon, *Chem. Soc. Rev.* **2008**, *37*, 123 - 150.
2. P. Wasserscheid and T. Welton, T. (eds). Ionic Liquids in Synthesis (Wiley-VCH, 2007).
3. R. Alcalde, G. García, M. Atilhan and S. Aparicio, *Ind. Eng. Chem. Res*, **2015**, *54*, 10918 - 10924.
4. M. Y. Lui, L. Crowhurst, J. P. Hallett, P. A. Hunt, H. Niedermeyer and T. Welton, *Chem. Sci.* **2011**, *2*, 1491 - 1496.
5. J. P. Hallett and T. Welton, *Chem. Re*v. **2011**, *5*, 3508 - 3576.
6. A. B. Pereiro, J. M. M. Araújo, F. S. Oliveira, J. M. S. S. Esperança, J. N. Canongia Lopes, I. M. Marrucho and L. P. N. Rebelo, *J. Chem. Thermodyn*, **2012**, *55*, 29 - 36.
7. F. Chen and M. Forsyth, *Phys. Chem. Chem. Phys*. **1933**, *18*, 19336 - 19344.
8. T. Méndez-Morales, J. Carrete, Ó. Cabeza, O. Russina, A. Triolo, L. J. Gallego and L. M. Varela , *J. Phys. Chem. B*. **2014**, *118*, 761 - 770.
9. P. C. Howlett, D. R. MacFarlane and A. F. Hollenkamp , *Electrochem. Solid State Lett*. **2004**, *7*, 97 - 101.
10. W. A. H. and and S. Passerini, *Chem. Mater.* **2004**, *15*, 2881 - 2885
11. I. Nicotera, C. Oliviero, W. A. Henderson, and G. B. Appetecchi and S. Passerini, *J. Phys. Chem. B*. **2005**, *48*, 22814 - 22819.
12. C. Roth, S. Chatzipapadopoulos, D. Kerlé, F. Friedriszik, M. Lütgens, S. Lochbrunner, O. Kühn and R. Ludwig, *New J. Phys*. **2012**, *14*, 1 - 16.
13. V. H. Paschoal, L. F. O. Faria and M. C. C. *Chem. Rev.* **2017**, *117*, 7053 - 7112.
14. Y. Jeon, J. Sung, C. Seo, H. Lim, H. Cheong, M. Kang, B. Moon, Y. Ouchi and D. Kim, *J. Phys. Chem. B*. **2008**, *15*, 4735 - 4740.
15. J. Kiefer, J. Fries and A. Leipertz, *Appl. Spectrosc.* **2007**, *61*, 1306 - 1311.
16. Y. Chen and T. Mu, *Appl. Spectrosc*. **2015**, *69*, 130 - 142.

17. B. Stuart. *Infrared spectroscopy*; J. Wiley and Sons: Chichester, United Kingdom, 2009.

18. J. Kiefer, J. Fries and A. Leipertz, *Appl. Spectrosc.* **2007**, *61*, 1306 - 1311.

19. R. Bini, O. Bortolini, C. Chiappe, D. Pieraccini and T. Siciliano, *J. Phys. Chem. B*. **2007**, *111*, 598 - 604.

Chapter 6

Future Work and Conclusions

6.1 Reflective Statement

The initial intention of this thesis was to not explore the relationship between contaminants and ILs. It was, however, designed to explore a more complex system within an IL medium. The original research concept aimed to investigate the relationship and potential interactions between several ILs (most of which are explored in this thesis) and the amino acids that make up the biopolymer, Keratin. This initial research determined the methodological format that is presented within this thesis. A concentration gradient of amino acid to IL was established and binary solutions were prepared and probed using vibrational spectroscopy as the major analytical technique. The amino acids explored, Arginine, Aspartic Acid, Cysteine, Glutamic Acid and Lysine account for a large percentage of the keratin protein. Each IL proved to be highly effective in dissolving each amino acid, with homogenous mixtures being formed. Similar to the work in Chapter 5 that explored alkali salts and ILs, the mixtures probed by ATR-FTIR spectroscopy were the ones that showed full dissolution by the IL.

The ATR-FTIR spectroscopy results obtained for each IL amino acid mixture proved to be vastly complex. The analysis of the individual bands from both components of the mixture failed to provide a deep insight into potential interactions between the amino acid and IL. The noticeable feature that was consistent for each system was a change in the IL and amino acid bands as the water was removed from the system. It was thus decided that the most effective approach in understanding the IL amino acid systems would be to explore the relationship between ILs and smaller, less complex

molecules, such as water. This thesis thus presents a bottom-up approach to the originally proposed research, with the ultimate aim in revisiting IL amino acid systems.

The choice to dismiss the preliminary study into ILs and amino acids from this thesis was one that was not flippantly decided. The absence of the results was decided as to not present a vast amount of complex data that could not be effectively assessed and communicated. This thesis has thus presented work that represents the foundation in understanding complex systems, such as IL amino acid solutions.

6.2 Thesis Summary

Although the initial intention of this thesis was to explore IL amino acid solutions it has not failed in tackling this. This thesis considered and explored an alternative approach to the initial research problem by investigating smaller, less complex systems.

This thesis has explored the impact that an assortment of contaminants, additives and lasting reagents has on both the physical properties and spectroscopic characteristics of an array of ILs. Each chapter has dealt with one of these additional components and investigated differences brought about from having a multicomponent IL-based system.

The conclusions for each chapter are unique to the individual systems explored within each chapter. The unanimous conclusion for this thesis is that the presence of additional components will impact the properties and characteristics of an IL. The extent of change on the IL is unique to each system. As discussed in chapter 1, ILs are easily contaminated in their preparation and synthesis along with exposure to the atmosphere. This thesis has explored three main contaminants; water, organic solvents and alkali salts. Chapters 3-5 explored each contaminant individually and drew individual conclusions based on the relationship between the contaminant and the IL.

This thesis has primarily utilised vibrational spectroscopy coupled with multivariate analysis to delve into multicomponent IL-based system. Each chapter has shown that the vibrational spectroscopic techniques, ATR-FTIR and Raman are powerful analytical tools in uncovering changes associated with binary mixtures. The use of multivariate analysis has further allowed binary systems to be explored with new information being uncovered to additionally explain the changes observed.

The main conclusions for chapters 3-5 are further detailed below,

6.2.1 Chapter 3 Conclusions

Chapter 3 explored the relationship between a range of imidazolium-based ILs with atmospheric water and bulk water. The use of the vibrational techniques, ATR-FTIR and Raman spectroscopy coupled with multivariate analysis in the form of MCR allowed for an in-depth investigation into IL water systems for a wide concentration gradient of water. ATR-FTIR and Raman spectroscopy allowed for the identification of points of interaction between each IL and water. MCR delved deeper into the datasets to reveal varying states of water at different concentrations points within the system. The major conclusions drawn from chapter 3 are as followed:

- The example IL [MMIM] [DMP] showed changes in vibrational nature for the C2-H position on the cation. An overall blueshift to higher energy was observed. This change was attributed to water weakening the original cation-anion interaction and observed for each IL studied.
- Significant vibrational changes were observed for the bonds associated with the anion of each IL. It was noted that significant interaction between water and the IL occurred at the anion. For the example IL, [MMIM] [DMP], both the ν(P=O) and ν(P-O) bonds showed a redshift to lower energy suggesting direct hydrogen bonding. The ν(C=O) of the anion showed a blueshift to higher

energy. This was hypothesised to be the anion counteracting the hydrogen bonding by redistributing the electron density of the anion.

- The shape and position of the water stretch showed variance for the range of ILs due to the strength of the hydrogen bond between the two components.
- The investigation into bulk water and the ILs revealed that water transitions through a variance of states as the concentration of water is increased. At lower concentrations water is viewed as being in a bound state. As the concentration of water is increased, water transitions into bulk water. ATR-FTIR and Raman spectroscopy was utilised to monitor this and showed varying shapes and positions of the peak maxima of the ν(O-H) stretch.
- MCR was used to further confirm the nature of the IL water mixtures. MCR showed a decrease in the IL component of the mixtures, an increase in the water component and two intermediates. These intermediates were assigned to bound water at distinct concentrations of 10 and 30 % water.
- Investigations into density and viscosity values showed that upon saturation with water, both the value of density and viscosity decreased. The uptake of water by the IL caused the IL to transition from a neatly packed system to a diffuse solution of ions

6.2.2 Chapter 4 Conclusions

As a result of the investigation of IL water mixtures, it was decided that IL molecular solvent mixtures would also be investigated to identify any significant trends between the different solvents that predominantly come into contact with ILs. Chapter 4 saw a range of IL molecular solvent binary mixtures probed with vibrational spectroscopy. This chapter saw the investigation into the relationship between molecular solvents and ILs along with the relationship between a tertiary

mixture of IL, solvent and water. The main conclusions drawn from this chapter are as followed:

- ATR-FTIR spectroscopy showed that miscible solvents displayed small vibrational changes to bonds associated with the IL. Both ACN and DCM alluded to interactions between the IL. The identified points of interaction occurred at the anion, overlapping peaks between the solvents and the IL introduced complexity in identifying the extent of the interaction. Analysis of the spectra showed that DCM was retained more effectively by the IL compared to ACN, despite being more volatile. ACN was seen to be evaporated from the IL quite readily, indicated by the disappearance of the ν(C≡N) feature.
- Immiscible solvents showed no significant spectral changes to the IL. Suggesting either no interaction or that further research using a range of analytical techniques is needed.
- The investigation into tertiary mixtures of ILs, molecular solvents and atmospheric water, showed that the rate at which water is absorbed is altered for these mixtures. In terms of water absorption, the sequence was determined to be acetonitrile > hexane > dichloromethane > toluene. DCM reduced the rate of water absorption more effective than the immiscible solvent hexane, which may be due to DCM interacting more readily with the IL and thus cannot be readily evaporated compared to ACN and hexane. The toluene IL mixture showed a delay in the absorption of water which was attributed to the toluene in the mixture arranging itself upon the surface of the IL creating a biphasic system.

6.2.3 Chapter 5 Conclusions

Chapter 5 detailed the investigation of IL alkali salt mixtures and explored the spectral variance brought about by increasing the concentration of alkali salts within an IL system. The chapter utilised ATR-FTIR spectroscopy to identify changes in the vibrational nature of the IL. The main conclusions drawn from this chapter are as followed:

- [EMIM] [Tf_2N] with varying concentrations of $LiNTf_2$ showed significant spectral variance to a number of bands associated with the IL. Identifying the extent of the changes became complex due to the severe overlap of peaks associated with both components present in the system.
- The peak at 843 cm^{-1} was identified to have no overlap with peaks associated with additional $LiNTf_2$. A redshift to lower energy was shown and implies a true interaction between the IL and the additional $LiNTf_2$. What can be deduced is that the spectral variance observed is reflective of an interaction between both components, the uncertainty in the results lies in the extent of the spectral variance due to overlapping peaks.
- Prominent vibrational changes are observed for the ν(S=O) bonding moieties of the anion, with the band showing a redshift to lower energy. The ν(C-F) bands show a blueshift to higher energy. The explanation used to describe the changes observed is that there is a direct interaction between the S=O bonds with surplus $[Li]^+$ cations in the system. The ν(C-F) changes may be explained as the anion readjusting to bonding at the S=O points.
- The observations observed for the [EMIM] $LiNTf_2$ can be linked with MD simulations in the literature. The MD simulations revealed that $[Li]^+$ cations

were typically coordinated, on average, to approximately four oxygen atoms with each oxygen atom being contributed by different $[Tf_2N]^-$ anions.

- Two other IL alkali salt systems were investigated, [EMIM] [Ac] - LiAc and [EMIM] $[BF_4]$ - $NaBF_4$. Both systems showed no significant spectral variance. The lack of vibrational change can be related back to the strength of the original anion - cation for each IL.
- Investigations into density and viscosity values showed that upon addition of $LiNTf_2$, both the value of density and viscosity increased. The increase in both parameters can be attributed to a more structured system compared to the pure IL.

6.3 Outlook and Future Work

Overall, this work has illustrated that as a result of additional components being present in an IL, changes are observed for both the physical and spectroscopic characteristics of the said IL. This work has also demonstrated the power of vibrational spectroscopy in identifying molecular interactions within a multicomponent IL system. Elaborating upon the work within this thesis, the following future experiments are suggested:

6.3.1 Investigation into Amino Acid Ionic Liquid Mixtures

As discussed in this chapter, the original concept of this thesis aimed to research IL amino acid mixtures. Due to the complexity of the mixtures, it was decided to explore less complex systems and build up knowledge that can be further applied to other IL mixtures.

The conclusions drawn from this thesis have revealed significant interactions between common contaminants and additives that can be present in IL. The interactions established have been a mix of intermolecular hydrogen bonding, electrostatic and Van der Waal interactions. Using the findings from each chapter the next appropriate step would be to apply this to the IL amino acid mixtures with the aim of dissecting the complexity of the original results.

Amino acids are naturally zwitterionic which opens up the potential for a multitude of interactions. Each amino acid and IL that would be revisited and investigated have multiple hydrogen bond acceptor and donor functionalities that may interact with one another. There is the potential for hydrogen donation between the two components, which may result in the formation of zwitterionic amino acids. This opens up the possibility for a change in the original anion - cation coulombic interaction with new coulombic interaction between ions potentially being formed. There is the possibility that one interaction will dominate in the mixture however, there is also the possibility of a collective of interactions being observed.

The amino acids may also have the ability to arrange around each IL and form aggregations in a way similar to what was observed in the anionic region is unique to each IL, however, the same approach is taken the water and alkali salt experiments. By altering the original concentration gradient of the IL amino acid mixtures and being more precise could reveal aggregation.

6.3.2 Monitoring Ionic Liquid facilitated Reactions *via* ATR-FTIR Spectroscopy

As seen in Chapter 1 the presence of additional components within an IL can interfere, change and inhibit chemical reactions that ILs facilitate. It has been shown within this

thesis that the presence of additional components changes the physical properties and spectroscopic characteristics of the IL. It would, therefore, be both prudent and productive to apply vibrational spectroscopy to IL facilitated chemistry and to asses and monitor how the presence of additional components influence the aspects of the reaction.

The use of FTIR Spectroscopy with in situ reaction monitoring would allow an understanding of reaction kinetics, pathway and mechanism with real-time FTIR Spectroscopy. A proposed experiment would see simultaneous reactions set up in order to distinguish differences between a control reaction, in which the IL was free of any potential contaminants or additives and one where the IL is knowingly doped with different contaminants or additives.

The use of FTIR Spectroscopy with in situ reaction monitoring in this way would allow for an understanding of:

- Initiation and termination of each reaction
- Reaction mechanisms
- The rate at which each reaction happens
- Potential interactions between the components in the system

This thesis has explored water, molecular solvents and alkali salts as additional components within IL systems. Applying the proposed simultaneous reaction set up to each of these systems, a number of features can be monitored, such as:

- If bound water has the ability to dissociate from the IL and interact with the other chemical components of the reaction
- If the additional components inhibit the efficiency of the IL performance
- If each component aids in the facilitation of the overall reaction. This may be useful when ILs are readily doped with additives to improve the properties of the IL.

Chapter 7

Appendices

Appendix A: NMR and Mass Spectrometry analysis for Chapter 2

This section contains the NMR and Mass Spectrometry analysis for the ILs investigated in this thesis. Chapter 2 details the methodology for the synthesis of each IL, the methodology is accompanied by NMR and Mass spectrometry values.

Mass Spectrometry

1, 3-Dimethylimidazolium dimethyl phosphate, [MMIM] [DMP]

ESI-MS (-ve) $[PO_4C_2H_6]^-$, calcd 125.04, found 125.00.

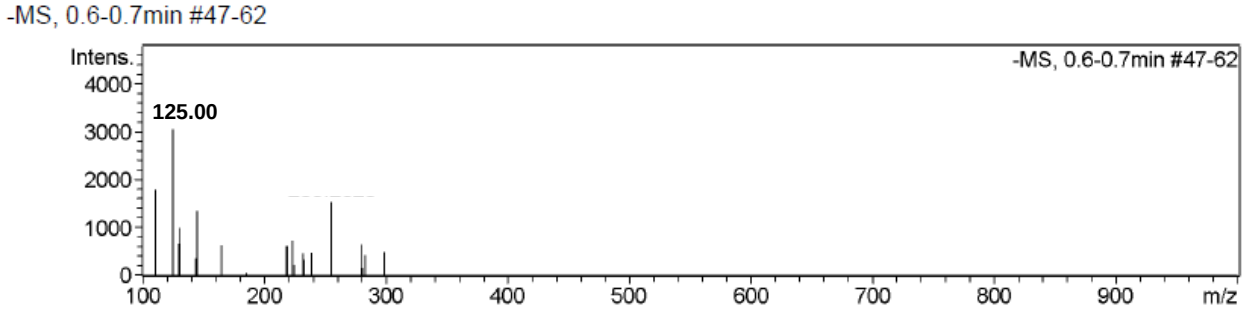


Figure 7.1. Mass Spectrometry analysis for [MMIM] [DMP].

1, 3-Dimethylimidazolium methyl sulphate, [MMIM] [$MeSO_4$]

ESI-MS (-ve) $[CH_3O_4S]^-$, calcd 110.98, found 110.90.

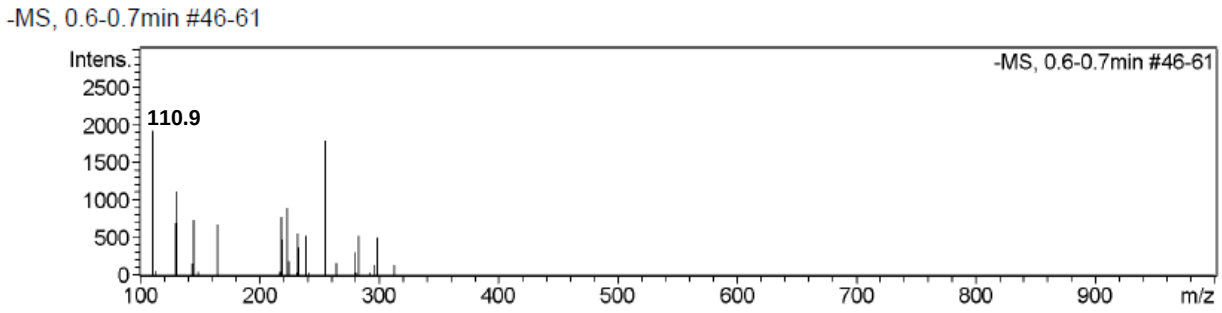


Figure 7.2. Mass Spectrometry analysis for [MMIM] [$MeSO_4$].

1-Ethyl-3-methylimidazolium chloride, [EMIM] Cl

ESI-MS (+ve) $[C_6H_{11}N_2]^+$ calcd 111.09, found 111.36.

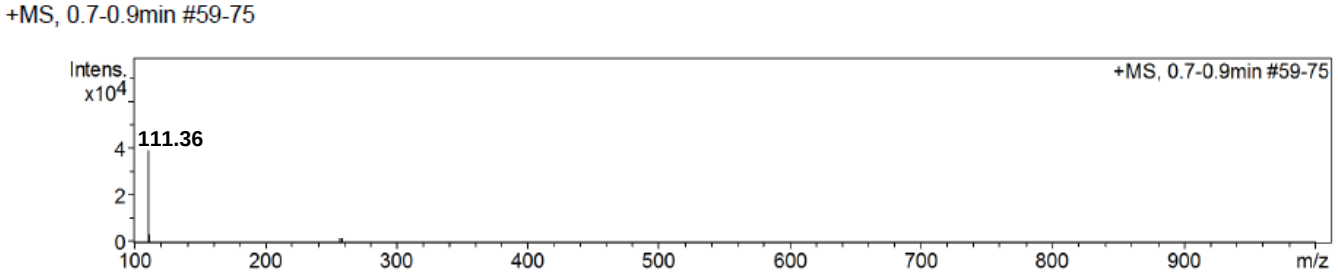


Figure 7.3. Mass Spectrometry analysis for [EMIM] Cl.

1-Methyl-3-octylimidazolium chloride

ESI-MS (+ve) $[C_{12}H_{23}N_2]^+$ calcd 195.19, found 195.49.

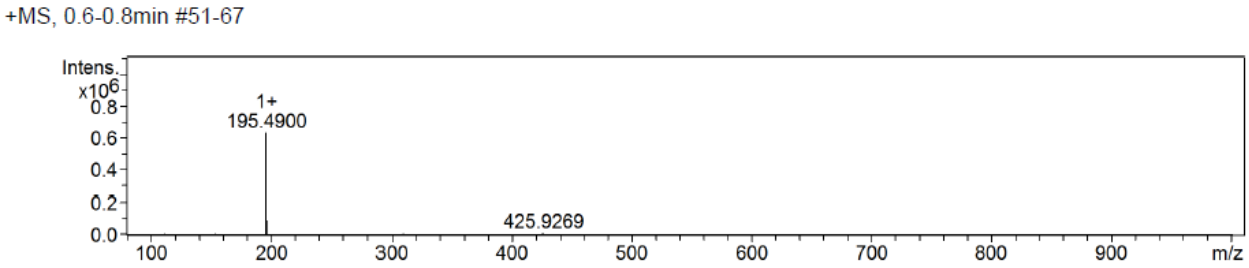


Figure 7.4. Mass Spectrometry analysis for [OMIM] Cl.

1-Ethyl-3-methylimidazolium acetate, [EMIM] [Ac]

ESI-MS (+ve) $[C_6H_{11}N_2]^+$ calcd 111.09, found 111.36.

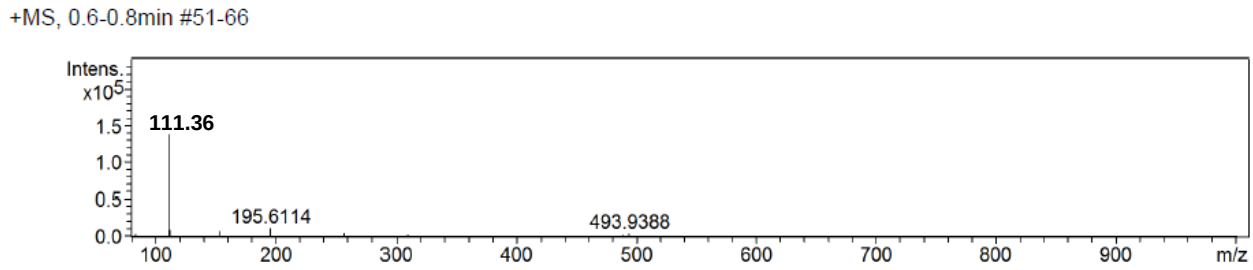


Figure 7.5. Mass Spectrometry analysis for [EMIM] Ac.

1-Ethyl-3-methylimidazolium bis (trifluoromethylsulfonyl) imide, [EMIM] [Tf_2N]

ESI-MS (+ve) $[C_6H_{11}N_2]^+$ calcd 111.09, found 111.09.

ESI-MS (-ve) $[C_2F_6NO_4S_2]^-$, calcd 279.92, found 279.91

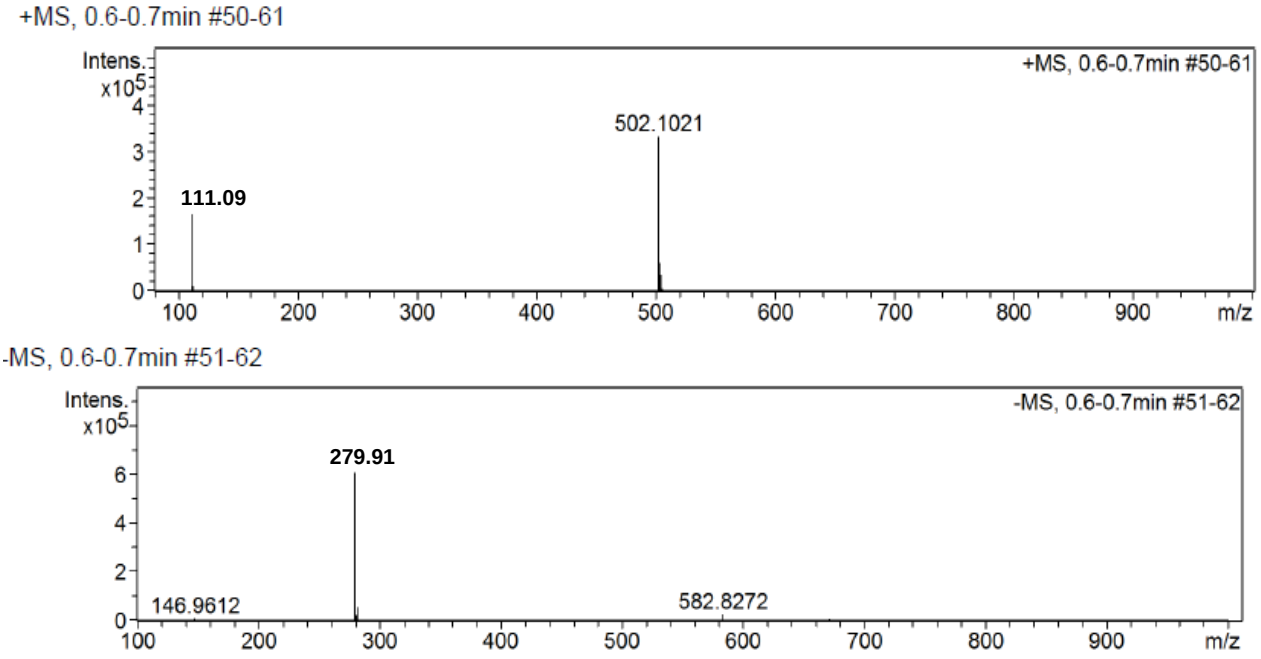


Figure 7.6. Mass Spectrometry analysis for [EMIM] [Tf_2N].

1-Ethyl-3-methylimidazolium tetrafluoroborate, [EMIM] [BF_4]

ESI-MS (+ve) $[C_6H_{11}N_2]^+$, calcd 111.09, found 111.09.

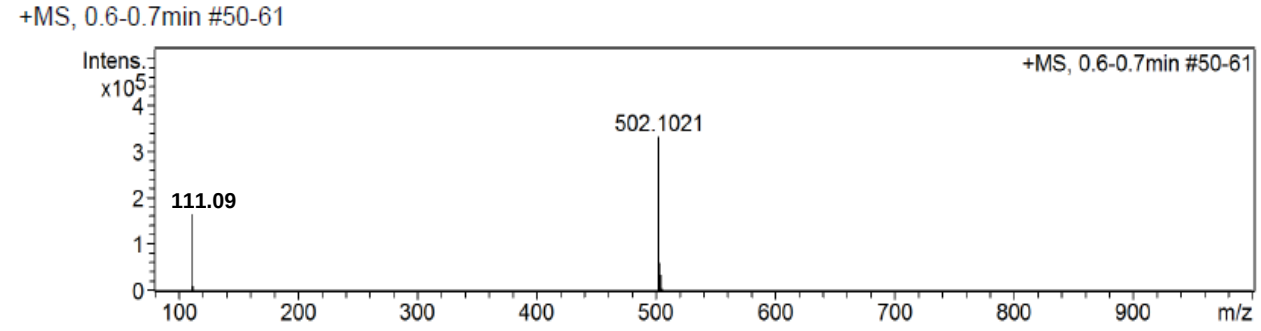


Figure 7.7. Mass Spectrometry analysis for [EMIM] [BF_4].

NMR spectrometry

1, 3-Dimethylimidazolium dimethyl phosphate, [MMIM] [DMP]

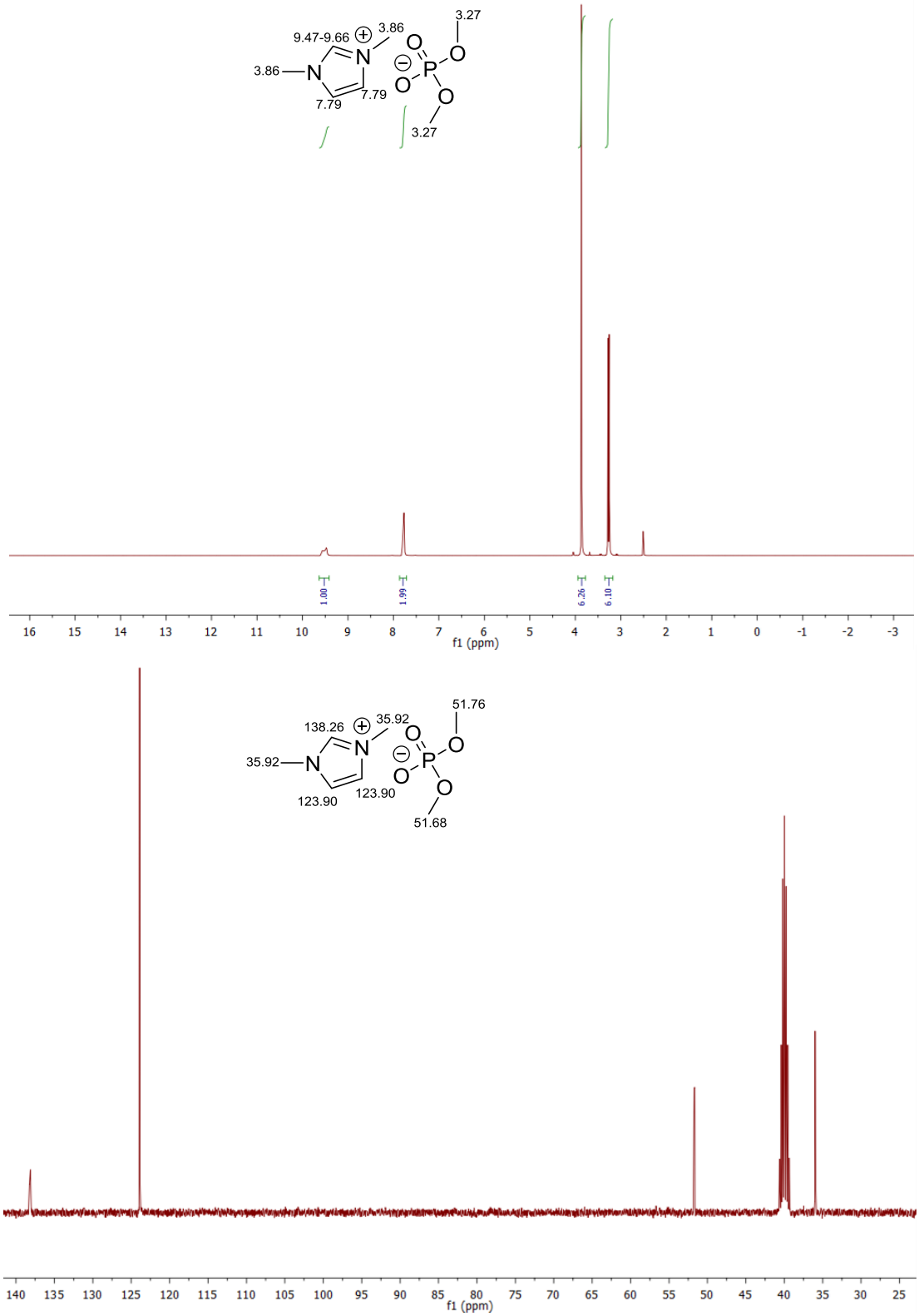


Figure 7.8. NMR analysis of [MMIM] [DMP] ^{1}H NMR (top) and ^{13}C NMR (bottom).

1, 3-Dimethylimidazolium methyl sulphate, [MMIM] [$MeSO_4$]

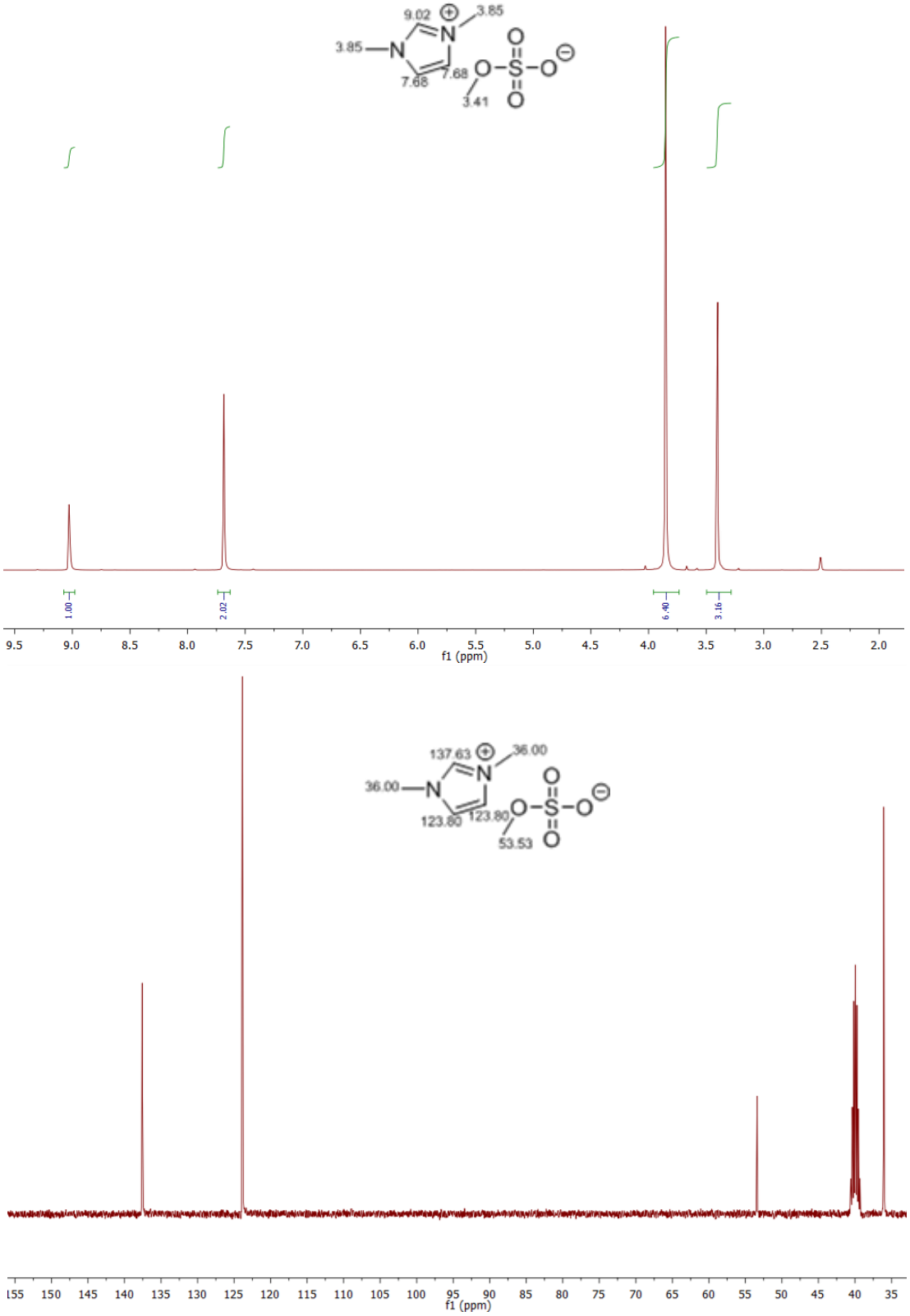


Figure 7.9. NMR analysis of [MMIM] [$MeSO_4$] ^{1}H NMR (top) and ^{13}C NMR (bottom).

1-Ethyl-3-methylimidazolium acetate, [EMIM] [Ac]

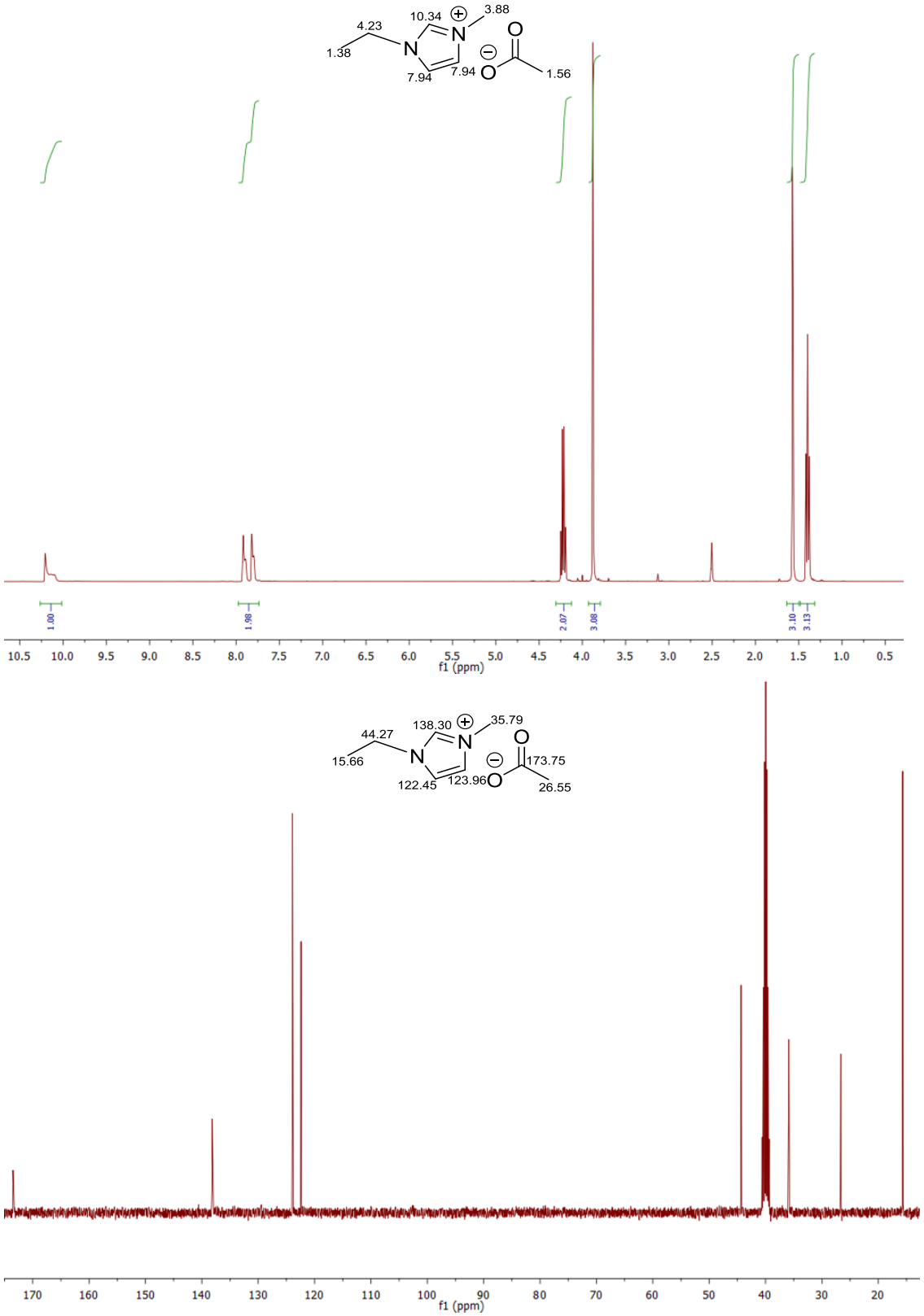


Figure 7.10. NMR analysis of [EMIM] Ac ^{1}H NMR (top) and ^{13}C NMR (bottom).

1-Ethyl-3-methylimidazolium chloride, [EMIM] Cl

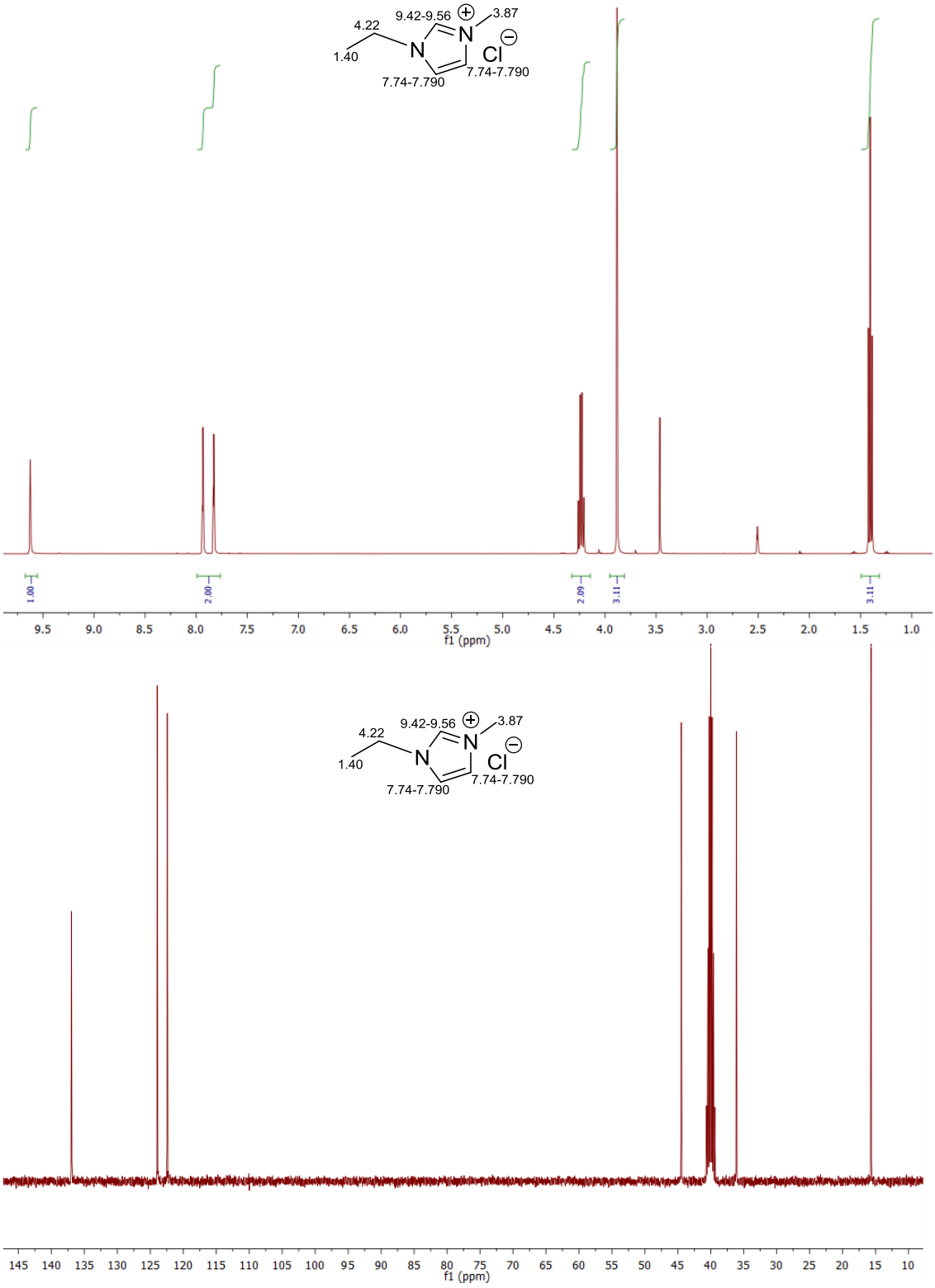


Figure 7.11. NMR analysis of [MMIM] Cl ^{1}H NMR (top) and ^{13}C NMR (bottom).

1-Methyl-3-octylimidazolium chloride, [OMIM] Cl

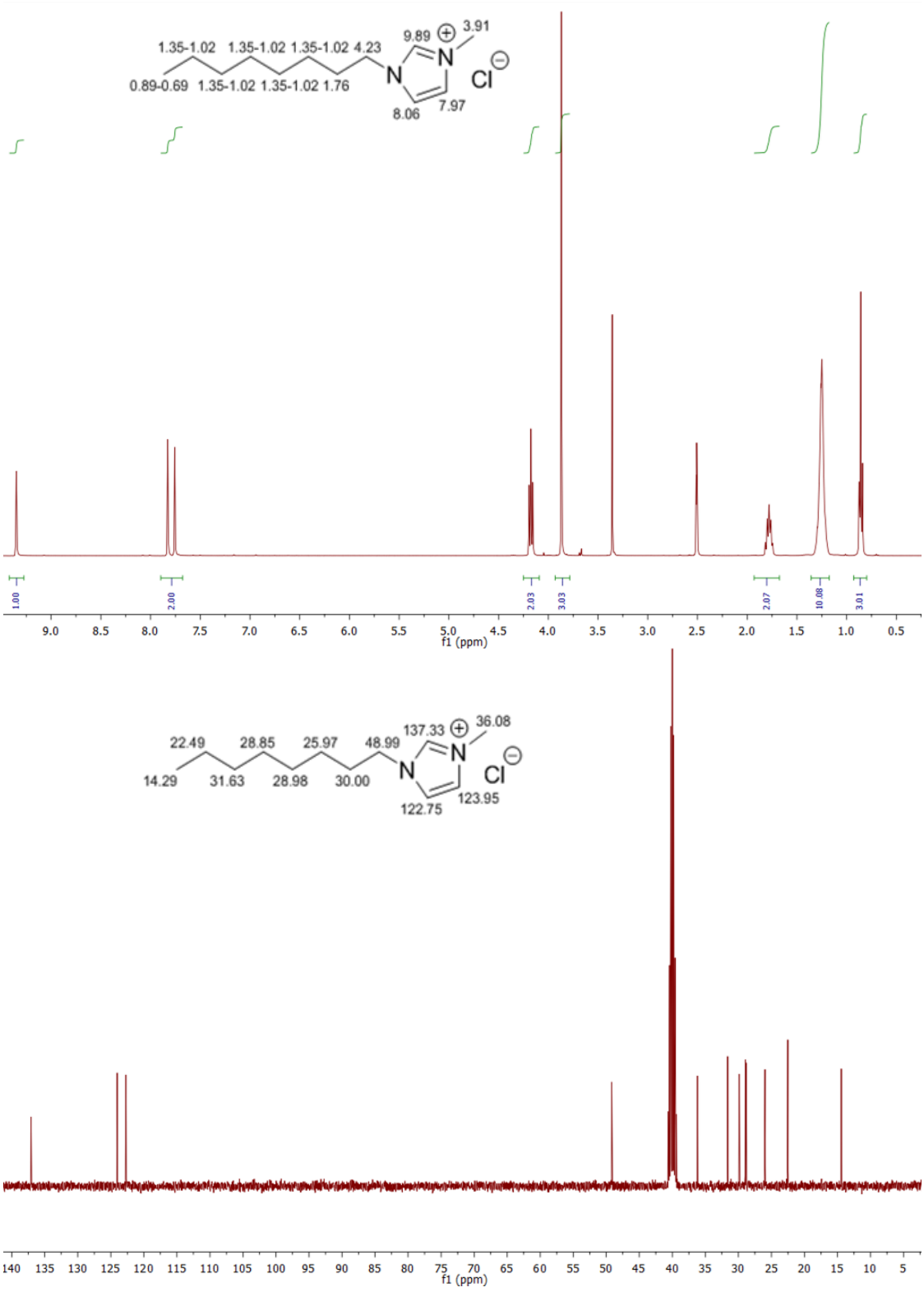


Figure 7.12. NMR analysis of [OMIM] Cl, ^{1}H NMR (top) and ^{13}C NMR (bottom).

1-Ethyl-3-methylimidazolium bis (trifluoromethylsulfonyl) imide, [EMIM] [Tf_2N]

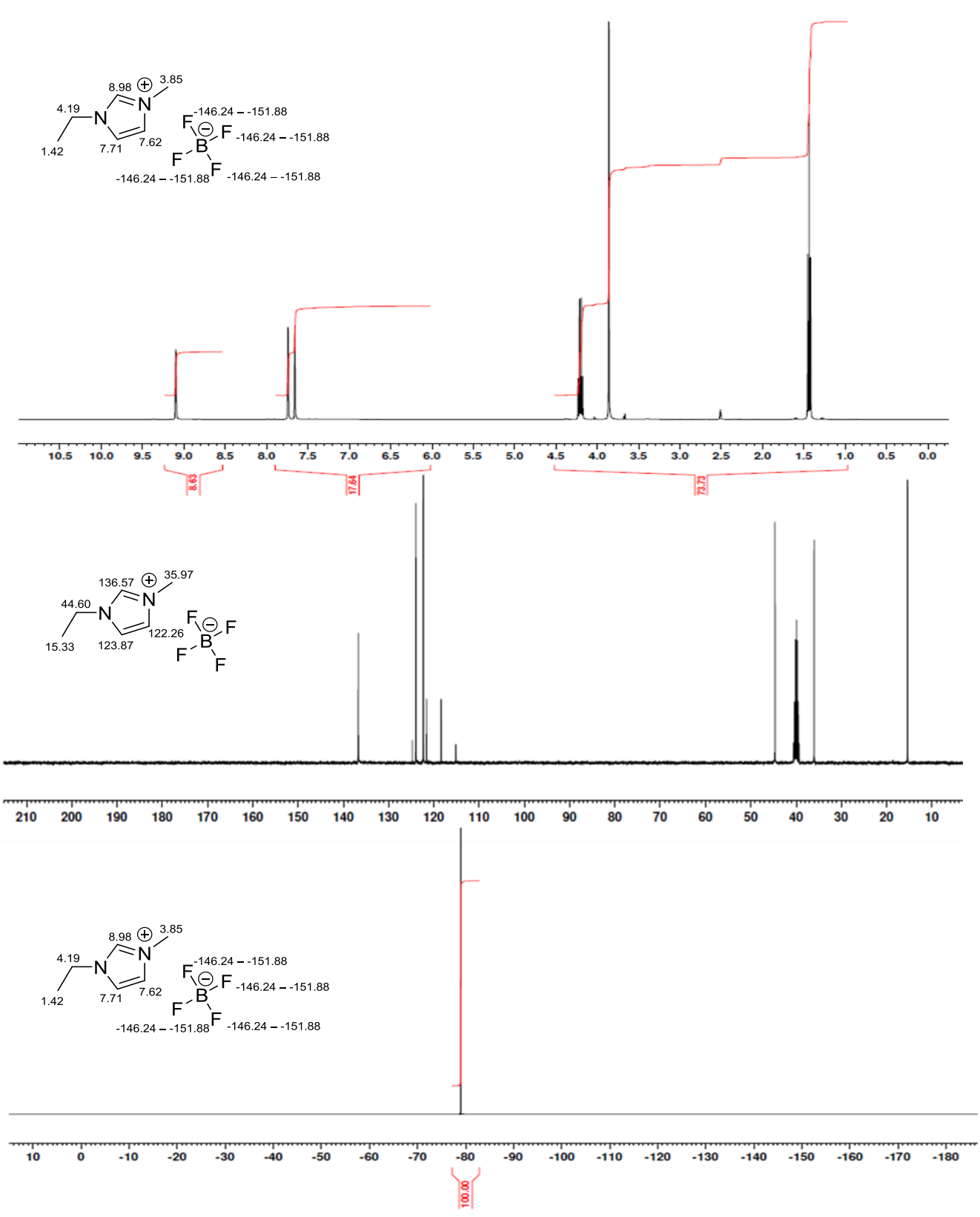


Figure 7.13. NMR analysis of [EMIM] [Tf_2N] ^{1}H NMR (top), ^{13}C NMR (middle) and ^{19}F (Bottom).

1-Ethyl-3-methylimidazolium tetrafluoroborate, [EMIM] [BF_4]

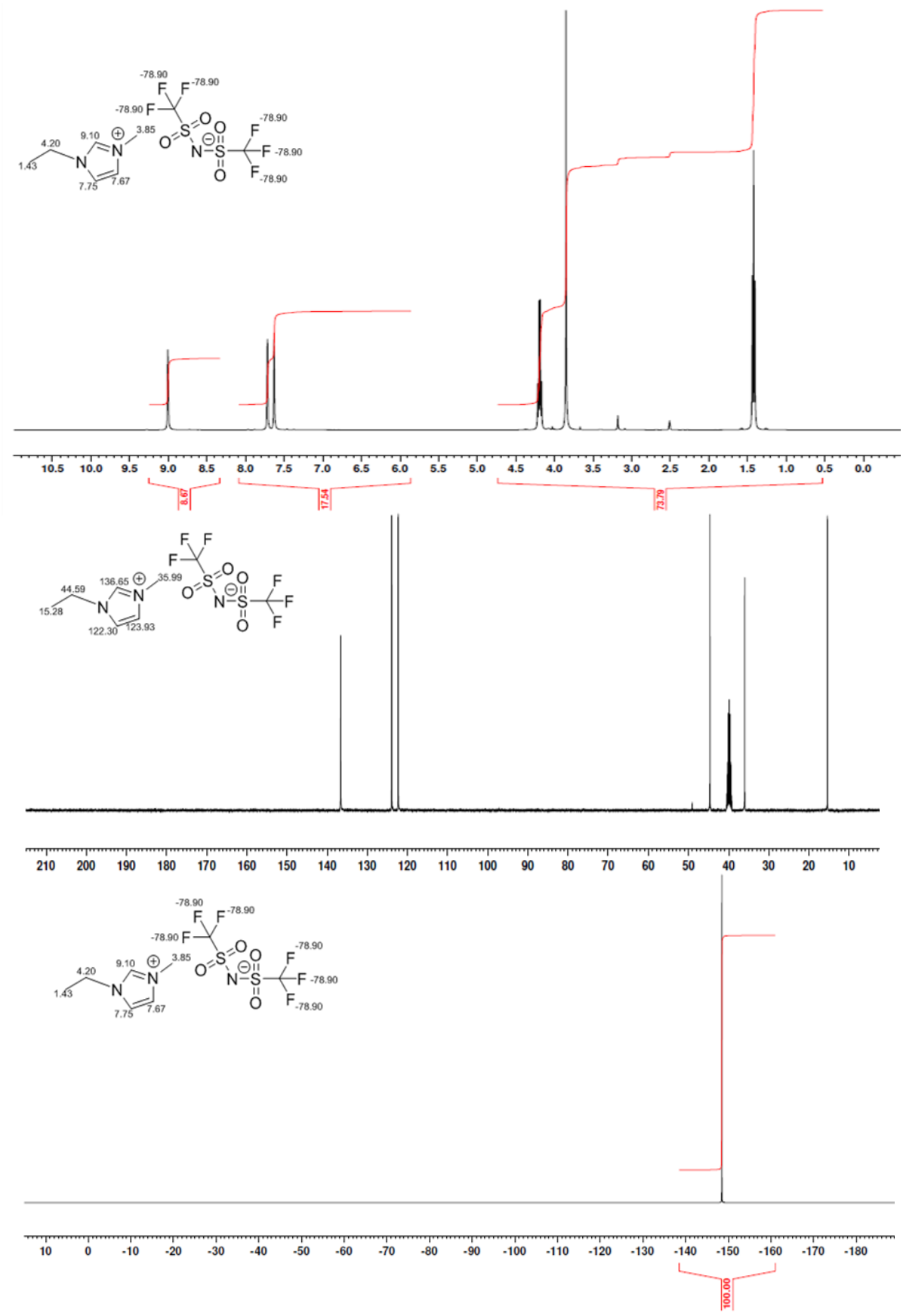


Figure 7.14. NMR analysis of [EMIM] [BF4]^{1}H NMR (top), ^{13}C NMR (middle) and ^{19}F (Bottom).

Appendix B: ATR-FTIR, Raman and Multivariate Spectra for Chapter 3.

This section contains the ATR-FTIR spectra, Raman spectra and the multivariate analysis of the ILs studied in Chapter 3. These spectra represent the hydration experiments for each individual IL with the multivariate analysis for the 0-95 % water concentration experiment. The ATR-FTIR and Raman vibrational assignment tables for each individual IL are displayed alongside the spectra collected.

1, 3-Dimethylimidazolium dimethyl phosphate, [MMIM] [DMP], Atmospheric Water Absorption

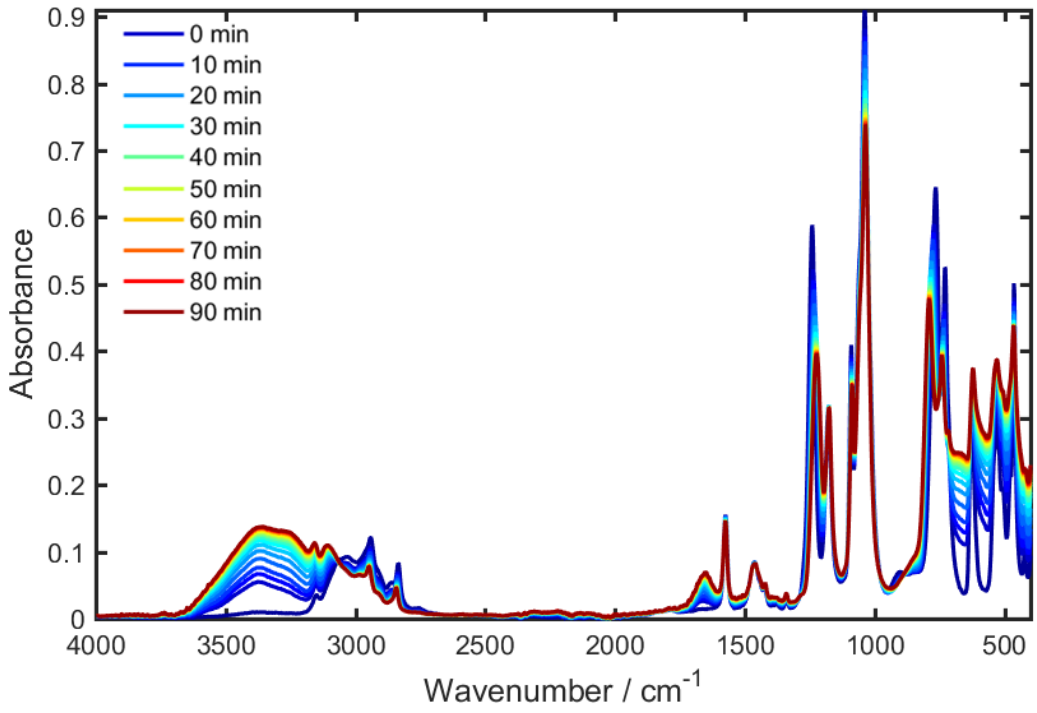


Figure 7.15. ATR-FTIR spectra of the absorption of atmospheric water in [MMIM] [DMP].

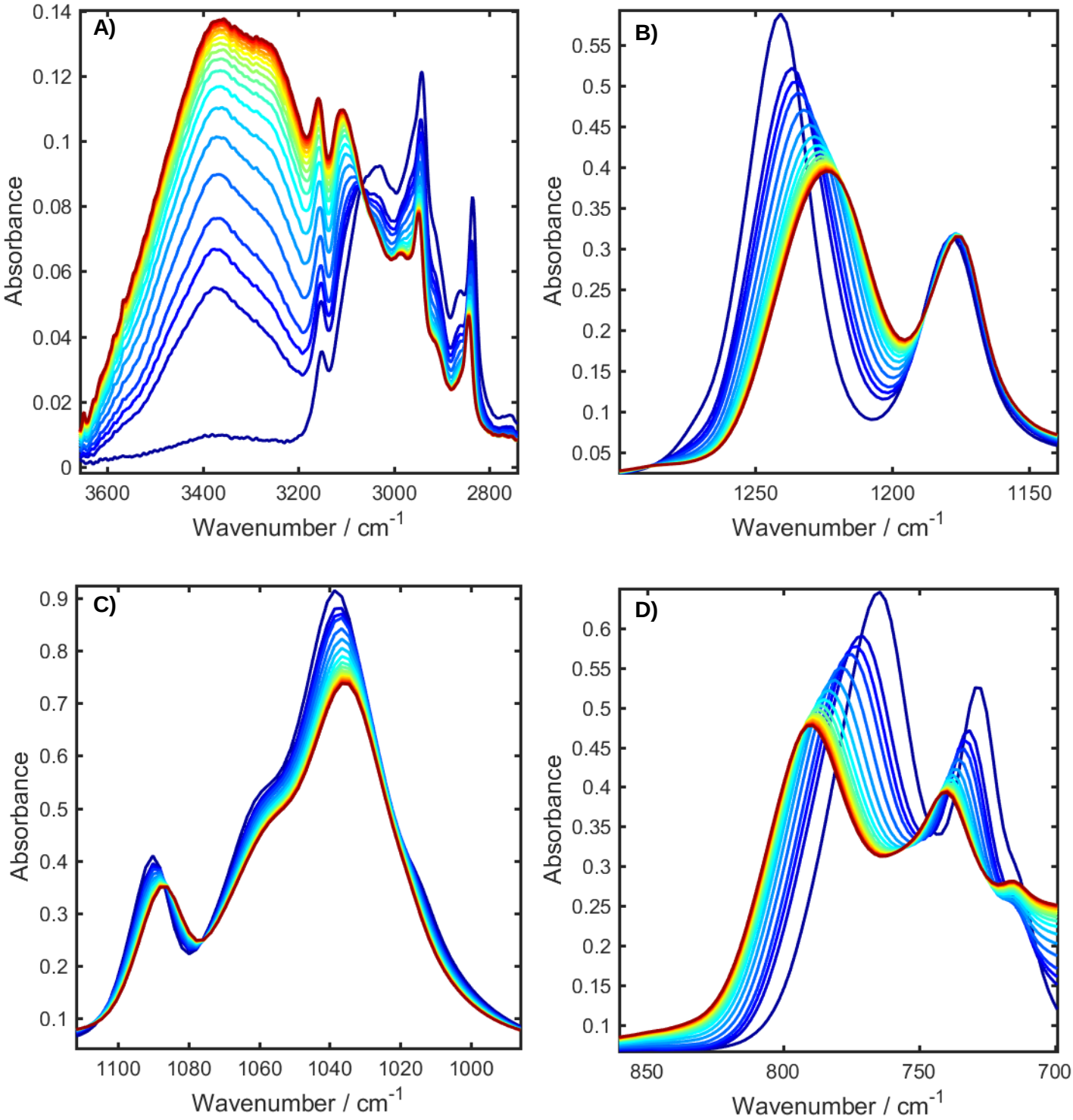


Figure 7.16. Major spectral changes observed in [MMIM] [DMP]. A) ν(O-H), B) ν(P=O), C) ν(C-O), D) ν(P-O).

1, 3-Dimethylimidazolium dimethyl phosphate, [MMIM] [DMP], Bulk Water

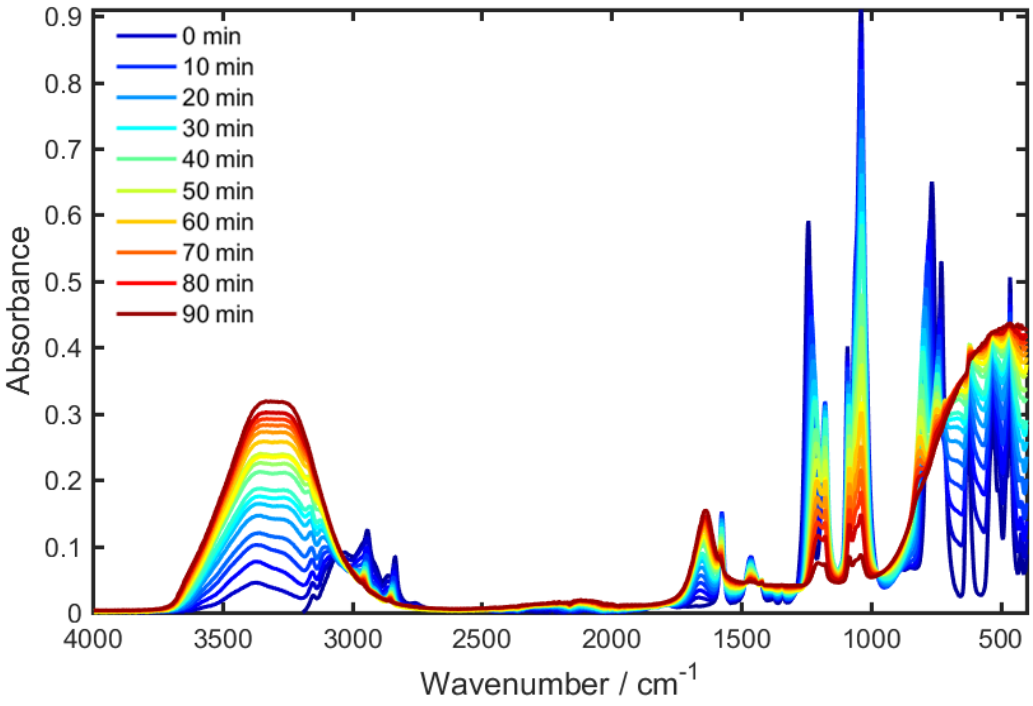


Figure 7.17. ATR-FTIR spectra of 5 % increases of water in [MMIM] [DMP].

1, 3-Dimethylimidazolium dimethyl phosphate, [MMIM] [DMP], Multivariate Analysis

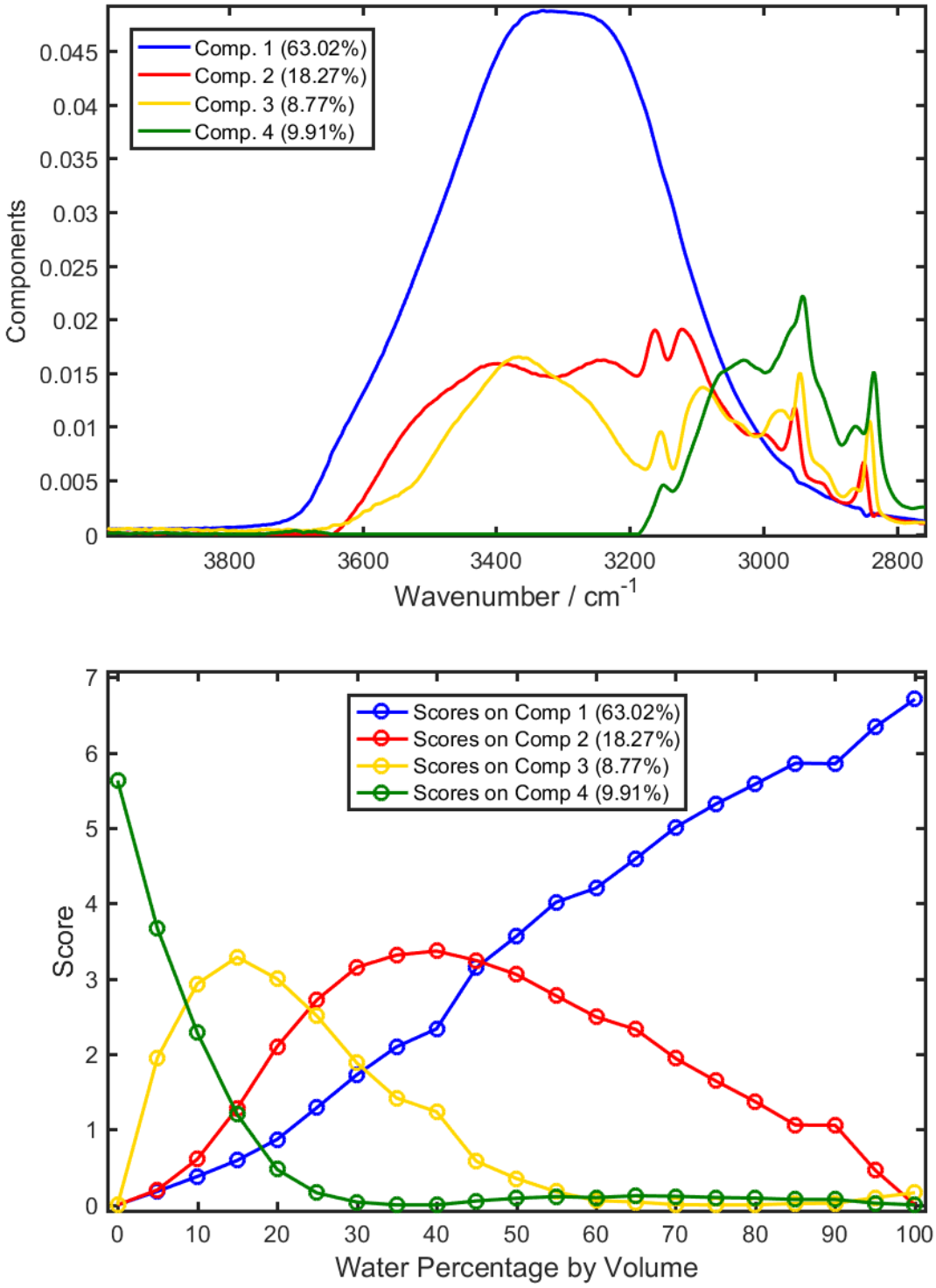


Figure 7.18. MCR components (top) and scores ("concentrations" bottom) for 0 - 95 % water in [MMIM] [DMP] mixture monitored by ATR-FTIR spectroscopy, showing only the high wavenumber region.

1, 3-Dimethylimidazolium dimethyl phosphate, [MMIM] [DMP], Bulk Water, Raman Analysis

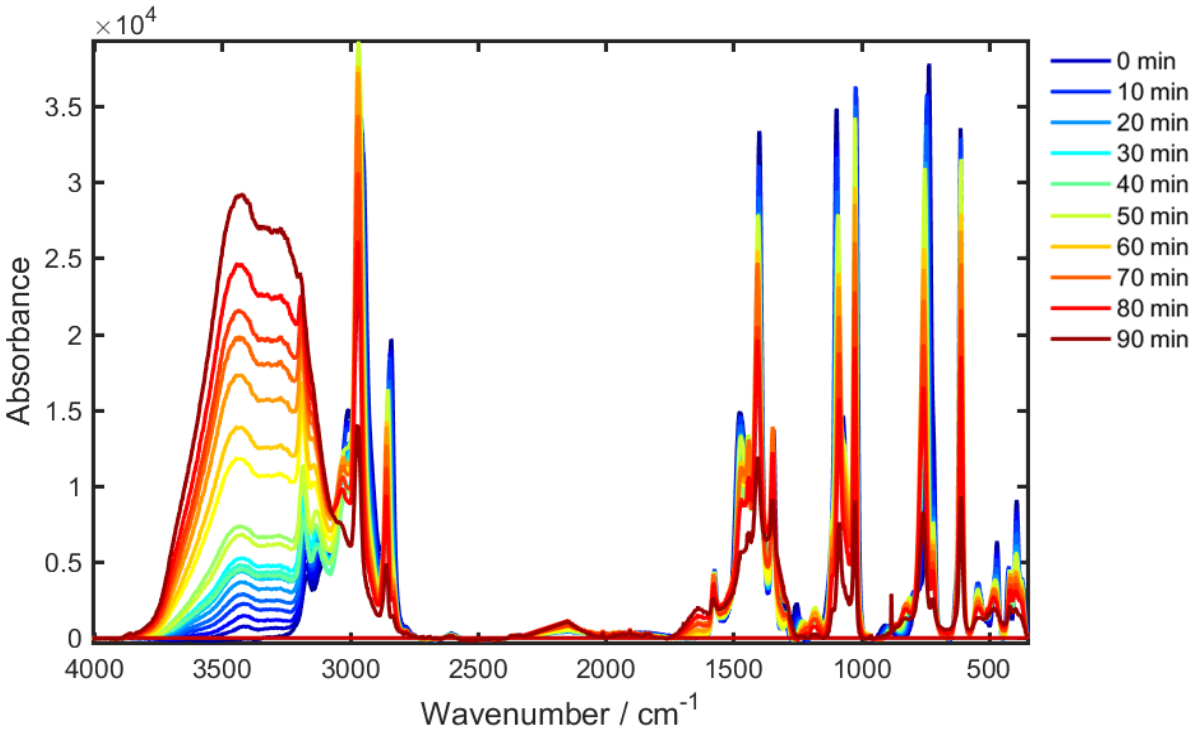


Figure 7.19. Raman spectra of 5 % increases of water in [MMIM] [DMP].

1-Ethyl-3-methylimidazolium acetate, [EMIM] [Ac], Atmospheric Water Absorption

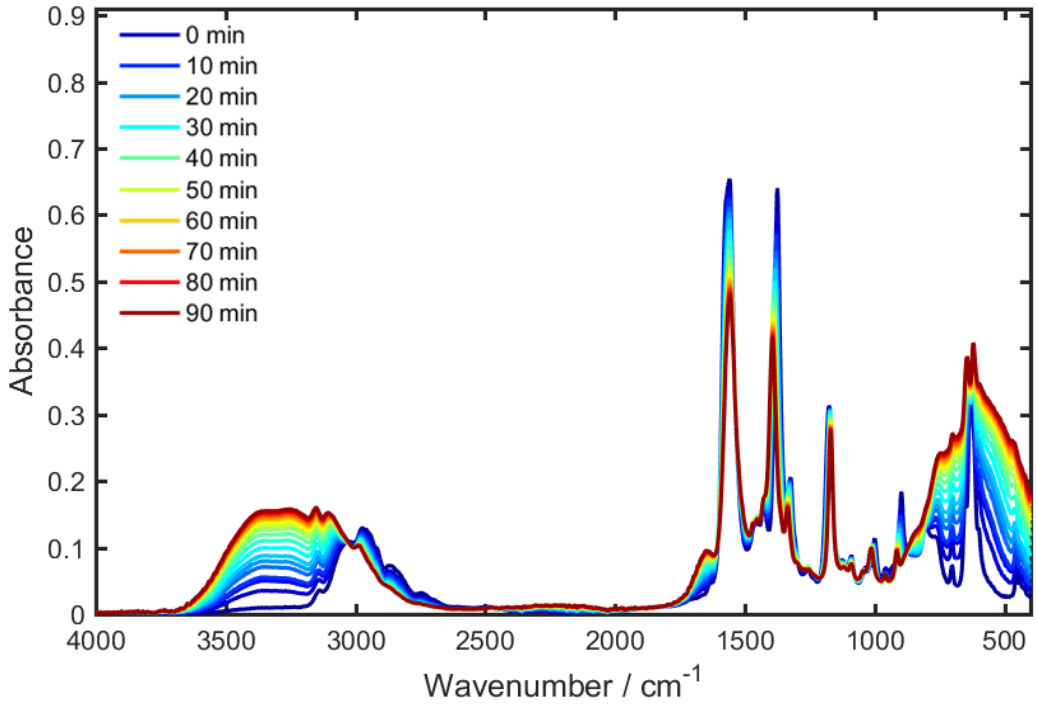


Figure 7.20. ATR-FTIR spectra of the absorption of atmospheric water in [EMIM] [Ac].

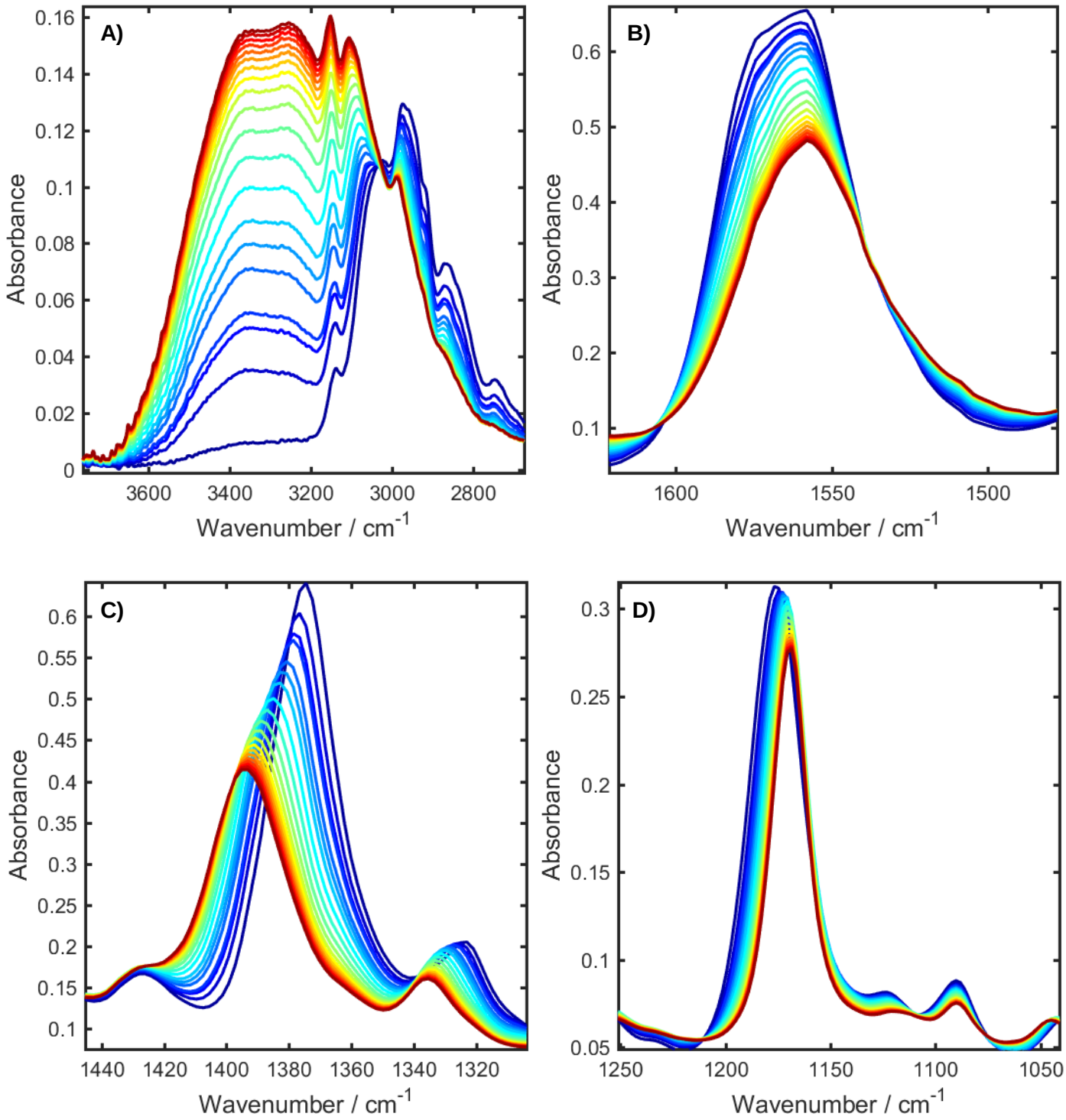


Figure 7.21. Major spectral changes observed in [EMIM] [Ac]. A) ν(O-H), B) ν(COO) asym, C) ν(COO) sym, D) ν(COC).

1-Ethyl-3-methylimidazolium acetate, [EMIM] [Ac], Bulk Water

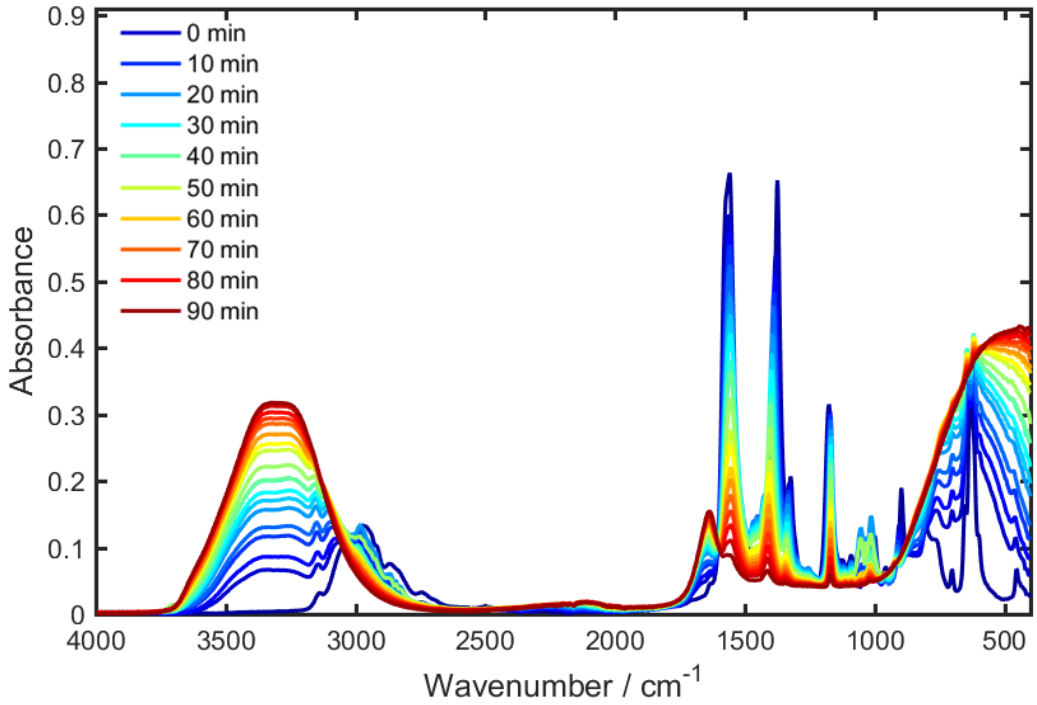


Figure 7.22. ATR-FTIR spectra of 5 % increases of water in [EMIM] [Ac].

1-Ethyl-3-methylimidazolium acetate, [EMIM] [Ac], Multivariate Analysis

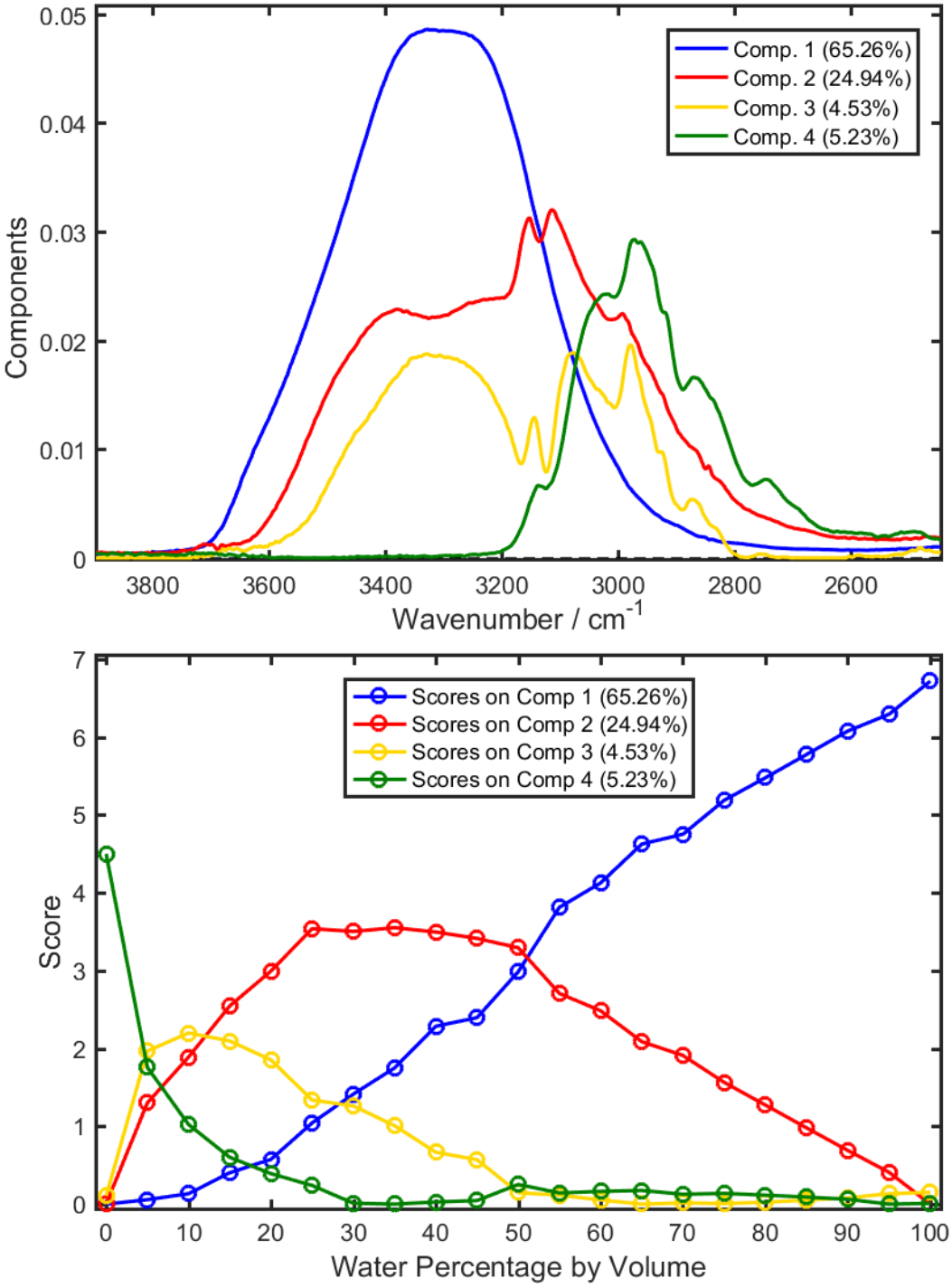


Figure 7.23. MCR components (top) and scores ("concentrations" bottom) for 0 - 95 % water in [EMIM] [Ac] mixture monitored by ATR-FTIR spectroscopy, showing only the high wavenumber region.

1-Ethyl-3-methylimidazolium acetate, [EMIM] [Ac], Bulk Water, Raman Analysis

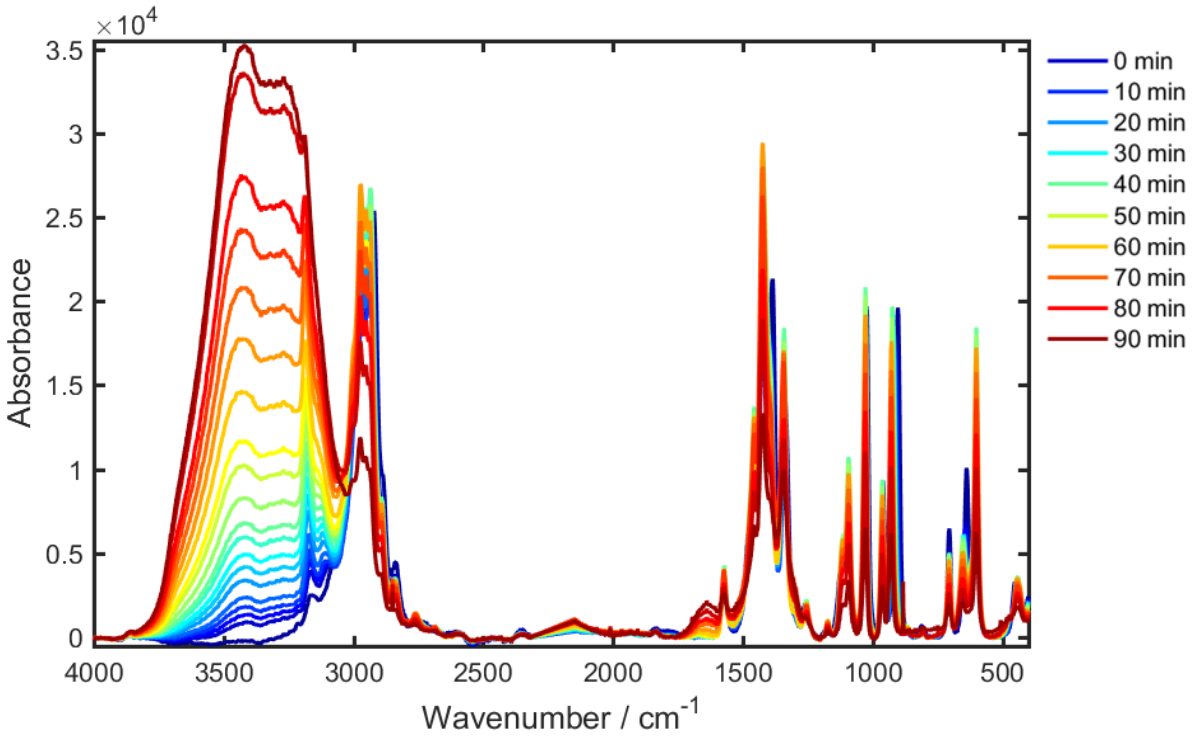


Figure 7.24. Raman spectra of 5 % increases of water in [EMIM] [Ac].

1-Methyl-3-octylimidazolium chloride, [OMIM] Cl, Atmospheric Water Absorption

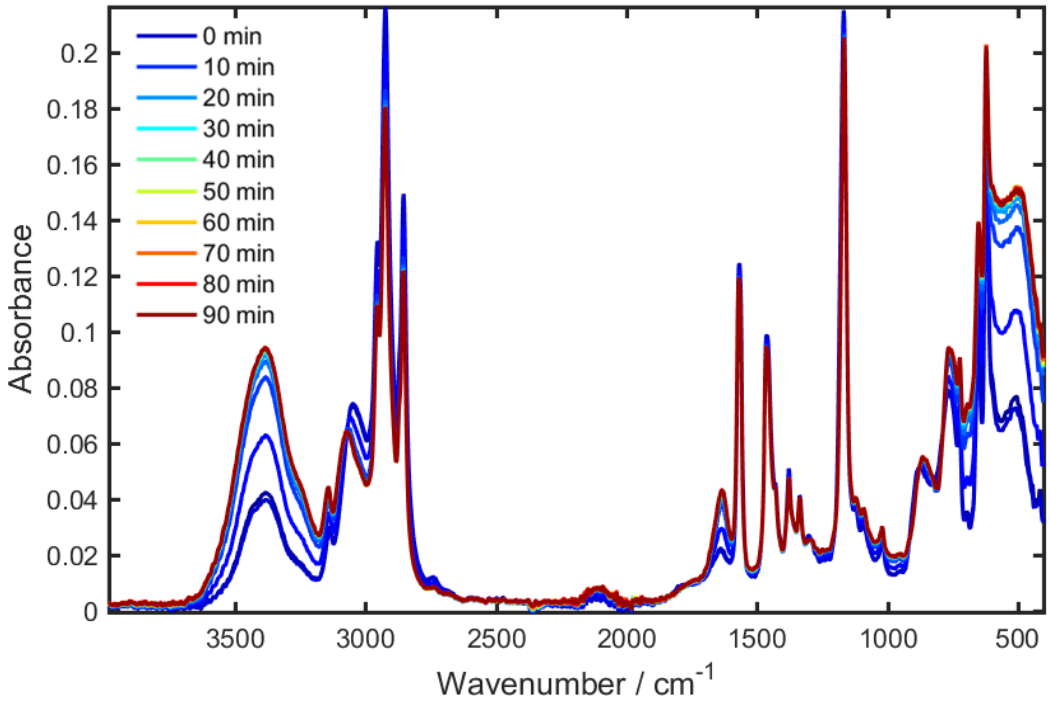


Figure 7.25. ATR-FTIR spectra of the absorption of atmospheric water in [OMIM] Cl.

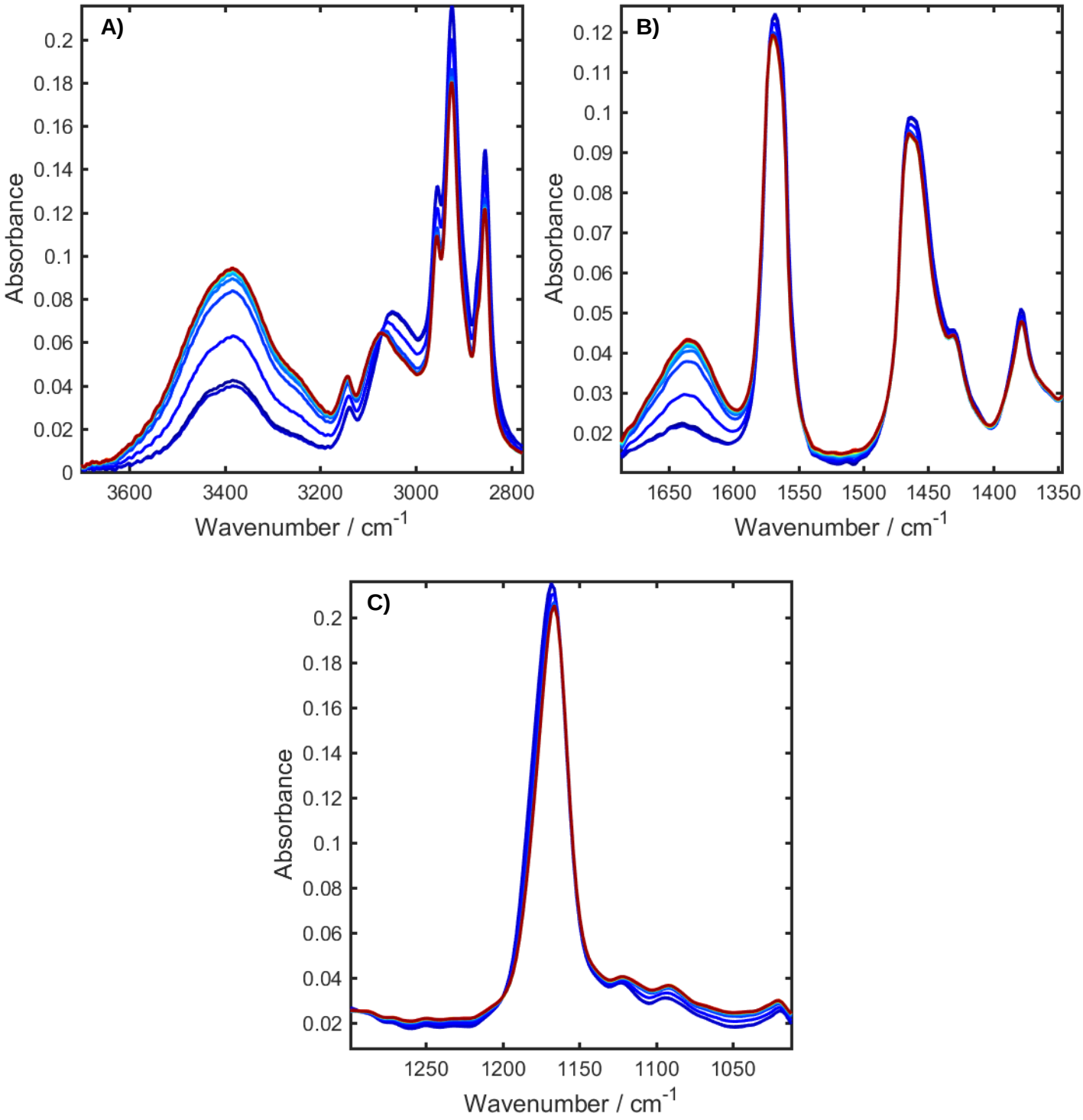


Figure 7.26. Major spectral changes observed in [OMIM] Cl. A) ν(O-H), B) ν(C=N) and ν(C=C), *C)* ν*(C-C).*

1-Methyl-3-octylimidazolium chloride, [OMIM] Cl, Bulk Water

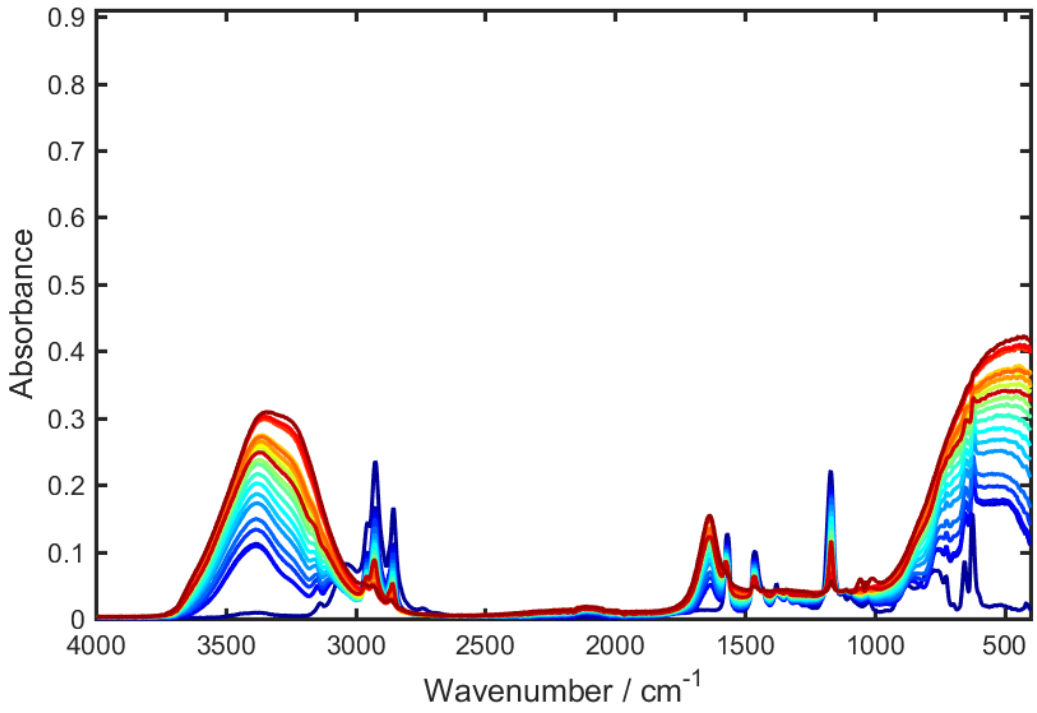


Figure 7.27. ATR-FTIR spectra of 5 % increases of water in [OMIM] Cl.

1-Methyl-3-octylimidazolium chloride, [OMIM] Cl, Multivariate Analysis

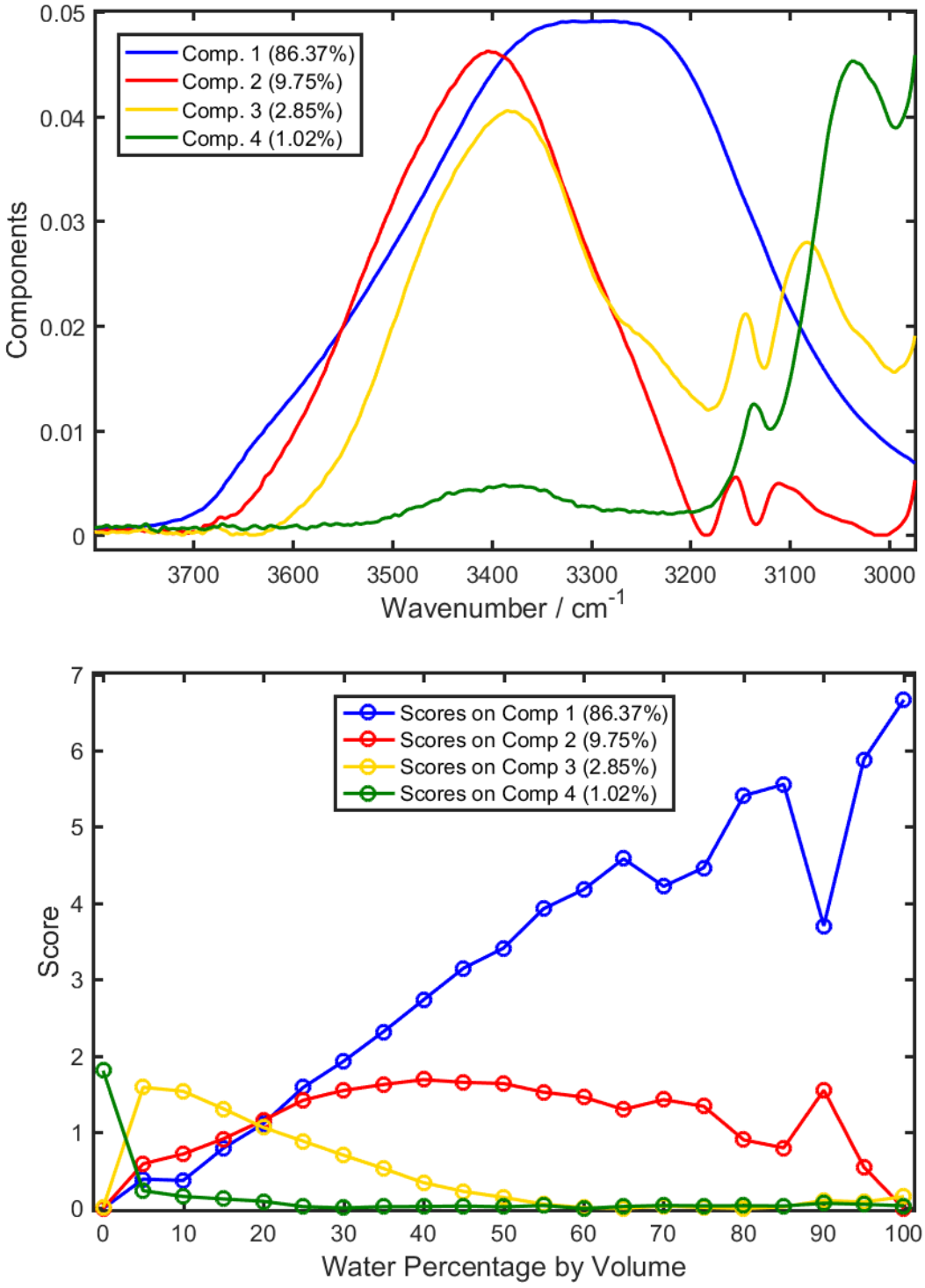


Figure 7.28. MCR components (top) and scores ("concentrations" bottom) for 0 - 95 % water in [OMIM] Cl mixture monitored by ATR-FTIR spectroscopy, showing only the high wavenumber region.

1-Methyl-3-octylimidazolium chloride, [OMIM] Cl, Bulk Water, Raman Analysis

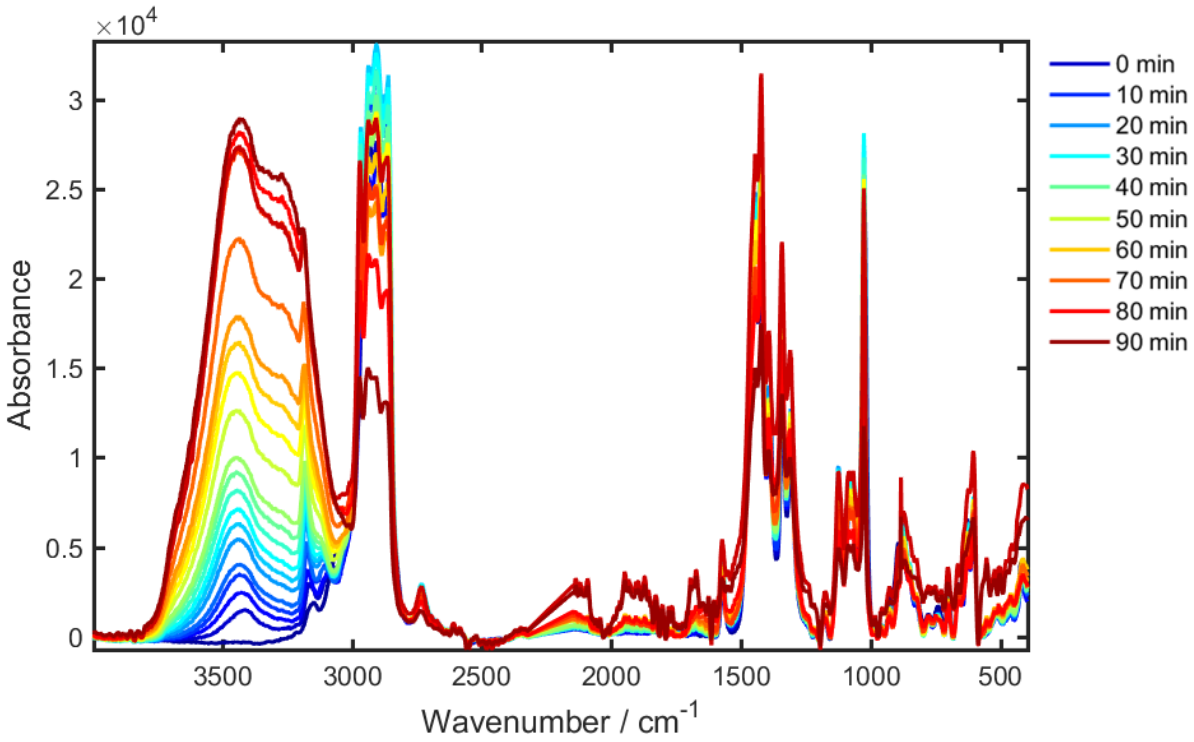


Figure 7.29. Raman spectra of 5 % increases of water in [OMIM] Cl.

Appendix C: ATR-FTIR spectra for Chapter 4.

This section contains the ATR-FTIR spectra for the IL solvent mixtures studied in Chapter 4. These spectra represent the glovebox and atmospheric experiments for each individual IL with the range of solvents studied. The ATR-FTIR vibrational assignment tables for each individual IL are displayed alongside the spectra collected.

Glovebox Measurements for Molecular Solvents and Ionic Liquid Binary Mixtures

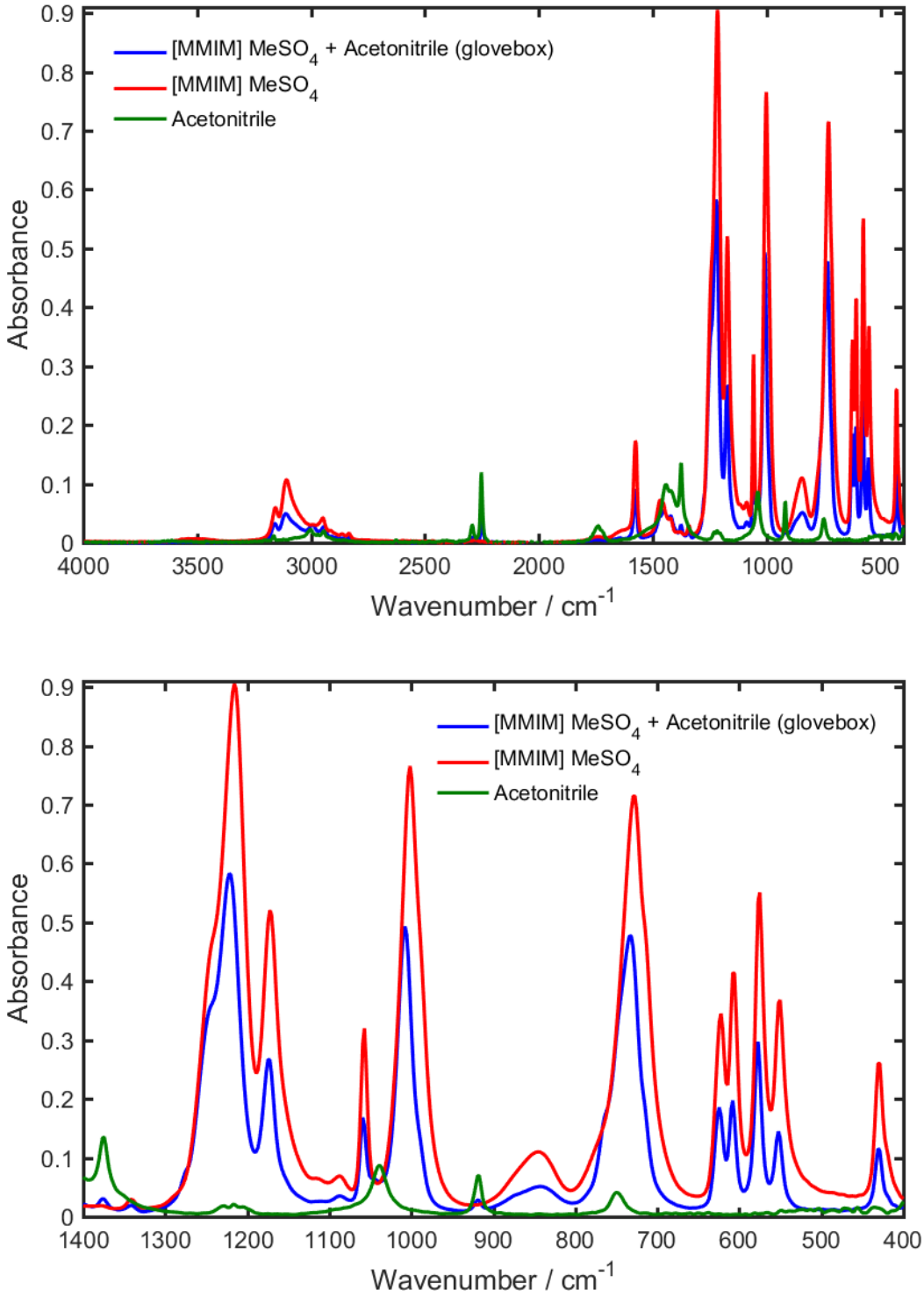


Figure 7.30. ATR-FTIR spectra of [MMIM] [MeSO$_4$] ACN binary mixture overlayed with pure [MMIM] [MeSO$_4$] and ACN (top spectra) a zoomed in version displaying the fingerprint region of the binary mixture (bottom).

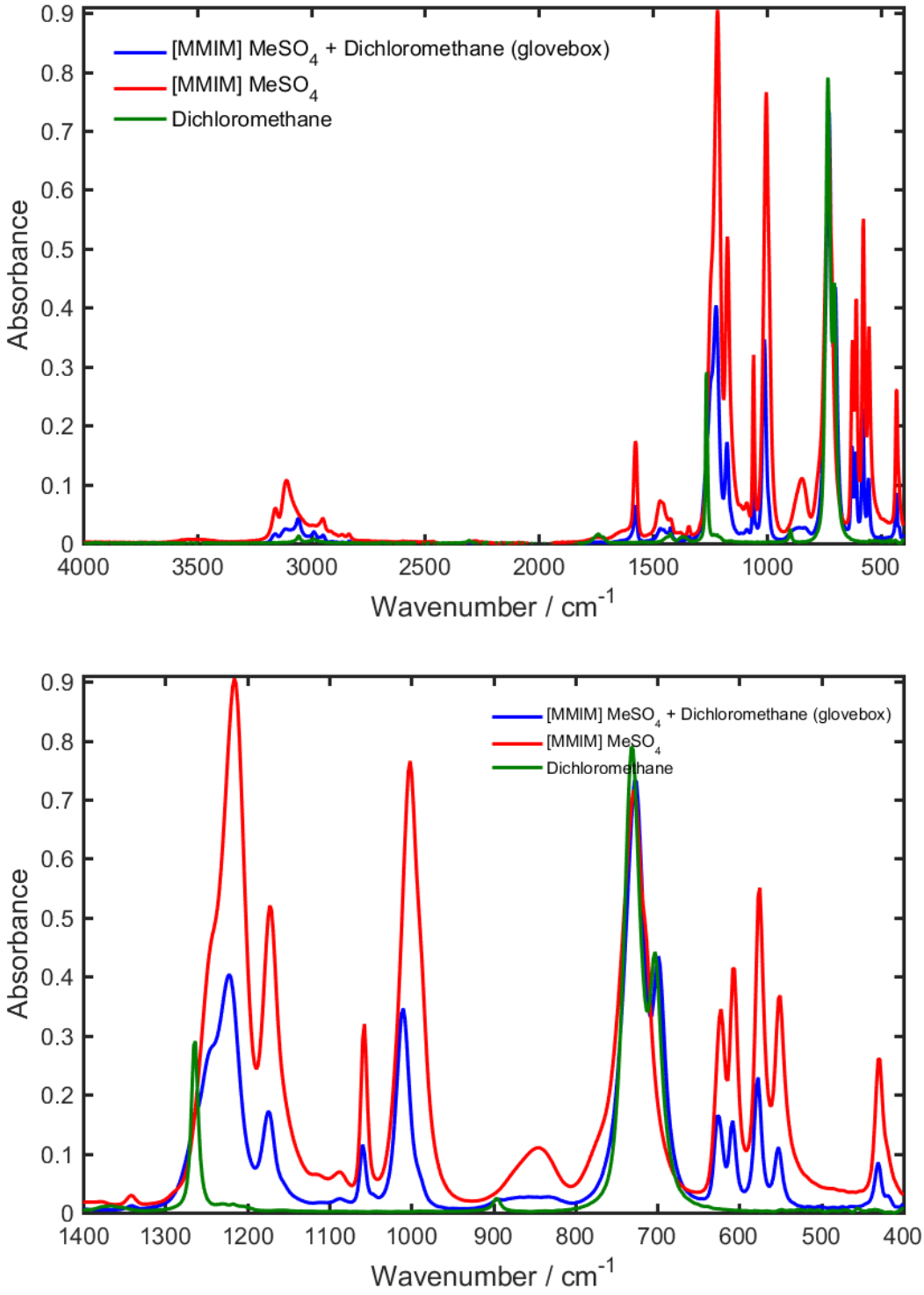


Figure 7.31. ATR-FTIR spectra of [MMIM] [$MeSO_4$] DCM binary mixture overlayed with pure [MMIM] [$MeSO_4$] and DCM (top spectra) a zoomed in version displaying the fingerprint region of the binary mixture (bottom).

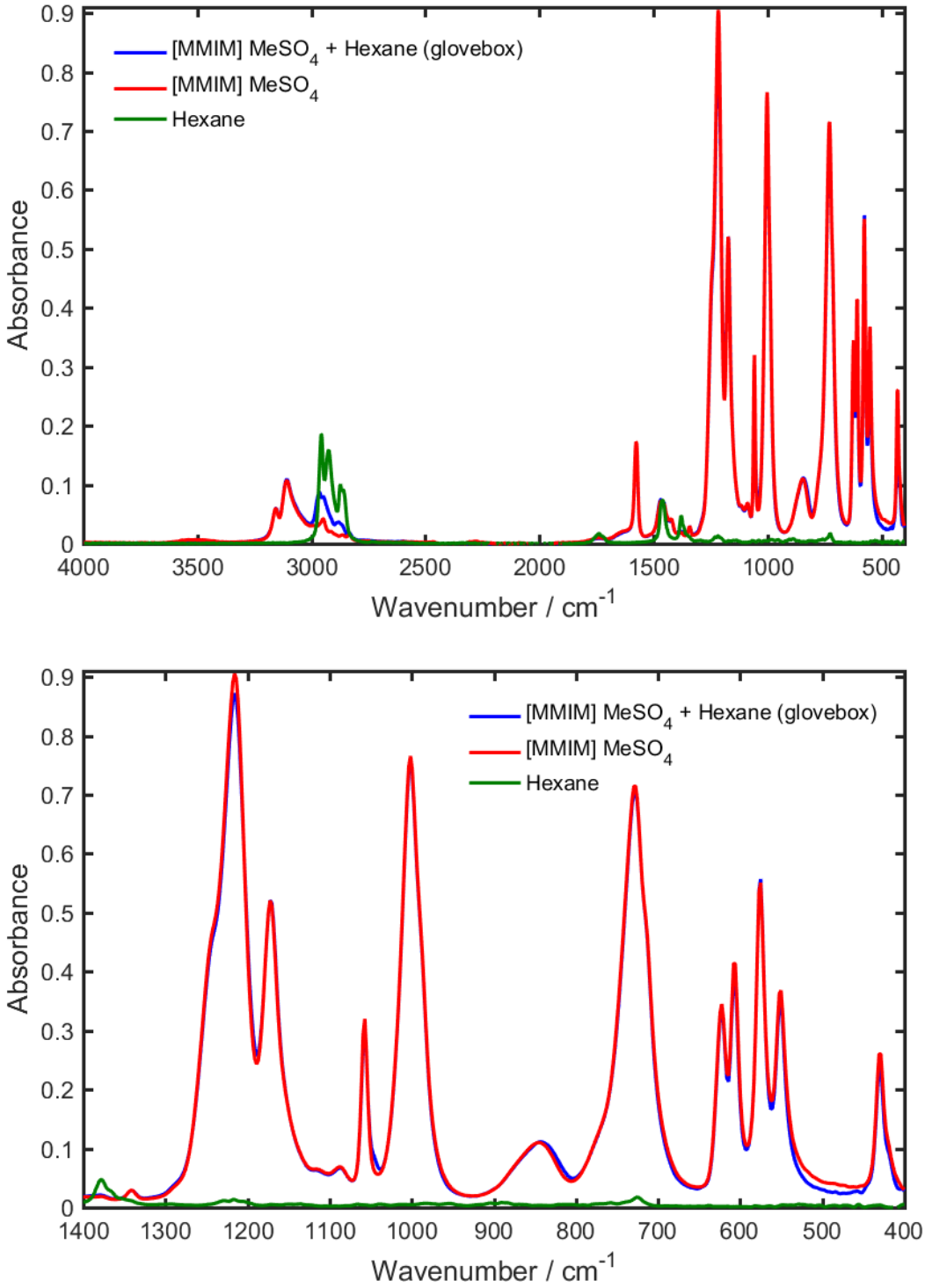


Figure 7.32. ATR-FTIR spectra of [MMIM] [$MeSO_4$] hexane binary mixture overlayed with pure [MMIM] [$MeSO_4$] and hexane (top spectra) a zoomed in version displaying the fingerprint region of the binary mixture (bottom).

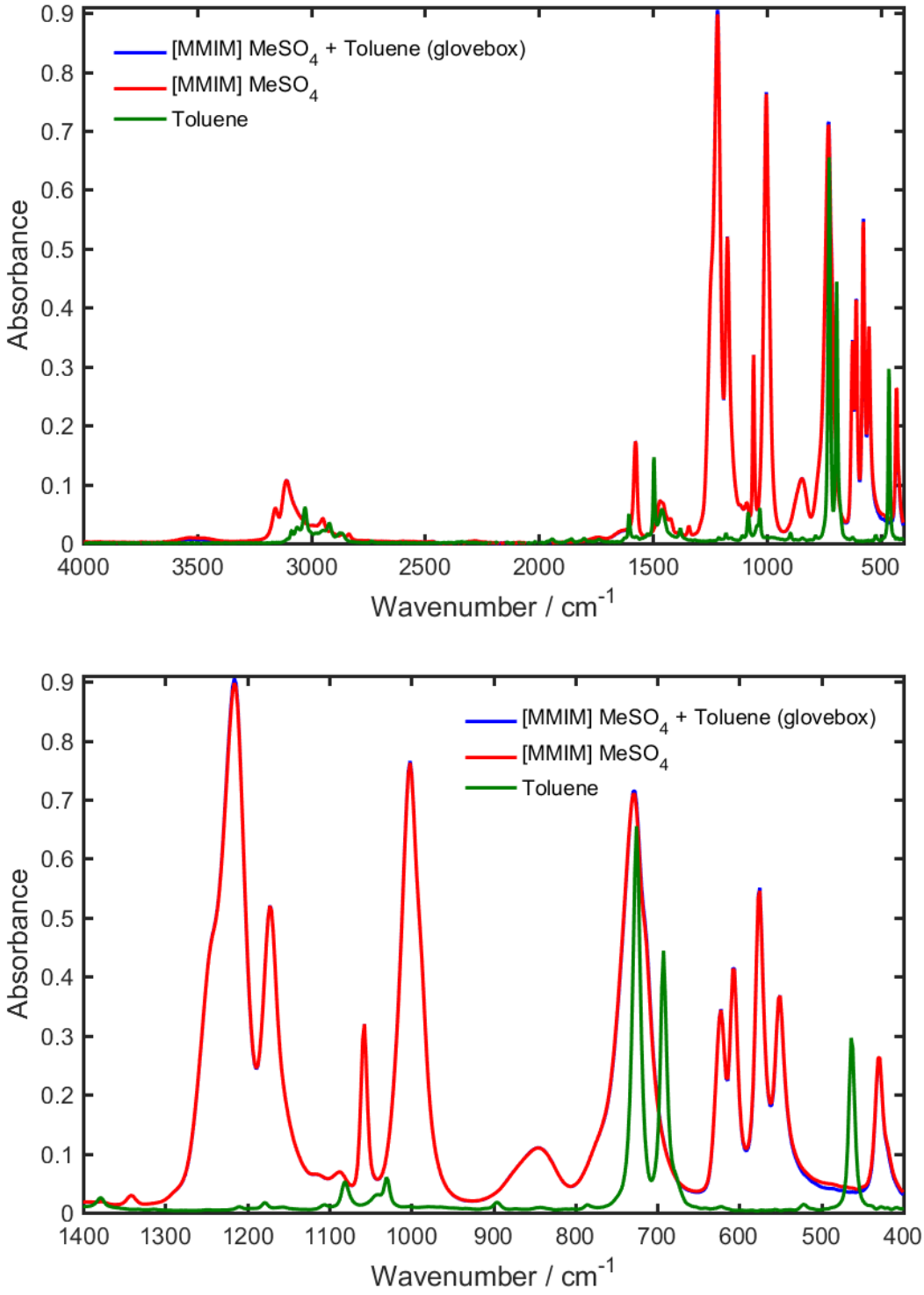


Figure 7.33. ATR-FTIR spectra of [MMIM] [$MeSO_4$] toluene binary mixture overlayed with pure [MMIM] [$MeSO_4$] and toluene (top spectra) a zoomed in version displaying the fingerprint region of the binary mixture (bottom).

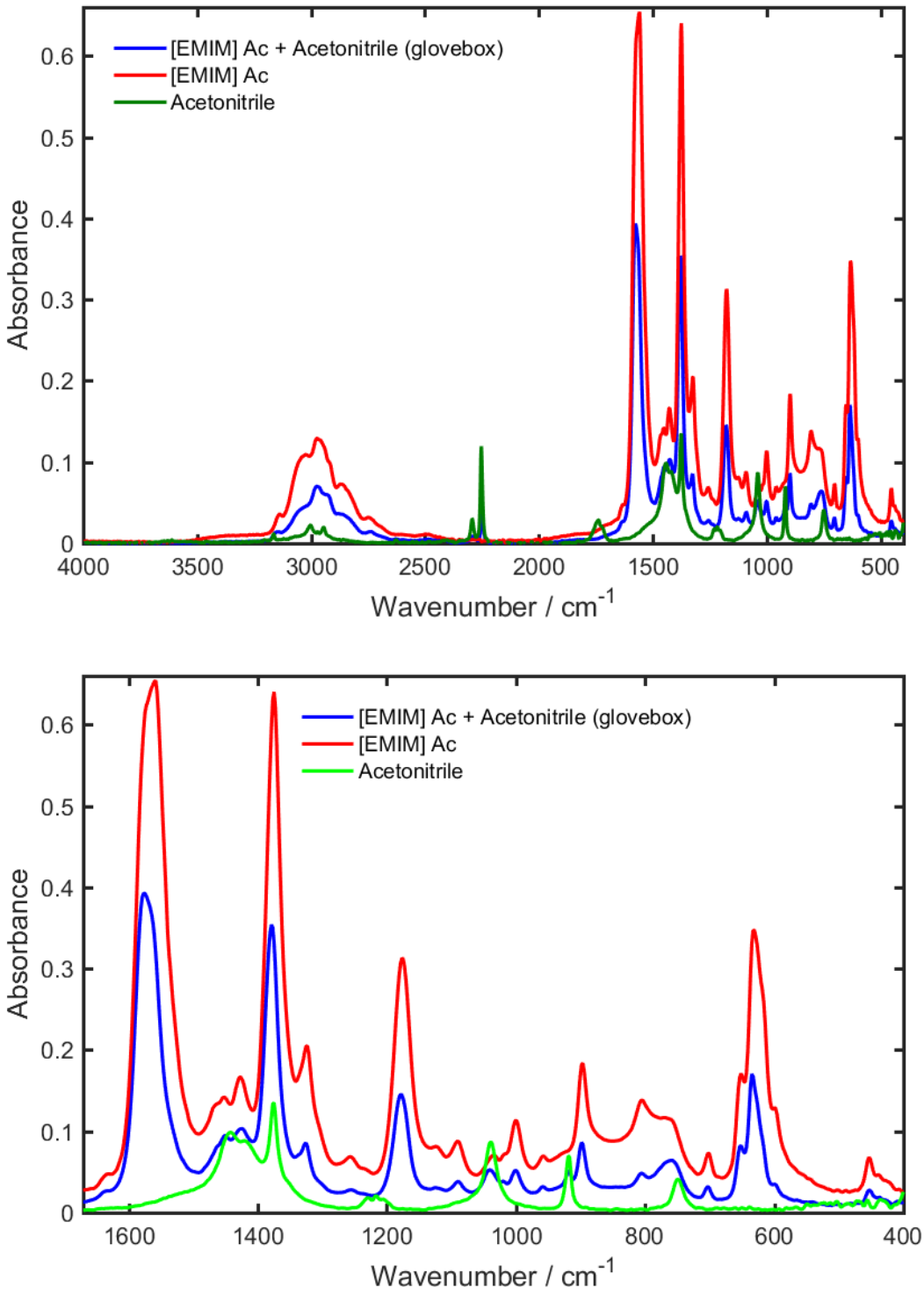


Figure 7.34. ATR-FTIR spectra of [EMIM] [Ac] ACN binary mixture overlayed with pure [EMIM] [Ac] and ACN (top spectra) a zoomed in version displaying the fingerprint region of the binary mixture (bottom).

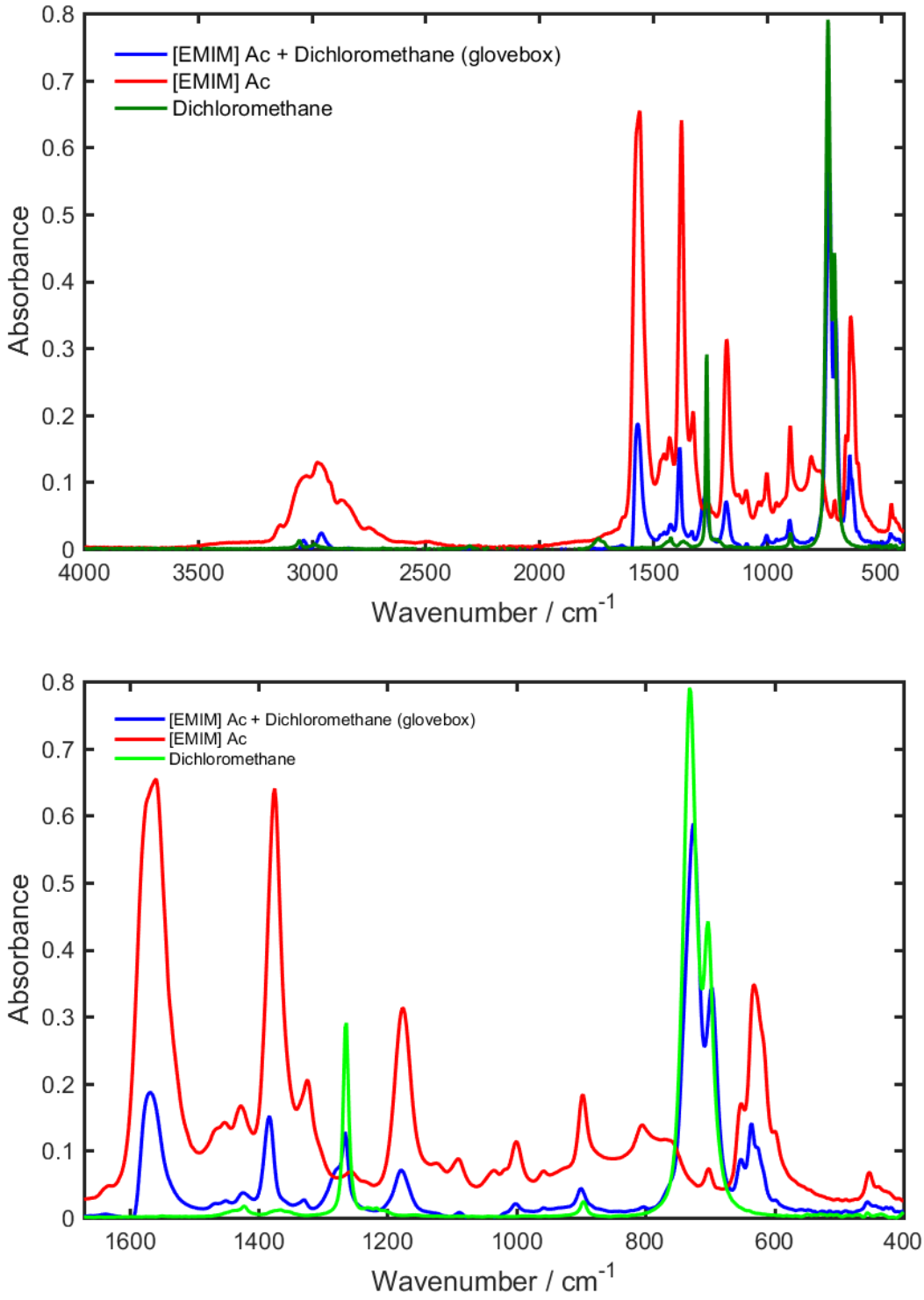


Figure 7.35. ATR-FTIR spectra of [EMIM] [Ac] DCM binary mixture overlayed with pure [EMIM] [Ac] and DCM (top spectra) a zoomed in version displaying the fingerprint region of the binary mixture (bottom).

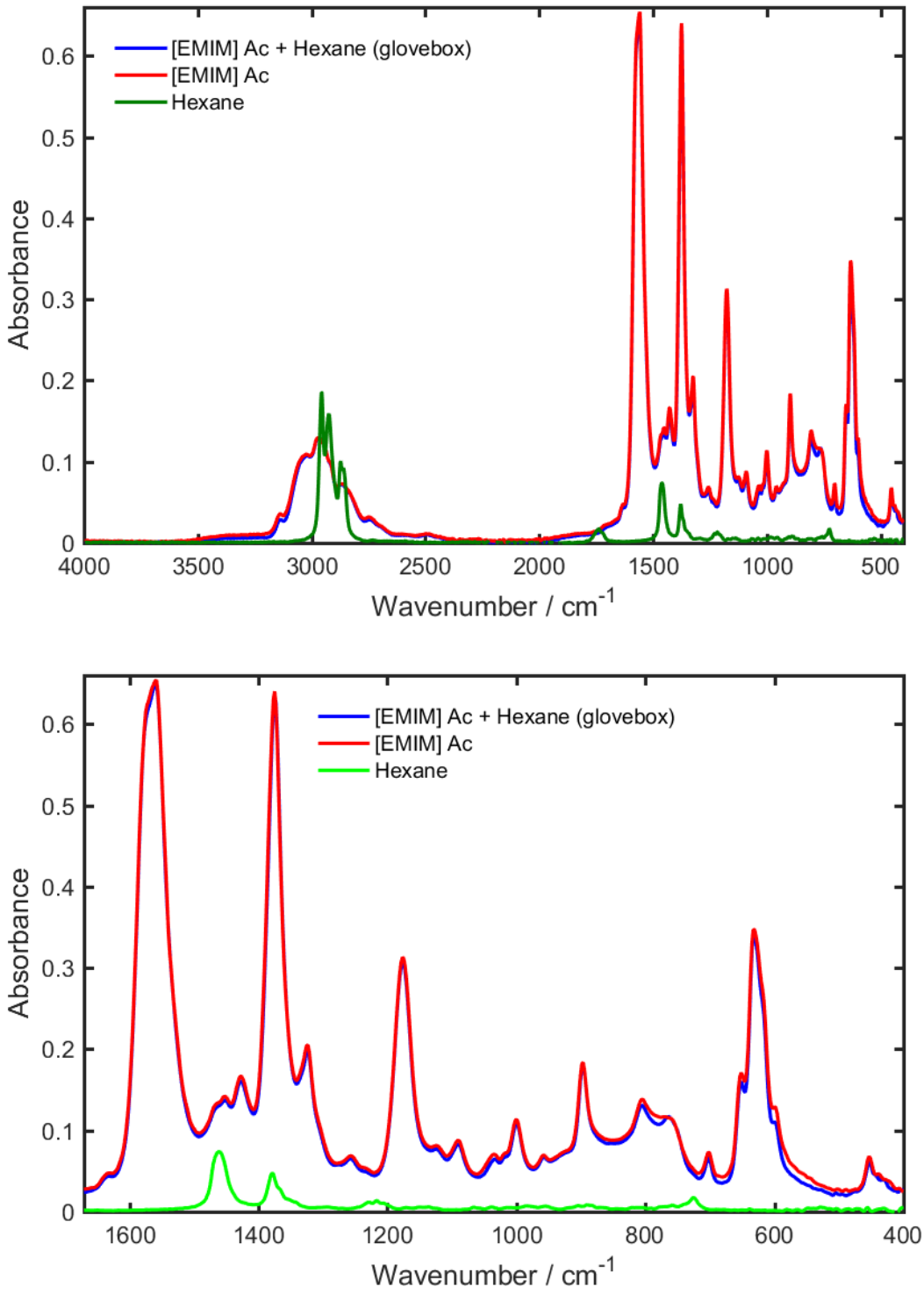


Figure 7.36. ATR-FTIR spectra of [EMIM] [Ac] hexane binary mixture overlayed with pure [EMIM] [Ac] and hexane (top spectra) a zoomed in version displaying the fingerprint region of the binary mixture (bottom).

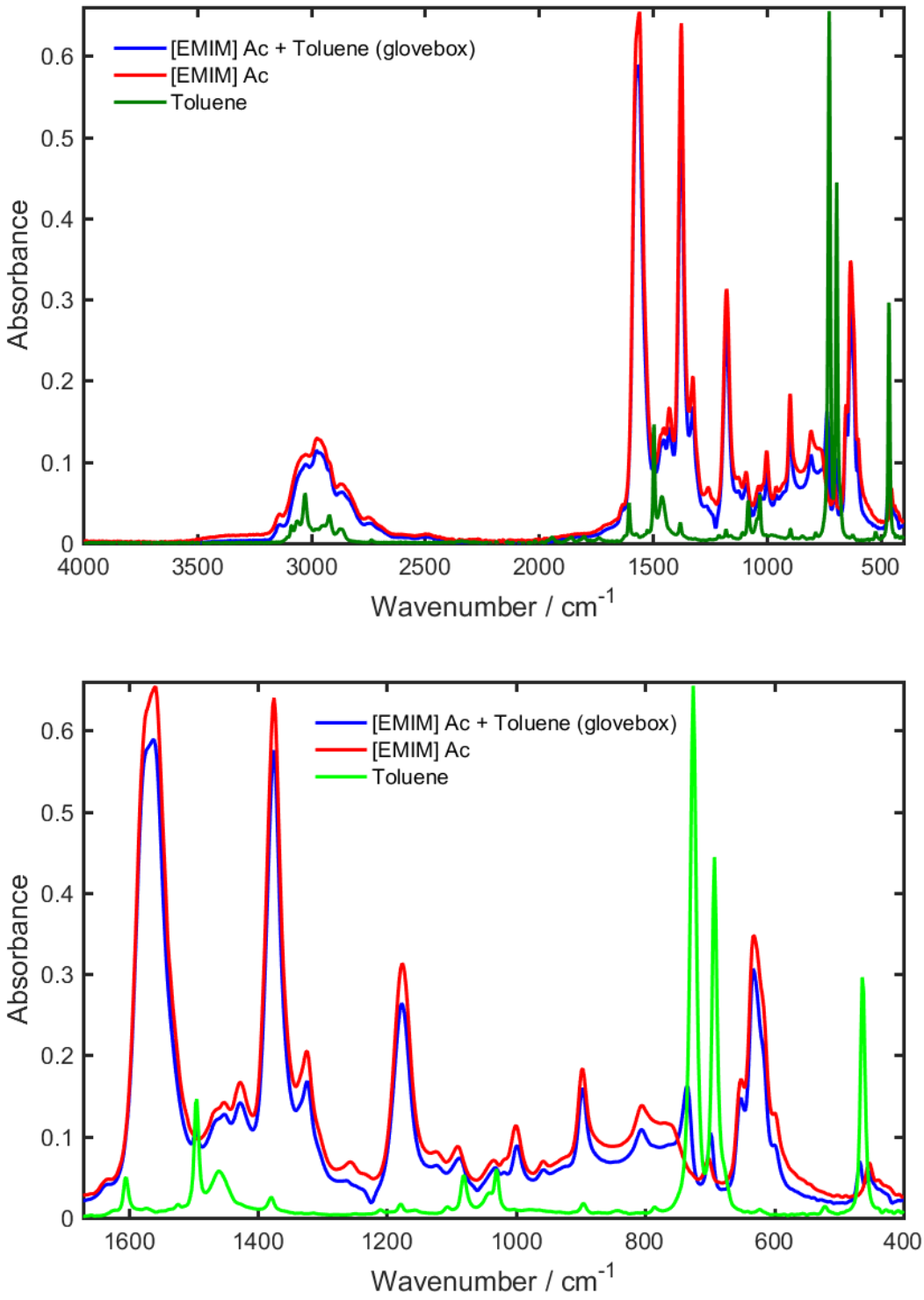


Figure 7.37. ATR-FTIR spectra of [EMIM] [Ac] toluene binary mixture overlayed with pure [EMIM] [Ac] and toluene (top spectra) a zoomed in version displaying the fingerprint region of the binary mixture (bottom).

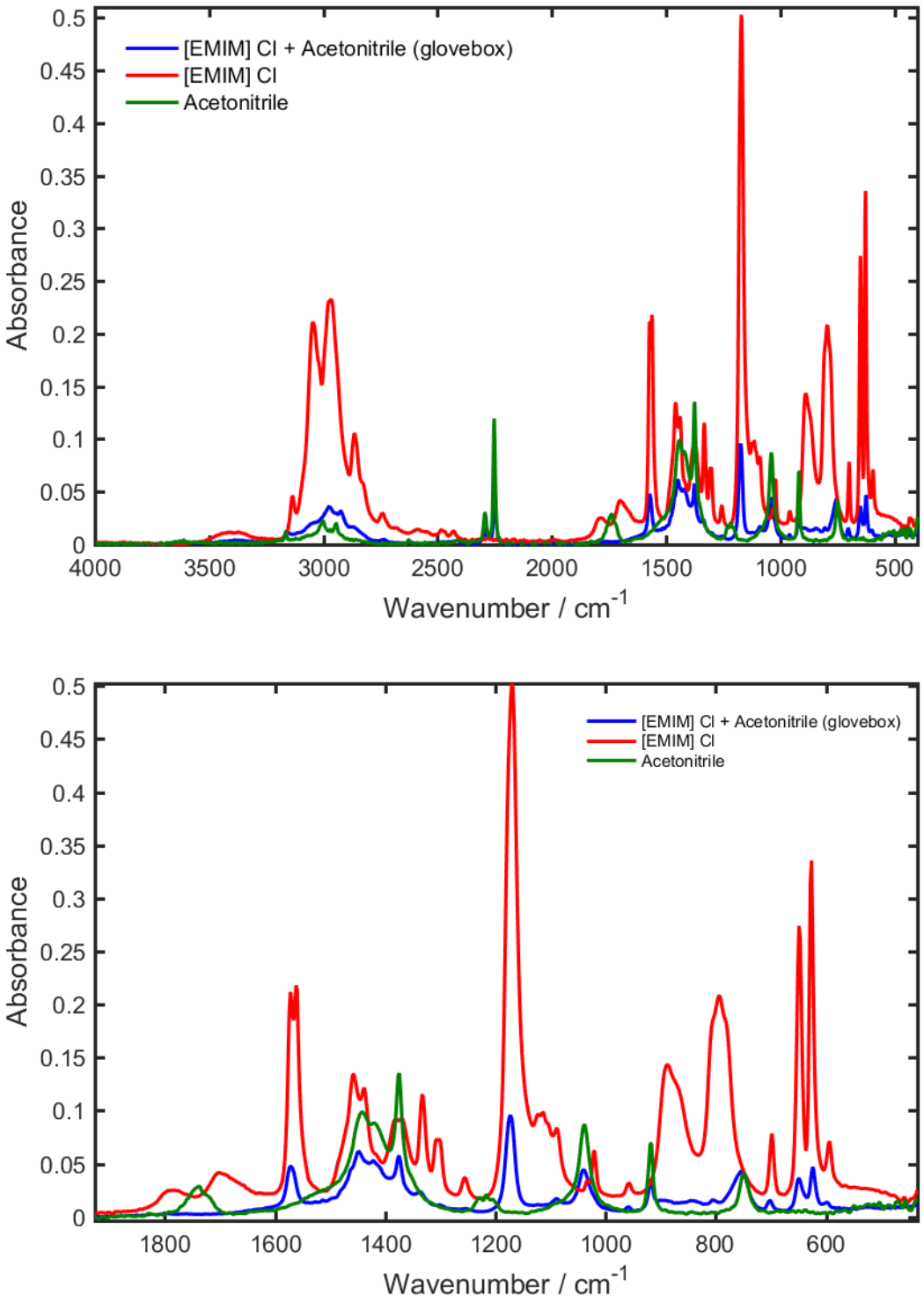


Figure 7.38. ATR-FTIR spectra of [EMIM] Cl ACN binary mixture overlayed with pure [EMIM] Cl and ACN (top spectra) a zoomed in version displaying the fingerprint region of the binary mixture (bottom).

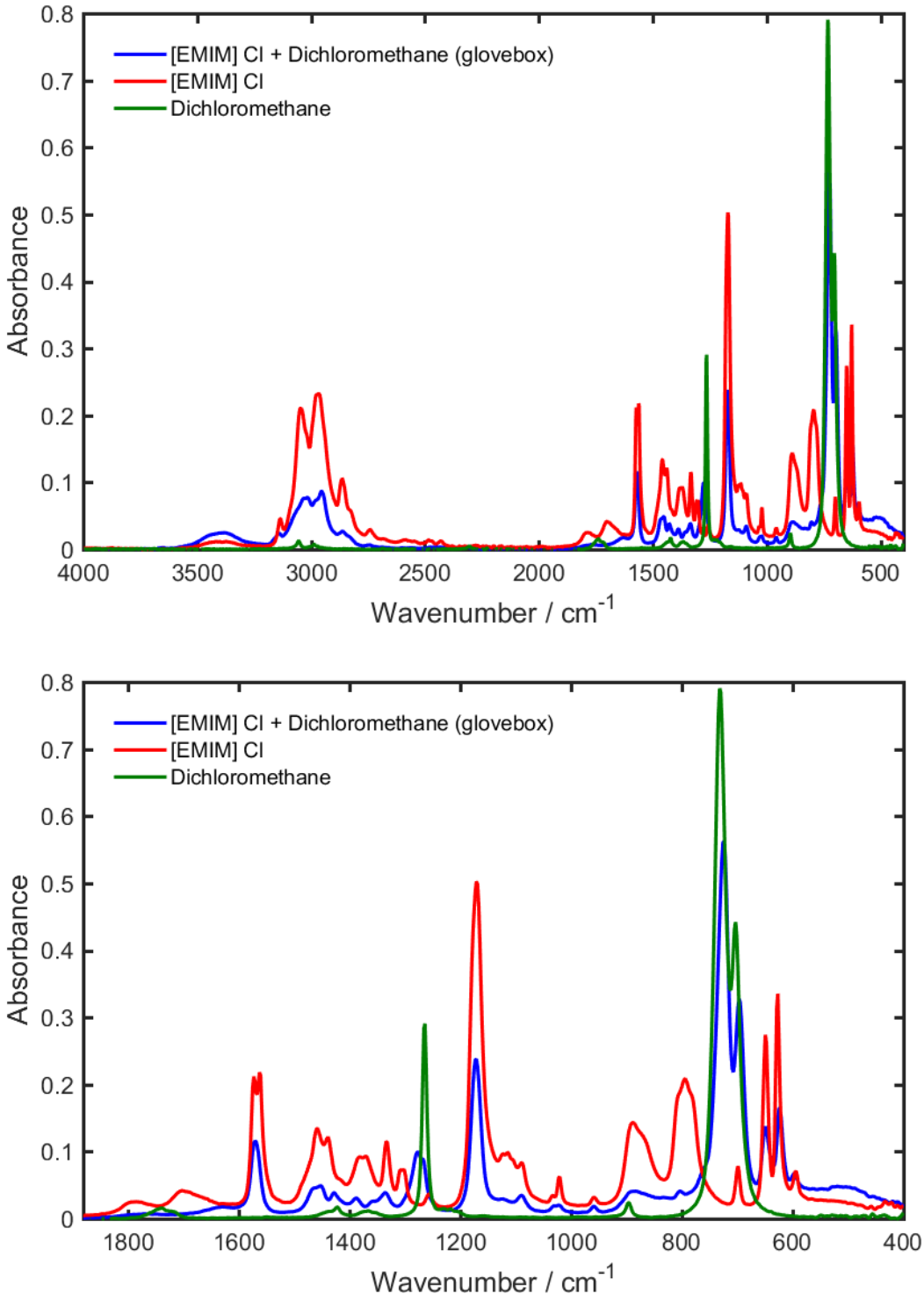


Figure 7.39. ATR-FTIR spectra of [EMIM] Cl DCM binary mixture overlayed with pure [EMIM] Cl and DCM (top spectra) a zoomed in version displaying the fingerprint region of the binary mixture (bottom).

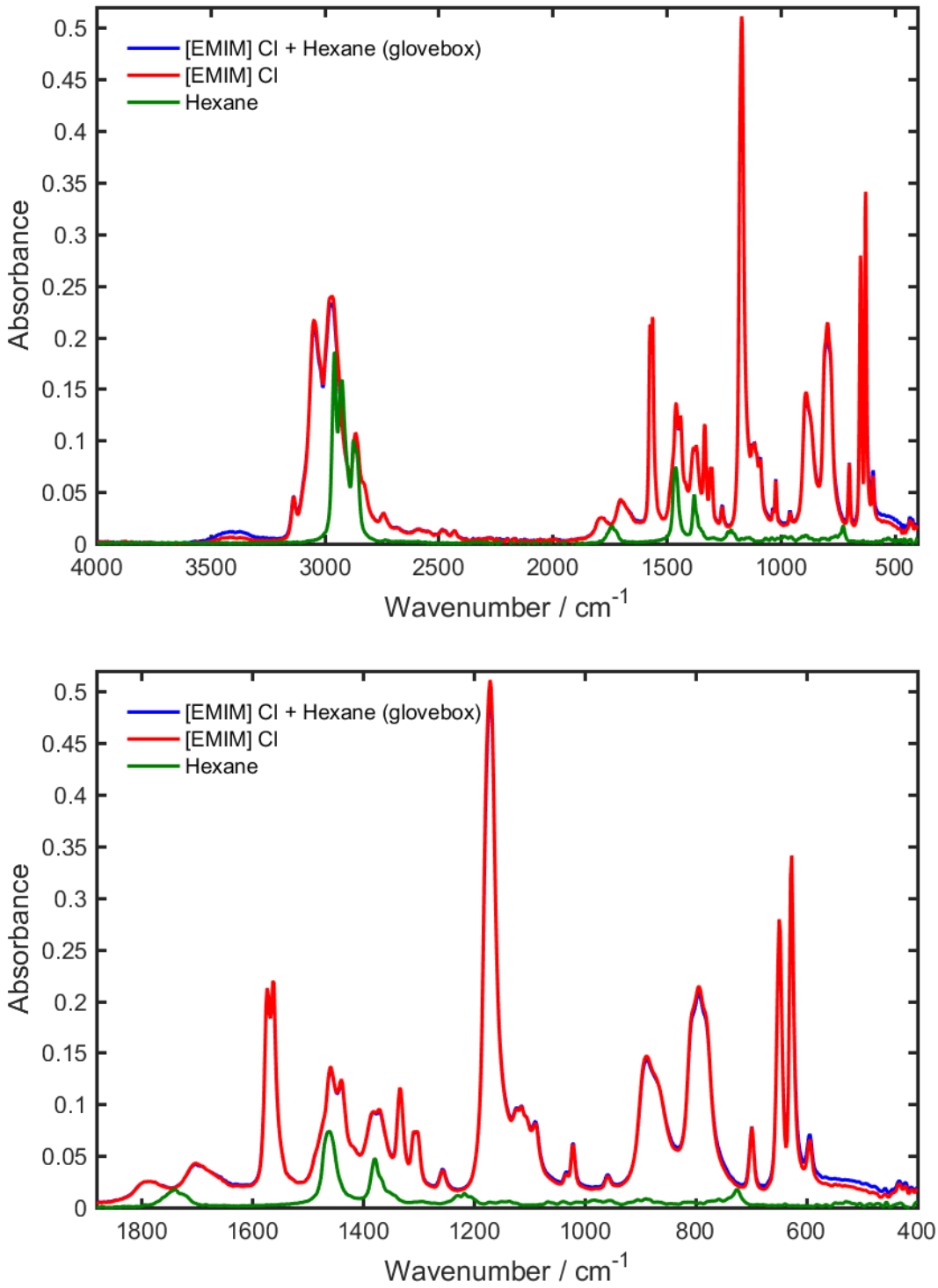


Figure 7.40. ATR-FTIR spectra of [EMIM] Cl hexane binary mixture overlayed with pure [EMIM] Cl and hexane (top spectra) a zoomed in version displaying the fingerprint region of the binary mixture (bottom).

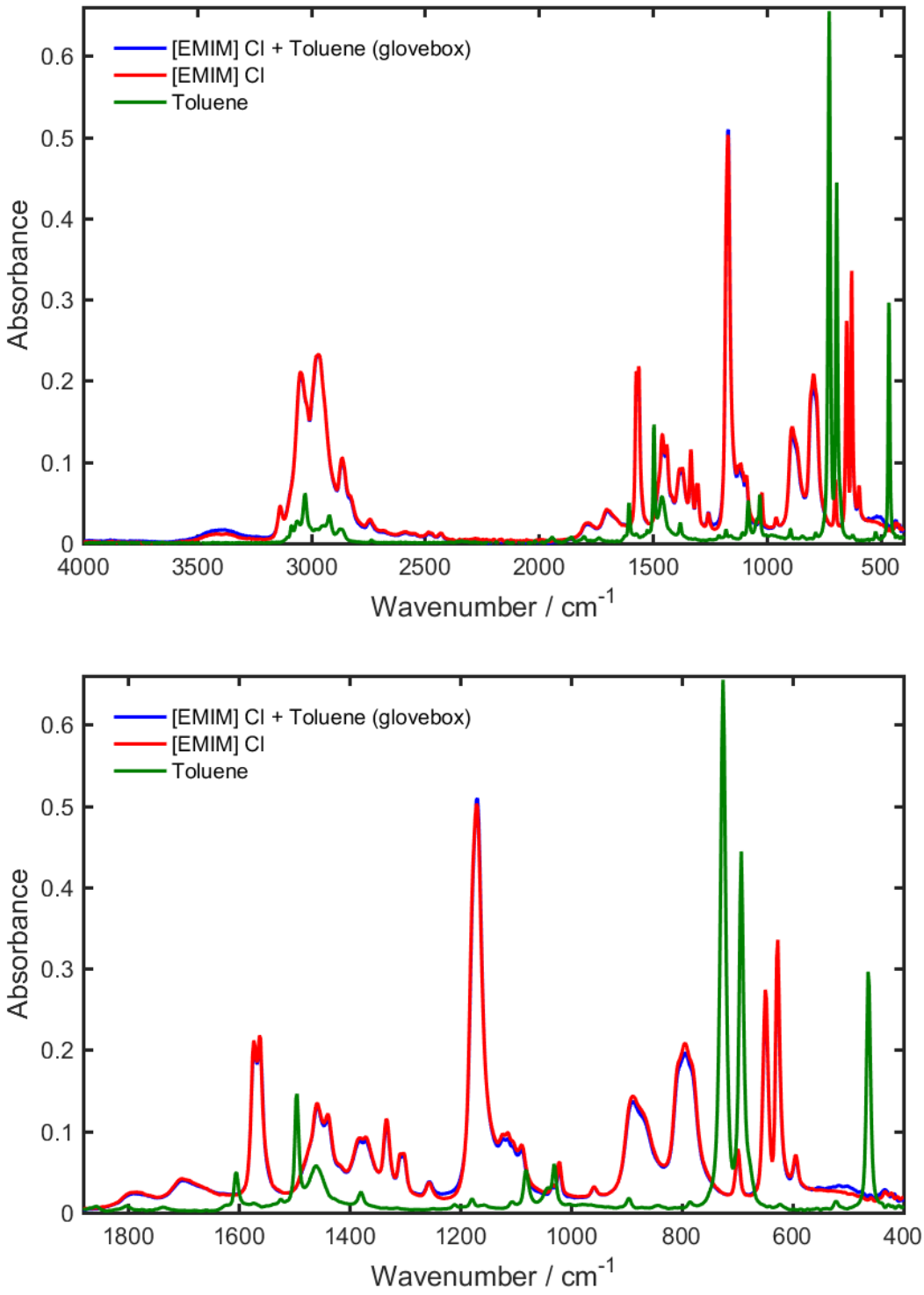


Figure 7.41. ATR-FTIR spectra of [EMIM] Cl toluene binary mixture overlayed with pure [EMIM] Cl and toluene (top spectra) a zoomed in version displaying the fingerprint region of the binary mixture (bottom).

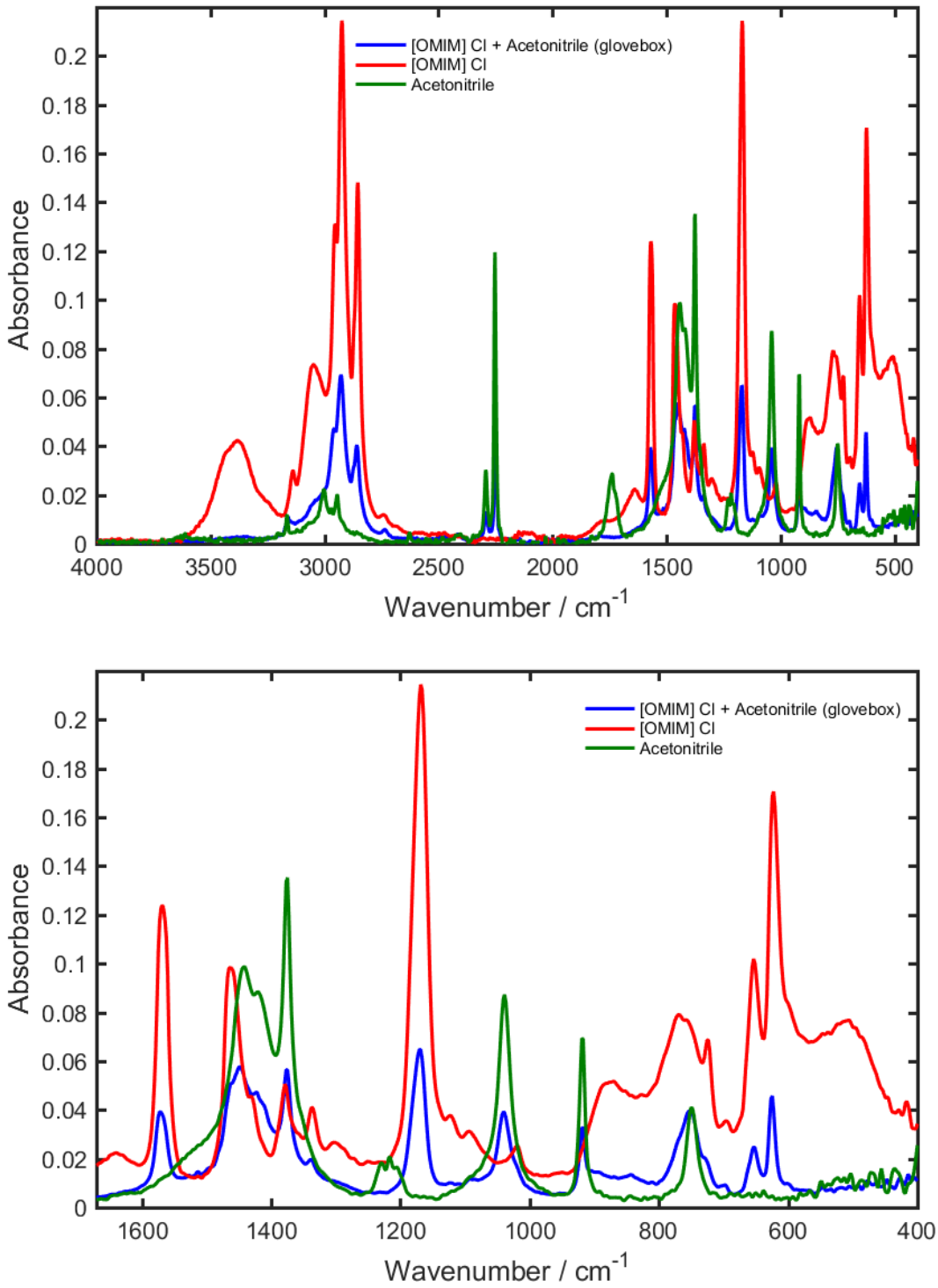


Figure 7.42. ATR-FTIR spectra of [OMIM] Cl ACN binary mixture overlayed with pure [OMIM] Cl and ACN (top spectra) a zoomed in version displaying the fingerprint region of the binary mixture (bottom).

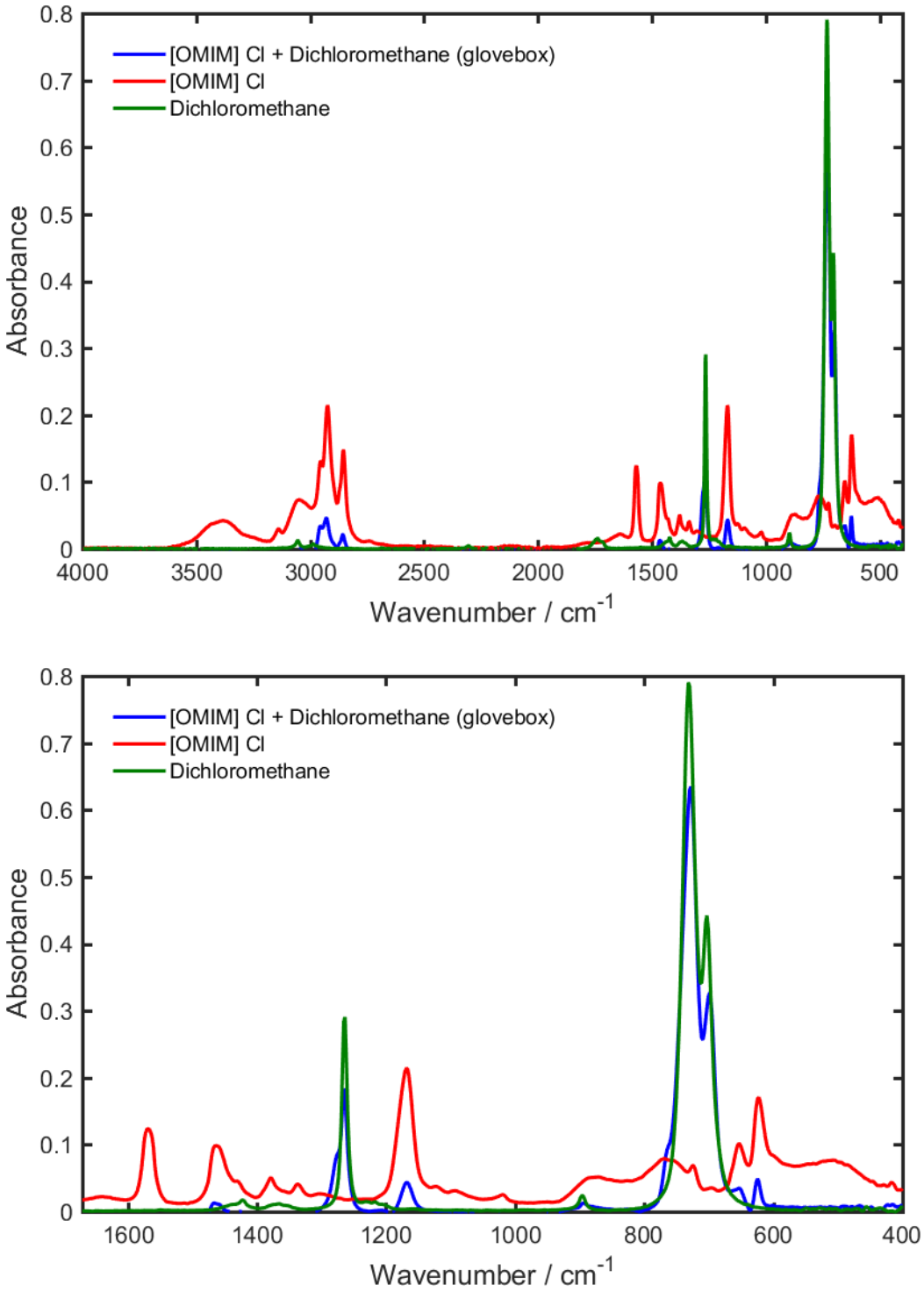


Figure 7.43. ATR-FTIR spectra of [OMIM] Cl DCM binary mixture overlayed with pure [OMIM] Cl and DCM (top spectra) a zoomed in version displaying the fingerprint region of the binary mixture (bottom).

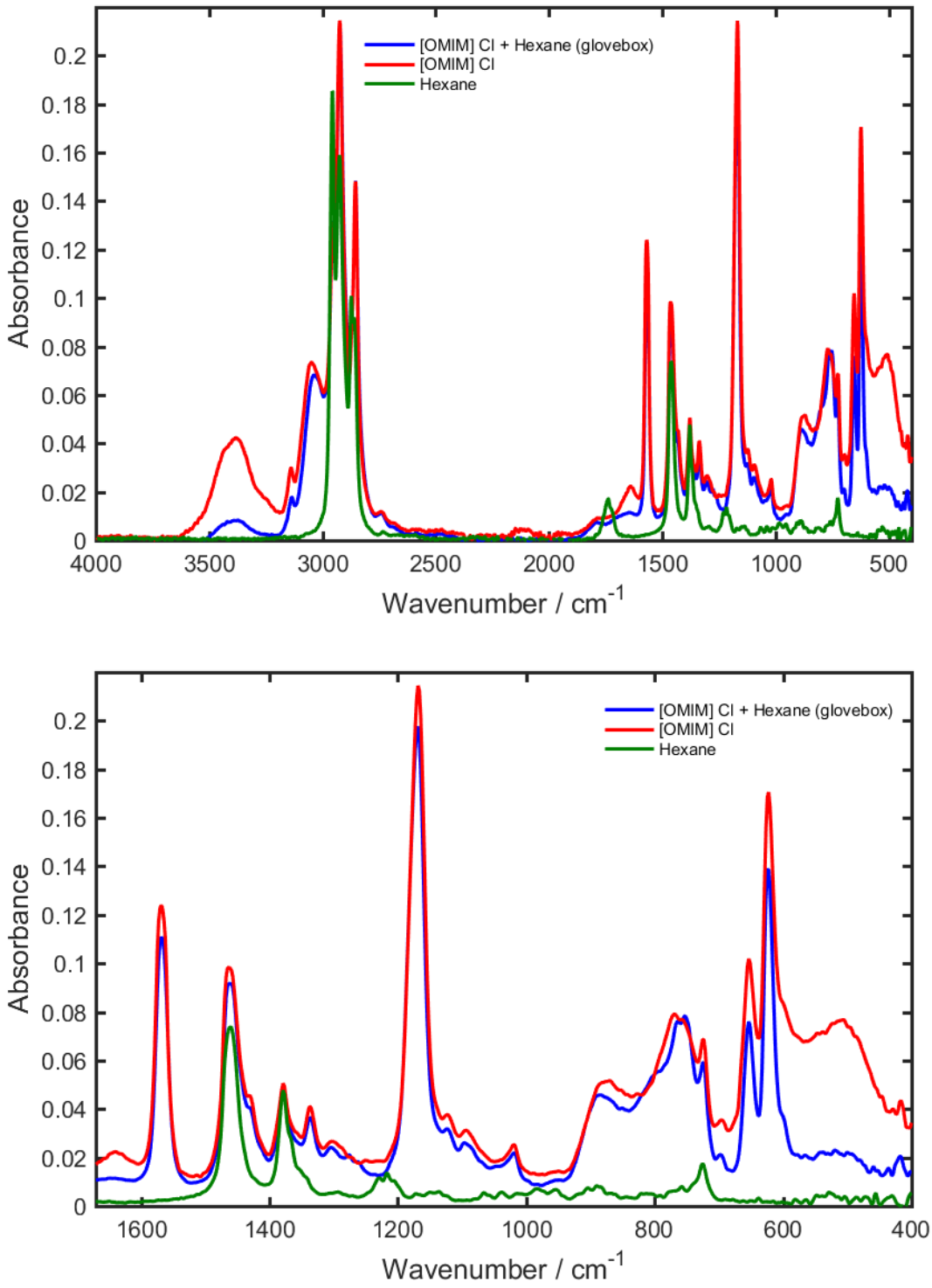


Figure 7.44. ATR-FTIR spectra of [OMIM] Cl hexane binary mixture overlayed with pure [OMIM] Cl and hexane (top spectra) a zoomed in version displaying the fingerprint region of the binary mixture (bottom).

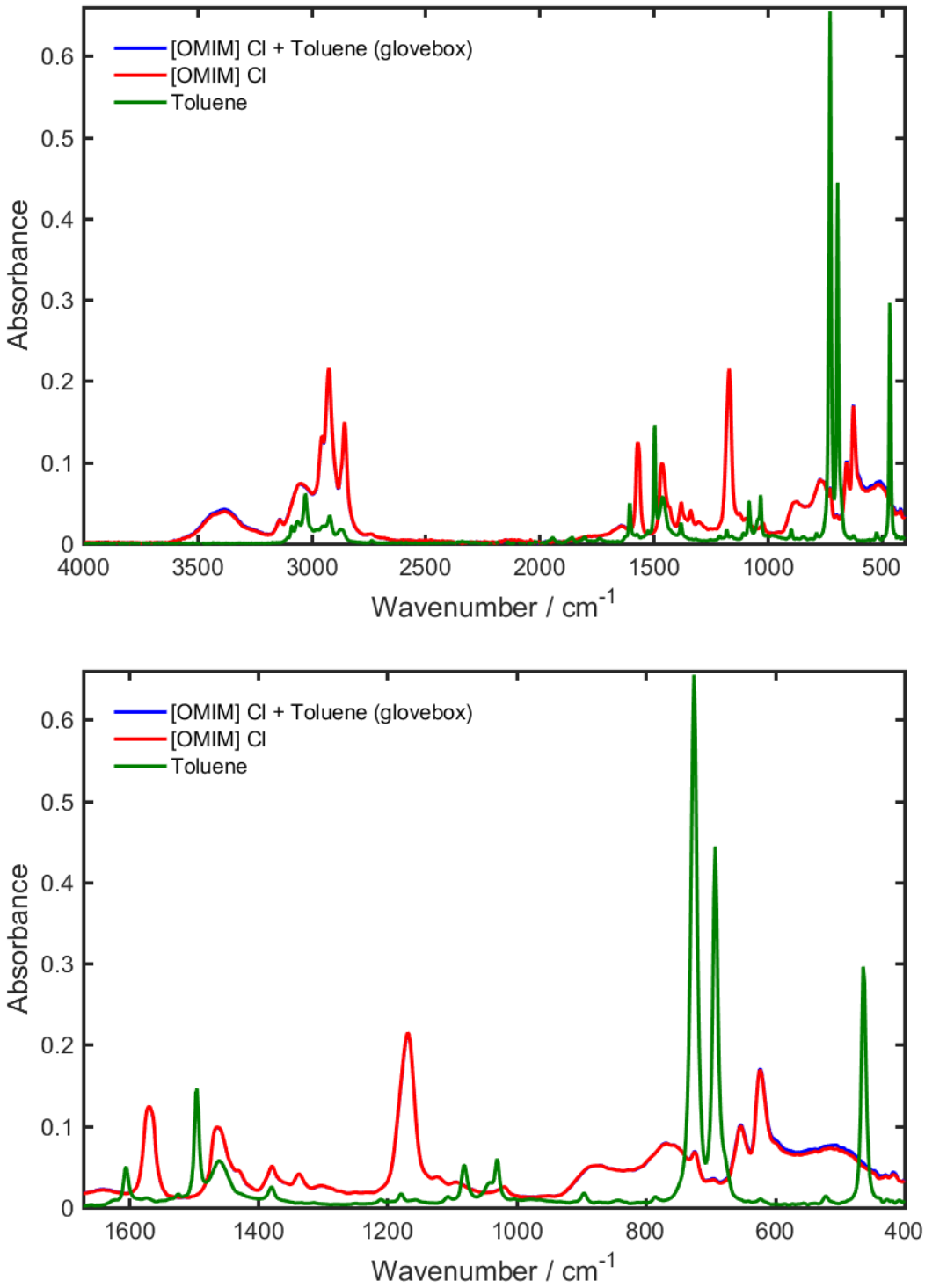


Figure 7.45. ATR-FTIR spectra of [OMIM] Cl toluene binary mixture overlayed with pure [OMIM] Cl and toluene (top spectra) a zoomed in version displaying the fingerprint region of the binary mixture (bottom).

Ionic Liquids, Molecular Solvents and Water Tertiary Mixtures

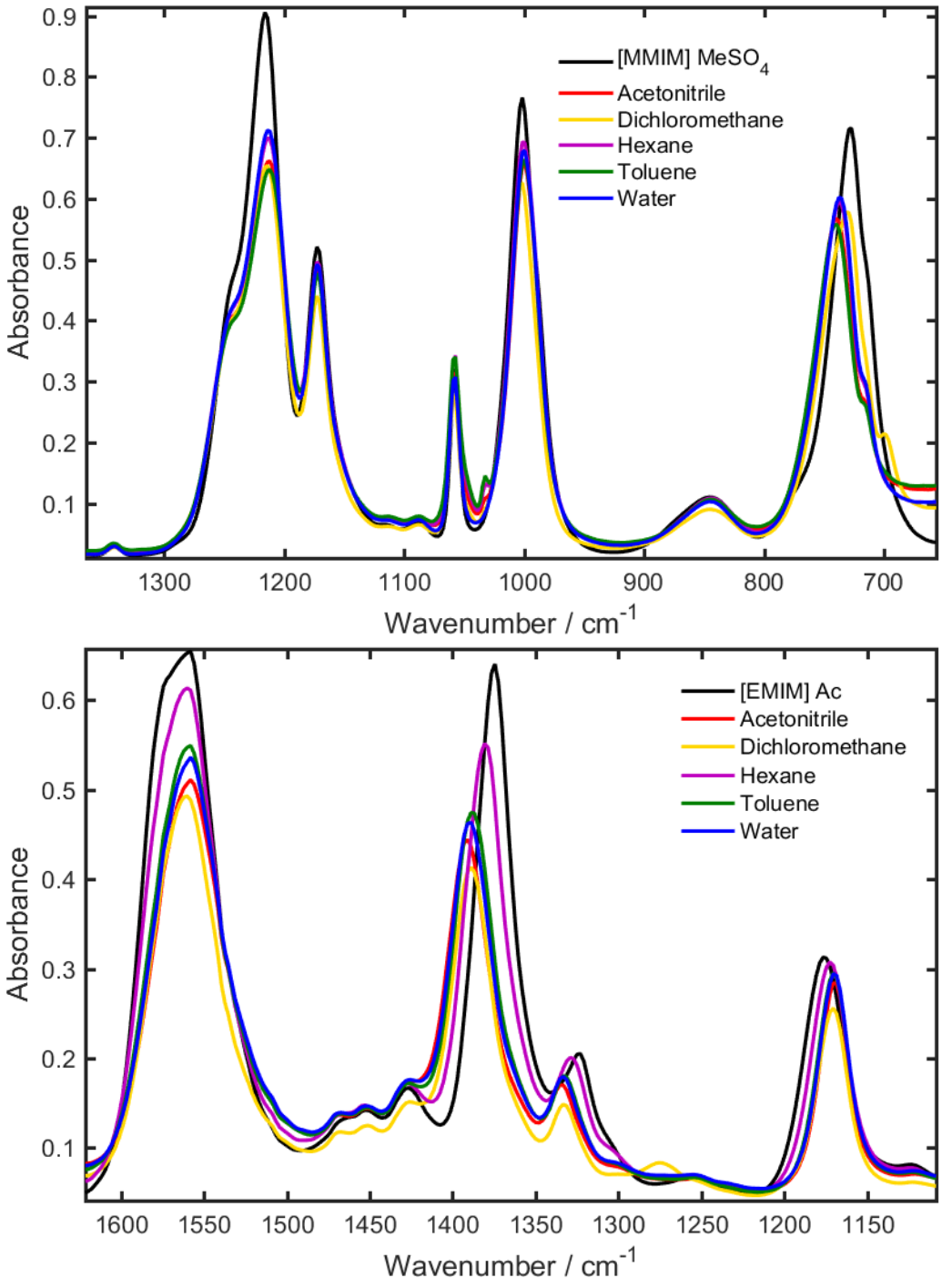


Figure 7.46. A zoomed in ATR-FTIR spectra of the fingerprint region for [MMIM] [$MeSO_4$] tertiary mixtures (top) and [EMIM] [Ac] tertiary mixtures (bottom

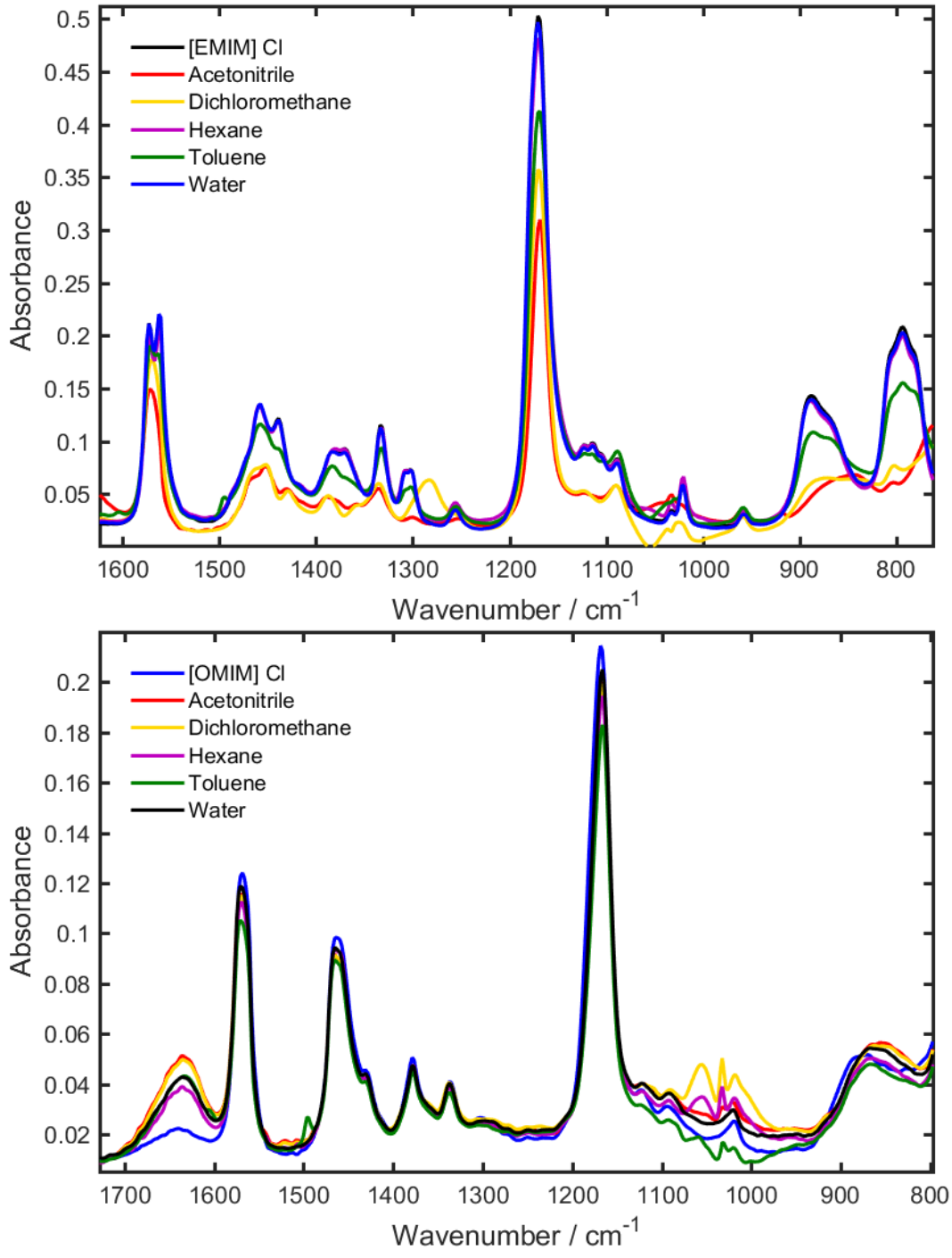


Figure 7.47. A zoomed in ATR-FTIR spectra of the fingerprint region for [EMIM] Cl tertiary mixtures (top) and [OMIM] Cl tertiary mixtures (bottom)